UNCLASSIFIED

REPORT NO. NASA CR-132380

A proposal for

EVALUATION OF A METAL FUSELAGE PANEL S SELECTIVELY REINFORCED WITH FILAMENTARY COMPOSITES FOR SPACE SHUTTLE APPLICATION

VOLUME II BUSINESS MANAGEMENT

by W. F. Wennhold

FINAL REPORT

January 1974

Submitted to
National Aeronautics and Space Administration

Submitted to
National Aeronautics and Space Administration
LANGLEY RESEARCH CENTER
Hampton, Virginia

Prepared by
CONVAIR DIVISION OF GENERAL DYNAMICS
San Diego, California

UNCLASSIFIED

FOREWORD

This report was prepared by the Convair Aerospace division of General Dynamics Corporation under Contract NAS1-10766 and covers the work performed during the period April 1, 1971 to June 1973. The contract was administered by Dr. M. F. Card and Mr. James Anderson of NASA Langley Research Center.

The author wishes to acknowledge the contributions of the following Convair Aerospace personnel:

M. G. Herbert, G. F. Foelsch	Stress Analysis
J. P. Hamm	Design
P. K. Shih	Thermal Analysis
T. C. Johnson	Cost Analysis
L. C. May, M. Maximovich	Materials
J. J. Christiana, C. R. Maikish, C. Bennett	Fabrication
R. Adsit, W. M. Parker	Subelement Testing
S. Chavez	Test Plan Preparation and Testing

The author also wishes to acknowledge the contribution of Mr. J. Joanides of Rockwell International Corporation, Space Division, for his assistance in providing design criteria data for the Space Shuttle Orbiter vehicle.

TABLE OF CONTENTS

TABLE OF CONTENTS (continued)

TABLE OF CONTENTS (continued)

TABLE OF CONTENTS (continued)

LIST OF FIGURES

LIST OF FIGURES (continued)

LIST OF FIGURES (continued)

LIST OF FIGURES (continued)

LIST OF FIGURES (continued)

LIST OF FIGURES (continued)

LIST OF TABLES

LIST OF TABLES (continued)

EVALUATION OF A METAL FUSELAGE PANEL SELECTIVELY REINFORCED WITH FILAMENTARY COMPOSITES FOR SPACE SHUTTLE APPLICATION

FINAL REPORT

by

W. F. Wennhold
Convair Aerospace division of General Dynamics Corp.

SUMMARY

This report summarizes the work accomplished in a three-phase program to demonstrate the feasibility of reinforcing a space shuttle orbiter fuselage panel with advanced composites. The three phases of this program were:

Phase I	-	Design and Technology Development
Phase II	-	Component Fabrication
Phase III	-	Component Testing

The component was chosen from the Rockwell International Corporation Space Division's design for a delta winged orbiter with internal propellant tanks.

A ground rule for the program was to investigate the use of those composite systems for which adequate mechanical property data was available. The initial parametric study considered five composite materials. These systems investigated were Boron/Aluminum, Narmco Ridgidite 5505, Boron Polyimide, Graphite/Epoxy GY-70/X-904, and Graphite/Epoxy HT-S/X-904.

The total task of Phase I was divided into several somewhat interrelated areas of investigation - these include:

1. A determination of loads and environmental conditions.

2. A parametric study of all metal and composite reinforced metal panels.

3. An analysis of the available composite systems and their applicability to this program.

4. The design of an all-metal orbiter fuselage panel.

5. The design of a composite reinforced metal orbiter fuselage panel.

6. A stress and thermal analysis of the metal and composite reinforced metal panels.

7. A cost analysis of the metal and composite reinforced panels.

8. The design, analysis, fabrication and testing of subelement test specimens.

9. The design of composite reinforced metal panel test specimens.

10. The preparation of a test plan and the fabrication of the test fixtures.

The work accomplished in Phase I substantiated the feasibility of building a compression panel test specimen using boron aluminum stiffeners on a titanium skin. The method used to predict the failure strength of the combined composite-metallic section appeared to be adequate and is similar in accuracy to the methods available for all-metal sections.

Phase II was devoted to the fabrication of two boron aluminum reinforced titanium compression panel test specimens. The boron aluminum stiffeners were fabricated from unidirectional boron aluminum sheet which was hot formed into the hat section shape. The stiffeners were attached to the titanium skin by means of a process called spot diffusion bonding. This process is performed on a conventional resistance welding machine and produces joints which have good strengths at room and elevated (600F)(589K)) temperature and also possess good fatigue characteristics.

Phase III of this program was devoted to the structural testing of the two compression panel components of a simulated space shuttle thermal environment. The first panel failed at 67.5% of design limit load. The premature failure was attributed primarily to test error.

The second panel failed at design limit load. Failure in this case was attributed to buckling of the titanium skin due to the lack of support by the stringers. Although the panels did not meet the design requirements, the tests did demonstrate that the basic concept is feasible and that more care is needed in the proportioning of stringer elements for this application.

INTRODUCTION

Numerous studies and investigations in the past and near term have shown the potential of using the high strength and modulus of advanced filamentary composites to reduce the structural weight of aerospace vehicles. The Space Shuttle is considered a prime candidate for composites, and several detailed investigations have been made.

In using composites for the structure, the designer has two options: to make the entire component from the selected composite material as a selective strengthening element on a basic member made from a conventional isotropic material. The latter course has considerable merit in that it provides a basic member made from a material relatively easy to fabricate and which has the inherent reliability that is derived from a long technological history, coupled with a vastly superior material from a specific strength standpoint. Further, the composite material is used primarily at the most structurally advantageous points on the reinforced member.

The objective of this program was to investigate the feasibility of using a composite reinforced metal panel on a space shuttle orbiter vehicle.

One of the goals was to utilize materials and processes which were presently available and which could be used to fabricate portions of the actual orbiter vehicle.

In the same light, the mechanical properties and allowables used for the design and analysis were those which were readily attainable. During the course of the contract the properties of boron/aluminum showed considerable improvement. As a result there will be some discrepancy in the mechanical properties data listed in this report. It is desired to utilize the most up-to-date data available.

The mechanical properties for the boron/epoxy, graphite/epoxy and polyimide data were obtained either from the design guide or from parallel in-house programs.

1

ESTABLISHING LOADS AND ENVIRONMENTAL CONDITIONS

INTRODUCTION

The space shuttle orbiter vehicle upon which this program was based was a delta winged, high cross range vehicle designated 161C (Figure 1.1). The data contained in this section were obtained under subcontract from Rockwell International Corporation Space Division, designer of the orbiter vehicle.

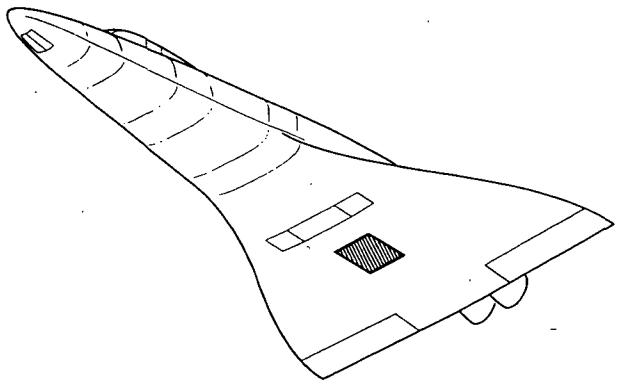

Figure 1.1. Orbiter Vehicle.

Panel Description

The fuselage panel selected for this study is located on the lower surface of the orbiter. The panel is between butt plane 70 and butt plane 240 and extends from the front spar bulkhead (STA 1899) to a position approximately 254cm (100 inches) forward of the bulkhead. The panel is a titanium (6Al-4V) stiffened hat section with an equivalent monocoque thickness ($\bar{t}$) 0.21 cm (0.083 inches). The skin thickness is 0.091 cm (0.036 inches) and the stringer spacing is 6.98 cm (2.75 inches). The panel's external insulation is 3.47 cm (1.37 inches) thick and the internal insulation is 5.63 cm (2.22 inches) thick.

General Requirements

The structure shall possess sufficient strength and rigidity to survive the critical loading conditions and associated environments that exist within the envelope of mission requirements.

The structure shall be designed to survive the specified number of missions with a minimum of structural refurbishment, and in a manner that does not reduce the probability of the successful completion of any mission. Consideration shall be given to the accumulative deteriorating effect of repeated exposure to the critical conditions such as temperatures, creep, and fatigue.

The structure shall be designed by flight conditions where possible. The non-flight conditions and environment shall influence the design to the minimum extent possible.

The proposed lifetime will be based on 100 orbiting missions with the associated flight testing and ferrying.

The structure shall be designed to withstand limit loads and pressures throughout its service life without experiencing detrimental deformation and to withstand ultimate conditions without rupture or collapse.

The structural design shall employ proven processes and procedures for manufacture and repair. The structural design shall permit the vehicle structure to be maintained in or restored to a flightworthy condition with a minimum of resources. The design should emphasize structural materials, forms, fasteners, and seals which minimize the need for maintenance and which properly consider the needs for access, inspection, service replacement, repair, and refurbishment. The structure shall be designed to minimize the total cost of the space shuttle for 100 missions, including costs of development, production, and any servicing, inspection, repair, or refurbishment necessary to carry out the missions.

When practicable, the structure shall incorporate fail safe designs concepts. A fail safe design is one in which the failure of a single structural element does not degrade the structure below a safe level, and which is detectable by "between mission" inspection procedures and requirements.

Where a fail safe design concept is not practicable, the structures shall be designed to a safe life requirement which incorporates a suitable factor of safety.

Factors of Safety for Lower Fuselage

CONDITION	CRITICAL LOADS	FS
Boost	Mechanical	1.4
Entry	Mechanical and	1.5
and	Thermal	1.0
Aircraft Flight	Thermal Only	1.25

Trajectory and Heating Data

Assumptions and Input Data for the Baseline Sizing Study

The trajectory profile represents nominal baseline data. The baseline configuration (161C/B9U) was sized using the following assumptions and input data:

185.2 x 185.2 km (100 x 100 NM)/90° Design Reference Mission

92.6 x 185.2 km (50 x 100 NM)/90° Insertion Orbit

3-g Maximum Acceleration

Zero Lift Ascent to Booster Separation

Optimum Pitch Plane Steering from Booster Separation to Orbit Insertion

Max $Q\alpha$ Unconstrained

Structural Loads

The design loads for the lower fuselage panel are:

Flight Condition	Ult. Stress Axial		Resultants Shear		Temp		Time
	KN/m	Nx(lb/in)	KN/m	q(lb/in)	K	F	
HiQ							
Headwind	532	(3040) Tension	108	(617)	338	(150)	80 sec.
Tailwind	334	(1910) Tension	91	(520)	338	(150)	80 sec.
End Boost	640	(3660) Tension	153	(875)	338	(150)	213 sec.
Landing							
Spring Back	-440	(-2515) Comp.	-	-	616	(650)	3500 sec.

Design Temperatures

Maximum outer surface temperatures (entry) 1283°K (1850°F)

Minimum inner surface temperature* (cold soak) 161°K (-170°F)

Figure 1.2 represents the convective flux history of the lower fuselage area under consideration. Table 1-1 summarizes the baseline vehicle characteristics.

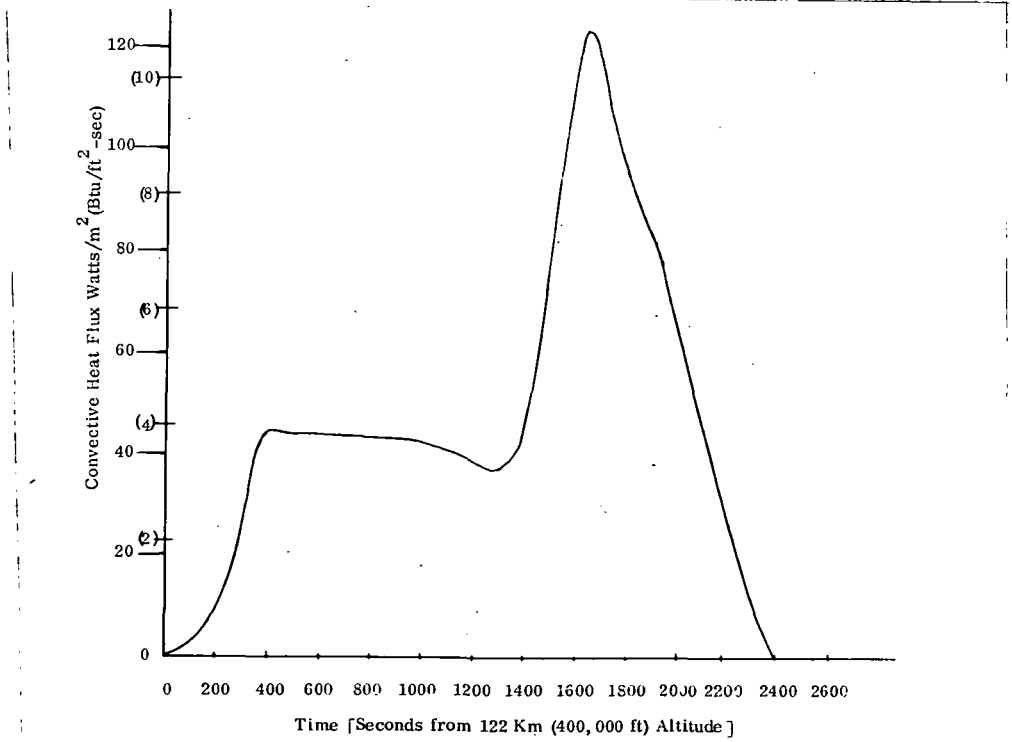

Figure 1.2. Convective Heat Flux for Lower Fuselage Area X/L = .80.

*External insulation bond line

Table 1-1. Selected Baseline Vehicle Summary

VEHICLE CHARACTERISTICS		
Lift-off Gross Weight	2.289 Gg (5,047,457 lb)	
Lift-off Thrust to Weight Ratio	1.308	
	BOOSTER	ORBITER
Gross Stage Weight	1.899 Gg (4,188,233 lb)	389.66 Mg (859,234 lb)
Thrust (S.L.)	29.356 MN (6,600,000 lb)	---
Thrust (VAC)	32.219 MN (7,243,400 lb)	251.88 Mg (1,263,810 lb)
I_{sp} (VAC)	439 sec	459 sec
Main Ascent Propellant	1.531 Gs (3,376,547 lb)	251.86 Mb (555,377 lb)
Ohms, Propellant	---	8.855 Mg (19,526 lb)
Ohms ΔV	---	304.8 m/sec (1,000 ft/sec)
Booster Flyback Propellant	67.765 Mg (149,427 lb)	---
Booster Flyback Range	772.2 KM (417 n.mi.)	---
Landing Weight	285.77 Mg (630,153 lb)	121.54 Mg (268,007 lb)
Max q, PSF	24.227 KN/m^2 (506 lb/ft^2)	

BOOSTER BURNOUT CHARACTERISTICS	
Rel. Velocity	3301.59 m/sec (10,832 ft/sec)
Altitude	73.784 KM (242,074 ft)
Rel. Flight Path Angle	6.0 degree
Time from Lift-off	213.5 sec

"Page missing from available version"

2

PARAMETRIC STUDY

2.1 INTRODUCTION

The purpose of this portion of the program was to investigate various compression panel stiffener configurations, both all metal and composite reinforced metal, in order to determine the optimum configurations. Initially a large number of configurations were envisioned and the list then reduced to the most efficient. Analysis subsequently showed that the hat section was the most efficient for both the all metal and for the composite reinforced metal panel.

Because of the relatively low compressive loading, the use of a titanium stringer with selective reinforcement was abandoned. The basic stringer in titanium was near minimum gage and hence a very small reduction in weight could be achieved by this method. The composite reinforced study then was directed toward using all composite stringers in metal sheets.

2.2 METAL PANEL PARAMETRIC STUDY

A parametric study was conducted on the basic titanium panel sections and the results are presented in Figure 2.1. The study made use of the structural efficiency factors as presented by Mr. D. H. Emero. (Ref. 1) The structural efficiency factors that were derived were based on the established principles, that for the optimization of a given structural cross section, local and general instability failure modes occur simultaneously. The resultant equation derived from the above requirements is

$$\frac{N_x}{L\bar{n}E} = (\epsilon)\left(\frac{\bar{t}}{L}\right)^2 \quad \text{where}$$

N_x = moment distributed load

L = length

E = modulus of elasticity

$\bar{t}$ = effective thickness

$\bar{n}$ = general plasticity correction

ϵ = efficiency factors

In this general form, various structural sections can be compared by comparing their relative structural efficiency factors. This method of establishing the most efficient

Configuration No.	Structure	Structural Efficiency Factor (1) Weight	Thermo-Prot.	Cost
1 	Provides good skin shear capability but stiffeners do not provide maximum skin panel edge support.	0.884(2) The lightest configuration has the highest efficiency factor	Good — Provides good exterior and fair interior insulation support structure.	High — Requires special thin or chem-milled extrusions to be spotwelded or riveted to skin.
2 	Provides good skin shear capability but stiffeners do not provide maximum skin panel edge support.	0.911	Good — Provides good exterior and fair interior insulation support structure.	Low — Simple formed stiffeners spotwelded or riveted to skin.
3 	Provides good skin shear capability but stiffeners do not provide maximum skin panel edge support.	0.793	Good — Provides good exterior and fair interior insulation support structure.	High — Requires special thin or chem-milled extrusions to be spotwelded or riveted to skin.
4 	Provides good skin shear capability but stiffeners do not provide maximum skin panel edge support.	0.656	Poor — Provides good exterior and poor interior insulation support structure.	Very High — Requires integral machining and chem-milling or diffusion bonding.
5 	Provides good skin shear capability and maximum skin panel edge support. (Greater torsional capability)	0.928	Very Good — Provides good exterior and good interior insulation support structure.	Low — Simple formed stiffeners spotwelded or riveted to skin.
6 	Provides good skin shear capability and maximum skin panel edge support. (Greater torsional capability)	0.685	Very Good — Provides good exterior and good interior insulation support structure.	Low — Simple formed stiffeners spotwelded or riveted to skin.
7 	Provides poor shear capability.	1.15 to 1.60(3)	Poor — Provides poor exterior and poor interior insulation support structure.	Lowest — Simple corrugated sheet.
8 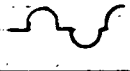	Provides poor shear capability.	1.15 to 1.60(3)	Poor — Provides poor exterior insulation support structure.	Low — Slightly more complicated forming required than in Configurations No. 7 and 9.
9 	Provides poor shear capability.	1.15 to 1.60(3)	Poor — Provides poor exterior and poor interior insulation support structure.	Lowest — Simple corrugated sheet.
10				

(1) Structural efficiency factors from Emero.

(2) This efficiency factor was derived by ratioing the integral Zee and the stiffened Zee to the integral hat. (Approximate)

(3) These efficiency factors cover trapezoidal corrugation ($\phi = 60$) to truss core corrugations but are in the range to cover configurations No. 7, 8, and 9.

Figure 2. 1. All metal panel parametric study summary.

stringer configuration and spacing proved to be a direct and economical approach to the optimization of the all-titanium panels. The efficiency factors not only provide a direct comparison between the various structural configurations from a theoretically optimum weight standpoint, but they also provide a good reference scale with which to compare other design problems such as manufacturing costs, thermal insulation attachment, and skin shear capability. By comparing all of these factors a configuration can be selected that has the highest efficiency factor consistent with low manufacturing costs, high skin shear capability and good thermal insulation attachment structure.

2.3 COMPOSITE REINFORCED PANEL

The initial consideration for the composite reinforced panel study had to include the thermal environment, the maximum operation temperature at the epoxy composite being around 449K (350F). The initial thermal analysis of the orbiter structure indicated that approximately 2 inches of REI insulation was required to reduce the REI bond line temperature to 449K (350F) from 589K (600F) temperature of the basic design. This is an increase of 1.6 cm (0.63 in.) insulation thickness and an increase in unit weight of 3.80 Kg/m^2 (0.78 lb/ft^2). There initially seemed to be little chance to save weight with this insulation penalty. The composite systems which can operate at 589K (600F) obviously have an advantage.

The study represented a different approach than that originally proposed and was undertaken to determine the maximum weight savings for each of the composite systems.

The parametric study for metal panels indicated that the hat section stiffener was the most efficient, so modifications of this basic hat were considered for this study.

Competitive designs to the all-titanium compression panel structure were investigated, where material substitution for the hat section included unidirectional boron/aluminum, graphite/epoxy, boron/epoxy and boron/polyimide. The boron/epoxy hats were combined with 2219-T81 aluminum skin while boron/aluminum, graphite/epoxy and boron/polyimide hats were combined with Ti-6Al-4V skin. The design temperatures selected for the various combinations were 589K (600F) for the all-titanium configuration, 589K (600F) for the aluminum boron, 449K (350F) for the graphite/epoxy, 449K (350F) for the boron/epoxy and, 561K (550F) for the boron/polyimide. A modified titanium hat configuration geometry was used as a starting point in this study in order to compare the weight of these five different configurations. Accordingly, the running cross section is shown in Figure 2.2 where the only unknowns are the height and thickness of the hats and the material and thickness of the skin.

Table 2-1 lists the materials properties used.

The following design criteria was used for this study:

1. No element buckling at limit load (2/3 of ultimate).

2. No wide column buckling at ultimate load.

No edge free plate element buckling was determined for the composite elements by the expression

$$N_{x_u} = \frac{2\pi^2}{b^2}\left\{\sqrt{D_{11}D_{22}} + D_{12} + 2D_{66}\right\} \quad (1)$$

where for unidirectional composites

$$D_{11} = \frac{E_{11}t^3}{12(1-\nu_{12}\nu_{21})} \qquad D_{22} = \frac{E_{22}t^3}{12(1-\nu_{12}\nu_{21})}$$

$$D_{12} = \nu_{21}D_{11} \qquad D_{66} = \frac{G_{12}t^3}{12}$$

However, Equation (1) appeared to be optimistic in some instances for boron/aluminum. Accordingly, the best available boron/aluminum crippling curve shown in Figure 2.3 was used when the crippling stress turned out to be less than the theoretical buckling stress as determined from Equation (1). Conventional buckling methods were used for the isotropic skin in the combined sections and conventional buckling and crippling methods were used for the all titanium configuration.

One edge free plate buckling was determined for the composites by the expression

$$\sigma_{x_a} = G_{12}(t/b)^2 + (\pi/2)^2(D_{11}/t)$$

where "a" is the length of the plate between fasteners. [2.54 cm (one inch) spacing is assumed in this study.]

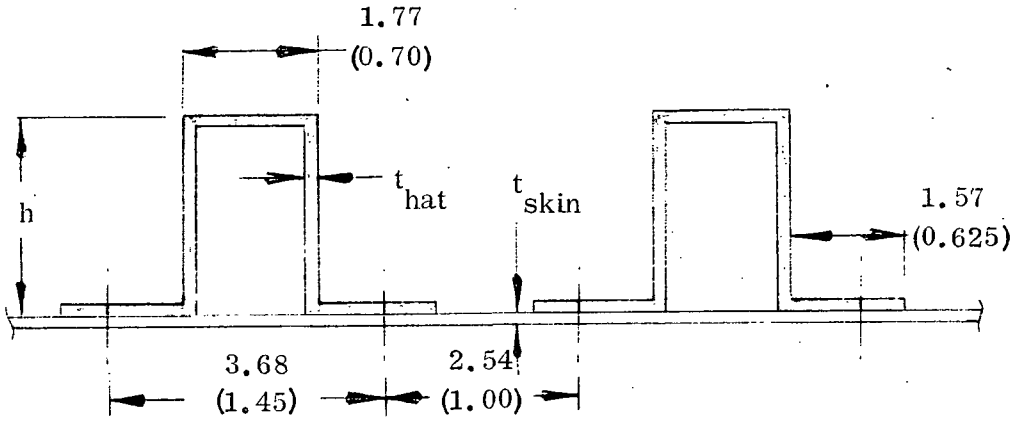

Figure 2.2. Composite Compression Panel Cross Section.

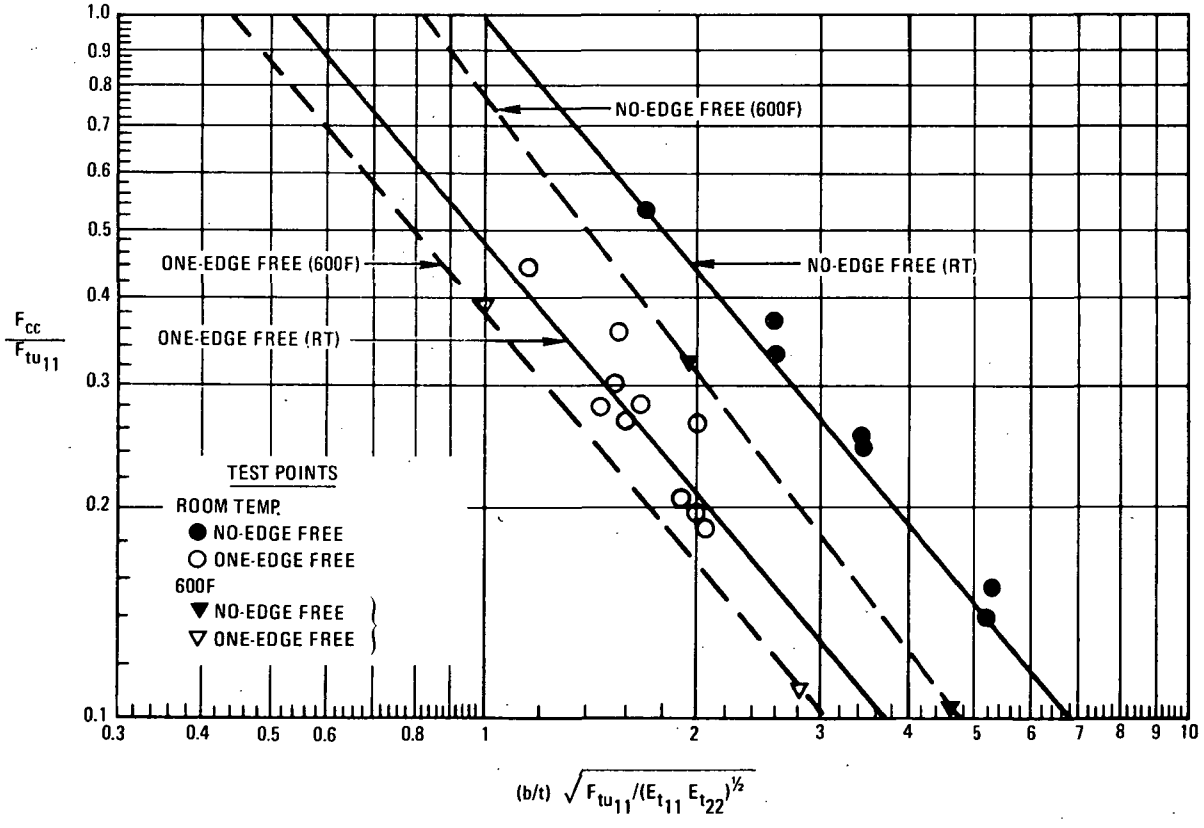

Figure 2.3. UD 50 V/O Boron/Aluminum.

Short column buckling was found by the expression

$$F_{co} = F_{u_{avg}} \left[1 - \frac{F_{cr_{avg}} (L'/\rho)^2}{4\pi^2 E_c} \right]$$

where

F_{co} = short column buckling stress

$F_{u_{avg}}$ = weighted average buckling stress ($\Sigma F_u A \ \Sigma A$)

L'/ρ = slenderness ratio $L' = L$

ρ = radius of gyration of combined section.

This study required several iterations of each configuration before arriving at what was felt to be a practical configuration section for a weight comparison. These sections are shown in Figure 2.4 and pertinent information summarized in Table 2-2.

2.3.1 THERMAL STRESS ANALYSIS. In order to compare the thermal stresses induced into the five composite stiffener configurations shown in Figure 2.4, due to different cross sections, moduli of elasticity, coefficients of thermal expansion and design temperatures, the following procedure was used. Each of the five configurations was idealized as an equivalent I-section as shown in Figure 2.5.

These idealized sections were then assumed to represent the stringer cross section and were analyzed by using a finite element computer program developed at the University of California at Berkeley called "Analysis of Plane Stress Structures." The basic computer structural idealization that was used in this thermal stress analysis represents one-half of a 254 cm (100-inch) long section of the compression panels supported on five frames. The ends of the compression panels were assumed to be simply supported for this thermal stress analysis comparison since it is slightly conservative. An attachment spacing of 254 cm (1-inch) was assumed in the idealization thus establishing the basic element length. The individual stiffener configurations were input into the program along with their appropriate mechanical and physical properties and nodal point temperatures. The temperature changes that were investigated in this analysis were as follows.

Table 2-1. Composite Material Properties used for Parametric Study

Material	Density		Temperature		F_{cu_x}		F_{cu_y}		E_{cx}		E_{cy}		G_{xy}	
	Kg/m^3	$(\#/in^3)$	K	(F)	MN/m^2	(ksi)	MN/m^2	(ksi)	GN/m^2	psi x 10^6	GN/m^2	psi x 10^6	GN/m^2	psi x 10^6
Boron/6061 Aluminum	2,657	(0.096)	589	(600)	1,171	(170)	68	(10)	193	(28)	75	(11)	48.2	7.0
GY-70/HM-S/X-904 Graphite/Epoxy	1,799	(0.065)	449	(350)	386	(56)	20	(3)	273	(39.7)	17.8	(2.59)	3.44	0.5
Boron/Epoxy AVCO 5505	1,992	(0.072)	449	(350)	1,296	(188)	62.7	(9.1)	206	(30)	18.61	(2.7)	3.58	.52
Boron/Polyimide	1,992	(0.072)	561	(550)	827	(120)	29.6	(4.3)	193	(28)	3.58	(.52)	5.2	.76

Table 2-2. Summary of Parametric Study Results

Material		Temp.		h		t_{hat}		t_{skin}		N_{co}		N_{ult}		M.S.	*Weight @ 600° F	
Hat	Skin	K	F	cm	(in)	cm	(in)	cm	(in)	KN/m	(lb/in)	KN/m	(lb/in)		Kg/m^2	(lb/ft^2)
Ti-6Al-4V	Ti-6Al-4V	589	600	2.54	(1.0)	0.08	(0.032)	0.08	(0.032)	434	(2482)	440	(2515)	-.01	9.3	(1.907)
B/Al	Ti-6Al-4V	589	600	2.92	(1.15)	0.068	(0.027)	0.08	(0.032)	449	(2568)	440	(2512)	.02	6.7	(1.377)
GY-70/HMS	Ti-6Al-4V	449	350	2.28	(0.90)	0.080	(0.0318)	0.08	(0.032)	488	(2788)	440	(2515)	.11	9.6	(1.957)
B/5505 Epoxy	2219-T8/Al	449	350	2.15	(0.85)	0.088	(0.035)	0.127	(0.050)	470	(2686)	440	(2515)	.07	9.9	(2.032)
B/PI	Ti-6Al-4V	561	550	2.03	(0.80)	0.129	(0.051)	0.08	(0.032)	471	(2695)	440	(2515)	.07	7.0	(1.436)

*This weight figure includes the weight of any addition insulation that may be required in order not to exceed the maximum design temperature in each configuration.

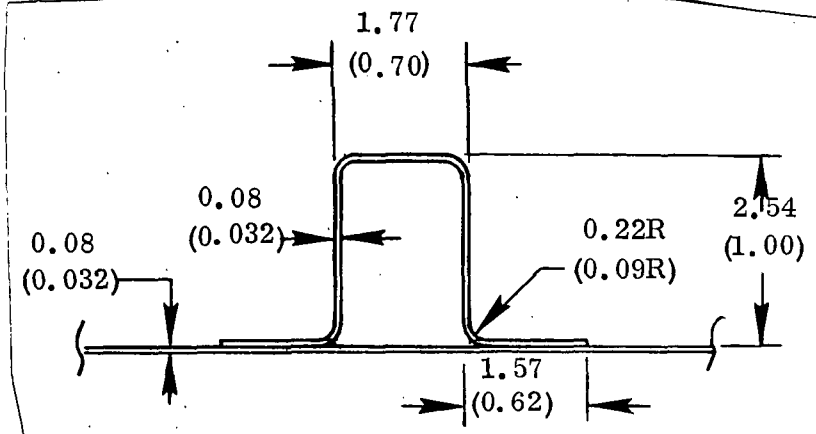

All Titanium Panel

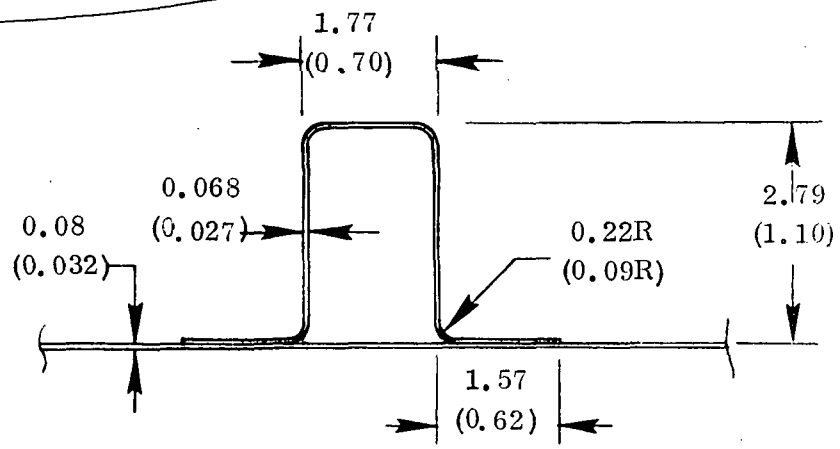

Boron Aluminum Stiffener
Titanium Panel

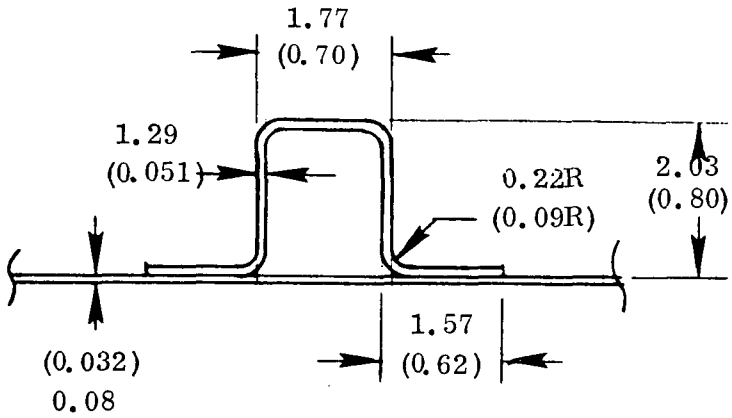

Boron Polyimide Stiffener
Titanium Panel

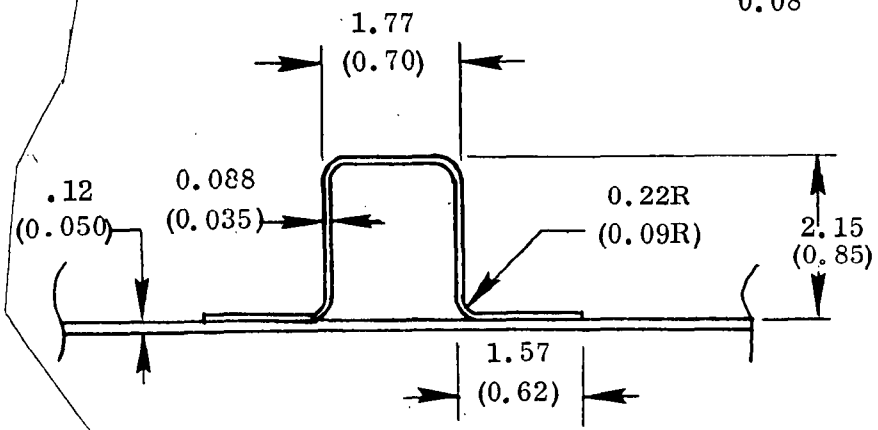

Narmco 5505 Boron Epoxy Stiffener
Aluminum Panel

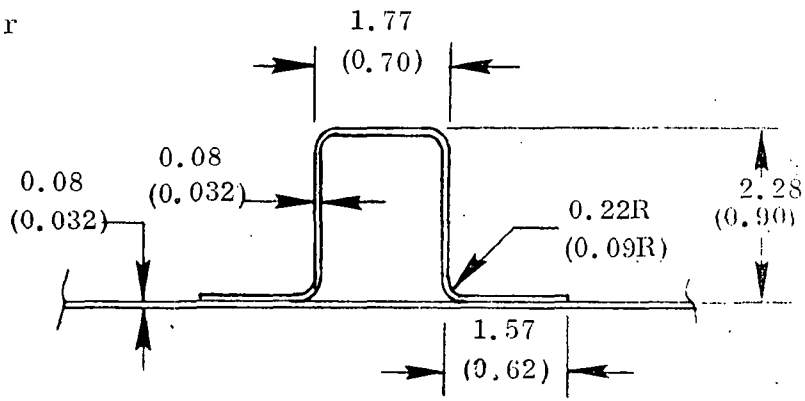

GY-70/HM-S/X-904 Graphite Epoxy
Stiffener Titanium Panel

Figure 2.4. Parametric Study Stiffened Configurations. (Stringer spacing for all)

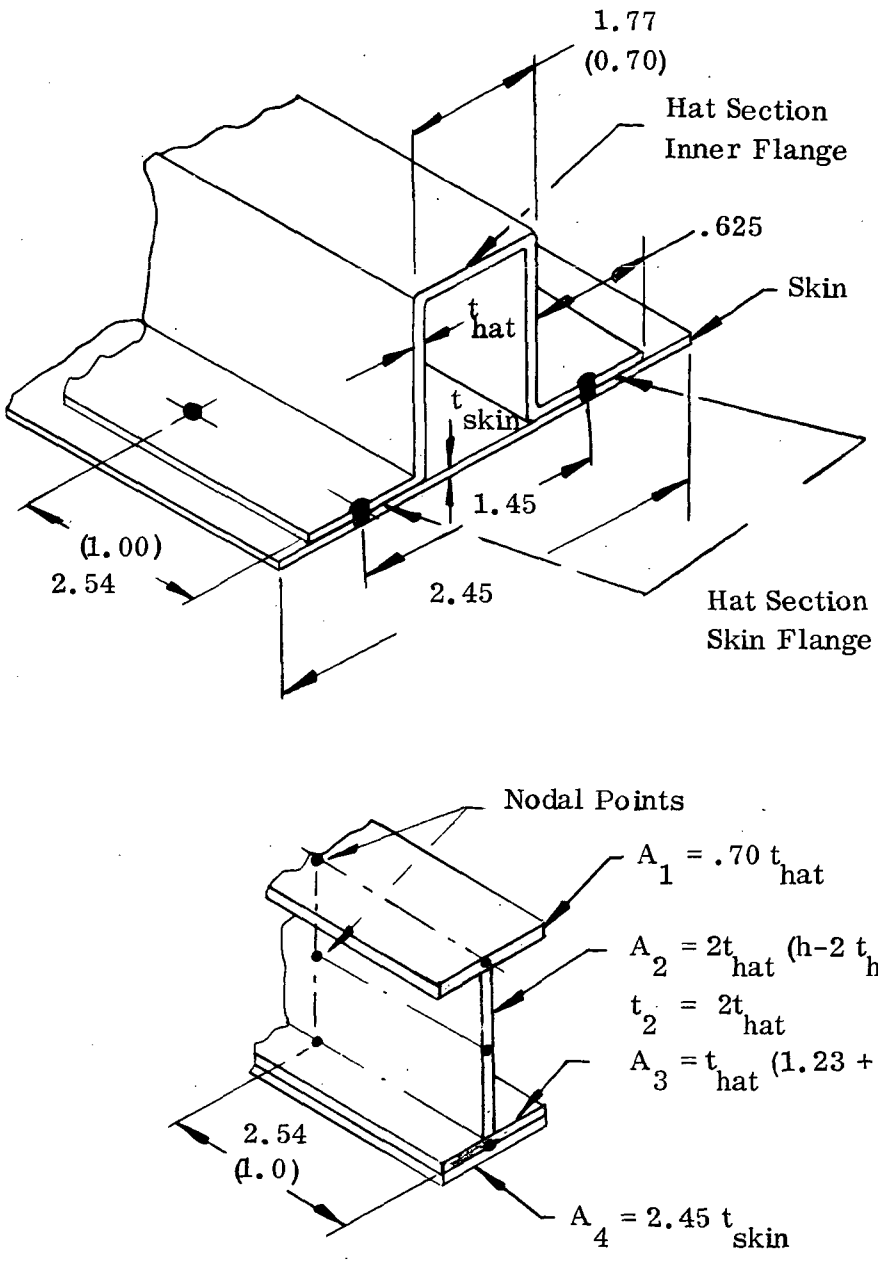

Figure 2.5. Equivalent I-Section.

1. A uniform increase from 279K to 589K (75F to 600F) for the boron/aluminum hat and titanium skin configuration,

2. A uniform increase from 279K to 449K (75F to 350F) for the GY-70/HM-S/X-904 hat and titanium skin and the boron/epoxy hat and 2219-T81 skin configurations, and

3. A uniform increase from 279K to 560K (75F to 350F) for the boron/polyimide hat and titanium skin configurations.

The thermal gradient condition that was used in the all titanium configuration was also 55.5K (100F). The skin was assumed to be 354K (175F) while the hat inner flange was assumed to be 297K (75F), since only the gradient produces thermal stresses in the one material configuration. The actual temperatures that the all titanium panel configuration will reach during a reentry flight cycle were determined subsequent to the assumed thermal gradient.

The thermal stresses that were obtained for the comparison were determined conservatively using a thermal model with pinned ends. The actual panels on the orbiter have continuous stringers except where there are cutouts or doors where the stringers stop. The continuous stringer thermal stress analysis requires that the rotation of the stringers at the frame support point be zero. This restriction was input into the thermal model for the all titanium configuration with 0.08 (0.036 inch) skin subjected to a 55.5K (100F) gradient and the boron aluminum hat with 0.08 (0.036) titanium skin subjected to a uniform temperature increase.

The most important effects of the uniform temperature change and temperature gradient analysis are the increased compression stresses on the skin. These thermal stresses add directly to the mechanical compression stresses and thus effect the compression buckling of the skin. A summary of the maximum thermal compressive stresses in the skin is shown in Table 2-3 for the five configurations and their uniform temperature changes and gradients.

Table 2-3. Maximum Compressive Thermal Stress in Skin

Configuration Material & Gage		Uniform Temperature Increase	Max. Comp. Stress in Skin MN/m^2 (psi)	Temperature Increase & 100° Gradient	Max. Comp. Stress in Skin MH/m^2 (psi)	Ref. Figure No.
Hat	Skin					
▲ Ti-6Al-4V 0.081 (.032)	Ti-6Al-4V 0.081 (.032)			297 to 352K (75 to 175F) & 55.5K (100F) Gradient	-20.6 (-3,000)	2.15
▲ Boron/Al 0.068 (.027)	Ti-6Al-4V 0.081 (.032)	297 to 589K (75 to 600F)	96.5 (-14,000 psi)	297 to 589K (75 to 175F) & 55.5K (100F) Gradient	109.6 -15,900	2.10
▲ GY-70/HMS X-904 (.0318)	Ti-6Al-4V 0.081 (.032)	297 to 449K (75 to 350F)	128.2 (-18,600 psi)	297 to 589K (75 to 600F) & 55.5K (100F) Gradient	130.2 -18,900	2.11
▲ Boron/5505 Epoxy (.035)	2219-T8/ Alum. 0.128 (.050)	297 to 449K (75 to 350F)	142.0 (-20,600 psi)	297 to 449K (75 to 350F) & 55.5K (100F) Gradient	151.6 -22,000	2.12
▲ Boron Polyimide 0.129 (.051)	Ti-6Al-4V 0.081	297 to 560K (75 to 550F)	-110 -16,000	297 to 560K (75 to 550F) & 55.5K (100F) Gradient	124.0 -18,000	2.13
▲ Ti-6Al-4V 0.08 (.032)	Ti-6Al-4V 0.091 (.036)			297 to 352K (75 to 175F) & 55.5K (100F) Gradient	20.1 -2,926	2.14
▲ Boron/Al 0.068 (.027)	Ti-6Al-4V 0.091 (.036)	297 to 589K (75 to 600F)	-94.4 (-13,700)			
* Ti-6Al-4V 0.081 (.032	Ti-6Al-4V 0.091 (.036)			297 to 352K (75 to 175F) & 55.5K (100F) Gradient	15.8 -2,300	2.16
* Boron/Al 0.060	Ti-6Al-4V 0.091	297 to 589K (75 to 600F)	87.5 -12,700			

▲ These configuration were analyzed using pin ended thermal model.

* These configuration were analyzed using the thermal model that restricted the rotation of the stringer at the support frame to zero.

Page intentionally left blank

Page intentionally left blank

3

MATERIAL ANALYSIS

3.1 SUMMARY

One of the ground rules for this program was that any composite system used must have sufficient mechanical property data available to permit a design and analysis to be performed with some reasonable level of confidence. For this reason 4 composite systems were chosen for which Convair Aerospace had fabrication experience and for which adequate data existed. These were 5.6 mil boron/6061 aluminum, boron/epoxy (Ridgidite 5505), graphite/epoxy HT-S/X-904, and graphite/epoxy GY-70/HM-S/X-904. Because of the possibility of use up to 589K (600F) boron/polyimide was also added to this list although adequate data did not exist nor was there the same level of confidence in the material. The mechanical property data used are shown in Section 2.

With a view toward potential low cost structural reinforcement, the initial work in this area was concentrated on utilizing graphite/epoxy to reinforce titanium structures. Preliminary work along these lines, under IRAD, funding had demonstrated the basic feasibility and had evolved processing parameters, adhesive systems and test procedures.

This work was then expanded to include boron/epoxy as a reinforcement system. A group of test specimens using boron/epoxy and graphite/epoxy on titanium were prepared, subjected to 200 thermal cycles from 161K (-170F) to 449K (+350F) and were structurally tested with good results. As a result of the selection of boron/aluminum reinforced titanium for the primary panel design approach, (Section 2) all further work with boron and graphite/epoxy was stopped.

3.2 PRELIMINARY TESTING

A series of tests was initiated under a Convair IRAD to investigate the problems associated in reinforcing metal structure with composite materials. Initial studies indicated that high modulus graphite combined with a titanium substructure offered a potentially economical and lightweight material having a good combination of high longitudinal modulus and good shear and transverse properties. The major problem presented by this combination is the difference in coefficient of thermal expansion. This series of tests was initiated to evaluate the problems involved in adhesive bonding the two materials and to determine optimum bonding parameters. Several adhesives were to be evaluated.

A review of the literature revealed that no existing test specimen met the requirements of this study, and it was therefore decided to experiment on a test specimen which is

composed of a strip of 6Al-4V titanium with graphite epoxy bonded to either side. It was planned that the specimen would be tested ultrasonically both before and after thermal cycling testing. Both high modulus and high strength graphites were tested.

Two specimen configurations were investigated. The longer of the two specimens has 1.14 mm (.045) thick graphite bonded to 1 mm (.040) titanium and represents a reinforcement ratio of 60%. The smaller of the two specimens was 1.14 (.045) thick graphite bonded to 5 mm (.020) titanium and represents an 80% reinforcement ratio. Three graphite surface preparation treatments were investigated. These included laying up against a peel ply, laying up against an armalon release, and vapor honing a surface laid up against teflon. The peel ply and release surfaces gave the best adhesion.

The titanium material was prepared for bonding by cleaning and etching using procedures which have produced the best results in previous development work.

Five adhesive systems were evaluated: Epon 934, Epon 951, HT 424, Narmco 2506, and FM 1000. The preliminary testing showed that Epon 951 gave the best compromise of properties and it was selected for the final group of specimens.

3.3 STRESS ANALYSIS OF THERMAL SPECIMENS

In order to study the thermally induced shear stresses in the bond line between the titanium and the GY-70/HM-S/X-904, seven different lap configurations were studied. The lap configurations were idealized and analyzed by using a computer program developed at the University of California at Berkeley called, "Analysis of Plane Stress Structures." The other six specimens studied were variations of the first which include different tapers in the GY-70/HM-S/X-904, varying bond line thickness, and tapering the bond line at the end of the specimens. The bond line shear stresses versus distance along the specimens were plotted for a temperature change from 449K to 199K (350F to -100F).

This study was conducted for a total delta temperature of 505K (450F) but the results can be extrapolated to cover the range from 449K to 161K (350F to -170F) by multiplying these bond shear stresses by 520/450 or 1.155.

Figure 3.1 illustrates a reinforced bar with straight cutoff end. The peak adhesive shear stress here is 43.4 MN/m^2 (6300 psi), a figure considered much too high for adhesives. Figures 3.2 and 3.3 show successive attempts to reduce the shear stress, the tapered adhesive thickness in Figure 3.4 being the most effective means to reduce the shear stress peaking. The configuration shown in Figure 3.3 was chosen for the test specimen as it was felt the double taper was uneconomical to produce.

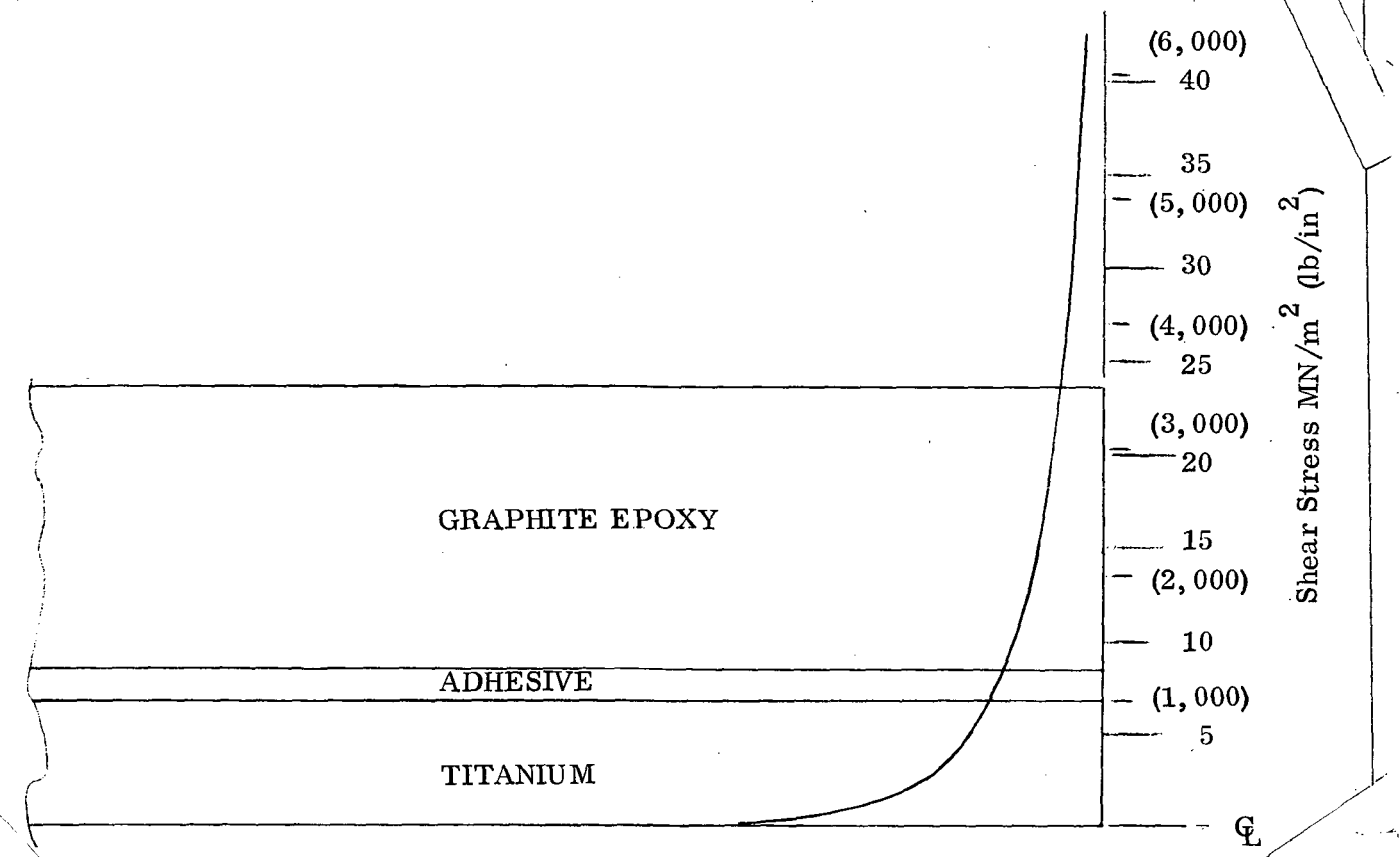

Figure 3.1. Peaking of Bond Line Shear Stress at End of Reinforcement.

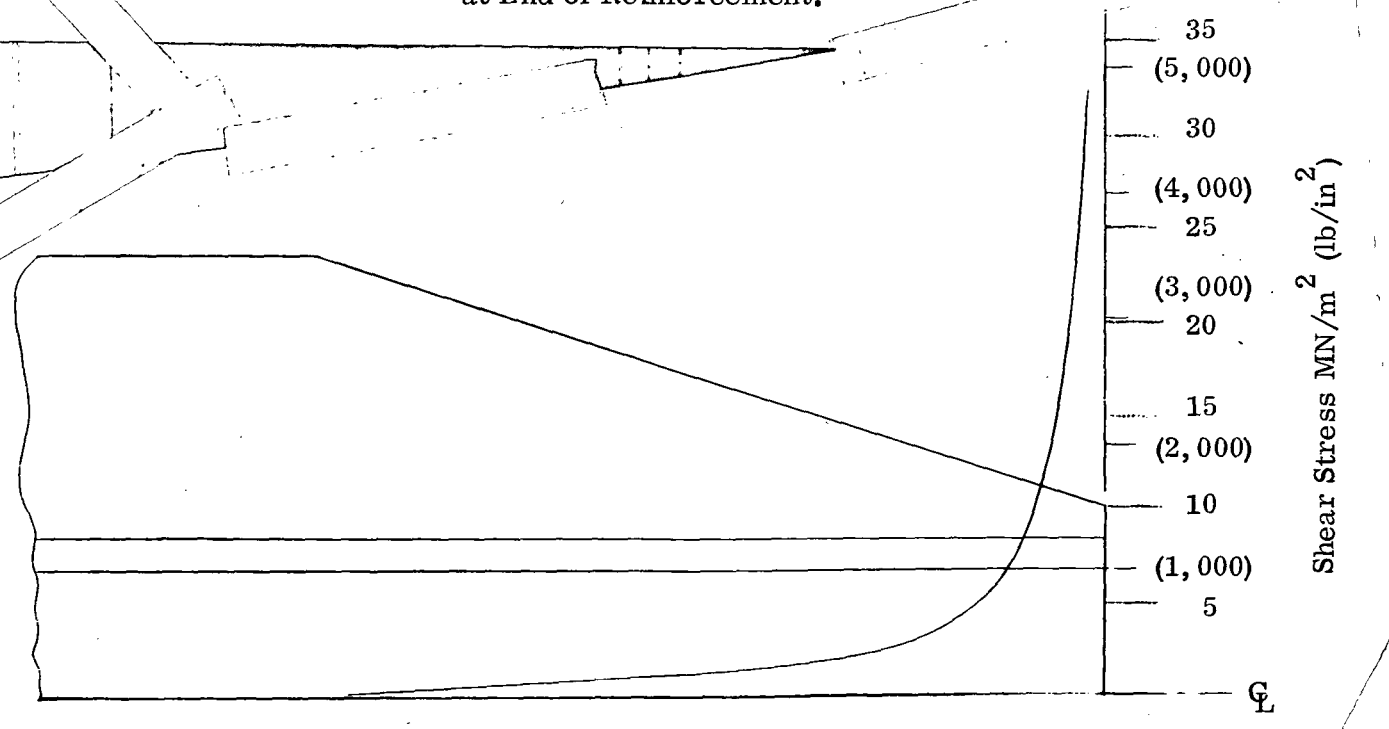

Figure 3.2. Peaking of Adhesive Shear Strength at End of Reinforcement.

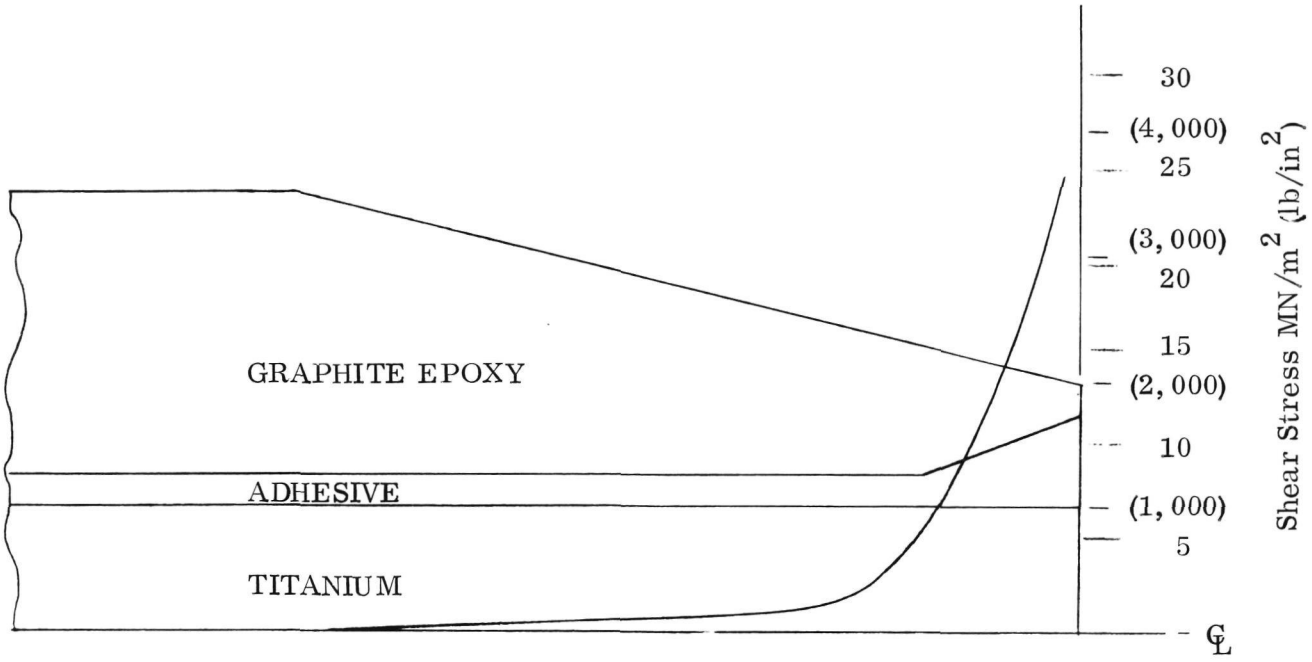

Figure 3.3. Peaking of Bond Line Shear Stress at End of Reinforcement.

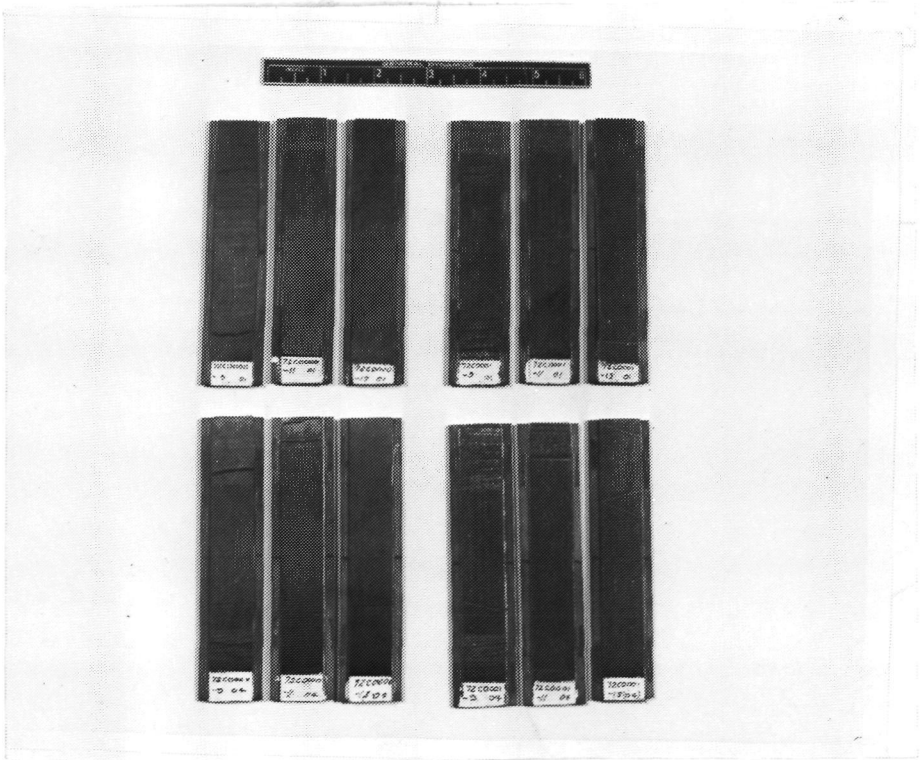

Figure 3.4. Thermal Cycling Specimens.

3.4 THERMAL CYCLING SPECIMENS

The two sets of thermal cycling specimens, P/N 72C0000 and 72C0001 (Figure 3.4), consisting of graphite epoxy and boron epoxy reinforced titanium bars were tested.

A total of 24 specimens were prepared, 12 boron and 12 graphite reinforced. The specimens were bonded using Epon 951 film adhesive and using the procedures previously developed. The surface preparation for the titanium included Pasajel treatment and thorough rinsing. The surface preparation for the graphite consisted of solvent wiping the surface of the material which had been laid up against a teflon release sheet. The completed specimens were divided into four groups identified by Serial Numbers 01-04. Two groups, 01 and 02, were subjected to the thermal cycling while the remaining groups, 03 and 04 , were stored.

The thermal cycling was performed in a special test setup. The specimens were placed in a slotted aluminum block which was surrounded by an electrical strip heater. This assembly was wrapped with foam insulation and placed into a Cres steel container and the container sealed.

The container was fitted with a tube through which the heater power leads and thermocouple wires were fed. The tubing also served as a pressure equalization vent. The vent was purged with dry helium to prevent the ingestion of air and the condensation of water inside the can. The can was placed in a cryostat into which was introduced a quantity of liquid nitrogen, the level of liquid nitrogen being maintained by a capacitance controlled level sensing system supplied from two 100-liter dewars.

The thermal cycle was controlled by means of a stripchart recorder and timer, the heating cycle being terminated when the temperature reached 449K + 5.6K (350F +10F). The cooling then took place for a period of approximately 83 minutes, by which time the temperature reached 161K (-170F). Figure 3.5 illustrates a typical stripchart record of one thermal cycle (in this case the last or 200th cycle). The gradual cooling allowed a timer to be used to control the minimum temperature, and the apparatus was operated continuously.

The 12 specimens were subjected to 200 thermal cycles using this apparatus. During one cycle accidental operation of an over temperature cutoff permitted the temperature of the parts to reach 89K (-300F), inadvertently exposing the parts to a 25% higher thermal stress loading than planned.

Upon completion of the thermal cycling, the specimens were subjected to a thorough visual inspection and were C-scanned. There was no apparent damage to any of the 12 specimens. Of particular importance was the complete absence of longitudinal splits in the GY-70 reinforced specimens. Some longitudinal cracks were found in early development specimens.

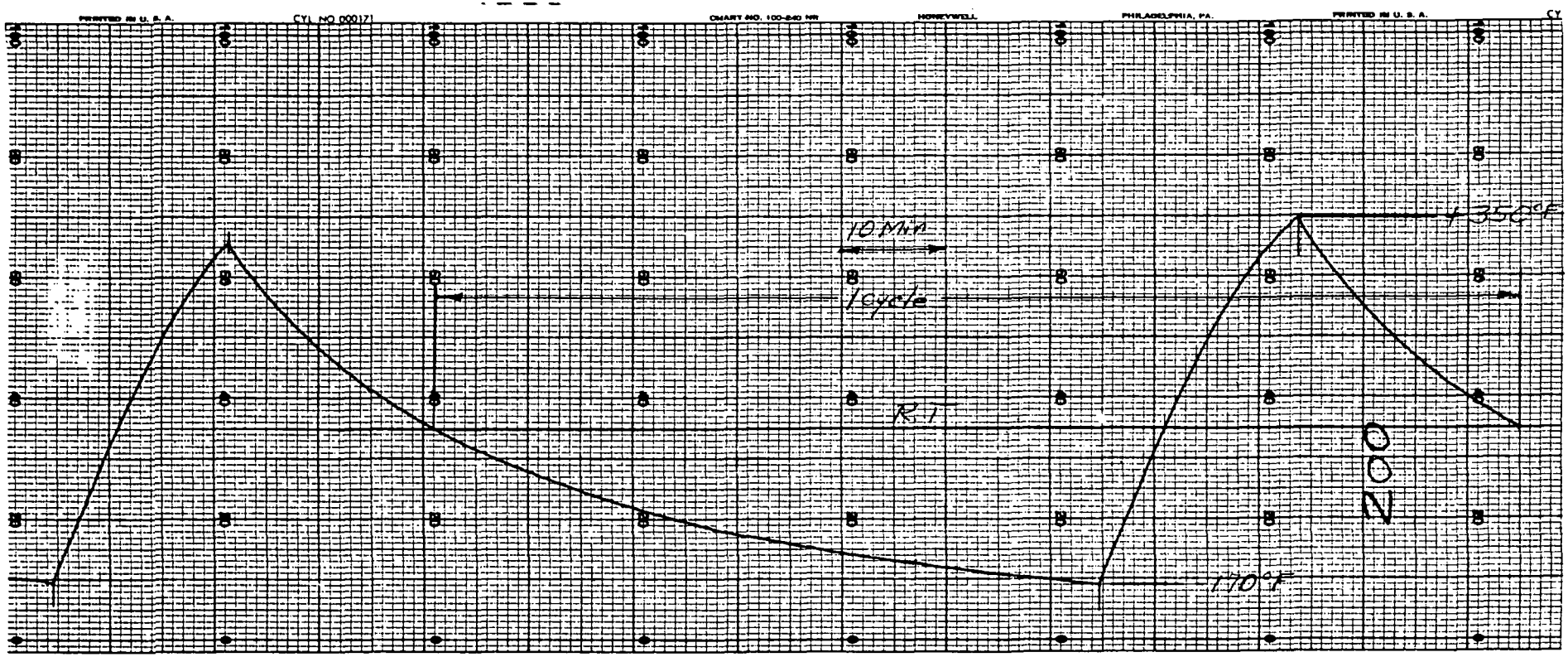

Figure 3.5. Thermal Cycle Record.

After inspection, the entire group of 24 specimens, including those stored, were subjected to a short beam shear test. This test is performed using a 3.8 cm (1.5 inch) beam length in a standard test machine. The testing induces a shear failure of the reinforced bar. The failure can occur in the adhesive or as an interlaminar shear failure in the composite. The VQ/I shear stress calculated from the failure load is a measure of the shear strength of the joint. These calculated strengths are not directly comparable with shear strengths obtained from lap shear specimens, primarily because of the shear stress peaking which occurs in the lap shear specimen.

3.5 SUMMARY

Table 3-1 summarizes the test results from the 24 specimens. Some interesting conclusions may be drawn from the data. First, the higher strength of the boron specimens is due to the higher interlaminar shear strength of that material, the ratio of the two failing loads being similar to the ratio of the shear strengths for the two materials. A somewhat startling result of these tests was the apparent increase in strength of the specimens subjected to thermal cycling. This phenomena is attributed to the viscoelastic behavior of the adhesive under the repeated cycling which in effect reduced the thermal stresses in the part at room temperature. The apparent increase in strength amounted to approximately 12% for the graphite reinforced specimens and 4% for the boron reinforced specimens.

The larger increase for the graphite specimens lends more support for the theory that adhesive creep is the cause. The calculated residual thermal stresses in the graphite reinforced specimens are almost twice as high as the boron reinforced specimens.

The specimens tested included three variations in the ends of the composite. Those with no taper in the end of the composite have theoretically twice the peak shear stress of the tapered specimens. The fact that all specimens satisfactorily passed the thermal cycling without failure indicates that the peak stress was not excessive in any of the specimens. Further, the failure loads in Table 3-1 show very little difference between end configurations.

From this and previous testing, it has been concluded that the detail of the end of reinforcement is not as critical from the thermal stress standpoint as is the choice of adhesive and preparation technology.

Table 3-1. Short Beam Shear Test Results;
Composite Reinforced Bars

72C0000		GY-70/HM-S/X-904 Failure Load	
Dash No.	Serial No.	KN	(lb.)
-9	01	3.36	(755)
	02	3.49	(785)
	03	3.06	(690)
	04	2.93	(660)
-11	01	3.27	(735)
	02	3.43	(770)
	03	2.78	(625)
	04	2.60	(585)
-13	01	3.20	(720)
	02	3.36	(755)
	03	3.18	(715)
	04	2.89	(650)
72C0001		5505 Boron Epoxy	
Dash No.	Serial No.		
-9	01	5.47	(1230)
	02	5.03	(1130)
	03	5.05	(1135)
	04	4.94	(1110)
-11	01	5.34	(1200)
	02	5.18	(1165)
	03	5.00	(1125)
	04	5.03	(1130)
-13	01	5.25	(1180)
	02	5.14	(1155)
	03	5.36	(1205)
	04	4.96	(1115)

4

ORBITER PANEL DESIGN

4.1 INTRODUCTION

The purpose of this portion of the program was to perform a predesign on an all metal orbiter fuselage panel area and a composite reinforced area. Both predesign studies were to be used upon the same design criteria as defined in Section 1.

The basic structural arrangement was obtained from Rockwell International and their design had not been developed past a very preliminary stage at the time of this study.

4.1.1 STRUCTURES DESIGN GROUND RULES.

1. Frame spacing set by Rockwell International (RI) design 63.5 cm (25 inches).

2. Column length is equal to frame spacing. Pin joint support.

3. Design loading and environment established based upon RI design criteria.

4. Design limit to ultimate factor is 1.40.

5. Buckling of panel elements is permitted between limit load and ultimate load where buckling distortion is not harmful. Where insulation systems or reinforcement are bonded to structural elements, such elements may not be allowed to buckle below ultimate load.

6. Maximum strain load in skin limited by REI material is 0.006 m/m.

7. Deflection of skin panels for aerodynamic reasons shall not exceed 0.4 cm (0.15 inch) in 45.7 cm (18 inch).

4.2 ALL METAL PANEL DESIGN

The space shuttle orbiter center fuselage configuration is shown in Figure 4.1. The area selected for this study lies in the center of the fuselage lower surface between Stations 1799 and 1899. The structure in the area consisted of heavy titanium frame members spanning the cargo bay between longerons. A hat section stiffened titanium skin was attached to the frame and support of the reuseable external insulation (REI). An internal insulation blanket was used to further reduce heat input into the fuselage area. Figure 4.2 shows a typical lower surface frame section with the skin and external insulation.

Page intentionally left blank

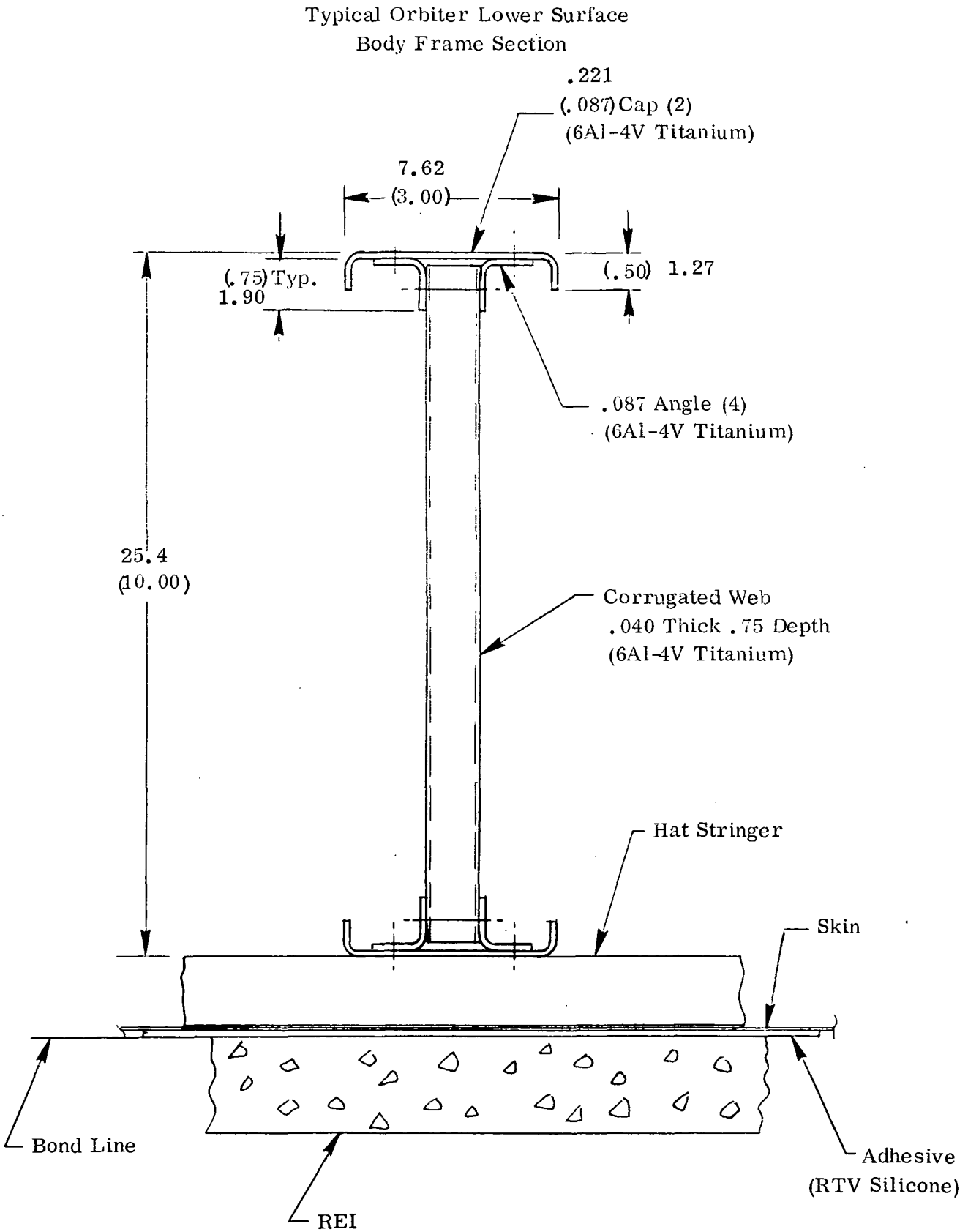

Figure 4.2. Typical Orbiter Lower Surface Body Frame Section.

The frames of the orbiter had a large moment of inertia requirement, therefore the cap members were thick, being in the area of 1.3 cm (.500 inch). Two basic design solutions were studied in order to solve the problem of attaching these heavy frames to the skin panels. Method one (Figure 4.3) consisted of attaching the frames directly to the hat sections at the cap. Method two (Figure 4.4) uses a shear clip which attaches to tabbed hat flanges and skin with mechanical fasteners. Method two eliminates the use of blind fasteners and allows the frames to take a more optimum shape.

It was decided and agreed to by RI engineers that both methods would be used in the actual design.

A potential problem with differential expansion of the skin and frames was investigated. Because of the heavy mass of the frames, the frame temperature will lag the skin temperature thus presenting the possibility of buckling the skin transversely due to induced compression. It was determined however, that the thermal gradients were not sufficient to cause buckling.

The metal panel was designed using the titanium stringer configuration obtained from the parametric study. For a typical panel section this produces a panel weight of 10.5 Kg/m^2 (2.15 lb/ft^2).

The final all metal design is shown in Figure 4.5.

4.3 COMPOSITE REINFORCED PANEL DESIGN

4.3.1 INTRODUCTION. This design is based upon the results of the parametric study. The panel design consists primarily of substitutions of boron/aluminum for the titanium stringers. The use of this material simplifies the design task as many of the conventional techniques used for titanium may also be used for boron/aluminum.

4.3.2 HAT SECTION FABRICATION METHODS. In order to proceed with the panel design, it became necessary to investigate the various methods of producing boron/aluminum hat sections as the method can affect the strength and final shape of the section.

The various manufacturing methods have been reviewed and a decision made as to the most promising method.

There are basically seven methods presently available to produce boron/aluminum hat section stiffeners. These are:

1. Continuous Case Sections

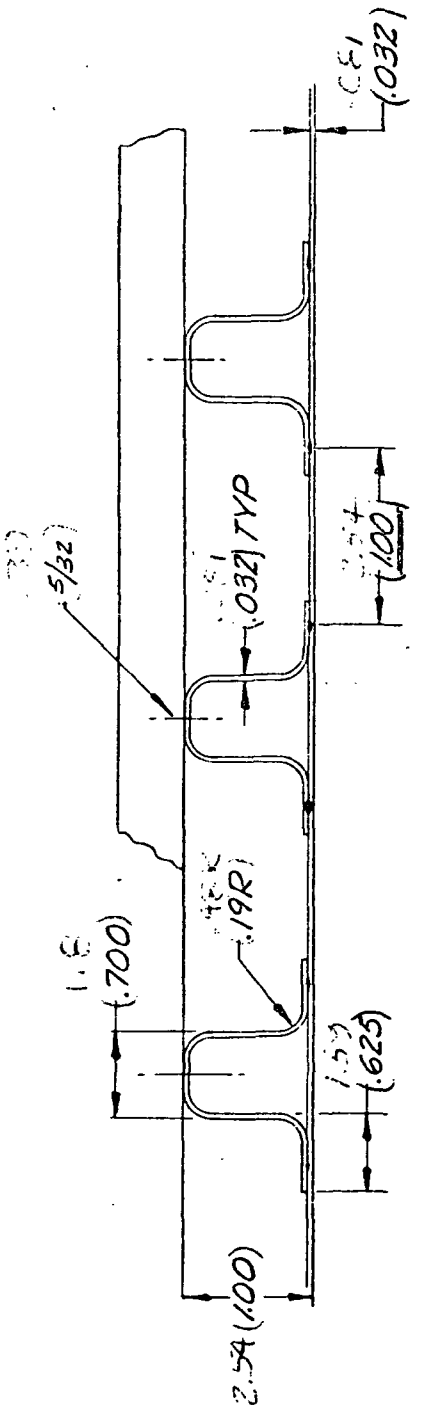

Figure 4.3. Typical all metal fuselage panel cross section.

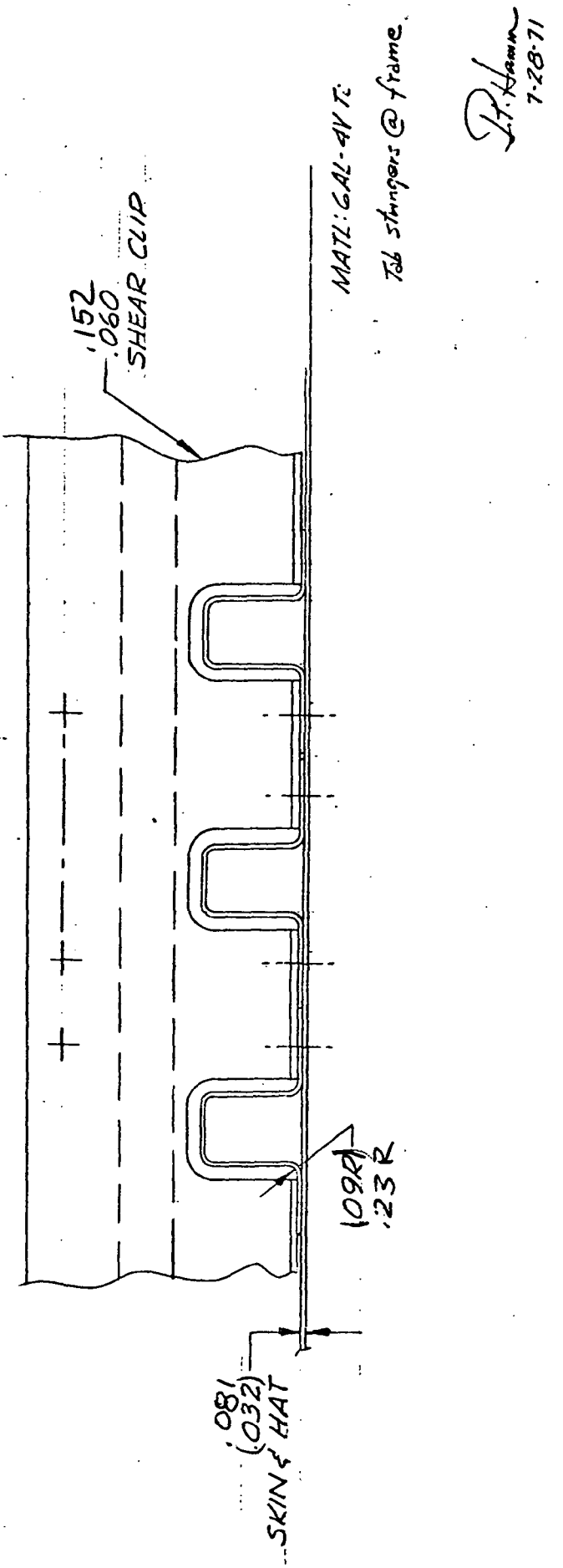

Figure 4.4. All metal fuselage panel cross section showing shear clips.

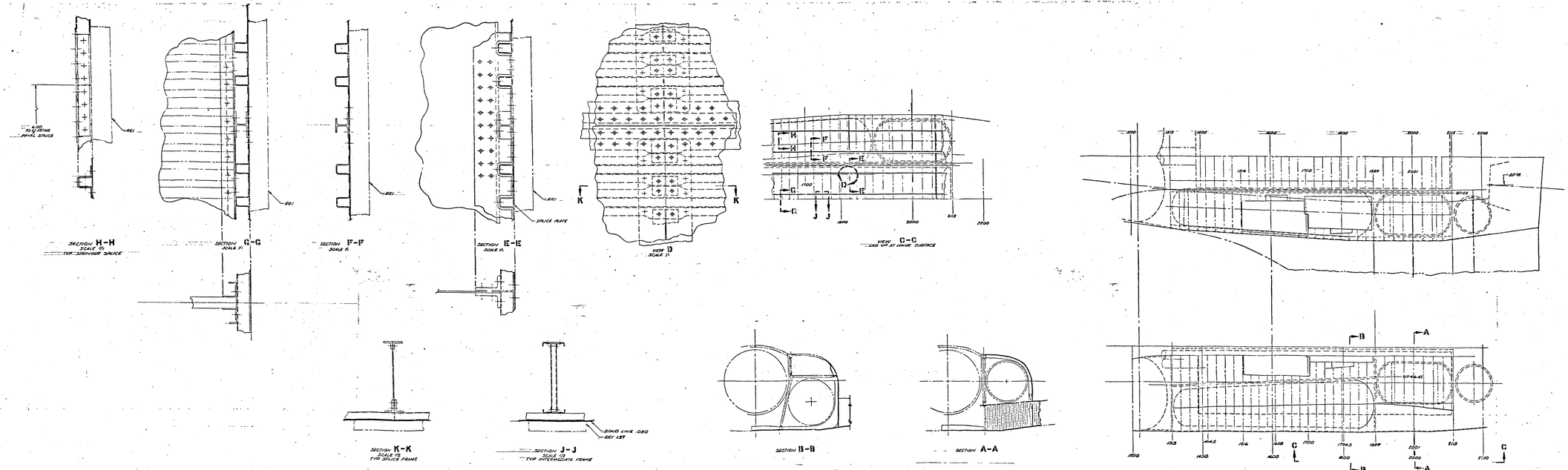

Figure 4.5

PRELIMINARY DESIGN DRAWING
METAL CRUISER FUSELAGE PANEL
CONVAIR DIVISION OF GENERAL DYNAMICS CORP. SAN DIEGO, CALIFORNIA

Page Intentionally Left Blank

2. Tape Material Diffusion Bonded

3. Tape Material Braze Bonded

4. Selectively Placed Filament (SPF) Sheet Hot Formed

5. Unidirectional Sheet Hot Formed to Shape

6. Sheet Material Elements Assembled by Brazing (Con Braz)

7. Conclad Forming

4.3.2.1 Continuous Cast Sections. The continuous casting method offers a potentially low cost method of producing very long continuous lengths of boron/aluminum structural shapes.

The sections produced by this method are generally much higher in filament volume (60%) than other forms of the material and hence tends to display lower matrix dependent properties. This method deserves consideration for future studies but was not considered sufficiently developed for this program. Much development work and a considerable amount of material characterization would be required.

4.3.2.2 Tape Material Diffusion Bonded. This process has been developed to a high degree at Convair Aerospace and a large amount of high quality structural shapes including hat sections have been fabricated. The process requires special tooling and the use of a high pressure (3,000-10,000 psi) autoclave and the price of the finished parts are high. The length of the parts is limited to the length of the autoclave which at Convair at this time was about 1 meter. The process did not lend itself to economical scaleup for space shuttle application.

4.3.2.3 Tape Material Braze Bonded. Several variations to this process are available. These include the low pressure consolidation of braze foil tape material and the eutectic bonding of monolayer sheets. Both processes produce good quality sections. Specialized tooling is required and the finished part cost is high.

Coated boron fibers are usually required to prevent degradation at the processing temperatures and the mechanical properties tend to be somewhat lower than diffusion bonded parts.

4.3.2.4 Selectively Placed Filament (SPF) Sheet Hot Formed. This type of construction utilizes boron filaments placed so that the areas of forming are pure aluminum. The cost of this type of material is high because of the fiber placement

and inspection. The strength is lower in the corners because of the lack of fibers and separation tends to occur where the filaments meet the aluminum. The buckling strength is also lower in the corners of the hat.

4.3.2.5 Unidirectional Sheet Hot Formed to Shape. This method of manufacture ensures good overall strength because the boron filaments are equally distributed around the hat section. The process is low in cost because the parts are formed from unidirectional sheet which is the lowest priced form of material. The minimum radius for this type of forming is R/t = 3. Sufficient development had been done to give confidence in the ability to form long sections. It was believed that this process offers the best choice for forming hat sections.

4.3.2.6 Sheet Elements Assembled by Brazing (Con Braz). This is an inexpensive process provided the temperature is held under 533K (500F) compatible with the braze alloys. In this application the structural temperature was too high (approximately 599K (600F) for use of this process. The number of joints necessary to make a hat tend to reduce the efficiency of the process and it lends itself more to fabrication of Tee and I-sections.

4.3.2.7 Con Clad Forming. This process permits the cold forming of boron/aluminum by the addition of steel cladding of the surface. It was not developed in time for use on this program, but has consequently been utilized to form long - heavy gage boron/aluminum parts.

4.3.3 JOINING. Several methods of joining the boron/aluminum hat sections to the titanium sheet were considered. Those methods available included:

1. Adhesive Bonding

2. Brazing

3. Diffusion Bonding

4. Spot Brazing

5. Spot Diffusion Bonding

Each of the methods was was investigated and a decision was made to use the Spot Diffusion Bonding.

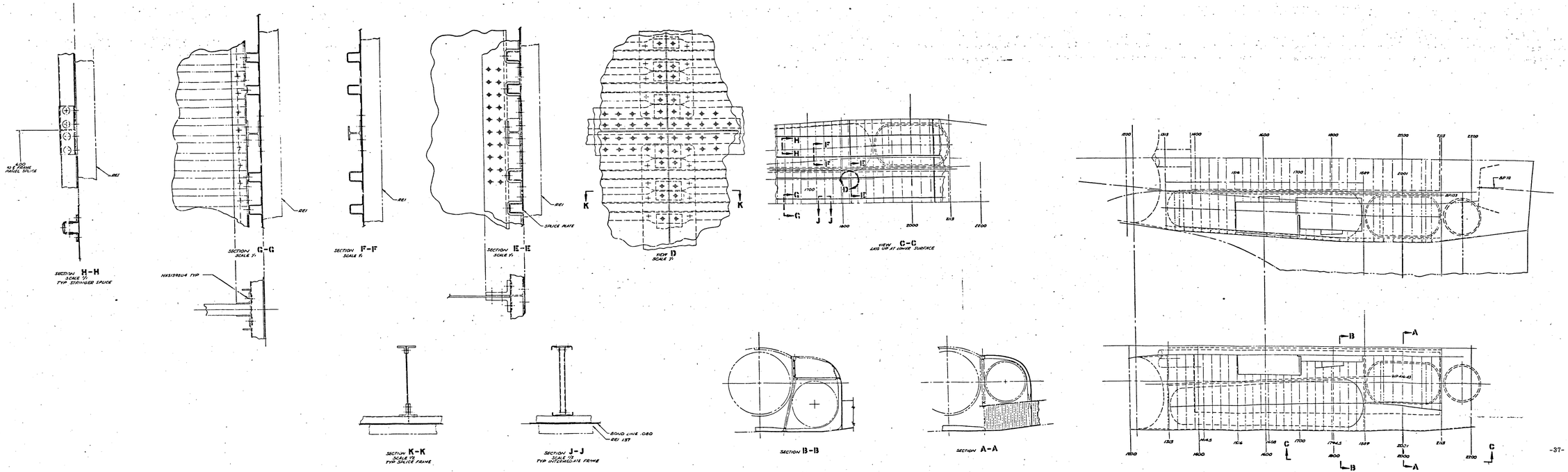
SECTION H-H
SCALE 1/1
TYP STRINGER SPLICE
SECTION G-G
SCALE 1/1
SECTION F-F
SCALE 1/1
SECTION E-E
SCALE 1/1
VIEW D
SCALE 1/1
VIEW C-C
LKG UP AT INNER SURFACE
SECTION K-K
SCALE 1/2
TYP SPLICE FRAME
SECTION J-J
SCALE 1/2
TYP INTERMEDIATE FRAME
SECTION B-B
SECTION A-A
COMPOSITE REINFORCED ORBITER
FUSELAGE PANEL

Figure 4.6.

Page Intentionally Left Blank

Adhesive bonding was considered and good results were obtained on a sample crippling specimen (Section 7) but loss of strength due to oxidation is also a problem.

Brazing was not considered feasible due to the lack of a good braze alloy for use at 600F.

Diffusion bonding could be utilized but was not considered practical for scale up to full size shuttle panels.

Spot brazing was evaluated (Section 7) and discarded as being poor quality above 533K (500F). A full description of the qualification testing of spot brazing is found in Section 7.

4.3.4 PANEL DESIGN. The panel configuration was based upon the results of the parametric study. The hat section size, shape and spacing is identical to that found to give the lightest weight.

Much effort was given to the aplices between sections of panel. During the panel design it was assumed that spot brazing could be used to make joints between the titanium and boron/aluminum, hence, the drawings show this method. It was found subsequently that spot diffusion bonding gave better results so all joints would be made using this process. Figure 4.6 shows the composite reinforced panel design.

Page intentionally left blank

5

THERMAL AND STRESS ANALYSIS

5.1 THERMAL ANALYSIS

5.1.1 INTRODUCTION. The thermal analysis work accomplished on this program was conducted in several phases. The initial work was accomplished on simplified models in order to obtain approximate temperatures for initial insulation trade studies. Later more detailed analyses were made to determine both maximum structural temperatures and also thermal gradients within the structure.

5.1.2 INITIAL STUDIES. Thermodynamic analysis of the TPS components were undertaken to determine the required reusable external insulation and the internal insulation thickness, with the maximum allowable temperature at the bond line as a constraint.

Structural temperature distributions were evaluated through the lumped parameter method of finite differences. The structure was divided into 33 nodes. Aerodynamic heating rates on the outer surface were obtained from Rockwell International as shown in Figure 1.2. The initial temperature of the nodes were assumed to be 3.11K (560R). This assumption was also used by RI in their thermal analysis of the orbiter. Figure 5.1 shows the temperature history on the bond line for different reusable external insulation thickness varied from 3.37 to 5.08 cm (1.37 to 2.00 inches). Changes of the internal insulation (TG 15000) thickness had a negligible effect on the bond line temperature.

Additional thermodynamic analyses were undertaken to study the effects of the panel structure thickness on the bond line temperature. The thickness of the external insulation was fixed at 5 cm (2.0 inch). The results are shown in Figure 5.2. The bond line temperature decreases with increasing the structure thickness. This decreasing of bond line temperature is due to more heat transferred to the inside insulation.

The structure temperature distributions were evaluated using Convair thermal analyzed Computer Program No. P4560. This program is a versatile heat conduction program which accommodates a broad variety of thermal analytical requirements. It accommodates simple or complex, transient, or steady state heat transfer problems. The program includes provisions to simulate natural convection, force convection, and radiative heat exchange. It is programmed for the CDC 6400 computer and has storage capacity for large problems approaching 2,000 nodes and 4,000 resistors. This program was developed for detailed analyses of internal heat transfer considering

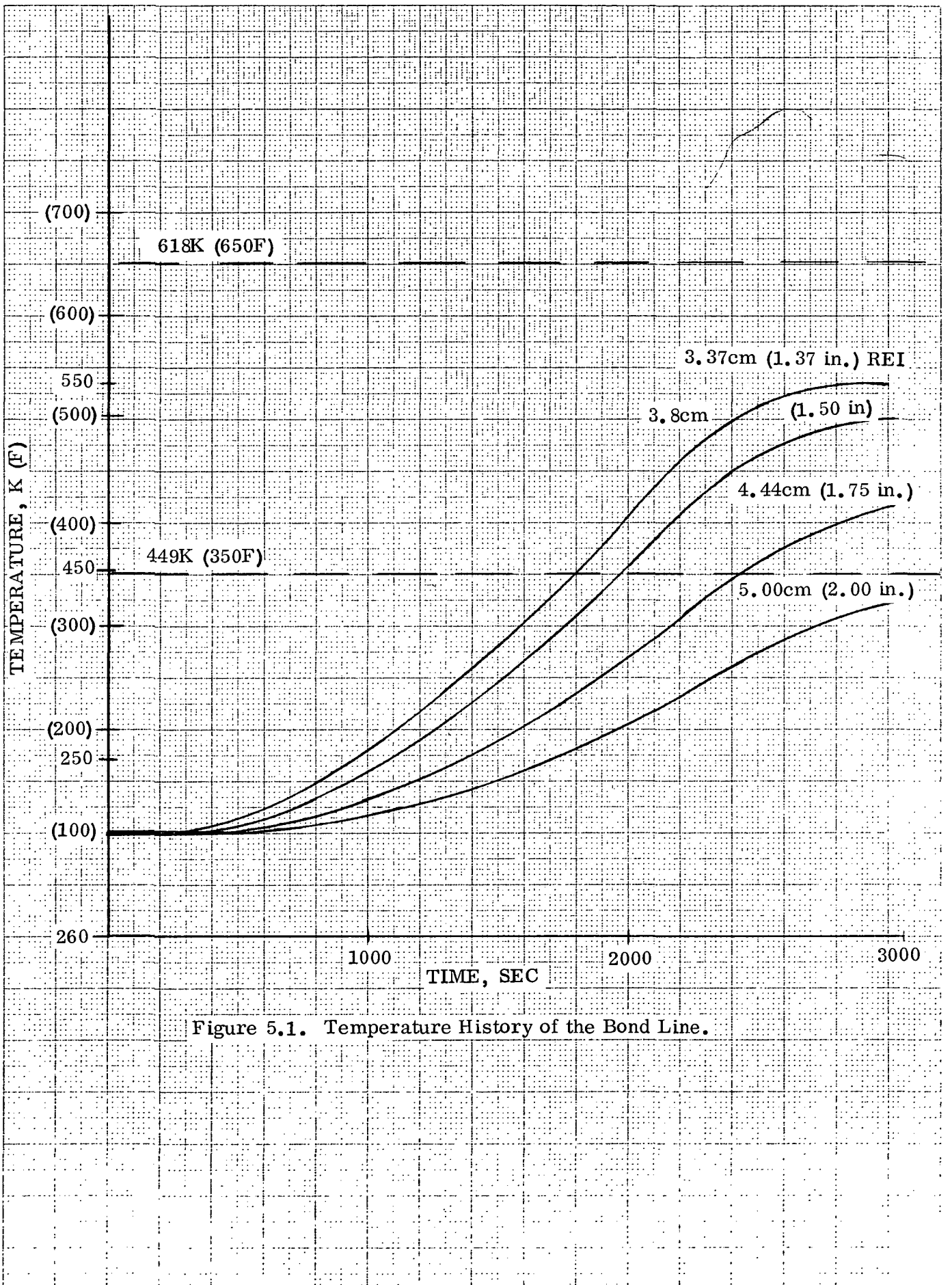

Figure 5.1. Temperature History of the Bond Line.

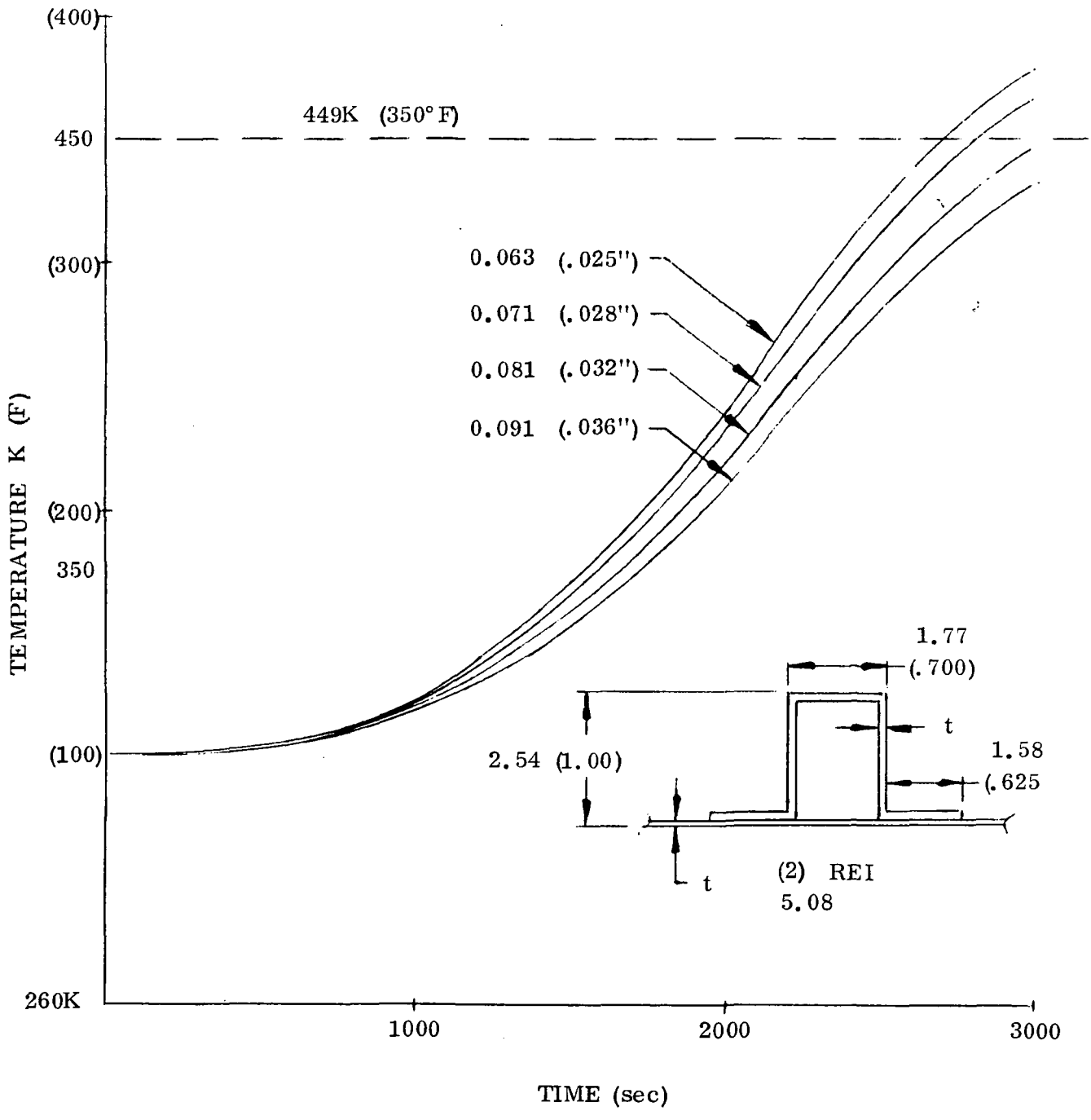

Figure 5.2. Bondline temperature for various structural thicknesses.

conduction, convection and radiation. The transient heat conduction problem is solved by using the Crank-Nickolson forward-backward differencing scheme. In this program, a special kind of node (no mass node) can be used to simulate the temperature at the juncture of dissimilar conductive materials and surface temperatures. Figure 5.3 shows the three dimensional model used for thermal analysis. The structure was divided into 103 nodes which includes 9 no-mass nodes for bondline temperature.

Structure temperatures were calculated for three sets of conditions:

1) 3.37 cm (1.37 in) REI, initial temperature of 161K (290R),

2) 3.37 cm (1.37 in) REI, initial temperature of 311K (560R), and

3) 5.06 cm (2.02 in) REI, initial temperature of 311K (560R).

Condition (1) gives worst temperature gradient in the structure while Condition (2) gives highest bondline temperature. Results of temperature response in bondline and hat stringer are shown in Figures 5.4 though 5.7.

5.1.3 THERMAL ANALYSIS OF TEST PANELS. The final thermal work accomplished was the analysis of a boron/aluminum stiffened titanium panel. This configuration represents the two test panels. The structural temperatures were calculated for two conditions:

1) 3.37 cm (1.37 in) REI thickness initial temperature 161K (290R) (maximum gradient), and

2) 3.37 cm (1.37 in) thickness initial temperature 311K (560R) (maximum temperature).

The REI thickness of 3.37 cm (1.37 in) was derived from Rockwell International's (RI) basic orbiter design. The 161K (290R) initial temperature is the minimum in orbit temperature permitted. The 311K (560R) temperature is the maximum structural temperature which is expected under any condition prior to reentry. Table 5-1 summarizes the thermal properties of the materials used in these analyses.

The method and model used were identical to the previous analyses. Figure 5.8 shows the structural temperature predicted for the 161K (290F) initial temperature case. The thermal gradient predicted by this analysis is considerably less than that for the titanium stringer case.

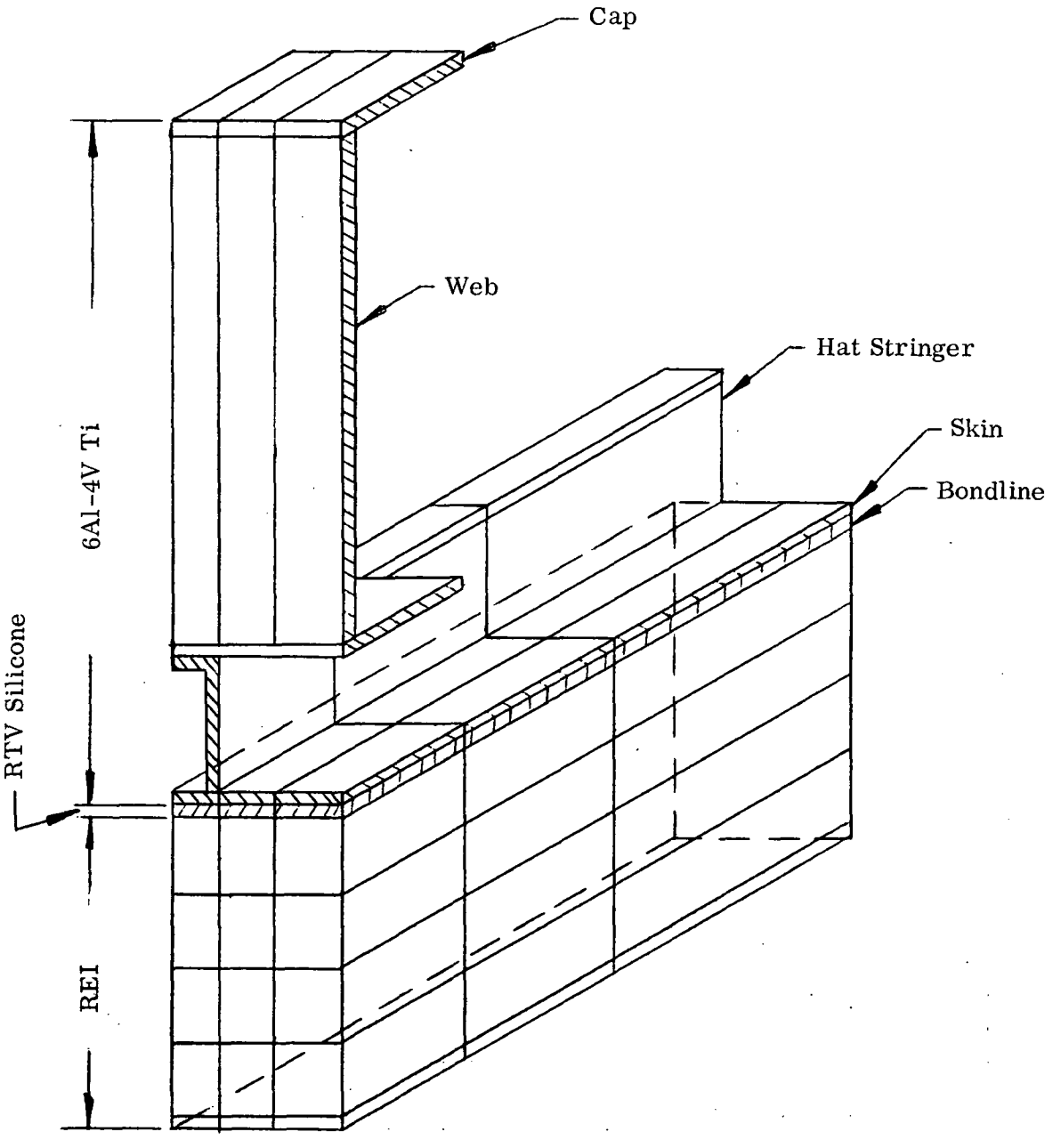

Figure 5.3. Three-Dimensional Structural Segmentation.

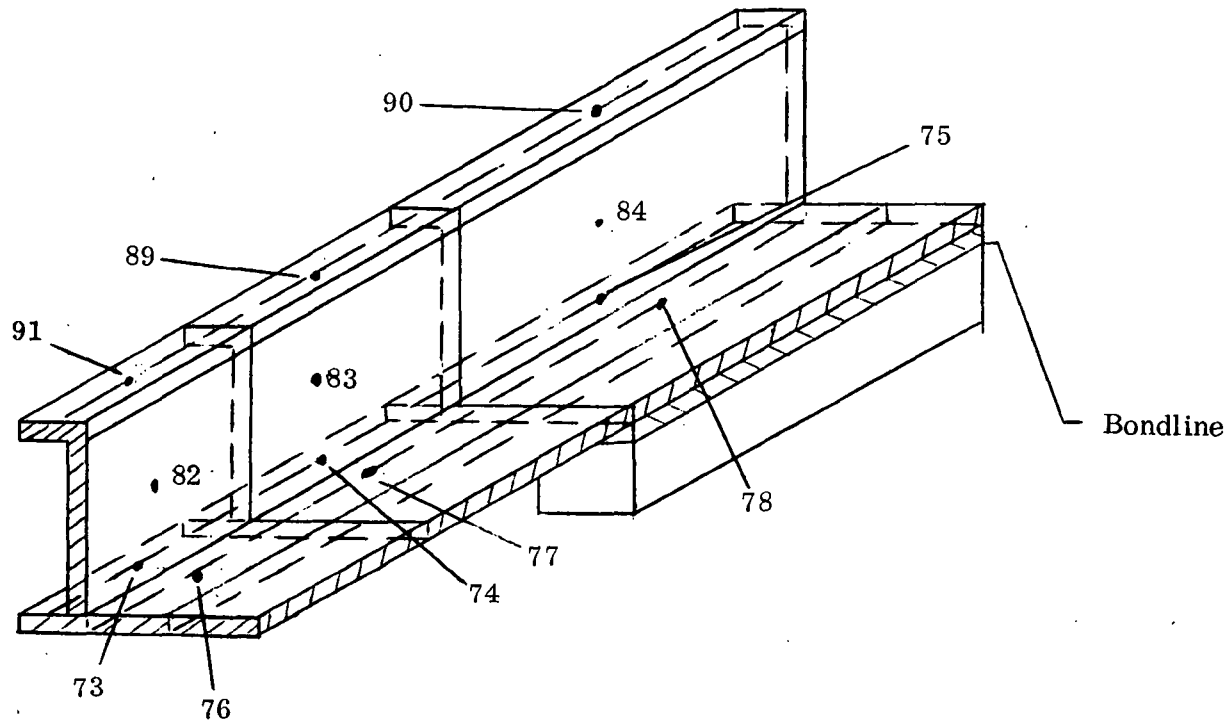

Figure 5.4. Bondline and Hat Stringer.

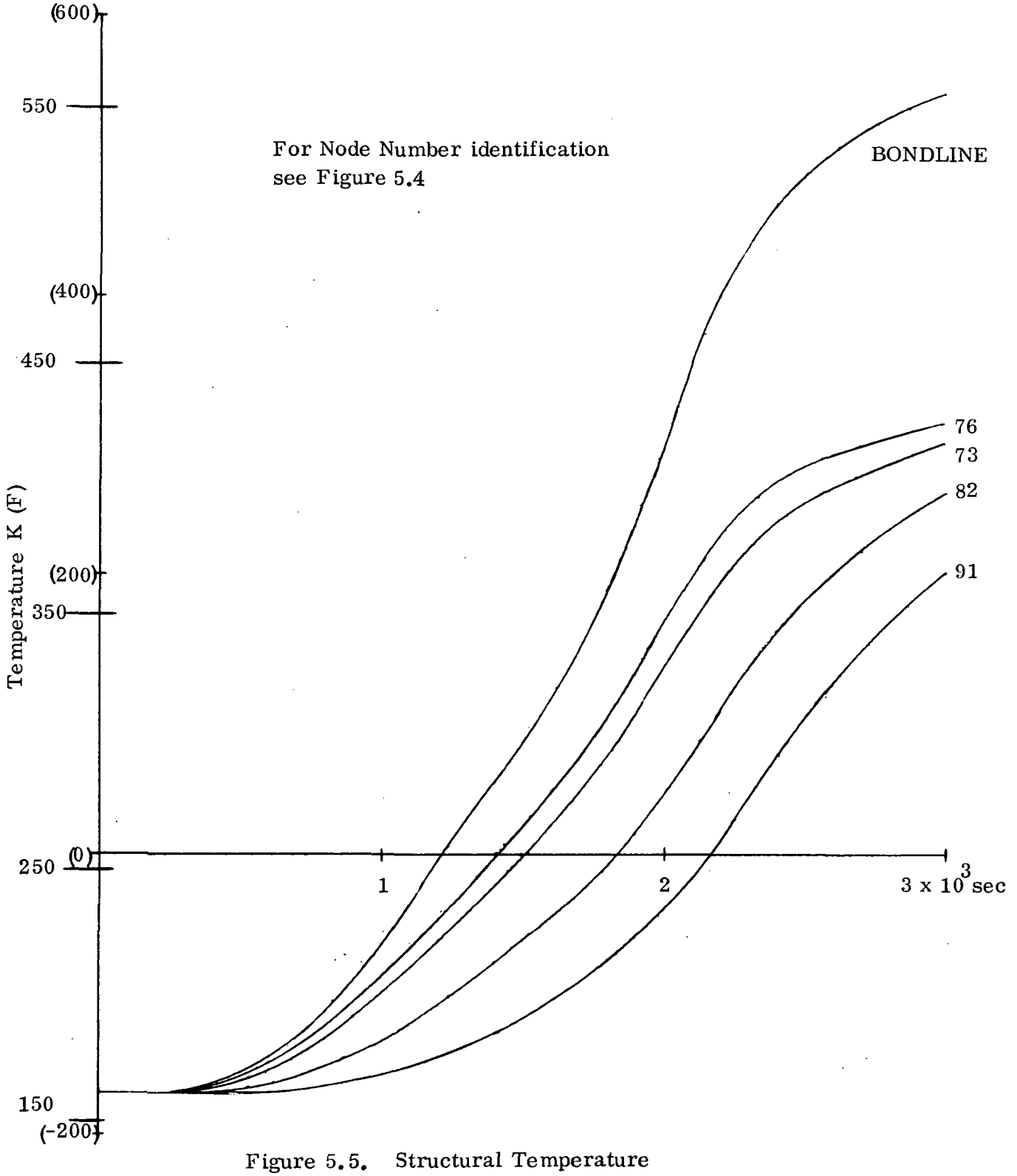

Figure 5.5. Structural Temperature
All Titanium
REI thickness (1.37) 3.37cm
Initial Temp -(170° F) 161K

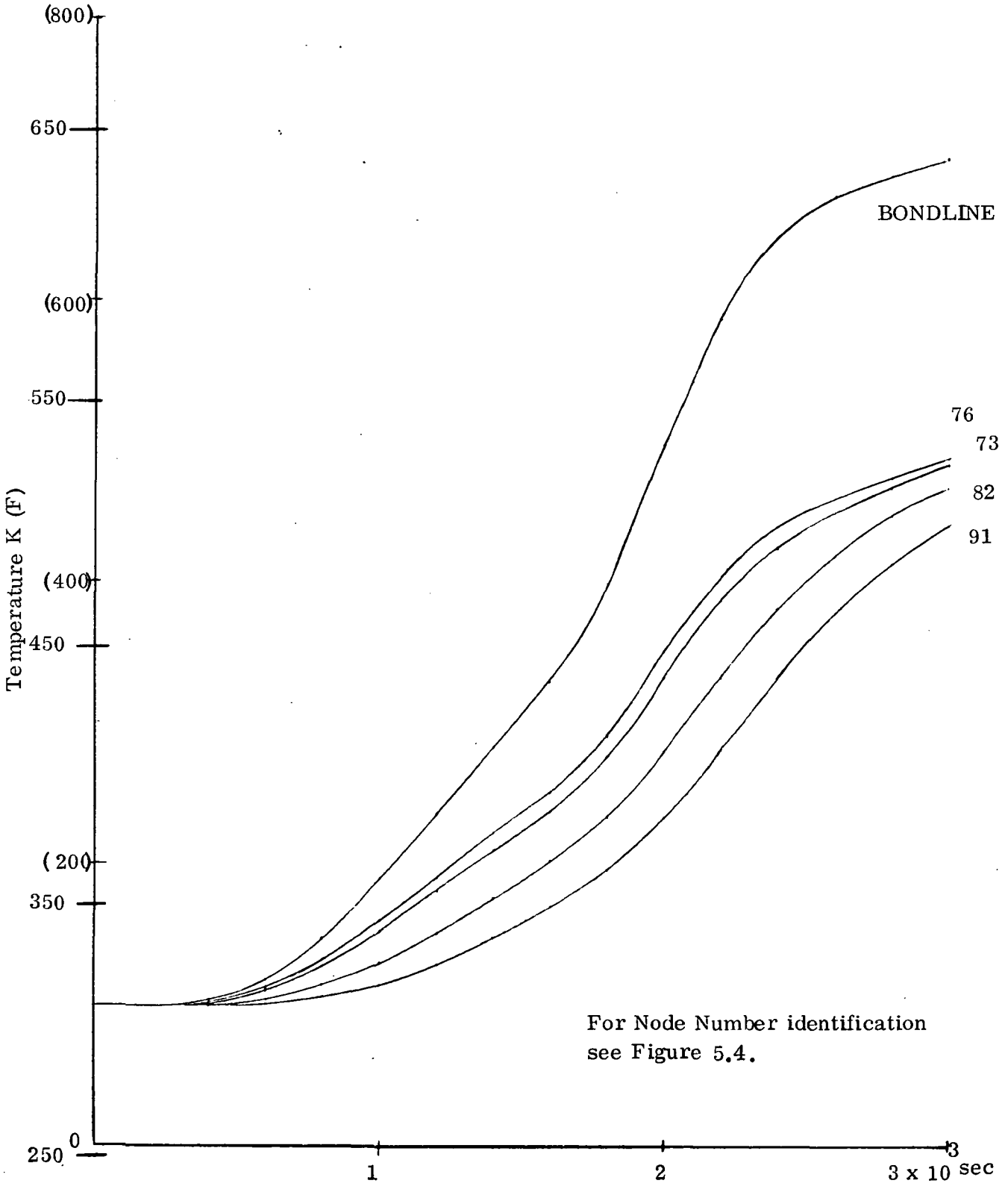

Figure 5.6. Structural Temperature
All Titanium
REI thickness (1.37 in.) 3.37cm
Initial Temp (100° F) 311K

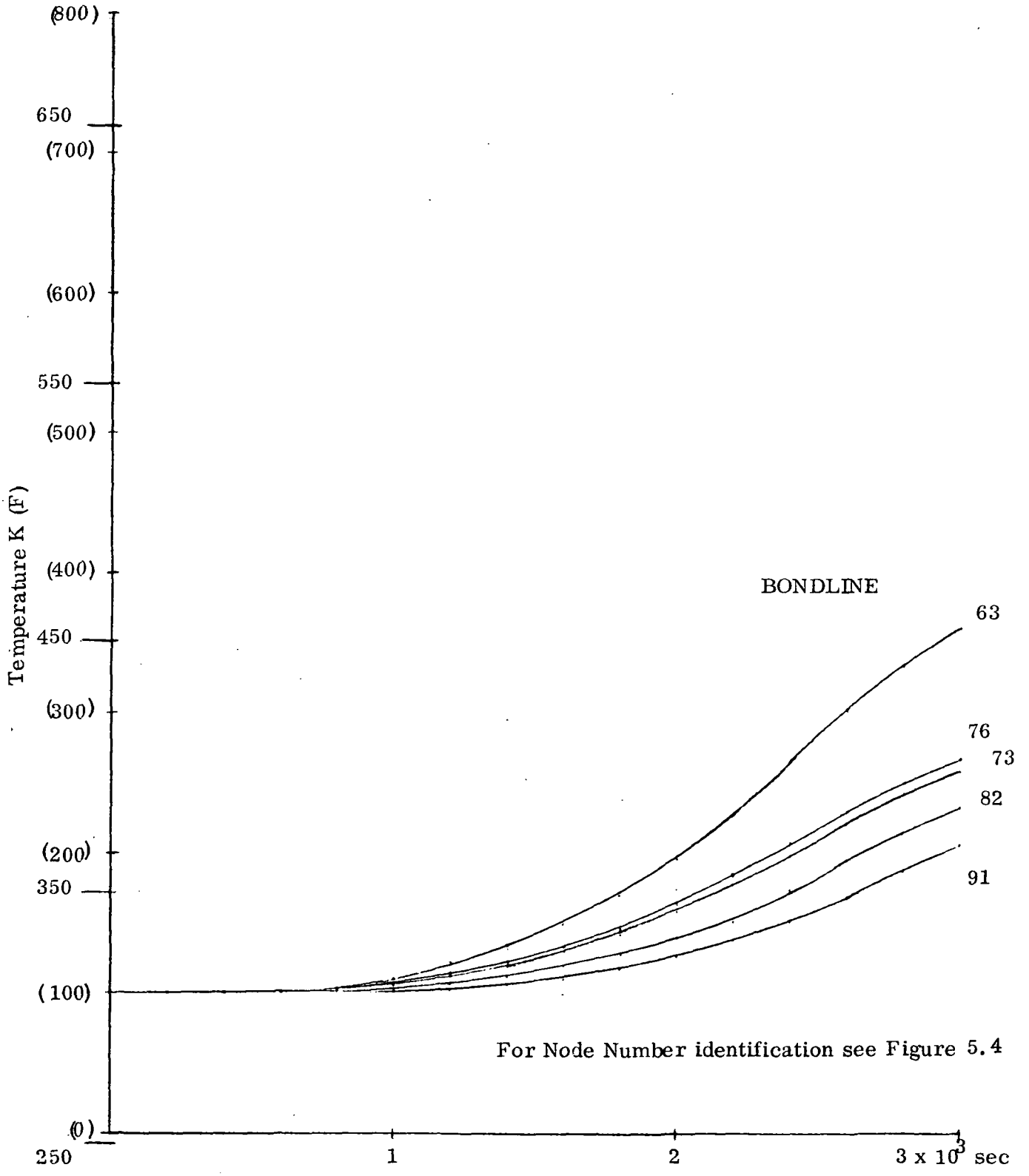

Figure 5.7. Structural Temperature
All Titanium
REI thickness = (2.02 in.) 5.13cm
Initial Temp = (100° F.) 311K

Table 5-1. Summary of Constants used for Thermal Analysis

Material	ρ Kg/m^3	ρ (lb/ft^3)	C_p BTU/lbm °R)	C_p Joules/KgK	K BTU/ft^{2}R hr)	K Watt/m^{2}K
Boron/Aluminum U. D. 50 v/o	2585	(161.4)	T K / R: 88.8 (160); 144.4 (260); 255 (460); 366 (660); 644 (1160)	C_p: (0.080) 334; (0.135) 564; (0.214) 895; (0.265) 1108; (0.380) 1589	(35)	198
REI	240	(15.0)	T K / R: 533 (960); 811 (1460); 1080 (1960); 1306 (2460); 1644 (2900)	C_p: (0.220) 920; (0.237) 1991; (0.247) 1038; (0.255) 1066; (0.262) 1096	T K / R: 255 (460); 533 (960); 811 (1460); 1088 (1960); 1644 (2960)	(0.0242) 0.137; (0.0350) 0.198; (0.0505) 0.292; (0.0740) 0.42; (0.1580) 0.897
RTV Silicone Adhesive	1079	(67.4)	0.246	1029	(0.1)	
6Al-4V	4485	(280.0)	$0.103 + 0.4 \times 10^{-4}T$		$2.5 + 0.3585 \times 10^{-2}T$	

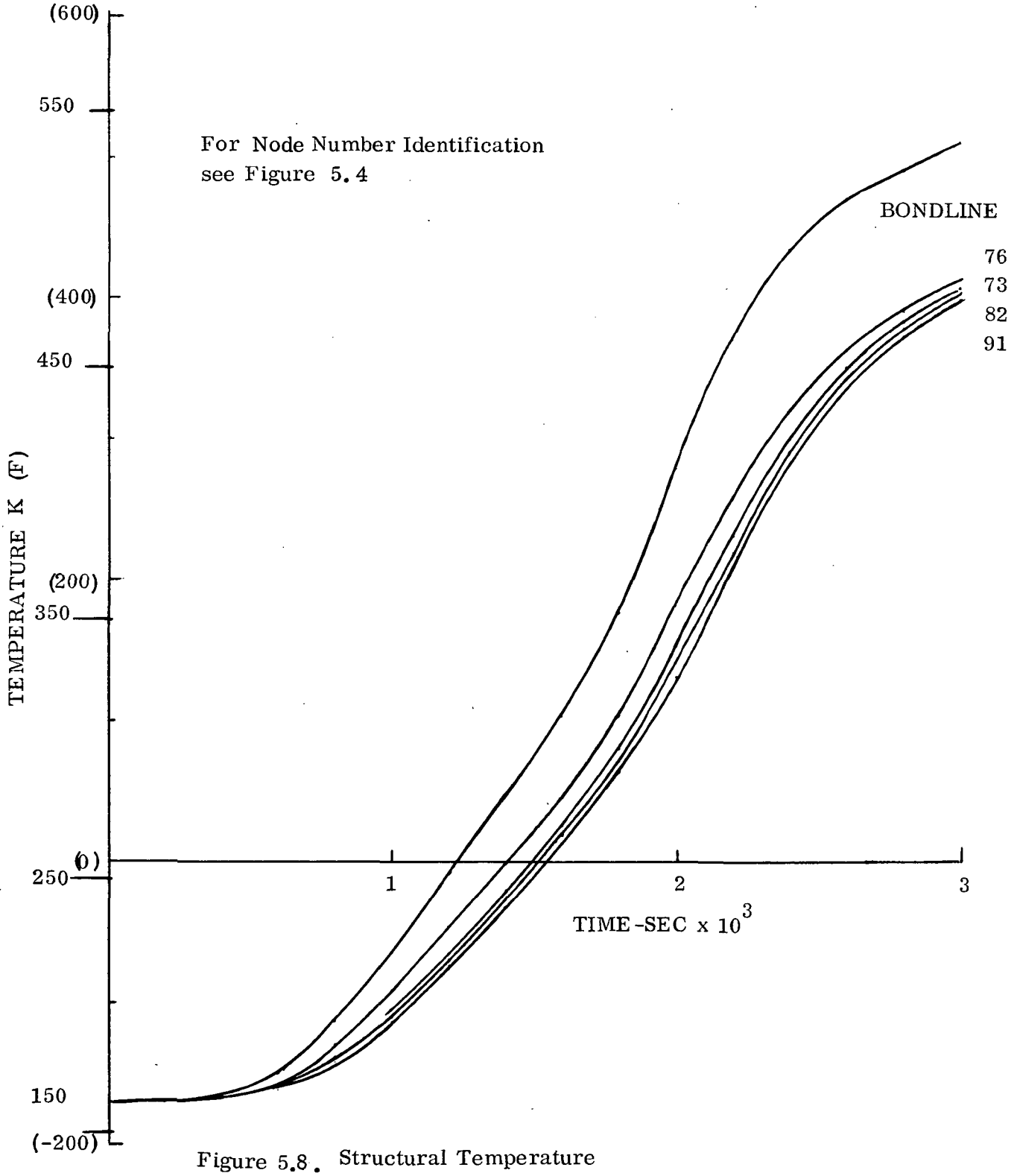

Figure 5.8. Structural Temperature
Boron Aluminum Stringer
Titanium Skin & Frames
REI Thickness (1.37-in) 3.37 cm
Initial Temp = (290°R) 161K

Figure 5.9 shows the structural temperature predictions for the 331K (560R) initial temperature case. Here too the thermal gradients are less and the structural temperatures are higher than the all titanium case.

First it was apparent that the thermal gradients in the titanium structure were higher than the boron/aluminum. Also the boron/aluminum stringer was operating at a somewhat higher temperature. Figure 5.10 is a plot of the bond line temperature and one of the backside hat node (91) temperatures for the all titanium and boron/aluminum cases. The 618K (650F) maximum bond line temperature is also shown. It is apparent from the plot that the predesign value of 3.37 cm (1.37 in) for the REI thickness selected by RI was insufficient, and that an increase in the thickness and weight of insulation would be required. The bond line temperature for the boron/aluminum stringer also exceeds the bond line allowable but by a much smaller magnitude. It has been estimated that the addition of from .20 to .25 lbs/ft^2 of REI material would be required to reduce the bond line temperature to 618K (650F) for the all titanium case.

The amount of insulation needed to be added for the boron/aluminum stringer would be small (.02 in). The boron/aluminum stringer, because of its higher thermal conductivity and specific heat, would appear to have a weight advantage. However, due to the uncertainties involved in the temperature predictions and the fact that the temperatures were not defined after 3,000 seconds, it was decided not to change the weight estimate for either systems.

5.2 STRESS ANALYSIS

5.2.1 MATERIAL PROPERTIES. The properties of the boron/aluminum and titanium used for this analysis are summarized in Table 5-2.

5.2.2 SECTION PROPERTIES. Due to the bend radii, the final configuration of the hat section stiffener has a somewhat smaller area and moment of inertia that the idealized sections previously studied. The final stress analysis was performed with the following properties.

A	=	0.817 μm^2	0.1267 in^2
$\bar{t}$	=	0.106 cm	0.0418 in
$\bar{Y}$	=	0.896 cm	0.353 in (from skin)
I	=	124 μm^4	0.030 in^4
ρ	=	1.06 cm	0.412 in

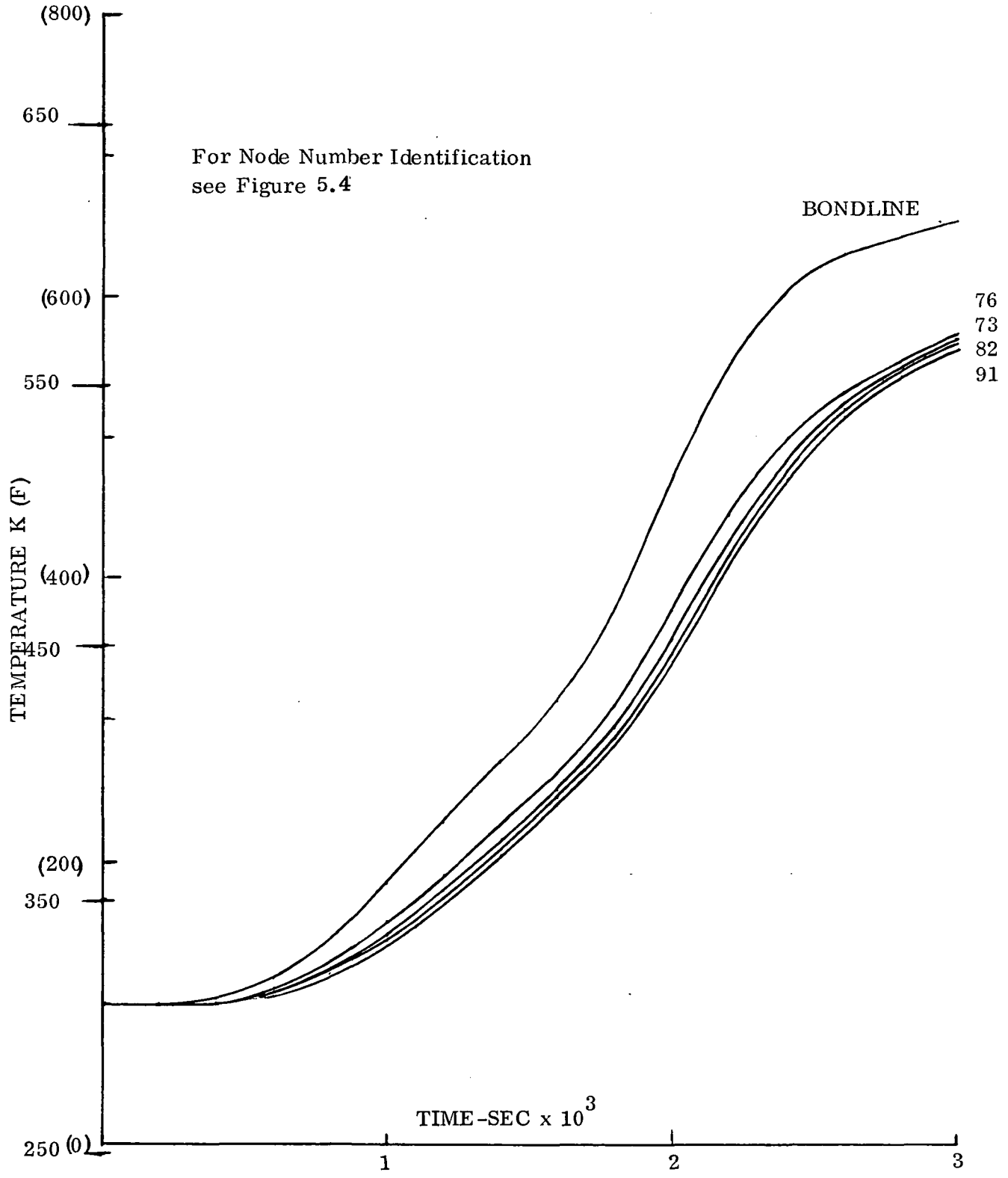

Figure 5.9. Structural Temperature.
Boron Aluminum Stringer
Titanium Skin & Frame
REI Thickness (1.37-in) 3.37 cm
Initial Temp. (560° R) 311K

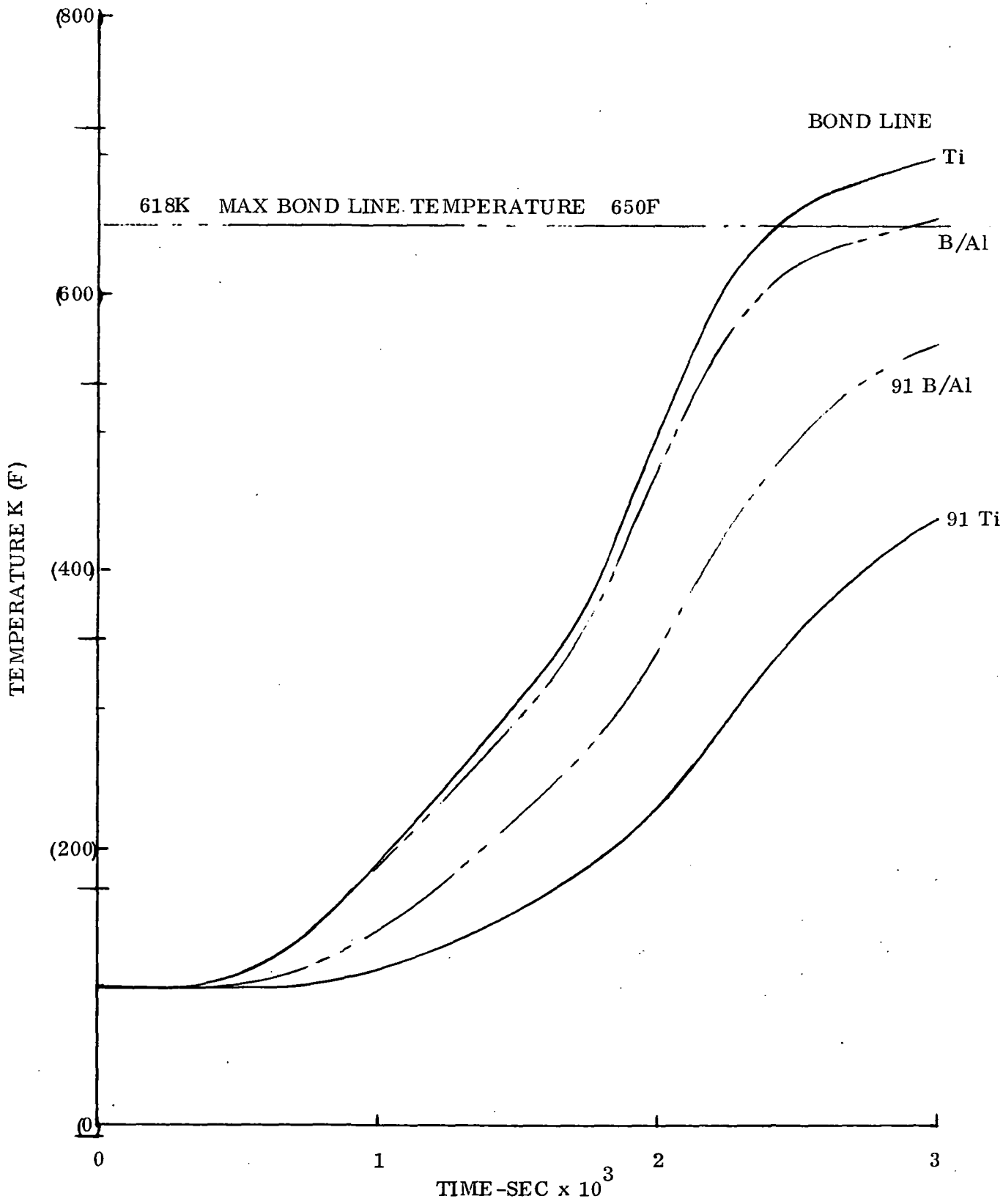

Figure 5.10. Difference in Bond Line Temperature and Typical Structural Temperature, B/Al and Titanium Stringers.

Table 5-2. Materials Properties

Titanium @ 589K (600F)		
F_{tu}	683 MN/m^2	(99,100 psi)
F_{cy}	618 MN/m^2	(89,700 psi)
F_{su}	402 MN/m^2	(58,400 psi)
E_x	9.03 GN/m^2	(13.1 x 10^6 psi)
E_y	9.24 GN/m^2	(13.4 x 10^6 psi)
G	3.45 GN/m^2	(5.0 x 10^6 psi)

Boron/Aluminum @ 589K (600F)		
$F_{tu_x} = F_{cu_x}$	1171 MN/m^2	(170,000 psi)
$F_{tu_y} = F_{cu_y}$	31 MN/m^2	(4,500 psi)
E_x	19.3 GN/m^2	(28 x 10^6 psi)
E_y	7.5 GN/m^2	(11 x 10^6 psi)
ν_{12}	.3	
ν_{21}	.118	
G	1.83 GN/m^2	2.66 x 10^6

5.2.3 THERMAL STRESSES. The basic proportions of the stringer and panel elements were analyzed as described in Section 2. The final configuration of the B/Al hat, Ti 6Al-4V skin plate stringer test specimen was checked for the temperature induced stresses of the flight profile. The study considers the thermal gradient at t = 2,200 seconds and 3,000 seconds.

Thermal stresses were computed for the structural model. The center reaction was deleted and the length was changed to 47.34 inches to simulate the test article. The middle 24.62 inches now represented the span between frames.

The thermal analysis gradients for the test specimen configuration defined by Drawing 72C0080 were used to compute actual anticipated thermal stresses. Two gradients were evaluated, one at 2,200 seconds and one at 3,000 seconds. The temperature variation is considered in the longitudinal panel direction and through the section. Figures 5.11 and 5.12 show the calculated thermal stress. The maximum stress-developed is seen to be 59 MN/m^2 (8,650 psi) for the B/Al hat and -52.7 MN/m^2 (-7,650 psi) for the titanium skin with a peak temperature of 436K (320F) at t = 2,200 seconds. The original analysis in the parametric study considered steady state temperature stresses for a peak of 589K (600F). The resulting thermal stresses were found to be 86.1 MN/m^2 (12,500 psi) and -93.06 MN/m^2 (-13,500 psi) for the B/Al hat and titanium skin respectively.

5.2.4 MARGINS OF SAFETY. Using the crippling curve, Figure 2.3

$$F_{cr_{avg}} = MN/m^2 \ (62,300 \text{ psi})$$

$$F_{co} = F_{cr_{avg}} \left[1 - \frac{F_{cr_{avg}} \left(\frac{L'}{\rho} \right)^2}{Y \pi^2 E_c} \right]$$

$$F_{cc} = 339.8 \ MN/m^2 = (49,300 \text{ psi})$$

$$P_{co} = F_{cc} \Sigma \Delta = 39.1 \text{ KN} = (8,800 \text{ lbs})$$

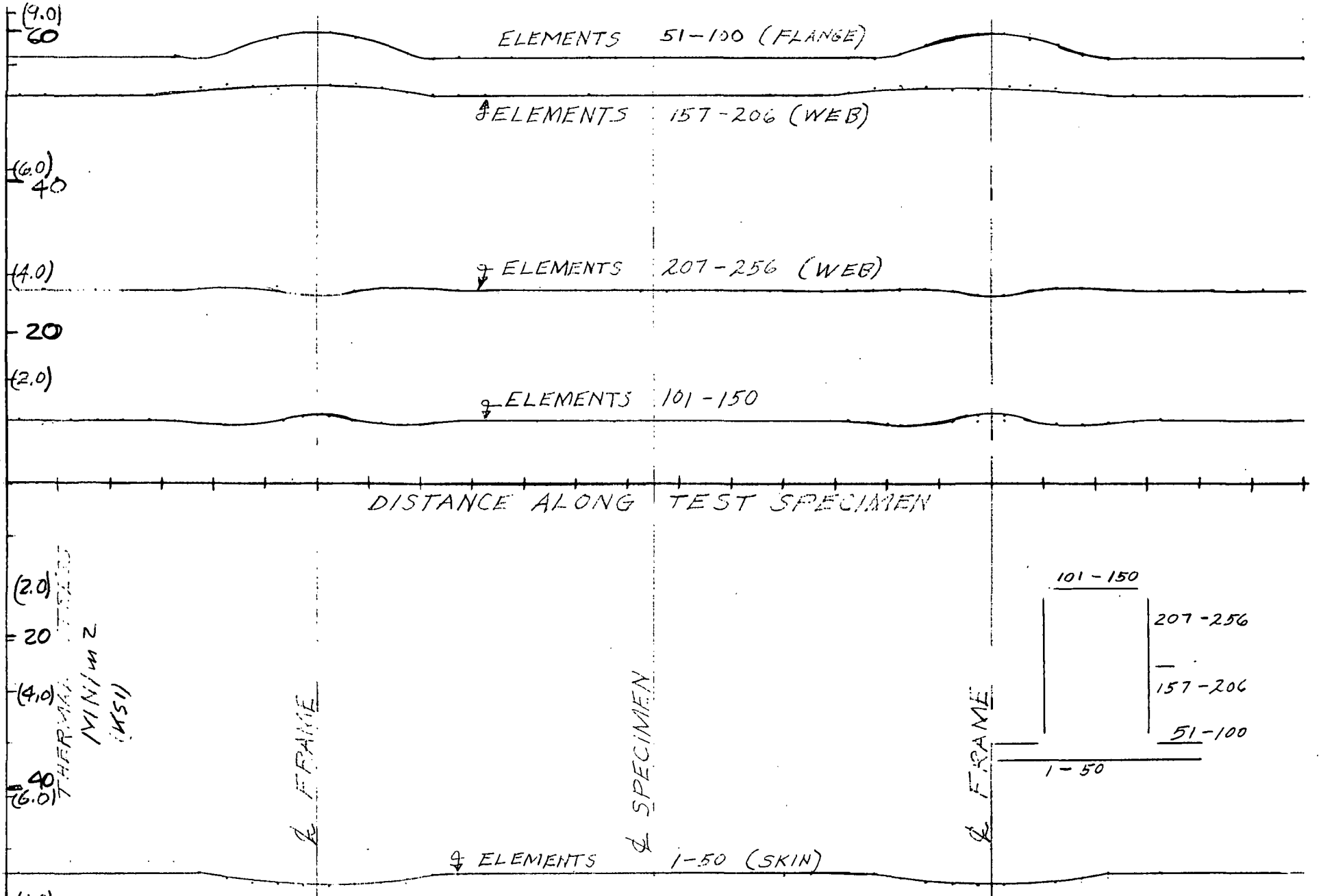

FIGURE 5.16. TEST PANEL TRANSIENT THERMAL STRESSES – $\tau = 3000$ SECONDS
B/AL. HAT; TITANIUM SKIN

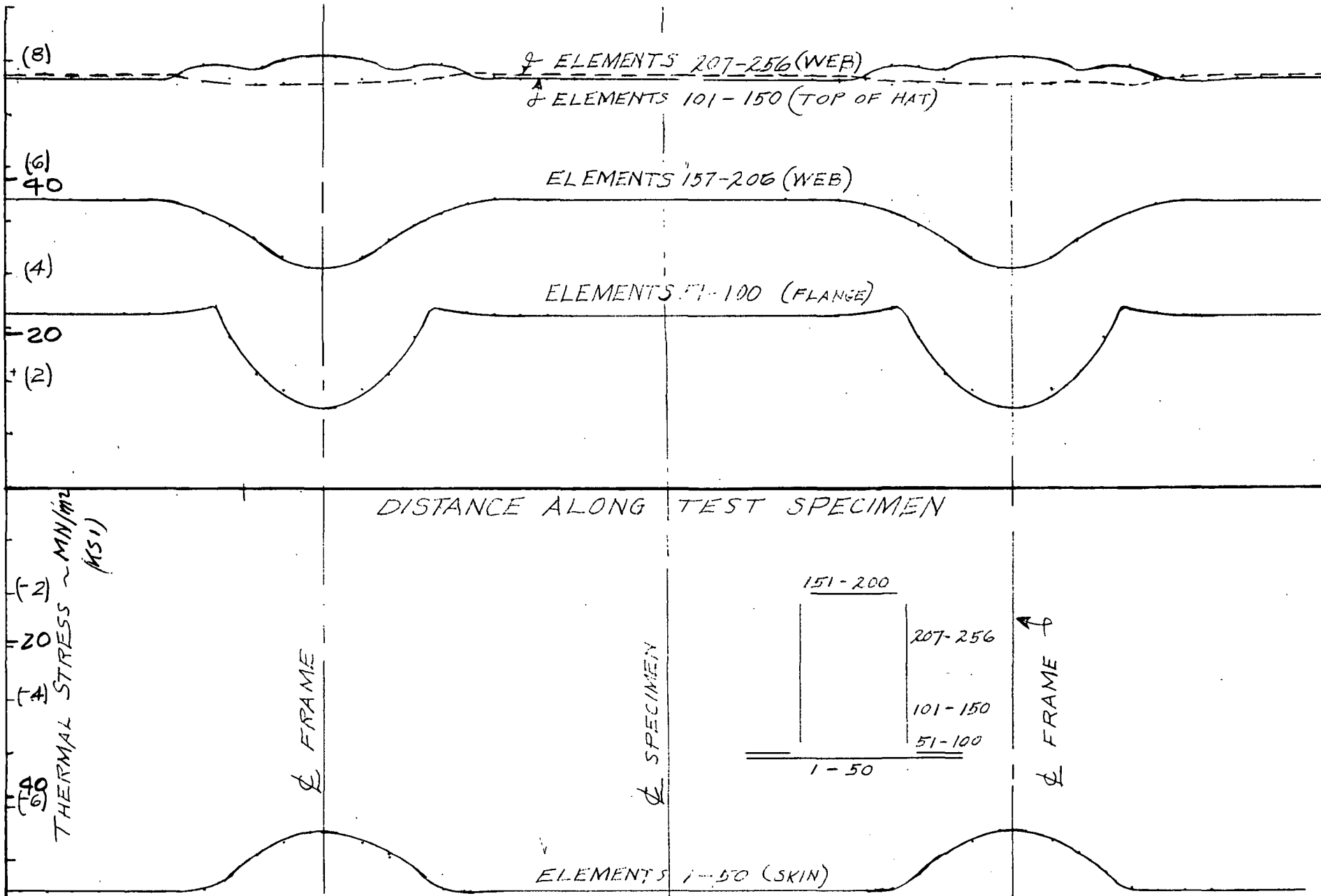

FIGURE 5.12 TEST PANEL TRANSIENT THERMAL STRESSES — $t = 2200$ SECONDS
B/AL. HAT; TITANIUM SKIN

Maximum Compressive Stress

$A' = A_{B,A} + .478\ (Ti\text{-}6Al\text{-}4V)$

$A' = .115\ mm^2 = 0.17892\ in^2$

$T_{c_{B,A}} = -293.7\ MN/m^2 = (-42,600\ psi)$

$T_{c_{Ti\text{-}6Al\text{-}4V}} = -139.9\ MN/m^2 = (-20,300\ psi)$

Column Check

$P_{column} = 33.91\ KN = (-7,625\ lbs)$

$P_{co} = 39.1\ KN = (-8,800\ psi)$

$M.S._{column} = \underline{\underline{.15}}$

Skin Compression Buckling Stress

$$\sigma_{cr} = \frac{\pi^2 K_c E}{12(1-\nu_e^2)} \left(\frac{t}{b}\right)^2$$

$b/t = 42.1$ Ref. 2

$K_c = 5.8$ (for hat)

$\sigma_{cr} = 273.6\ MN/m^2$ (39,700 psi) for hat supported skin

Shear Buckling 338K (150F) (assume S.S. edge)

$$\tau_{cr} = \frac{\pi^2 K_s E}{12(1-\nu_e^2)} \left(\frac{t}{b}\right)^2 \text{ Ref. 2}$$

$K_s = 4.8$

$\tau_{cr} = 260\ MN/m^2$ (37,800)

Skin Buckling

$$f_{c_{\substack{\text{Ti-6Al-4V} \\ \text{total}}}} = f_{c_{\text{Ti-6Al-4V}}} + f_{c_{\text{thermal}}}$$

$$f_{c_{\substack{\text{Ti-6Al-4V} \\ \text{total}}}} = 230.9 \text{ MN/m}^2 \text{ (-33,350 psi)}$$

$$\sigma_{cr} = 235.7 \text{ MN/m}^2 \text{ (34,200 psi)}$$

$$\text{M.S.} = \frac{\sigma_{cr}}{f_{c_{\text{total}}}} - 1 = \underline{\underline{.02}}$$

Net Section Crippling

$$f_{c_{B,A}} = 293.68 \text{ (-42,600 psi)}$$

$$F_{cr_{avg}} = 429.4 \text{ MN/m}^2 \text{ (62,300 psi)}$$

$$\text{M.S.} = \frac{F_{cr_{avg}}}{f_{c_{B,A}}} - 1 = \underline{\underline{.46}}$$

Maximum Tension

$$f_{t_{B,A}} = 427.4 \text{ MN/m}^2 \text{ (62,000 psi)}$$

$$f_{t_{\text{Ti-6Al-4V}}} = 204. \text{ MN/m}^2 \text{ (29,600 psi)}$$

$$f_{t_{\substack{B,A \\ \text{thermal}}}} = 9.7 \text{ MN/m}^2 \text{ (1,415 psi)}$$

$f_{t_{\text{Ti-6Al-4V thermal}}} = 12.8\ \text{MN/m}^2$ (-1,865 psi)

$f_{t_{B,A\ \text{total}}} = 437\ \text{MN/m}^2$ (63,415 psi)

$F_{tu_{B,A}} = 1,171\ \text{MN/m}^2$ (170,000 psi)

Boron Aluminum M.S. = <u>1.68</u>

$f_{t_{\text{Ti-6Al-4V}}} = 191\ \text{MN/m}^2$ (27,735 psi)

$F_{tu\ @\ 150°\ \text{Ti-6Al-4V}} = 868\ \text{MN/m}^2$ (126,000 psi)

Ti-6Al-4V M.S. = LARGE

<u>Shear Stresses @ 338K (150F)</u>

$\tau = q/t = 167.5\ \text{MN/m}^2$ (24,300 psi)

$$\tau_{cr} = \frac{\pi^2 K_s E}{12(1-\nu_c)^2}\left(\frac{t}{b}\right)^2$$

$K_s = 4.8$

$\tau_{cr} = 260.5\ \text{MN/m}^2$ (37,800 psi)

$$\text{M.S.} = \frac{\tau_{cr}}{\tau} - 1 = \underline{.55}$$

5.2.5 BUCKLING BEHAVIOR. A computer simulation of the panel was run by NASA Langley using BUCLASP (Ref. 3).

The calculated buckling load for the first mode at 589K (600F) was 458 KN (102,946 lbs) which compares with an applied ultimate load of 268 KN (60, 360 lbs).

6

COST ANALYSIS

SUMMARY

An economic analysis was conducted to evaluate the cost differences that could be expected by substituting a boron/aluminum composite reinforced fuselage panel for an existing all-titanium panel on the orbiter vehicle documented in the North American/ Convair Phase B Space Shuttle study. A parametric approach was utilized in conjunction with comparative detailed estimates of panel fabrication cost. Resizing cost effects due to the reduced weight of the composite panel were determined for the orbiter and booster vehicles. The results of the analysis indicated that a total program cost increase of about $6.8 million could be expected for about 54 Kg (120 lb) of direct weight saved. Cost sensitivities to major program variables were determined and the effects of constraints unique to the study are discussed.

INTRODUCTION

The introduction of advanced materials in small quantities on an uncommitted design are difficult to justify on the basis of cost alone. A limited application results in relatively small resizing benefits that have to carry the entire penalty associated with introducing the new technology. Since a change on an uncommitted design is only a "paper" change, this penalty, which acts in favor of the advanced material introduction, is small. For the case of a nearly completed development program where performance (payload, range, landing distance, etc.) is found to be below predicted levels, this resizing cost penalty may approach the total program costs already expended. The incremental costs of introducing advanced technologies (composite materials for example) are likely to be economically attractive in this case. A design effort with extensive application of advanced materials is likely to be economically attractive because large decreases in size are obtainable, thereby giving a greater economic base to offset the costs of introducing the new technology. The constraints of this study of filamentary reinforced orbiter fuselage panels represent a case of relatively limited application of 28 m^2 (200 ft^2) on an uncommitted design. As might be expected, these constraints prohibit the showing of an economic advantage for boron/aluminum composite reinforced panel designs.

APPROACH

The methodology used in this study to evaluate boron/aluminum reinforced fuselage panels resulted in an estimated shuttle program cost delta from a baseline all titanium design. Two distinct cost effects were determined in comparing the candidate composite design with the all titanium design baseline panel. One cost effect was the decrease in

program costs due to the weight reduction (resizing) attributable to the more structurally efficient composite panel. These program cost savings were determined by an analysis of orbiter and booster vehicle program weight and cost sensitivities for the selected baseline space shuttle program. The other cost effect determined was the cost increases due to the introduction of composite panels. Detailed manufacturing cost estimates for the baseline all titanium and the candidate composite-reinforced panel were generated. Representative costs for the baseline 161-C orbiter's all-titanium type structure, as reported in the space shuttle Phase B study final report, were obtained. The results of the comparative detailed estimates, in the form of a relative complexity ratio, were then applied to baseline 161-C orbiter's reported cost to obtain the composite reinforced panel cost. These unit costs were then multiplied by the appropriate hardware quantities to get the total cost increase for introduction of the composite panel.

The following costing ground rules and assumptions were made for the cost analysis.

1. Costs based on 161-C (delta-wing) orbiter and B9U (aft-wing canard) booster.

2. All costs in 1970 dollars and exclude vehicle contractor fee.

3. The space shuttle Phase C/D master program schedule MPS-05, Revision 1, is assumed for baseline program costs.

4. The following total vehicle requirements are assumed:

   a. Five orbiter and four booster operational flight vehicles.

   b. One (1) orbiter and two (2) booster structural test articles for static and fatigue test program.

   c. An orbiter and a booster main propulsion cluster firing development test article.

5. Detail hardware element requirements for typical orbiter elements are assumed to be as follows and are compatible with the vehicle requirements above.

a.	Major test hardware	= 4.95 equiv. units
b.	Production hardware	= 2.21 equiv. units
c.	Refurbishment of test article to operational config.	= .25 equiv. units
d.	Operational spares (444 flights)	= .47 equiv. units
	Total	= +7.88 equiv. units.

6. The 161-C orbiter baseline payloads are 29,470 Kg (65,000 lbs) to 185 Km (100 n.mi.) circular orbit from ETR and 11,340 Kg (25,000) to 500 Km (270 n.mi.) 55° orbit from ETR.

7. All main rocket engine costs are excluded.

8. A composite panel application area of 28 m^2 (300 ft^2) was assumed for the baseline comparison.

9. For the initial cost comparison case no additional engineering design and development complexity was assumed for the composite reinforced panel concept.

10. A boron/aluminum raw material cost of $331/Kg ($150/lb) was assumed for the baseline comparison calculations.

11. The difference in weight per unit area between the all titanium and composite panels was set at 1.99 Kg/m^2 (0.408 lbs/sq. ft) for determining the direct weight reduction of 54 Kg (210 lbs).

Because there is significant variation in assessments of the state-of-the-art for boron/aluminum composites, cost sensitivity analyses were conducted around the baseline comparison calculations. This approach was felt to be invaluable to this study because many of the assumptions and parameters (such as composite raw material costs) are likely to change with time. Also, these sensitivities will facilitate the use of this cost data in other applications where the constraints unique to this study may not apply. For clarity in the following charts and tables material and structural costs are given in $/lb.

RESULTS

For cost purposes the final Phase B costs as documented in the "Program Cost and Schedule Estimates Plan for Phase C/D," 25 June 1971, were utilized for the baseline. This baseline total program costs, exclusive of main rocket engines, amounts to about $9.6 billion. Figure 6.1 shows the orbiter and booster vehicle portions of the space shuttle costs - final baseline as well as the flight testing, operations and management. A breakdown of the baseline orbiter vehicle cost representing the all titanium panel configuration is shown in Figure 6.2.

Based on an analysis of the 161-C orbiter body cent section costs, the all titanium panel section unit manufacturing cost was established at $435,000. Similarly, the 28 m^2 (300 ft^2) panel's share of ED&D (Engineering Design and Development) cost was established at $798,000. The detailed manufacturing cost comparisons result in

Table 6-1. Space Shuttle Costs, Final Baseline
161C Orbiter/B9U Booster

WBS Level 3 - Description	Cost ($ Million)			
	DDT&E	Production	Operations	Total Program
1.0 Orbiter	$3437.5	$ 873.1	$ 322.2	$4632.8
2.0 Main Engine	-0-	-0-	-0-	-0-
3.0 Booster	3208.8	440.9	142.7	3792.4
4.0 Flight test	287.8	-0-	-0-	287.8
5.0 Operations	-0-	-0-	703.9	703.9
6.0 Shuttle management and integration	166.3	31.5	27.9	225.7
Total costs	$7100.4	$1345.5	$1196.7	$9642.6

TFU orbiter $204.3 million
TFU booster $285.9 million

Table 6-2. Baseline All-Metal Orbiter Cost ($ Millions)

WBS Element	DDT&E	Production	Operations	Total
Structure GP	1104	425	88	1617
Propulsion GP	631	165	57	853
Avionics GP	367	69	72	508
Power GP	234	68	25	327
ECLS GP	187	38	15	240
IA & C/O	100	96	--	196
Development Test	97	--	--	97
Sys Engr	230	--	--	230
Facilities	2	--	--	2
System Support	414	--	31	445
Management	47	13	35	95
Payload Integ.	25	--	--	25
TOTAL	3438	874	323	4635

an overall complexity ratio of 3.3 (composite/all-titanium) with the baseline raw material cost assumption of $331/Kg ($150/lb) for boron/aluminum. This results in an estimated composite panel unit manufacturing cost of $1,435,000. The ED&D cost was kept constant for the initial comparison as stated in the assumptions. Figure 6.3 summarizes the unit cost and ED&D values used to establish the direct cost increases for the composite panel application.

The decreases in program cost were due to the weight reduction effected by the composite panel application. For this study, the reductions in weight were taken on the orbiter vehicle and booster vehicles only. No program cost savings in the areas of Flight Test, Operations, or Shuttle Management were felt to be directly attributable to the substitution of composite panels in the orbiter. An analysis of these program cost elements found that they were relatively insensitive to vehicle size differences of the magnitude realized in this study. In addition, these three items contribute only about 13% to the total program cost. The orbiter and booster program cost sensitivities used to evaluate weight reduction (resizing) effects are shown in Figures 6.4 and 6.5 respectively. The slope of these sensitivity lines represent the change in orbiter or booster total program cost that would result from taking one pound of weight out of the respective vehicle. The design, development, test and engineering (DDT&E) portion of these total program sensitivities account for 77% and 82% of the orbiter and booster totals respectively. The recurring production portions are 15% and 7% respectively, and the recurring operations portions account for the remaining 8% and 11%. The resizing cost decreases for the orbiter vehicle were calculated as follows:

$$\begin{aligned} \text{Orbiter Program } \Delta \text{ Cost} &= \text{weight change x cost partial} \\ &= -120 \text{ lbs x } \$6500/\text{lbs} \\ &= \$793,000 \end{aligned}$$

The resizing cost decreases attributable to the booster vehicle were calculated in a similar fashion except that an additional weight calculation was required to establish the amount of booster weight change resulting from the 120 pounds of orbiter panel weight reduction. A booster weight partial based on previous Phase B study results showed the following:

$$\partial \text{ Booster Dry Weight}/\partial (\Delta \text{Orbiter Weight}) = 2.5$$

Using this partial, the resizing cost decrease calculation was made as shown below:

$$\text{Booster Weight Change} = 2.5 \times -120 \text{ lbs} = -300 \text{ lbs.}$$

$$\begin{aligned} \text{Booster Program } \Delta \text{ Cost} &= -300 \text{ lbs x } \$1121/\text{lb} \\ &= \$336,000 \end{aligned}$$

Table 6-3. Program Cost Increases for Composite Panel Application

	Area (sq.ft.)	Costing Weight (lbs)	TFU[1] ($M)	Hardw. Consumption[2] ($M)	ED&D ($M)
Composite Panel Section	300	450	1.435	11.310	0.798
All-titanium Panel Section	300	570	0.435	3.430	0.798
Program Cost Increase				+7.880	+0

(1) TFU = Theoretical First Unit manufacturing cost
(2) Based on 7.88 equivalent units at TFU cost

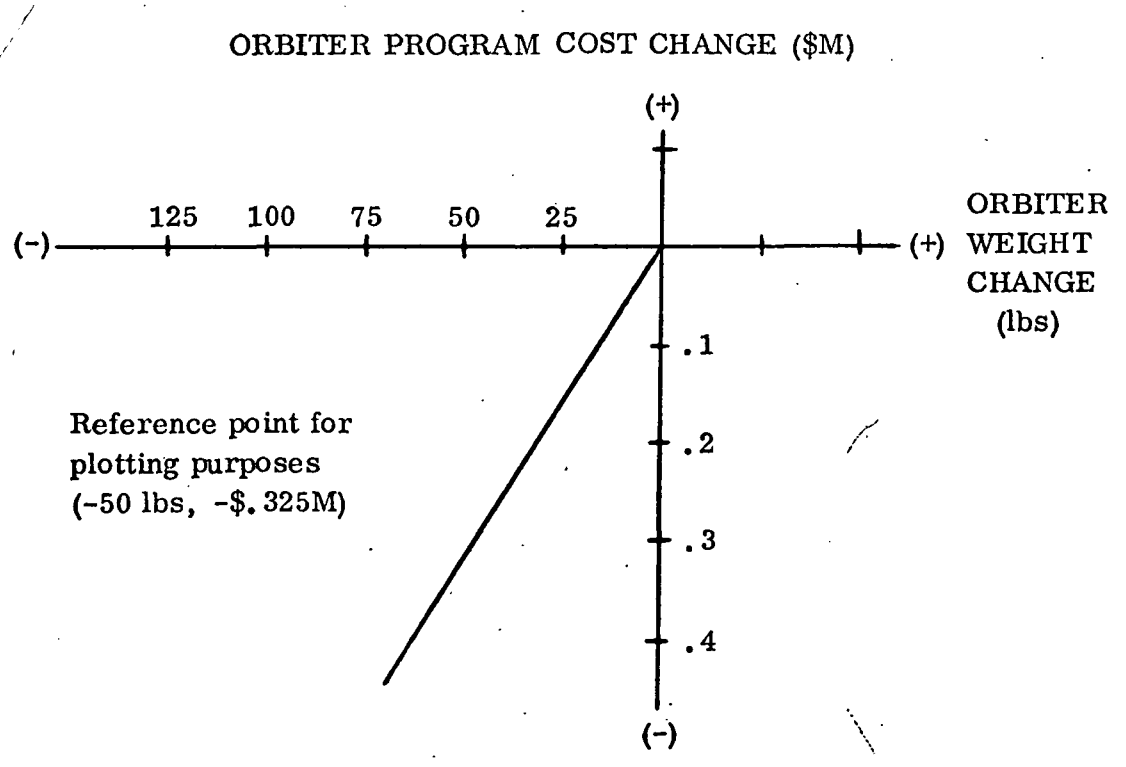

Figure 6.1. Orbiter Program Cost Sensitivity.

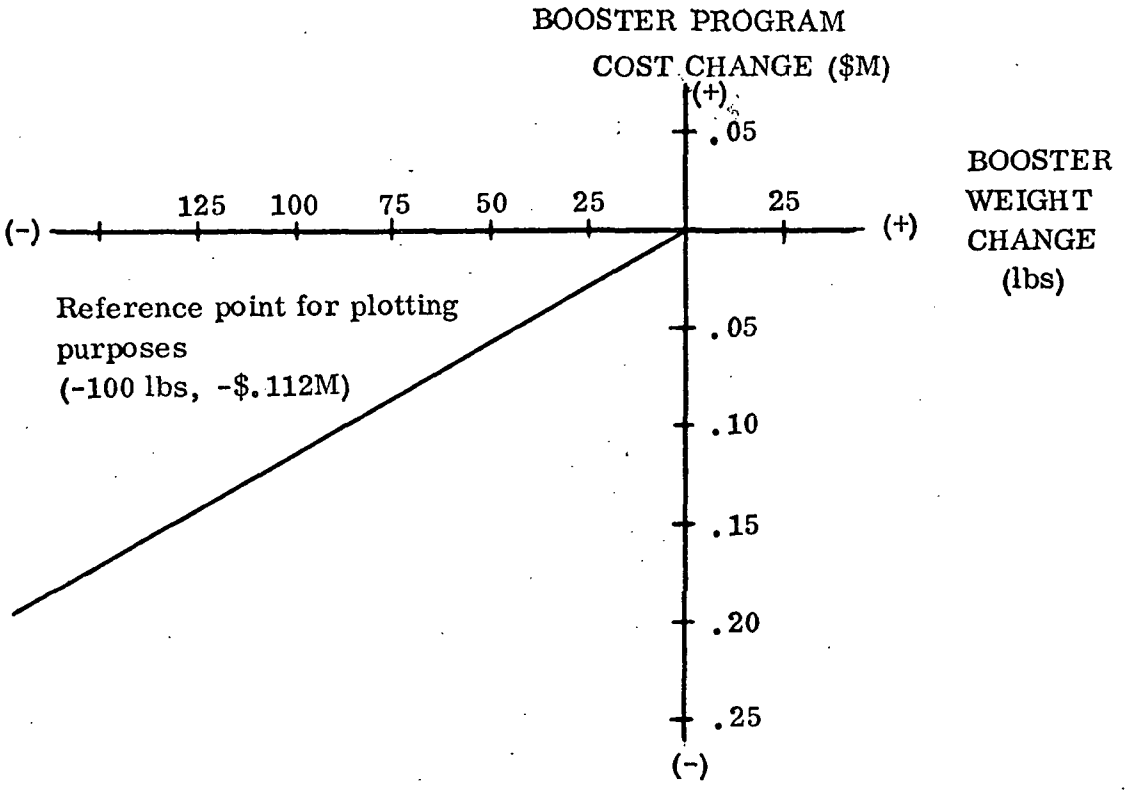

Figure 6.2. Booster Program Cost Sensitivity.

Table 6-4. Baseline Comparison - B/Al vs All-Titanium Panel Program Δ Cost Summary

Direct Cost Increase	+$7.880M
Resizing Cost Decreases	-$1.129M
Net Program Δ Cost	+$6.753M

The combined booster and orbiter resizing cost decrease was equal to $1.129M. This resulted in the net program cost difference summarized in Figure 6.6.

The sensitivity of the net program delta cost shown in Figure 6.6 was investigated with respect to six major variables (or assumptions) that were utilized in the baseline cost comparison. The variables whose sensitivities were analyzed included:

1. Composite Panel Manufacturing Cost Complexity
2. B/Al Raw Material Cost
3. All-titanium Panel Cost per Pound
4. Composite Panel Application Area
5. Engineering Design and Development Complexity
6. Payload Growth

The sensitivity of program Δ cost to variations in the manufacturing complexity of the composite panel is shown in Figure 6.7. The baseline composite panel is shown at a complexity of 7.6 relative to aluminum sheet stringer construction. This is 3.3 times as complex as the comparative all titanium panel which would have a complexity value of 2.3 compared with an equivalent aluminum sheet stringer constructed panel. This complexity for Ti construction was used in the Phase B Booster study costing and is in good agreement with the orbiter contractor's cost for this type structure. Note that at a complexity of 2.3 (equal to the all titanium panel) the program cost savings for resizing ($\sim$ $1.1M) still exist due to the lighter weight (see Figure 24) of the composite design. The baseline complexity ratio of 3.3 applied to the all titanium panels was, of course, based on the detailed manufacturing cost comparison utilizing a materials cost of $150/pound.

The sensitivity of program Δ cost to boron aluminum material cost is shown in Figure 6.8. The baseline boron/aluminum material cost of $150/lb was based on an analysis of recent composite materials cost histories (see Figure 6.9). The slope of these plots indicate about a 33% reduction every two years. Currently (1970-1971), boron/aluminum is being supplied at about $300/lb, and assuming a 1974 space shuttle application, a figure of around $150 is not unreasonable.

The sensitivity of program Δcost to the manufacturing cost of the all titanium panel is shown in Figure 6.10. The baseline point is shown at $763/lb which corresponds to the first unit manufacturing cost as shown in the Phase B final report. This average cost per pound was closely confirmed by using Convair Aerospace Division's booster fuselage structure parametric cost estimating relationship and titanium complexity factor on the orbiter center fuselage sections as shown below:

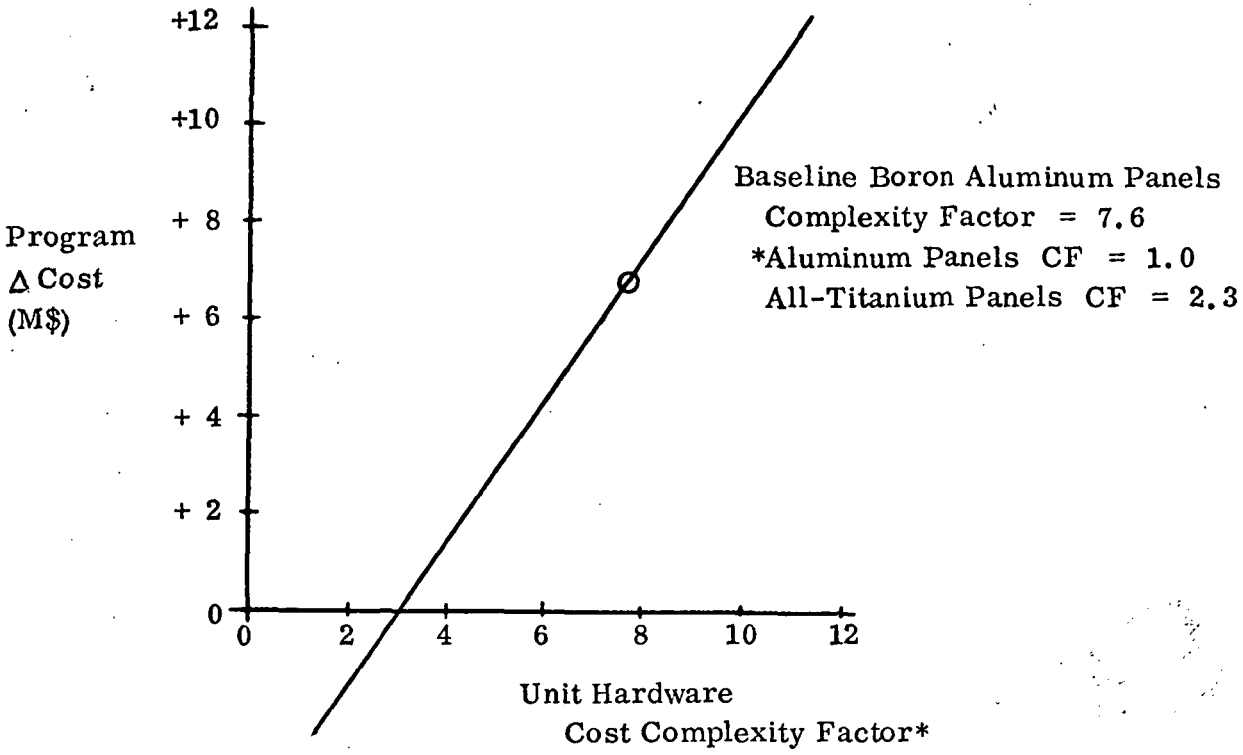

Figure 6.3. Manufacturing Cost Complexity Sensitivity.

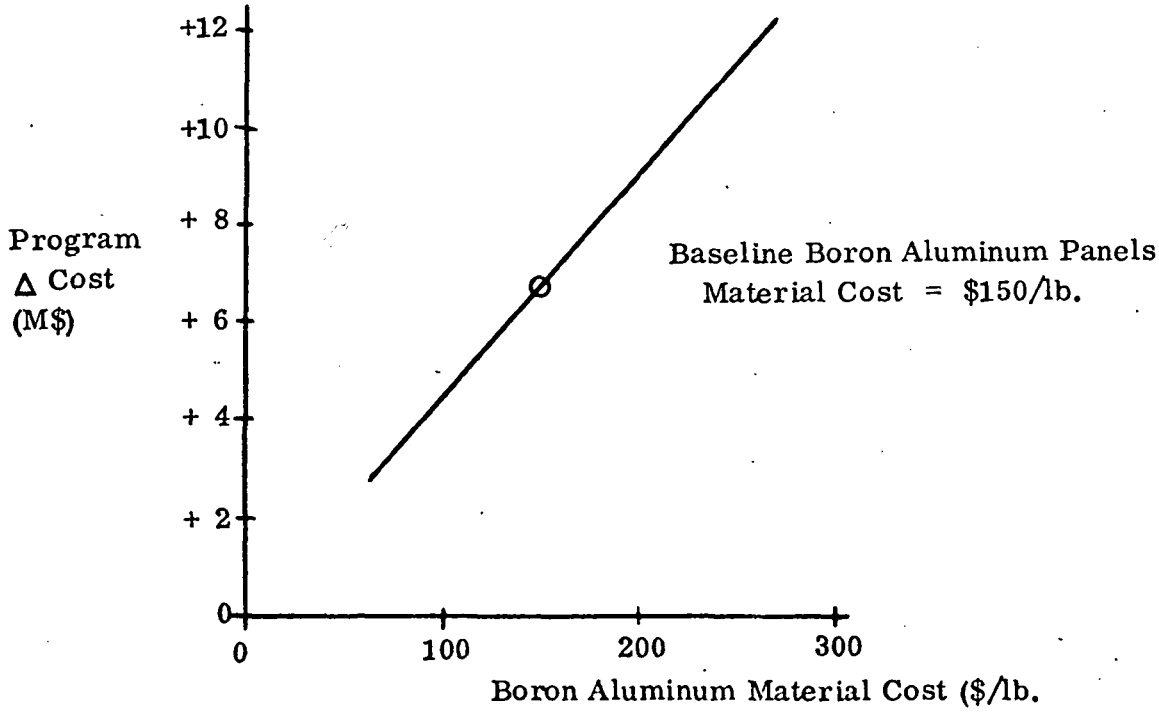

Figure 6.4. Material Cost Sensitivity.

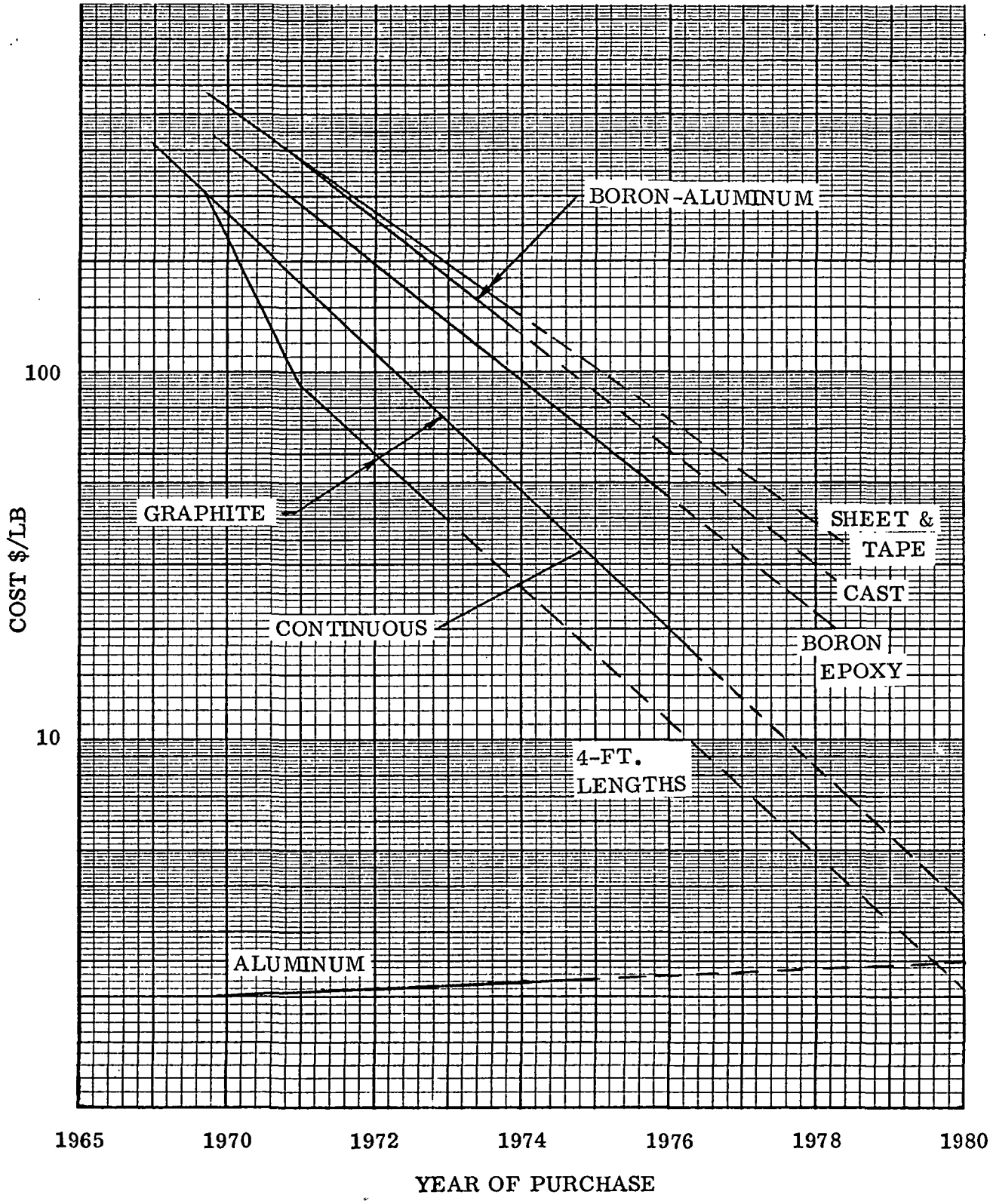

Figure 6.5. Composite Material Costs.

$$TFU = 2.3\,(.00655)(8080\ \text{lbs})^{.667} = \$6.08M$$

Average cost per pound of structure = \$735/lb

Figure 6.11 shows the program Δ cost change with variations in the area of composite panel applicability. It is important because it shows the relative impact that the 300 ft^2 assumption has on the magnitude of the total program cost change. This assumption was a constraint associated with the scope of the study. Composite designs, such as the one studied here, would be more likely to provide a cost savings if applied in an area such as the thrust structure where much greater weights are involved and where second-order effects such as stability and balance would tend to pyramid the vehicle resizing savings.

ED&D is historically less sensitive to design complexity than hardware costs. Since the specific design of this study represents a relatively modest increment in design sophistication (when compared with an all B/Al design), the assumption of a baseline ED&D cost ratio of 1 is not unrealistic. The effect on program cost of changes to this assumption are shown in Figure 6.12.

The final sensitivity curve shown in Figure 6.13 shows the program cost for incremental payload increases. This viewpoint of composite application represents one of the most promising aspects of this technology from an economic standpoint. The constraints of a study such as this (i.e., single panel in a new design) inherently legislate against a favorable answer for advanced materials. However, as a replacement article on an existing design, composite panels are likely to provide an attractive solution (less expensive) to the problem. For example, if weight growth in a program whose design phase is well underway were to threaten the mission capability, the incremental costs for weight savings or payload growth shown in Figure 6.13 would certainly be attractive. In this case the alternatives to composite panel substitution would be extensive (and costly) redesign of the entire vehicle to reduce drag, improve fractions, incorporate uprated propulsion systems, etc.

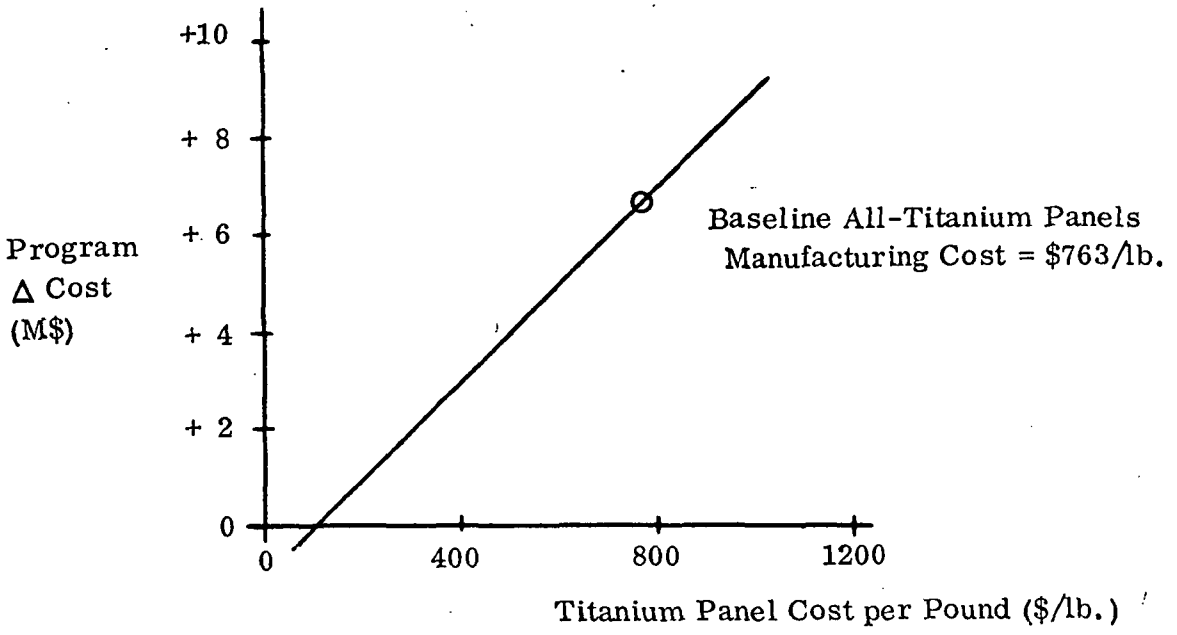

Figure 6.6. All-Titanium Panel Cost Sensitivity.

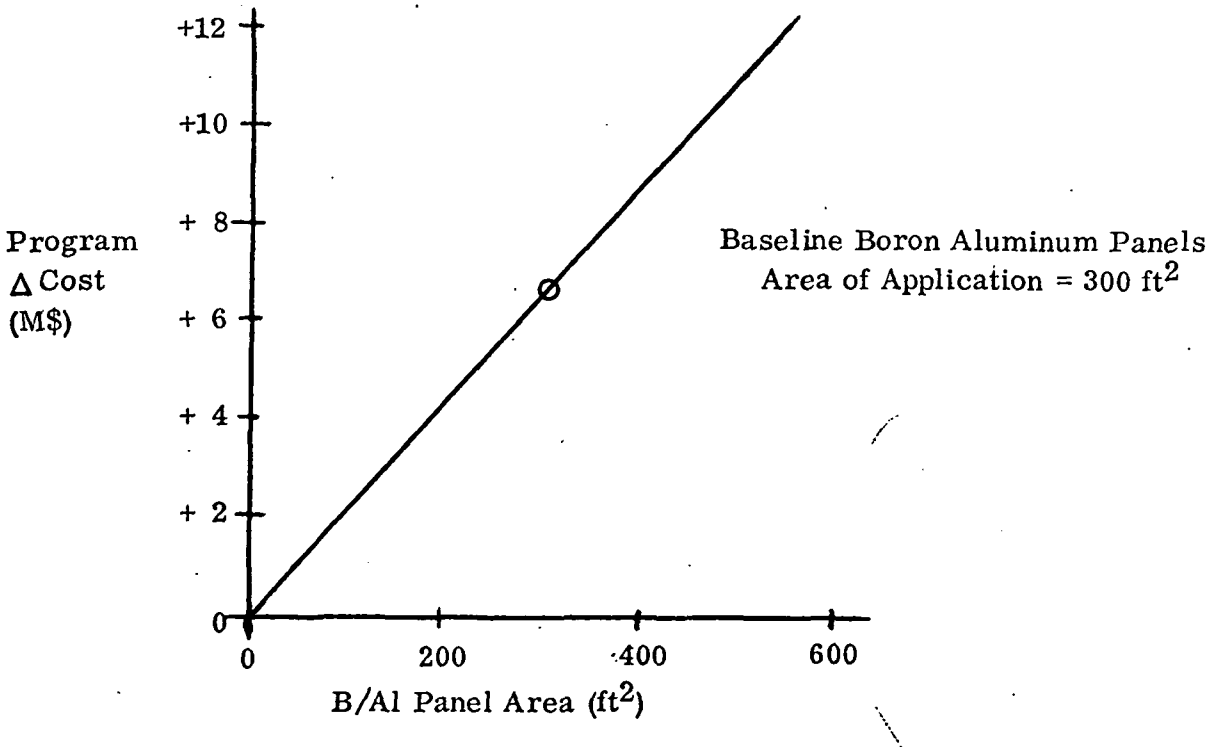

Figure 6.7. Area of Application Sensitivity.

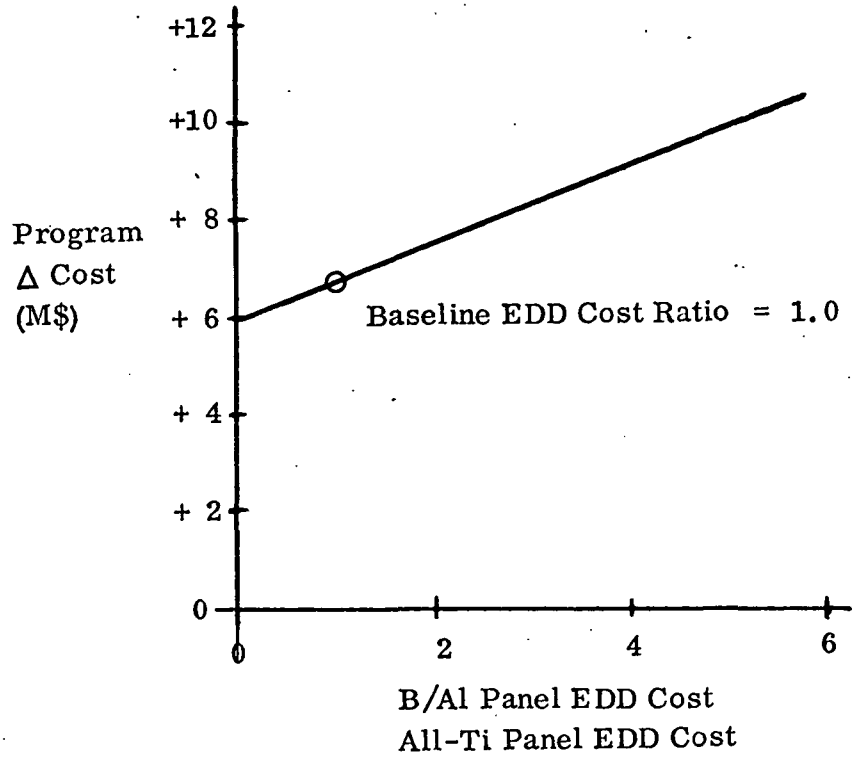

Figure 6.8. Engineering Design and Development (EDD) Cost Sensitivity.

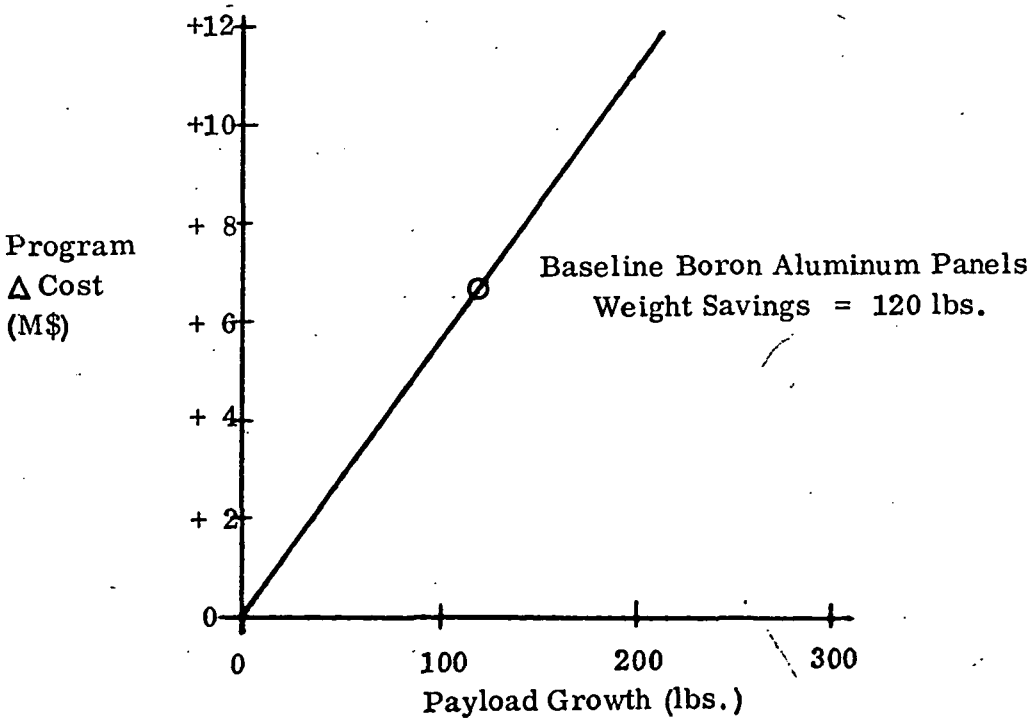

Figure 6.9. Payload Growth Sensitivity.

7

SUBELEMENT SPECIMEN DESIGN FABRICATION AND TESTING

7.1 INTRODUCTION

The purpose of the subelement testing portion of this program was to substantiate the design approaches and to obtain design allowable information in those instances where existing data did not exist.

Table 7-1 summarizes the subelement testing program. In addition to those tests listed, numerous minor tests were performed to determine basic properties of joining systems.

The total testing program was modified somewhat as the program progressed in order to keep pace with the panel parametric and predesign studies.

7.2 JOINING AND FASTENING INVESTIGATIONS

This portion of the program was intended to investigate the characteristics of various joining techniques applicable to the selective reinforcement of metal structure with composite material.

When the parametric study revealed that the optimum configuration for the fuselage panel consisted of boron/aluminum hat sections attached to a titanium skin, methods of joining the two materials were investigated.

The two methods which were originally envisioned were spot brazing and bonding with polyimide adhesive. Accordingly, the subelement specimens were planned using those processes.

7.2.1 SPOT BRAZING. The method of assembly considered first was spot brazing. This process was initially investigated on Air Force Contract F33615-70-1460. The brazing process consists of joining the two materials which have been copper plated by means of a standard resistance welding machine.

The initial work on this program consisted of fabrication of two sets of spot brazed specimens. The first set had 2 spots and the second set of a 4 spot pattern. The initial set of 14 specimens was inspected using ultrasonic techniques. The C-scan showed some variability in the apparent spot braze area and two of the specimens were rejected. The specimens were then tested at room temperature and at 589K (600F).

Table7-1. Subelement Testing Summary

TEST	TEST SPECIMEN	DRAWING NUMBER	TEST TEMPERATURE	TEST METHOD	NUMBER OF SPECIMENS	INSTRUMENTATION	COMMENTS
Braze Lap	Single Lap	72C0065-1 & -2	162 K (-170F) RT & 589K (600F)	Tensile Test Machine	36	Load Deflection	RT and 600F completed -170F deleted
Joint Fatigue	Single Lap Shear Spot Join	72C0099	RT 589 K (600F)	Fatigue Machine	18	Cycles to Failure	
Joint Creep	Single Lap Shear Spot Join	72C0099	589 K (600F)	Creep Machine	6	Deflection	Cumulative Creep Simulation
Panel Stiffener Crippling	Short Column	72C0067	589 K (600F)	Compressive Test	6	Load Deflection	
		72C0068	RT	Compressive Test	6	Load Deflection	
Stringer Joint	Compres-sion	72C0079	589 K (600F)	Standard Test Machine	2	Load Deflection	
Stringer Joint	Tension	72C0078	338 K (150F)	Standard Test	2	Load Deflection	
Spot Joined Lap Shear	Single Lap Shear	—	RT 394 K (250F) 589 K (600F)	Tensile Test Machine	18	Load Deflection	
Adhesive Bonded Lap Shear	Single Lap Shear	—	RT 394 K (250F) 589 K (600F)	Tensile Test Machine	12	Load at Failure	
Development Crippling	Short Column	—	RT	Standard Test Machine	4	Load at Failure	End potting testing
Development Crippling	Short Column	—	589 K (600F)	Standard Test Machine	1	Load at Failure	Part from previous program
Spot Brazed Rivet Reinforcement	Lap Shear	—	RT 589 K (600F)	Tensile Test Machine	12	Load at Failure	

The results of this testing are shown in Table 7-2. Significant observations of these data include the rather large scatter in both the room temperature and 589K (600F), and the lack of correlation between the apparent shear area and shear strength. An attempt was made to correlate the failure load and the shear area found in each specimen. There are two zones in each spot which are found in the joints after shear testing at room temperature. There is an inner zone in which the failure occurs in the surface layer of aluminum in the composite. There is in most cases an outer zone which surrounds the inner zone in which the failure occurs in the braze metal. There appeared initially to be some correlation between the area of the outer zone and the shear strength of the joint but this was soon found to be inconclusive.

The 589K (600F) specimens show only the initial inner zone failure, the outer zone having been oxidized and destroyed prior to testing. Here again there is no apparent correlation between the measured shear area and the strength of the joint.

A second set of specimens with 4 spots was prepared, inspected and tested. In this case, 4 each of the specimens were tested at room temperature, 394K (250F) and 589K (600F). The results of these tests are shown in Table 7-3. Here again we note the very large scatter and the low values at 589K (600F).

Figure 7.1 is a plot of data from Table 7-3 and even more graphically shows the large scatter. No attempt was made to plot shear stress as the variation on apparent shear area gave even more scatter in the stress values.

As a result of this work, it was concluded that the spot brazing process did not have sufficient strength or consistency to permit its use. Alternate methods for attachment were therefore investigated.

7.2.2 SPOT BRAZE RIVET REINFORCEMENT SPECIMENS. As part of the task of designing a typical stringer splice, it became necessary to determine a method of introducing fastener loads into the unidirectional boron/aluminum stringers.

Previous experience with mechanical fasteners in U.D. boron/aluminum showed that the use of an adhesively bonded titanium washer through which fastener is installed will serve to distribute the fastener load over a larger area and avoid a shear out failure of the boron/aluminum. It was calculated for the stringer splice that, due to the low shear strength of boron/aluminum, the shear out load of a single 0.55 cm (1/8 in) rivet at 589K (600F) would be in the vicinity of 534 N (120 lb). In order to make an efficient joint, it was necessary to obtain individual rivet joint strengths of 2890 N (650 lb) or more.

It was therefore decided that the most logical course to pursue would be some variation of the bonded washer technique. One method chosen was the attachment of titanium

Table 7-2. Ambient and Elevated Temperature Tests of Lap Shear Joint Double Spot Braze

Sample	Ultimate Load		Test Temperature	
	N	(lbs)	K	(F)
1	4106	(923)		RT
2	3852	(866)		
3	5694	(1280)		
4	4902	(1102)		
5	6139	(1380)		
6	4279	(962)		RT
7	1001	(225)	589K	(600F)
8	1081	(243)		
9	463	(104)		
12	832	(187)		
13	707	(159)		
14	1001	(225)	589K	(600F)

Load Rate — Crosshead Speed 0.13 cm (0.050 in)/minute

Time at Test Temperature - 20 minutes

Table 7-3. Ambient and Elevated Temperature - Tests of Lap Shear Joint - Quad Spot Braze

Sample	Ultimate Load		Test Temperature	
	N	(lbs)	K	(F)
15	5293	(1190)		RT
18	5418	(1218)		RT
21	4782	(1075)		RT
24	6530	(1468)		RT
16	7762	(1745)	394K	(250F)
19	2749	(618)	394K	(250F)
22	6539	(1470)	394K	(250F)
25	4195	(943)	394K	(250F)
17	979	(220)	589K	(600F)
20	Test Error		589K	(600F)
23	53	(12)	589K	(600F)
26	1121	(252)	589K	(600F)

Elevated temperature soak time at temperature - 20 minutes.

Load Rate = Crosshead speed setting of 0.13 cm (0.050 in) /minute.

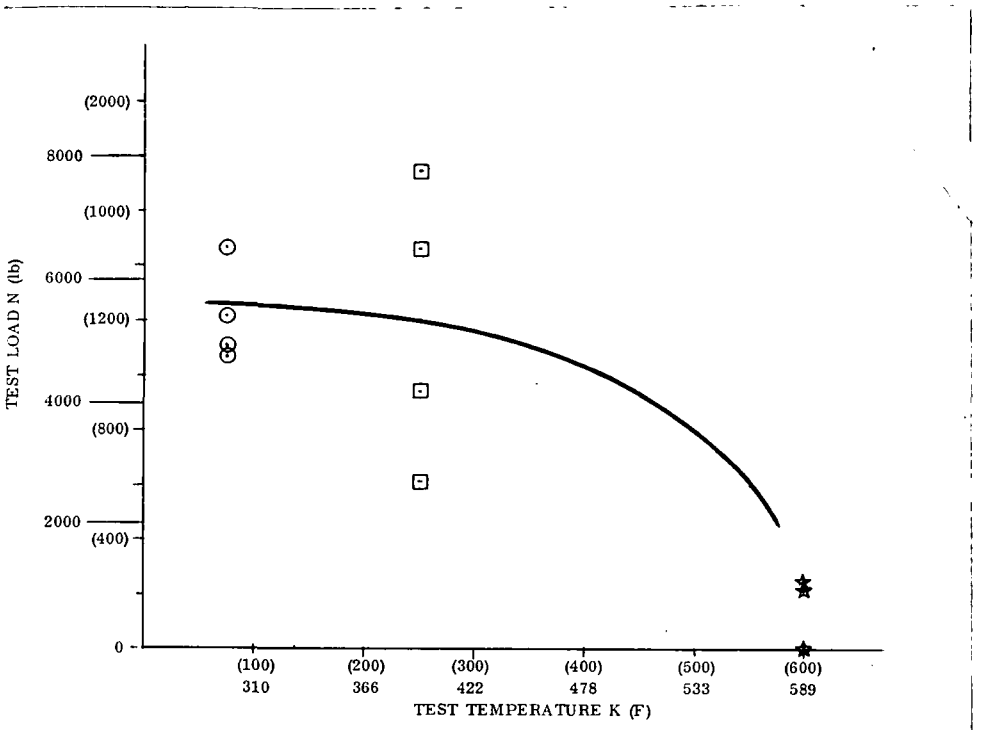

Figure 7.1. Shear Strength vs Temperature 4 Spot Specimens.

doublers to the boron/aluminum by means of spot brazing. A group of 12 specimens were fabricated, inspected and tested. Six of the specimens were tested at room temperature and 6 at 589K (600F). Table 7-4 gives the results of the testing. It is evident from the test results and from examination of the failed specimens that the spot brazed joint failed to provide adequate attachment of the boron/aluminum. The failure load of the high temperature specimens was about 1/3 of the required load and only about 75% better than the strength of the basic boron/aluminum. An examination of the surfaces of the spot brazed joint reveals an oxidized surface which is typical of the surface of other 589K (600F) spot braze tests. As a result of this testing, it was decided that other methods must be pursued.

7.2.3 ADHESIVE BONDING. Adhesive bonding utlizing polyimide adhesives had been considered an alternate system for joining titanium and boron/aluminum. A group of PI bonded lapshear specimens were fabricated and tested. After reviewing the available adhesive systems, Hexcel 951 was chosen for this test because of availability and past experience.

The results of testing 12 specimens are shown in Table 7-5. From this testing, it has been concluded that this material would be acceptable as a structural adhesive for use on this program.

Table 7-4. Cherry Riveted (NAS 1398C) Lap Shear Tests — Boron Aluminum and Titanium Sheet

Sample	Loads		Failure Mode	Test Temperature	
	N	(lbs)			
1	3327	748	Rivet Shear	Room	
2	3385	761			
3	3510	789			
4	3470	780			
5	3452	776			
6	3479	782	Rivet Shear	Room	
	3434	772 Avg.			
7	845	190	Sht. Shear Fail.	589K	(600F)
8	1005	226			
9	979	220			
10	783	176			
11	1001	225			
12	983	221	Sht. Shear Fail.	589K	(600F)
	934	210 Avg.			

Elevated Temperature soak time wo minutes @ temperature

Load Rate = 0.13 cm (0.050 in)/minute crosshead speed

Table 7-5. Hexcel 951 Polyimide Lap Shear Specimens

Sample	Area		Ultimate Load		Stress		Test Temperature	
	cm^2	(in^2)	KN	(lbs)	KN/m^2	(kpsi)	K	(F)
A1	2.56	(.398)	5.61	(1262)	21.8	(3.17)	Ambient	
A2	2.57	(.399)	5.67	(1275)	22.0	(3.20)		
A3	2.62	(.407)	5.50	(1238)	20.9	(3.04)		
A4	2.58	(.400)	5.48	(1232)	21.2	(3.08)	Ambient	
					21.5	(3.12) Avg.		
A5	2.36	(.366)	5.38	(1210)	22.8	(3.31)	394K	(250F)
A6	2.43	(.377)	5.47	(1223)	22.3	(3.24)	394K	(250F)
A7	2.50	(.389)	4.75	(1068)	18.9	(2.75)	394K	(250F)
A8	2.58	(.401)	5.03	(1130)	19.4	(2.82)	394K	(250F)
					20.8	(3.03 Avg.		
A9	2.49	(.386)	2.44	(547)	9.7	(1.42)	589K	(600F)
A10	2.33	(.362)	2.50	(563)	10.7	(1.56)	589K	(600F)
A11	2.46	(.382)	2.49	(560)	10.1	(1.47)	589K	(600F)
A12	2.40	(.372)	2.35	(480)	8.8	(1.29)	589K	(600F)
					9.8	(1.43) Avg.		

Note 1. Load Rate = Crosshead speed of 0.13 cm (0.050 in)/minute
Note 2. Soak Time at temperature equals 20 minutes

No additional work was accomplished on PI bonding as a decision had been made to use a different joining system.

7.2.4 SPOT JOINING. A third attachment method was available at the start of this program but was not initially proposed due to the lack of processing parameters and test data. The process had been discovered several years previously and consisted of the direct attachment of boron/aluminum to titanium by means of a diffusion bond made with a resistance spot welder. Although not technically correct, this process had been called spot welding. A more accurate description of the process is spot diffusion bonding and for simplicity it has been called here spot joining.

More recent experience with this process has shown that high quality, high strength, consistent joints can be made. Parallel work on another program has shown that high temperature strengths were good.

It was decided to further explore this attachment method using material gages similar to those needed on this program.

A series of 24 lap shear spot joined specimens were fabricated using two gages of boron/aluminum 0.68 mm (0.027 in) and 0.86 mm (0.034 in) jointed to 0.01 mm (0.036 in) titanium. These specimens were tested at 3 temperatures. These results are shown in Table 7-6.

Figures 7.2 and 7.3 show these specimens after testing.

As a result of this testing, spot joining was selected as the primary joining process for this program.

Figure 7.4 summarizes the static strength of the spot joined specimens,

7.2.4.1 Joint Fatigue and Creep Specimens. As a result of the change in primary attachment method from that previously planned, the fatigue and creep specimens were redesigned. The configuration was selected because it is essentially identical to a standard titanium spotweld fatigue specimen used previously. Figure 7.5 shows a completed specimen.

The plan for testing was to subject half of the eighteen fatigue specimens to 3-load levels at room temperature and the remainder at 3-load levels at 589K (600F). The six creep specimens were to be tested at several load intensities for a maximum of 200 hours.

Fatigue test data is summarized in Figures 7.6 and 7.7.

Table 7-6. Lap Shear Strength Boron/Aluminum Spot Joined

Specimen No.	B/Al Gage		Ultimate Load		Average Load		Test Temperature	
	mm	(in.)	N	(lbs.)	N	(lbs.)	K	(F)
01A	0.86	(0.034)	5604	(1260)				RT
02A	0.86	(0.034)	5338	(1200)	5179	(1164.3)		RT
06A	0.86	(0.034)	4595	(1033)				RT
01B	0.68	(0.027)	3172	(713)				RT
02B	0.68	(0.027)	3202	(720)	3556	(799.6)		RT
06B	0.68	(0.027)	4341	(976)				RT
07A	0.86	(0.034)	5440	(1223)			394	(250)
08A	0.86	(0.034)	6552	(1473)	5805	(1305)	394	(250)
09A	0.86	(0.034)	5916	(1330)			394	(250)
07B	0.68	(0.027)	4070	(910)			394	(250)
08B	0.68	(0.027)	5694	(1280)	4152	(933.3)	394	(250)
09B	0.68	(0.027)	3514	(790)			394	(250)
03A	0.86	(0.034)	4590	(1032)			589	(600)
04A	0.86	(0.034)	4742	(1066)	4666	(1049)	589	(600)
03B	0.68	(0.027)	3469	(780.5)			589	(600)
04B	0.68	(0.027)	3700	(832)	3254	(731.6)	589	(600)
05B	0.68	(0.027)	2588	(582.5)			589	(600)

Titanium gage 0.91 mm (0.036 in)

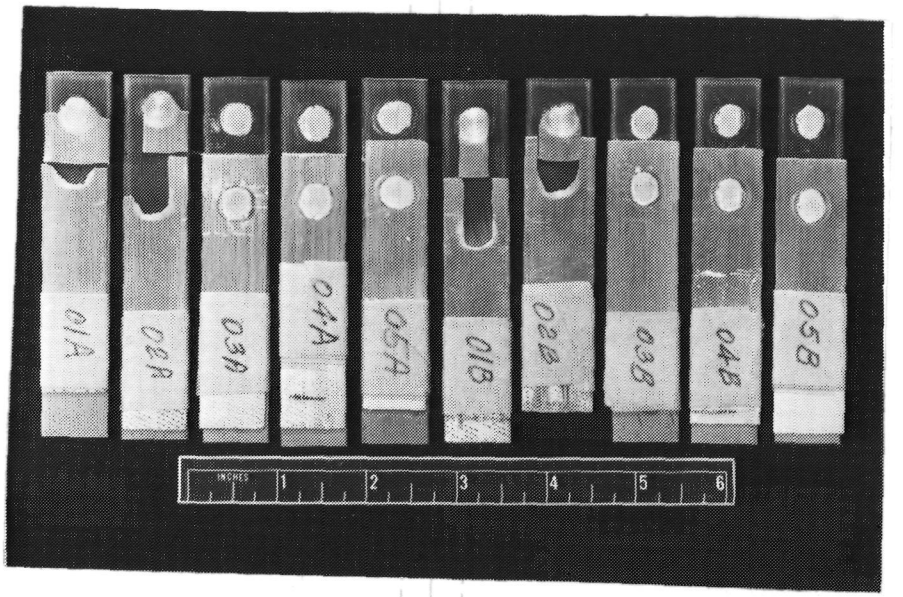

Figure 7.2. Boron/Aluminum-Titanium Spot Joined Specimens after Testing.

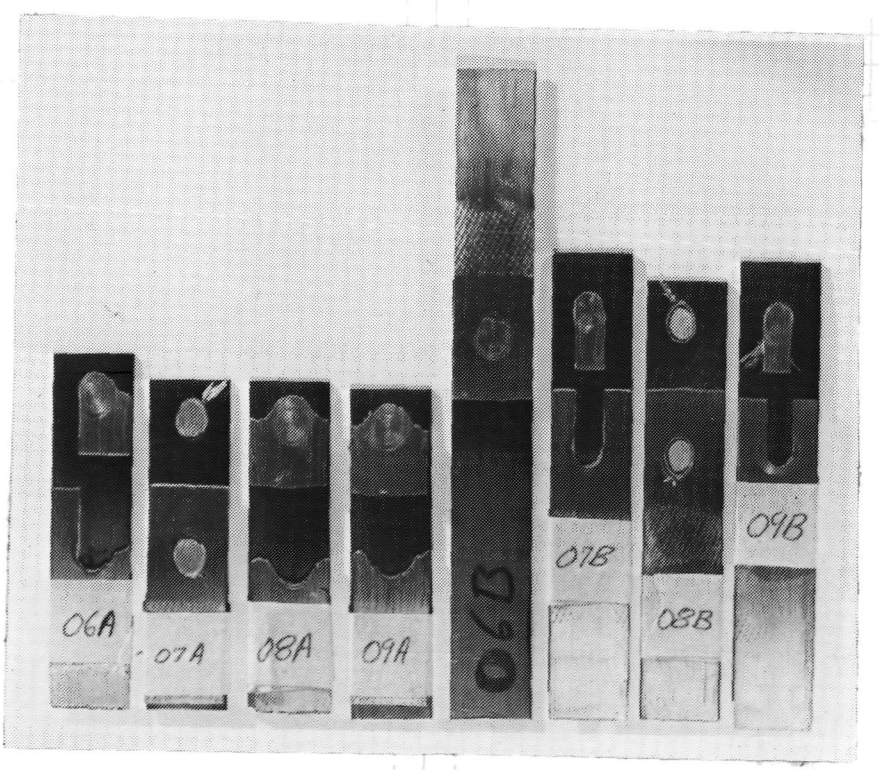

Figure 7.3. Appearance of Spot Joined Boron/Aluminum-Titanium Lap Shear Specimens after Testing.

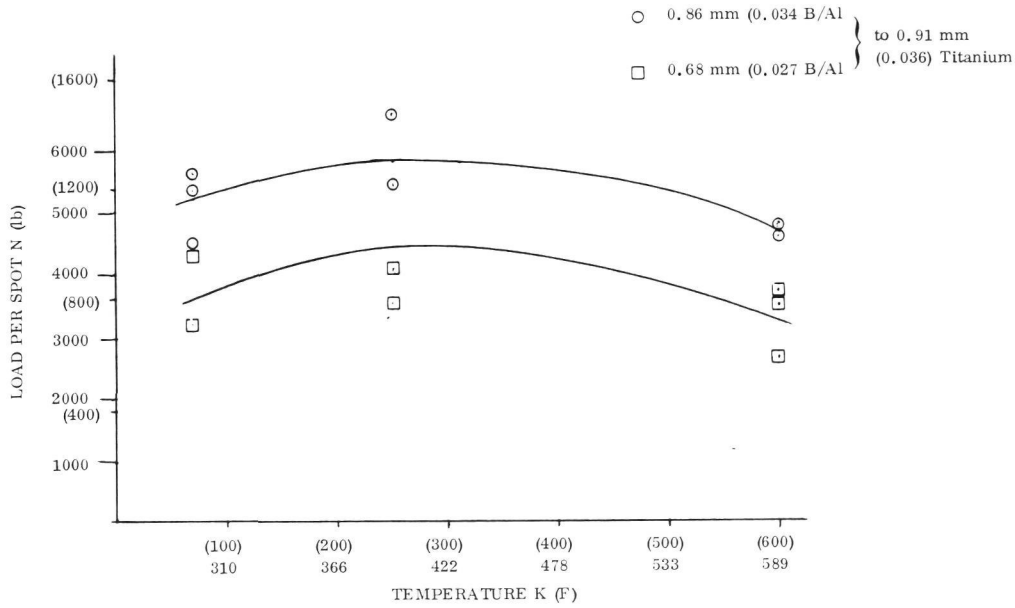

Figure 7.4. Boron Aluminum-Titanium Spot Joining Lap Shear Strength.

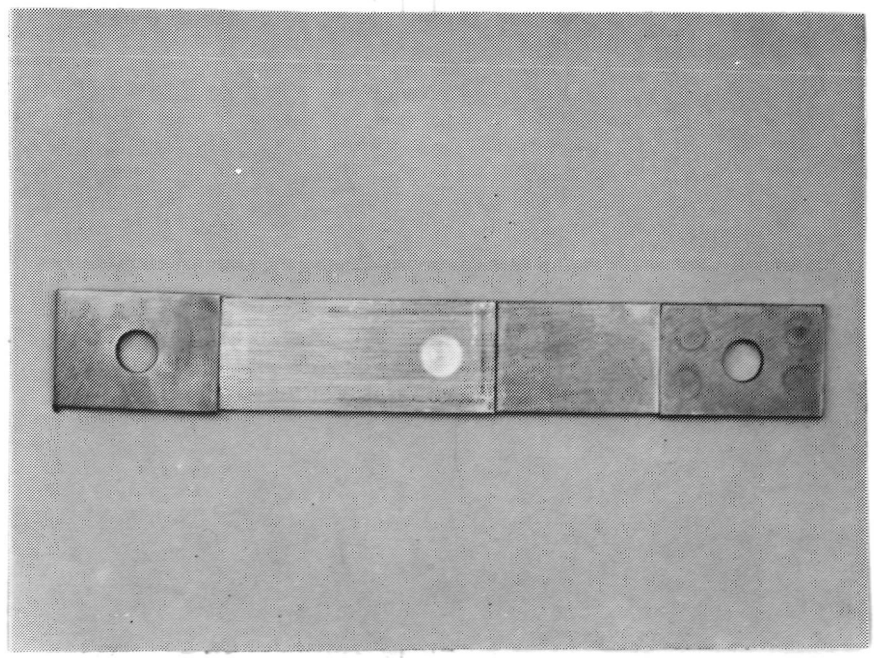

Figure 7.5. Boron/Aluminum-Titanium Spot Joined Fatigue and Creep Specimen.

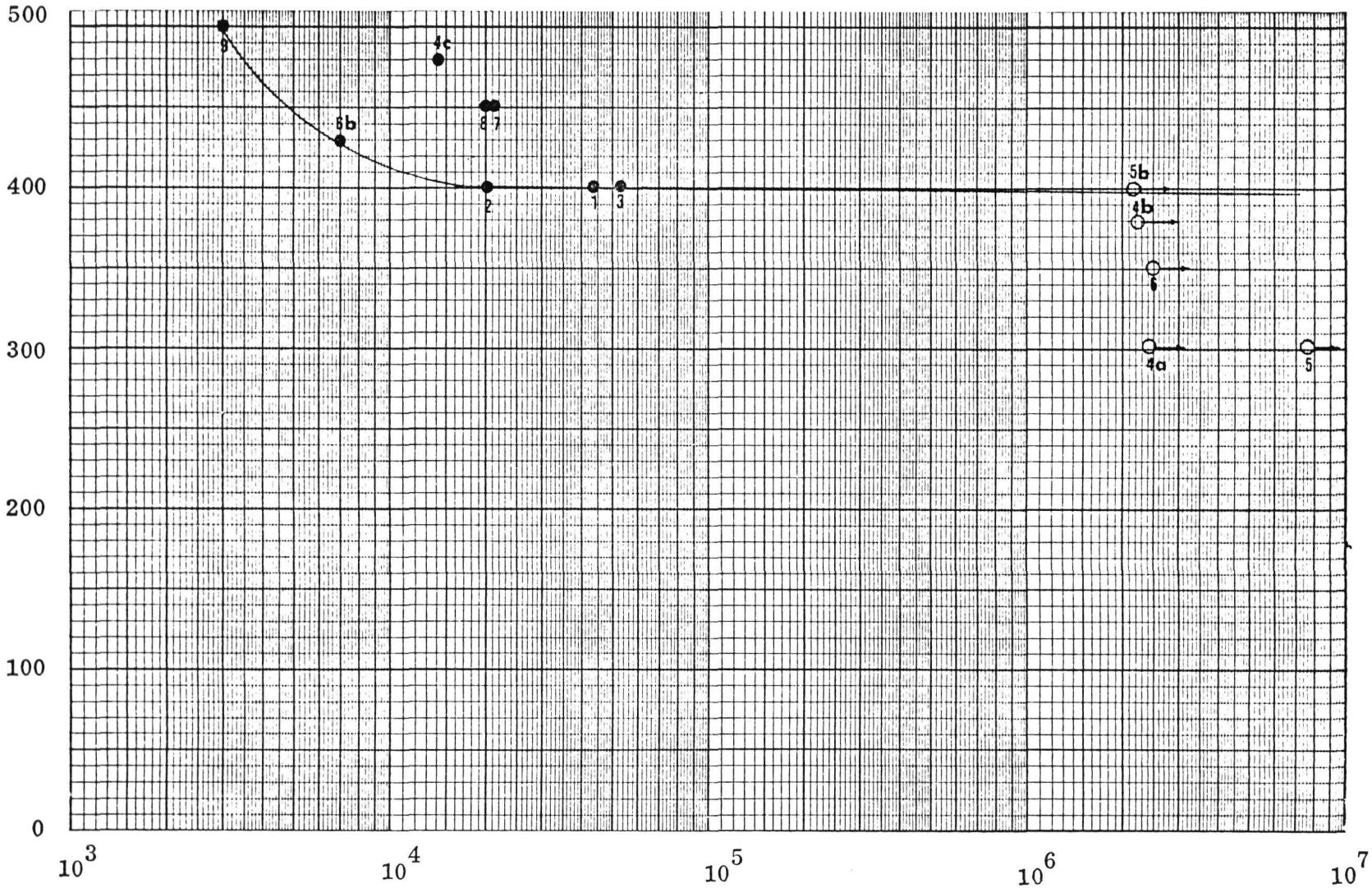

Figure 7.6 . Room Temperature Fatigue Strength
Spot Joined Lap Shear Specimens. 0.027 B/Al 0.036 Ti

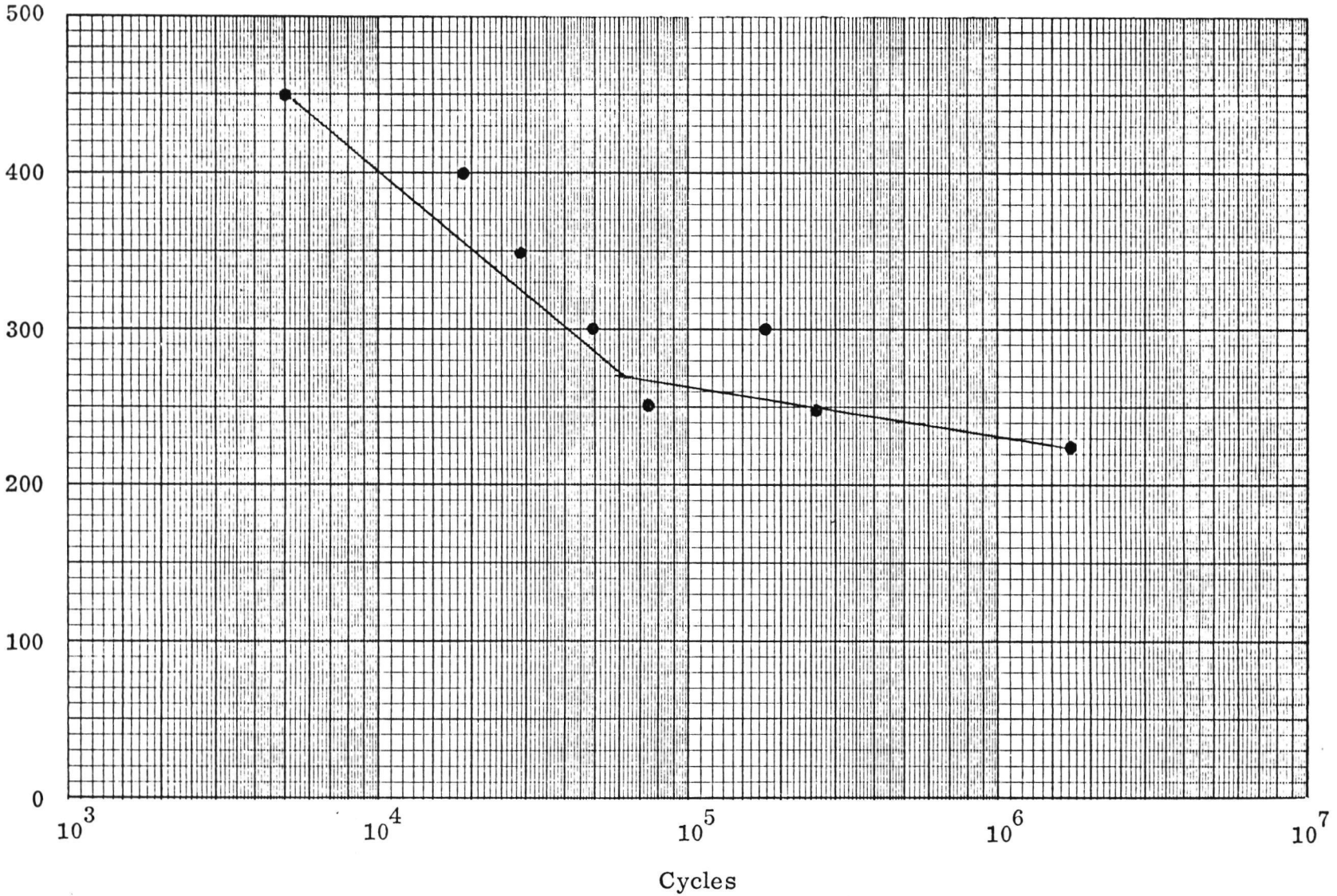

Figure 7. 7 . 600F Fatigue Strength Spot Joined Lap Shear Specimens.
0.027 B/Al to 0.036 Ti.

Fatigue testing results were better than initially expected. Room temperature fatigue values were about 50% of the static strength. The 589K (600F) fatigue data shows a definite creep effect but exhibits strengths in excess of 30% of static values. The creep testing is summarized in Figure 7.8. Here we find a useful strength of 890 N (200 lb) at 589K (600F) for over 200 hours of exposure.

Before the joining method could be used, it was necessary to determine something of the nature of the joint itself, and so several metallurgical specimens were prepared. Figure 7.9 shows a photomicrograph of a sectioned spot. The joint in question had previously undergone approximately 10^7 fatigue cycles at room temperature at loads up to 1780 KN (400 lb). Figures 7.10 and 7.11 are electron photomicrographs of sections of the joint at moderate and high magnification. They show the area between the aluminum and titanium where the intermetallic bond is formed. The prepared joints were scanned from end to end and showed the joint to be consistent throughout.

7.3 CRIPPLING SPECIMENS

7.3.1 DESIGN. The crippling specimens were intended to evaluate the local crippling strength of the compression panel stiffeners. An evaluation was to be made at both room temperature and the maximum operating temperature 589K (600F) which necessitated the use of two groups of specimens.

Convair Aerospace has standardized the use of an L'/ρ of 12 for crippling specimens as recommended by Peery (Ref. 4). For the section involved and using an effective end fixity of 3.6 results in a specimen length of 15.88 cm (6.25 in). The room temperature crippling specimens were patterned after previous examples and utilized Epon 934 epoxy end potting material.

The design of the high temperature specimen necessitated the investigation of methods to contain the end of the specimen and to provide the necessary fixity at 589K (600F). Two methods were investigated. The first consisted of substituting a more heat resistent material for the Epon epoxy. After screening available materials, Epoxylite was selected. Several attempts to cast this material around the ends of specimens resulted in poor bonds and cracked epoxy; therefore, the investigation was dropped.

A second method was tried wherein the end of the specimen was to be placed in a slotted steel block and Hexcel 901 foaming polyimide adhesive cured in the slots. This method proved very satisfactory and was utilized for the high temperature specimens.

7.3.2 FABRICATION. After a review of available forming techniques a decision was made to develop the technology to hot form boron/aluminum hat sections from sheet material. This process offered the potential of being the lowest cost method of producing unidirectional boron/aluminum shapes.

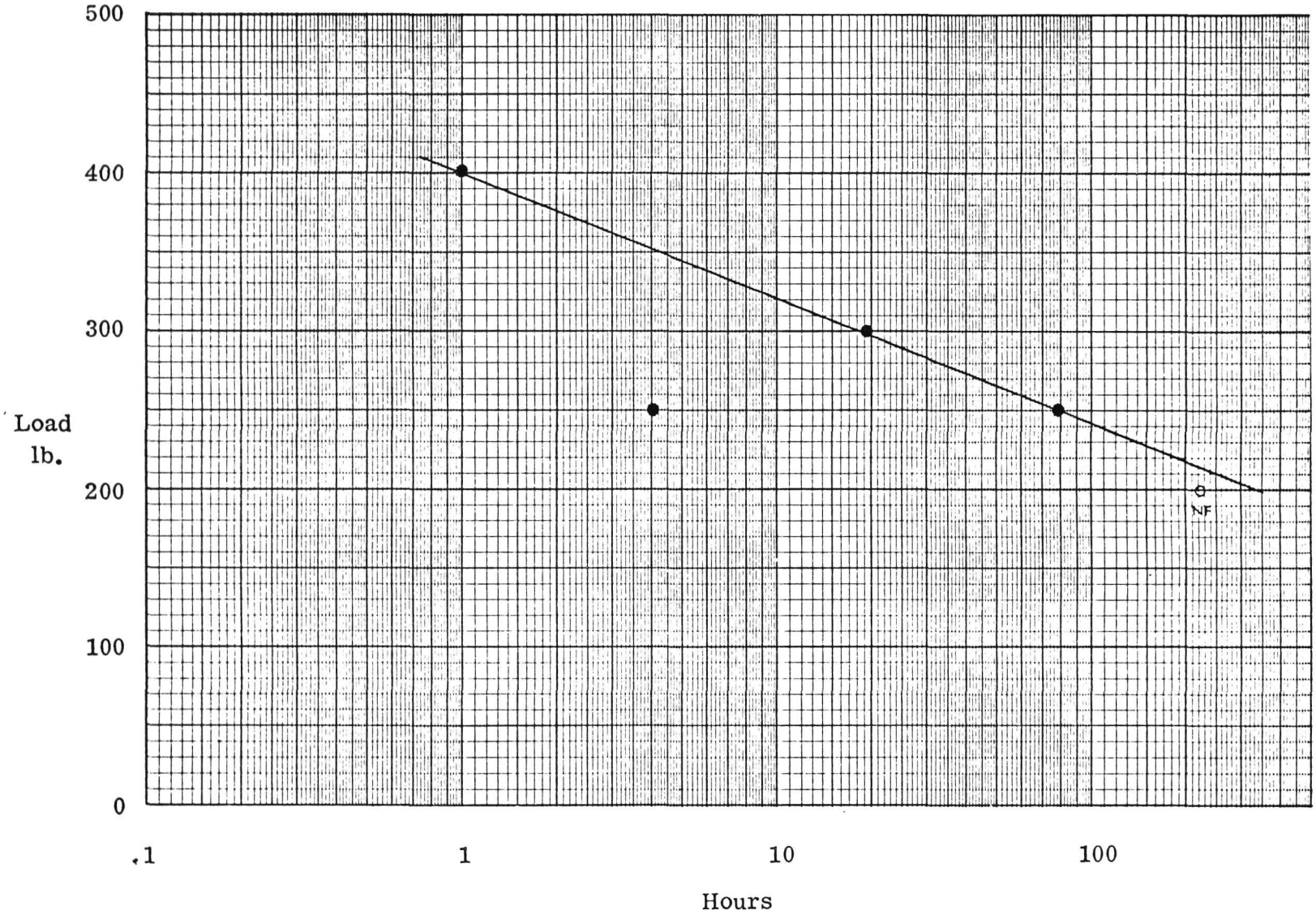

Figure 7.8. Creep Rupture Strength Spot Joined Lap Shear Specimens. 600F to 0.027 B/Al 0.036 Ti.

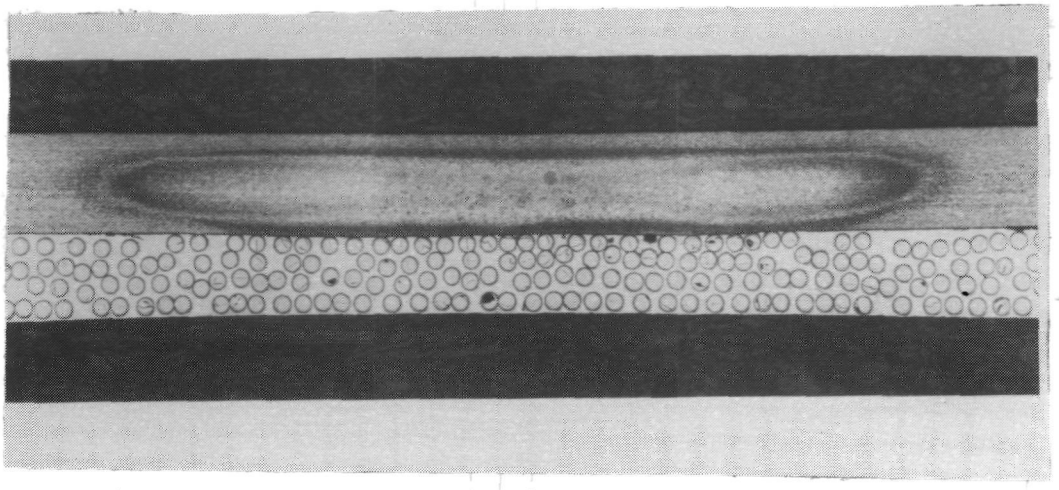

Figure 7.9. Photomicrograph at Sectioned Spot between Boron/Aluminum and Titanium (approx. 20X).

Figure 7.10. Electron Photomicrograph at Spot between Ti (lower) and B/Al (approx. 6,000X).

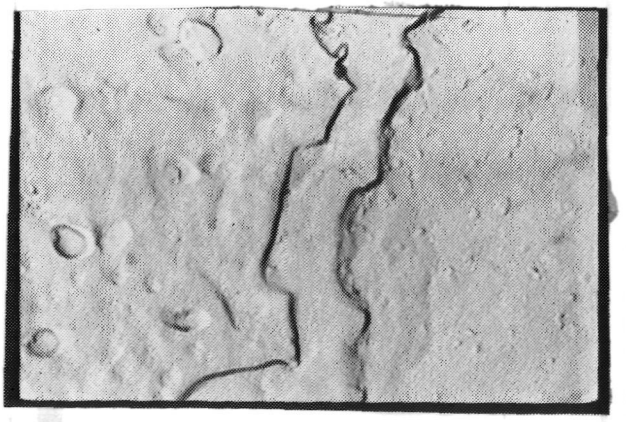

Figure 7.11. Electron Photomicrograph of Spot between Ti (left) and B/Al (approx. 22,000X).

7.3.2.1 Equipment and Tooling. The equipment used to fabricate the hats was a "Pneuco" pneumatic press brake of 311 KN (35 ton) capacity. The press was operated by foot treadle and forming rate was controlled by presetting a speed control valve or by adjustment of pressure on the foot treadle.

Heat was supplied to the tools by a "Honeywell" power cart and temperature controller. The Honeywell unit had six control circuits, each supplying 480 volts, 30 amps, 3 ϕ power. Figure 7.12 shows the tooling setup in the press. In order to reduce costs, an existing heated die holder was utilized. The die holder had 3 "Calrod" cartridge heaters imbedded in it. A 30 cm (12 in) long punch and Vee die were fabricated from hot rolled steel to suit the die holder. The tools were 90° matched dies and the punch was made in a "Gooseneck" shape to accommodate the narrow width of the hat. Indexing was accomplished by press fitting dowel pins in the Vee die which accommodated slots in the ends of the blank along the bend axis. (Initially the pins were placed in the punch but preliminary testing indicated handling of the blank with this particular hat configuration was difficult with the pins in the punch.)

Figure 7.12. Hot Forming Facilities (Neg. 11952B).

7.3.2.2 Fabrication Procedure. Prior to forming the hat sections, a series of bend tests were made with 2.54 cm x 6.4 cm (1.0 in x 2.5 in) specimens to establish forming conditions such as part heating method, tool temperature, part preheat time, forming rate, dwell time, and blank support or backup requirements.

The method selected to attain and monitor temperature is shown in Figure 7.13. Prior to placing the specimen on the die, the tools were covered with Q felt insulation and the die heated to 805K (990F). The punch attained a temperature of 639K (690F). The specimen and thermocouples backup were then placed between the punch and die and the insulation replaced. After 3 minutes, the temperatures stabilized at 700K (800F) — Specimen: 811K (1000F) — Die: 589K (600F) — Punch. All of the bend tests were then made by monitoring the temperature of the punch and die only.

7.3.2.3 Test Results. The formed hat is shown in Figure 7.14. After hot forming the parts were cleaned by vapor honing and penetrant inspected. Based on these tests, it was decided to employ the following forming conditions for the hat stringers.

Die temperature	811K (1000F)
Punch temperature	589K (600F)
Preheat time	5 minutes
Forming time	0.5 minutes
Dwell time	1.0 minute
Backup	0.63 mm (0.025 in) annealed stainless steel

The tools were modified by moving the indexing pins to accommodate a 18.8 cm (7.4 in) blank and six hat sections were formed with the above conditions. Figure 7.15 shows the completed sections.

Penetrant inspection revealed cracks ranging between 1.3 cm (1/2 in) and 3.8 cm (1-1/2 in) in length in some of the bends. Straightness and transverse flatness across the flanges was good. The parts had a very slight twist which could be removed with light finger pressure.

7.3.2.4 Evaluation. An analysis of the bend test data indicates that forming rate may be critical during hot forming. However, insufficient tests were run to draw conclusions. The intent of the tests was to establish forming conditions that would produce good parts rather than make a quantitative evaluation of forming parameters.

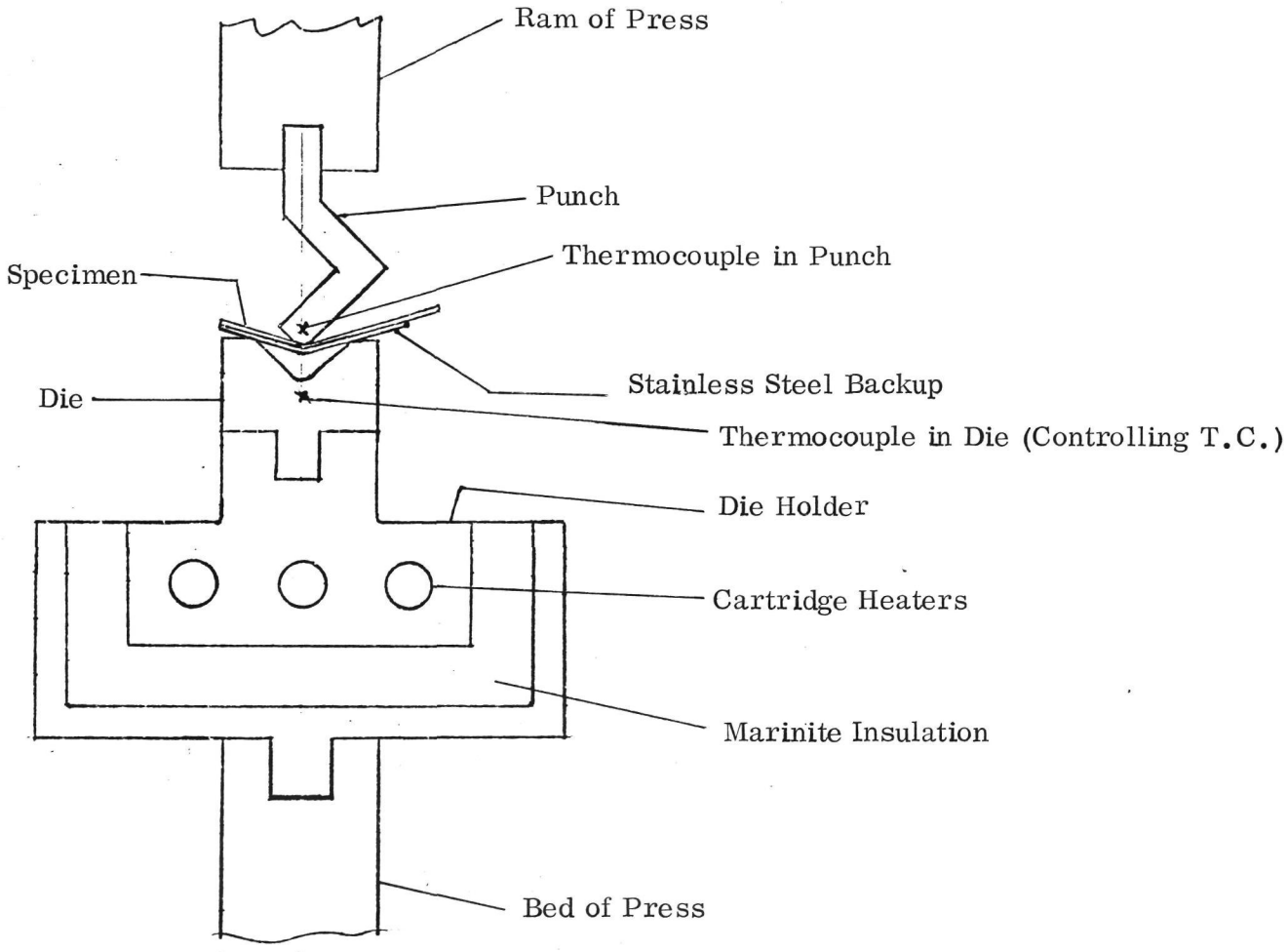

Figure 7.13. Diagram of Brake Arrangement.

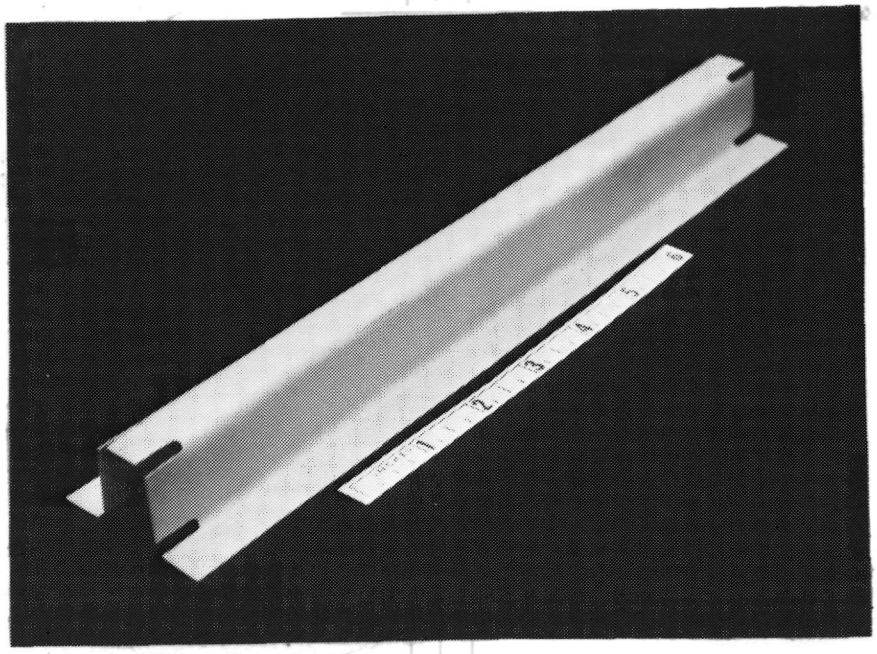

Figure 7.14. Hat Section After Forming and Cleaning.

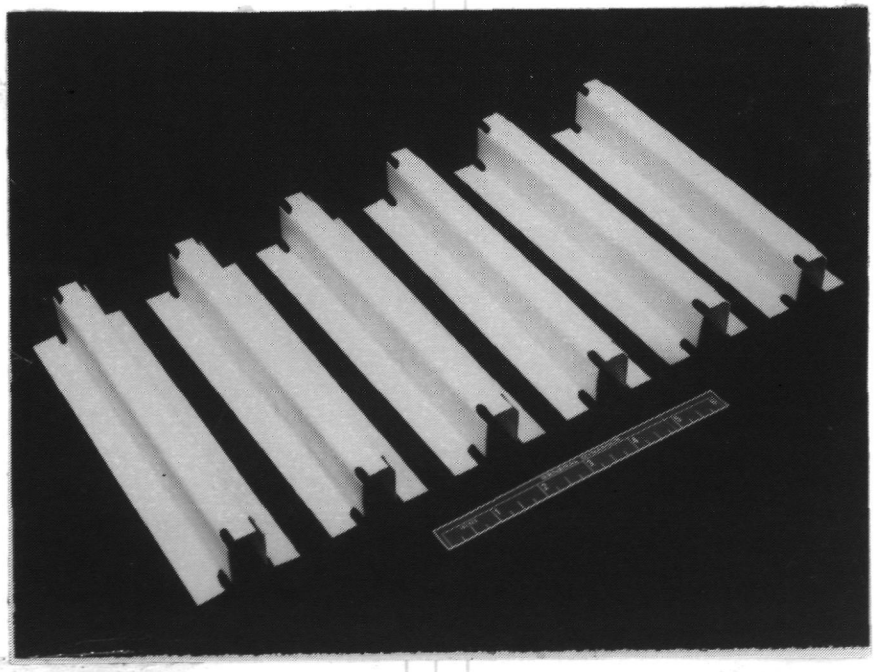

Figure 7.15. Group of Six Production Crippling Specimens.

The reason for obtaining some cracks in the parts was not readily apparent. Tool temperature variations in the six production parts were small [783K (950F) to 811K (1000F) on the Die and 519K (475F) to 560K (550F) on the Punch] and no correlation could be found between cracks and temperature.

To evaluate the cracks, photomicrographs were taken across the bend radius of Bend 3 of Part #2. Figure 7.16 shows two cross sections across the same radius. The specimen on the upper right side of Figure 7.16 was taken across the 1.8 cm (0.7 in) long crack. The specimen on the lower left side of Figure 7.16 was taken on an uncracked portion of the radius approximately 1.3 cm (1/2 in) away from the first specimen.

Figure 7.17 is a photomicrograph of the cracked radius, while Figure 7.18 shows the uncracked portion of the radius. The crack is 0.20 mm (0.008 in) deep. It can be seen that the orientation of the fibers varied considerably in the 1.3 cm (1.2 in) distance between the specimens. What appeared to be happening was that the fibers along some portion of the bend line are crowded together and touching. When this portion of the bend line was strained, the fibers were separated leaving a void between them which showed up as a crack. The data indicates that the most critical parameter in forming B/Al composites is the orientation of the boron fibers in the sheet material. The large number of striations in the outside surface of the radius was considered simply a widening of striations already present in the flat sheet. This can be seen clearly in Figure 7.19 which is a closeup plan view of a flat sheet. It appeared that an additional layer of aluminum on the outside of the sheet would greatly improve the surface finish of the blank and eliminate the problem with striations and cracking.

Figure 7.19 also shows the filaments in the outer layer to be wavy. To further identify this condition and to assess any damage to the material, an X-ray was taken of a 10.2 cm (4 in) length of hat section which had a 2.54 cm (1.0 in) long crack in one of the radii. The X-ray confirmed the wavy filaments and in addition indicated there were no broken or damaged filaments even along the crack. Specimens containing cracks were included for testing along with uncracked specimens.

Amercom Inc., the material supplier was contacted in regard to the wavy filaments and filament placement. It was ascertained that the panel from which the hats were made was one of several which suffered from filament wandering due to processing errors. They made assurances that all subsequent material would have closer control of filament spacing and straightness. They also agreed to increase the thickness of the surface aluminum on subsequent orders in order to minimize the potential of cracking.

Twelve crippling specimens were fabricated using new material with better filament control and with additional surface aluminum. The forming parameters were the same as previously developed. All parts formed satisfactorily with no cracks.

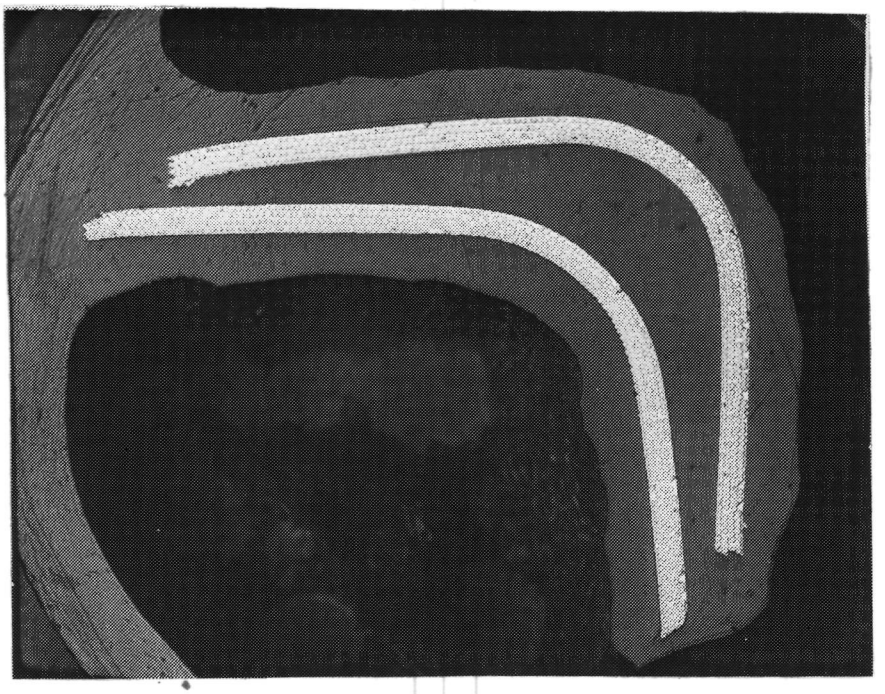

Figure 7.16. Cracked and Uncracked Specimens.

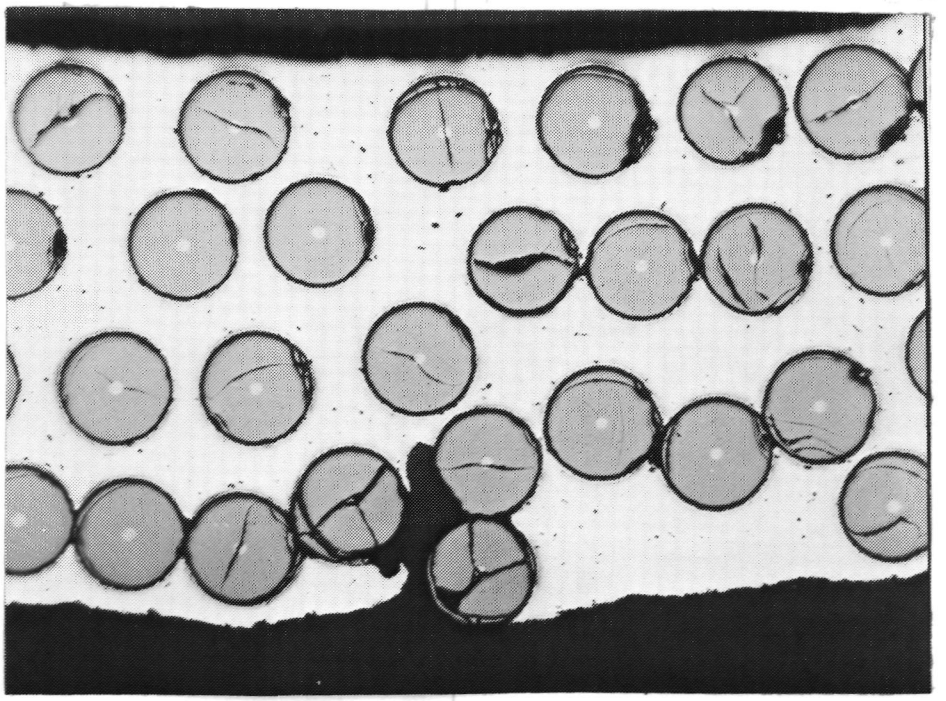

Figure 7.17. Photomicrograph of Cracked Corner.

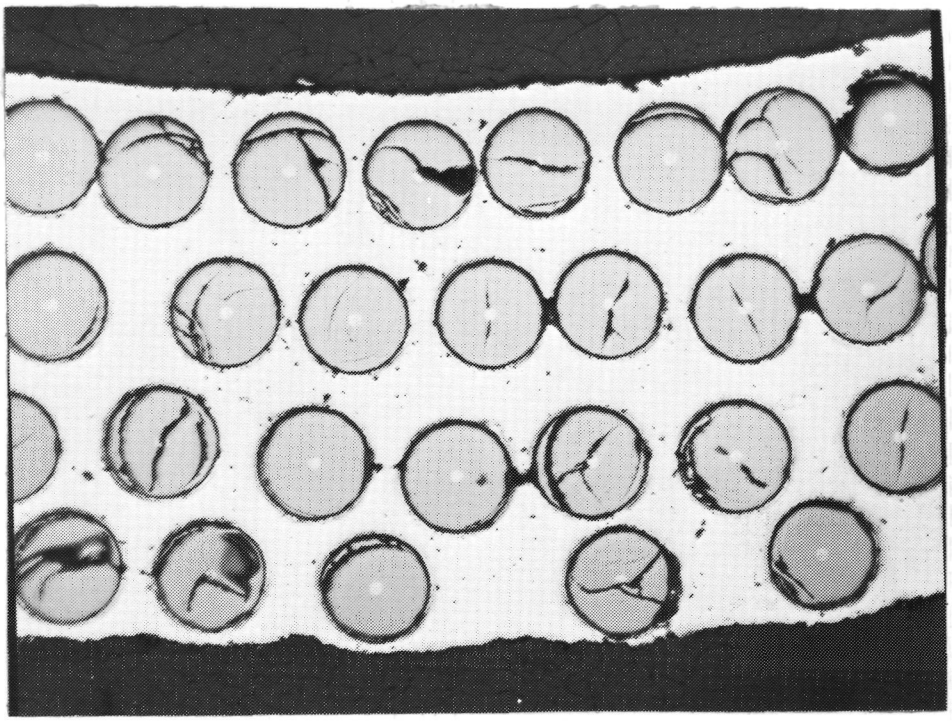

Figure 7.18. Photomicrograph of Uncracked Corner.

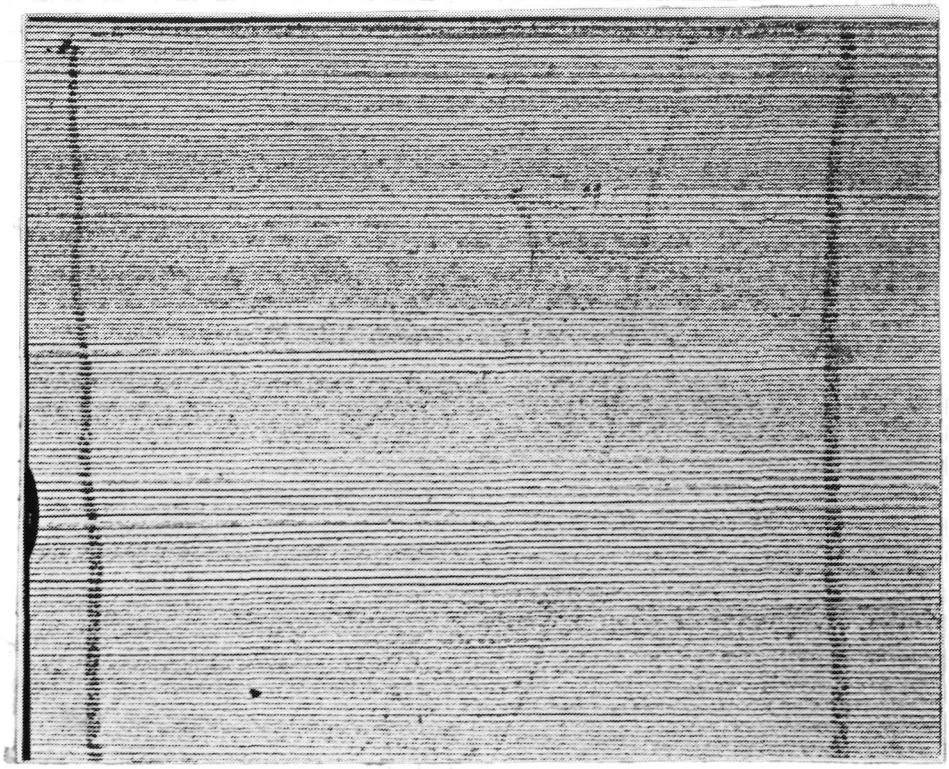

Figure 7.19. Surface of Boron Aluminum Sheet Showing Striations.

These parts were trimmed to length and had holes punched in the flanges for setup bolts. The boron/aluminum hats were then spot joined to the titanium skins by means of spot joining and rivets placed in the holes previously occupied by the setup bolts.

The ends of the specimens were prepared for testing by potting with Epon 934 or by being bonded into the steel end blocks with Hexcel 901 adhesive. Figures 7.20 and 7.21 show a typical room temperature crippling specimen.

7.3.3 CRIPPLING TESTING. Crippling testing was accomplished by means of a 533 KN (120,000 lb) Tinius Olsen Universal testing machine. Room temperature specimens were tested directly between the machine plattens while the 589K (600F) specimens were placed in a Pacific Scientific Electrically Heated Oven placed in the test machine.

All testing was accomplished at a loading rate of .13 cm (0.05 in/min).

Figure 7.22 shows 5 of the room temperature specimens after testing. Figures 7.23 and 7.24 show the general appearance of the buckles in two of the specimens. No evidence of spot joining failure were evident in any of the specimens.

Figures 7.25 and 7.26 show the high temperature specimens after testing. A close up of one of the specimens is shown in Figure 7.27. Here again no evidence of spot joining failure was evident on any of these specimens.

7.3.4 ANALYSIS OF CRIPPLING DATA.

7.3.4.1 Material Characteristics. The longitudinal and transverse stress-strain curves of UD boron/aluminum (0.0056 dia.) are shown in Figures 7.28 and 7.29. Basic material properties of UD boron/aluminum and 6Al-4V annealed titanium alloy are shown in Table 7-7. A crippling parameter

$$(b/t)\sqrt{F_{tu_{11}}/(E_{t_{11}}E_{t_{22}})}^{1/2}$$

was arbitrarily chosen for use in the presentation of UD boron/aluminum crippling analysis curves on log scale. This is analogous to the parameter

$$(b/t)\sqrt{F_{cy}/E}$$

used by Gerard (Reference 5) in the presentation of crippling data for aluminum alloys, magnesium alloys and stainless steel. The crippling parameter for boron/aluminum at room temperature is a constant and is shown in Table 7.7, and that at 589K (600F)

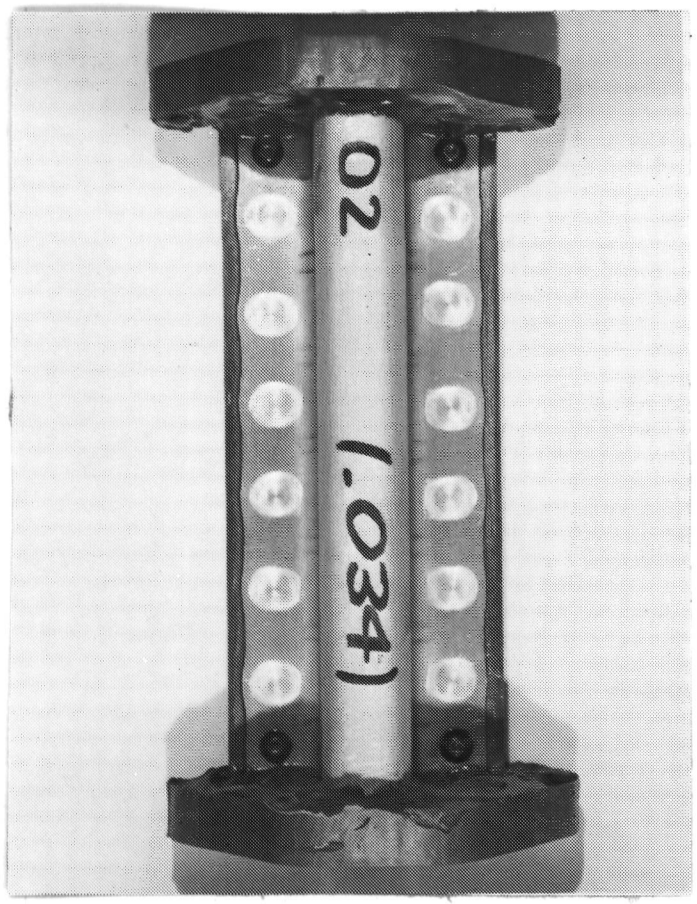

Figure 7.20. Stringer Side of Room Temperature Crippling Specimen.

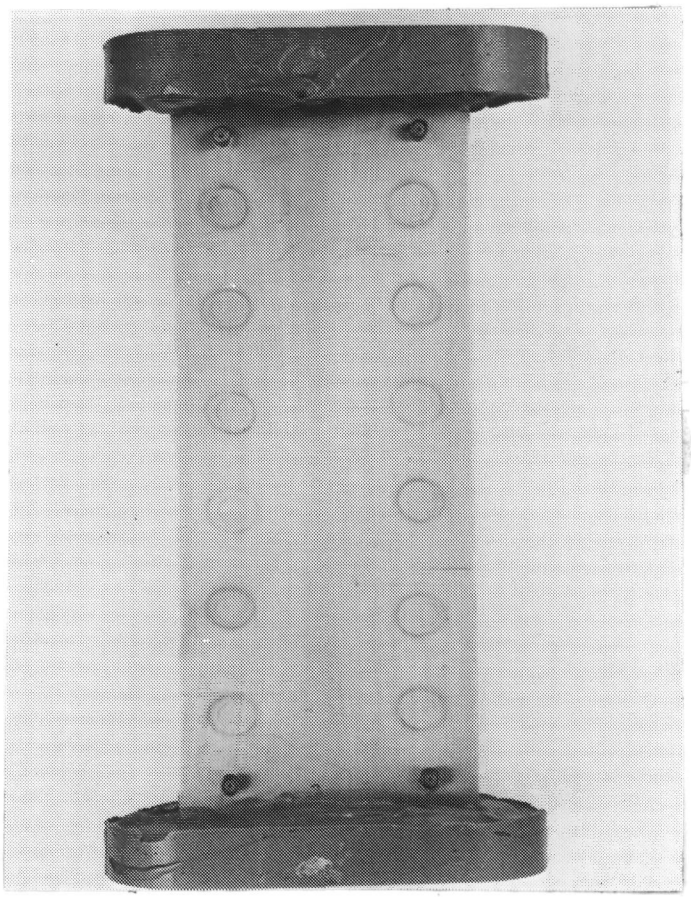

Figure 7.21. Skin Side of R. T. Crippling Specimen.

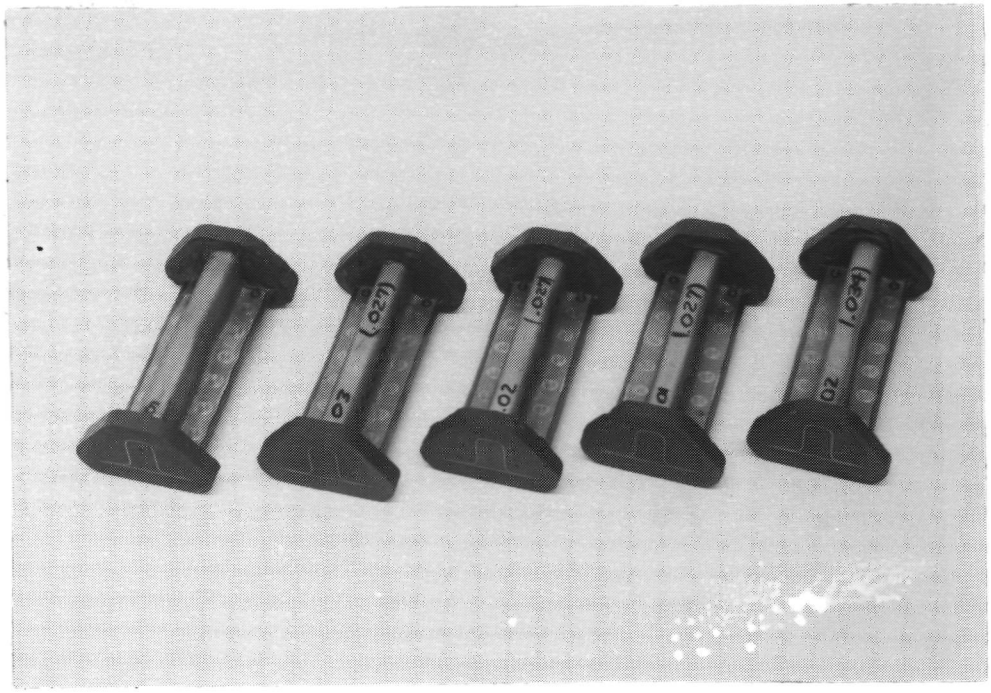

Figure 7.22. Room Temperature Crippling Specimen after Testing.

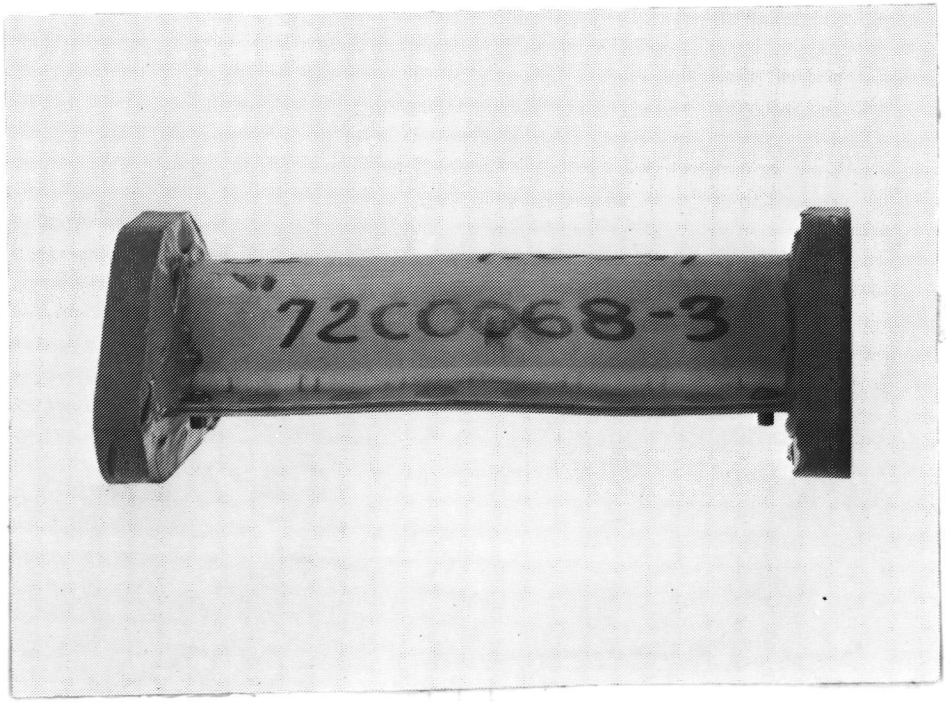

Figure 7.23. Buckled Shape of R.T. Crippling Specimen.

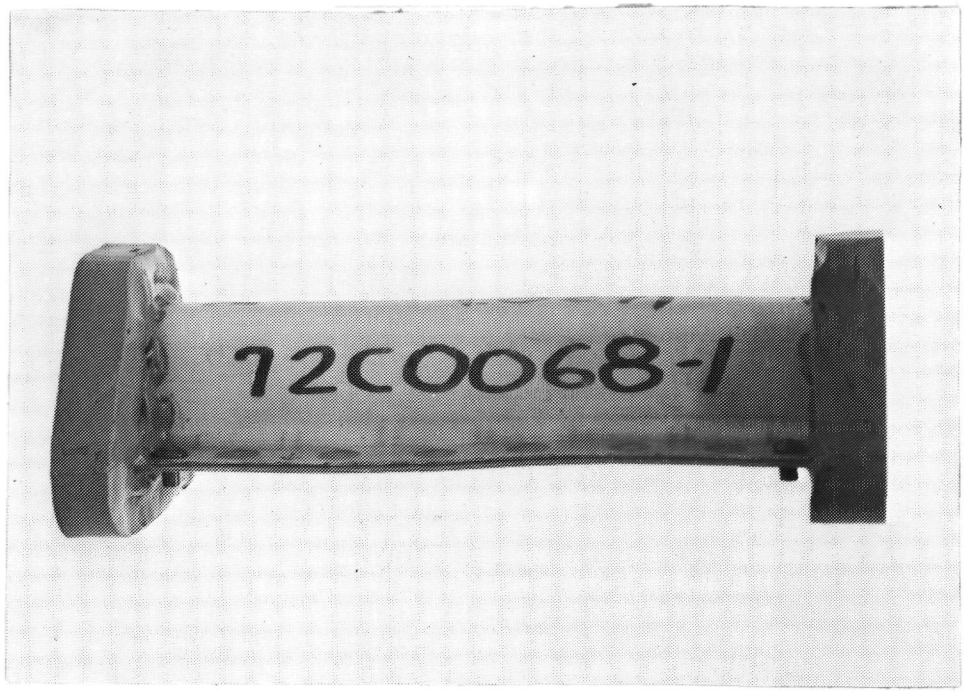

Figure 7.24. Buckled R. T. Crippling Specimen.

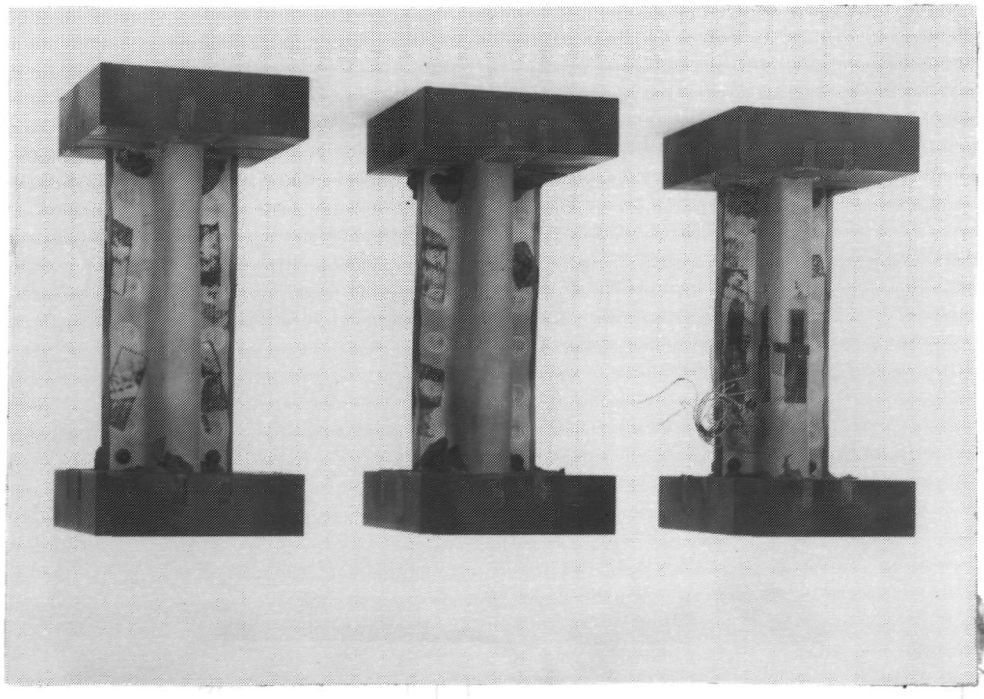

Figure 7.25. 72C0067-3 (0.034) Crippling Specimens.

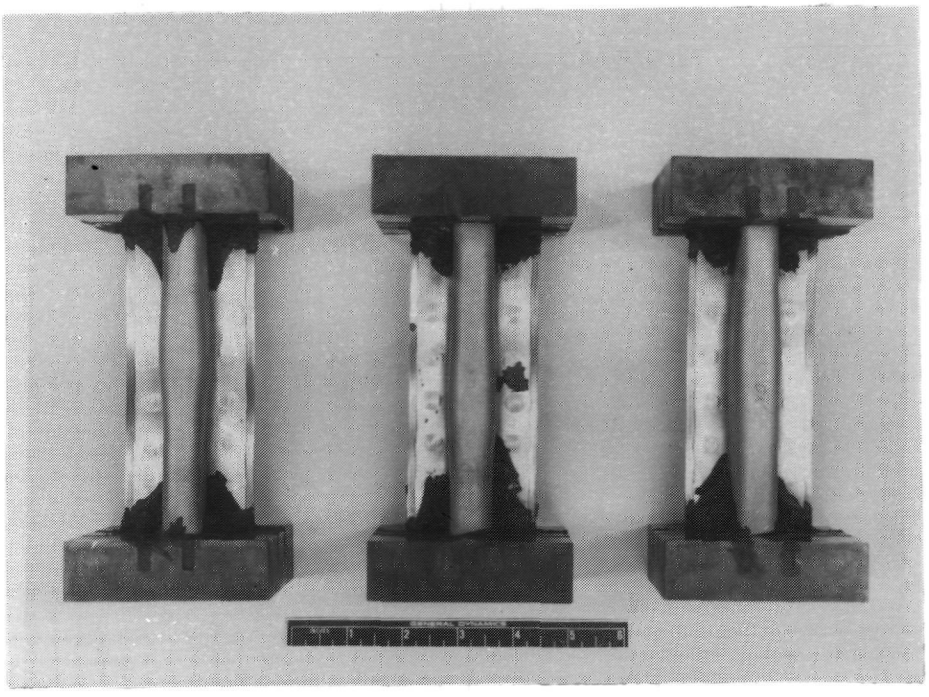

Figure 7.26. 72C0067-1 (0.027) Crippling Specimen after Testing.

Figure 7.27. Thin 0.027 Crippling Specimens after Test.

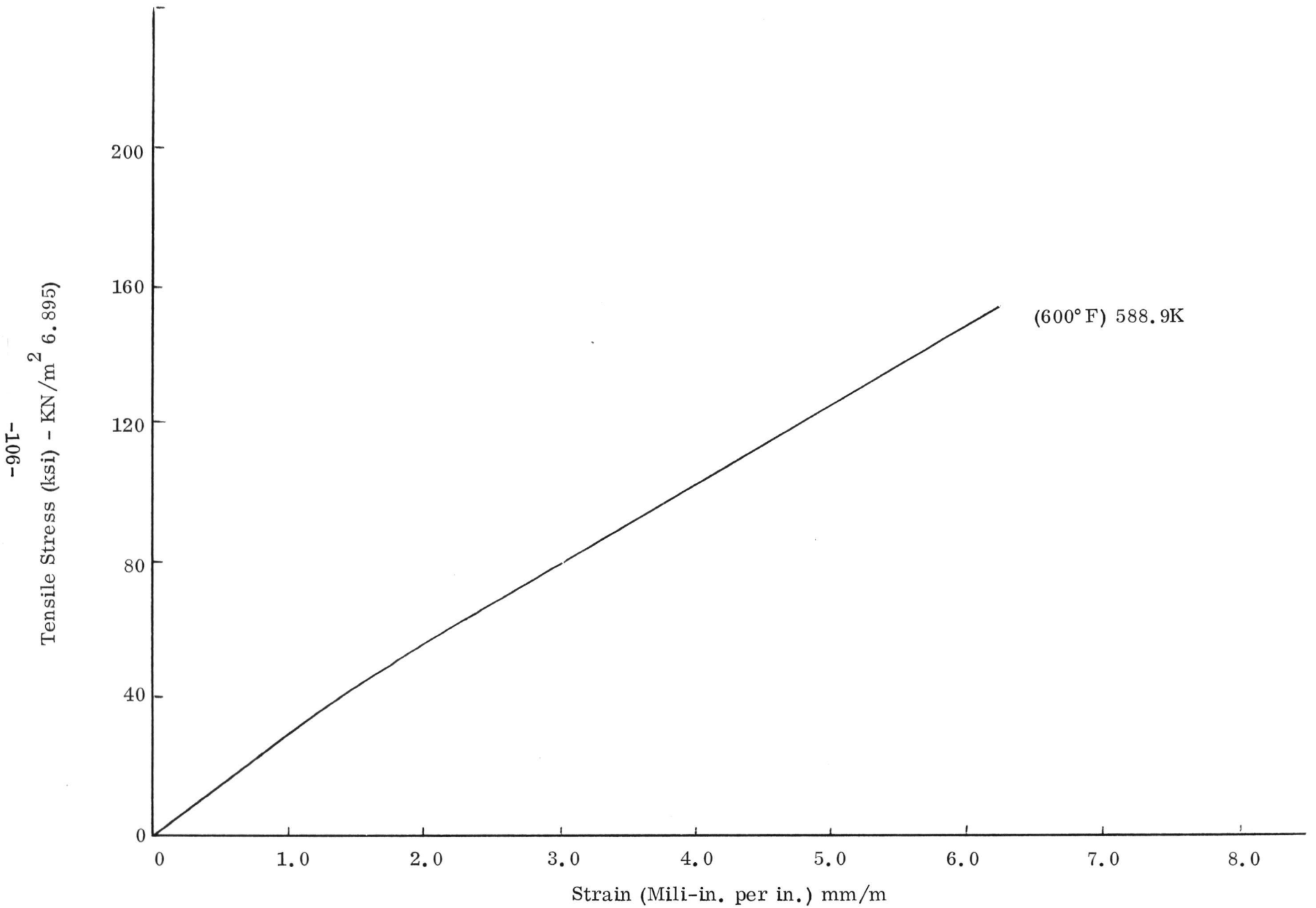

Figure 7.28. Longitudinal Tensile Stress Strain Curve for U.D. B/Al - 588.9K (600°F).

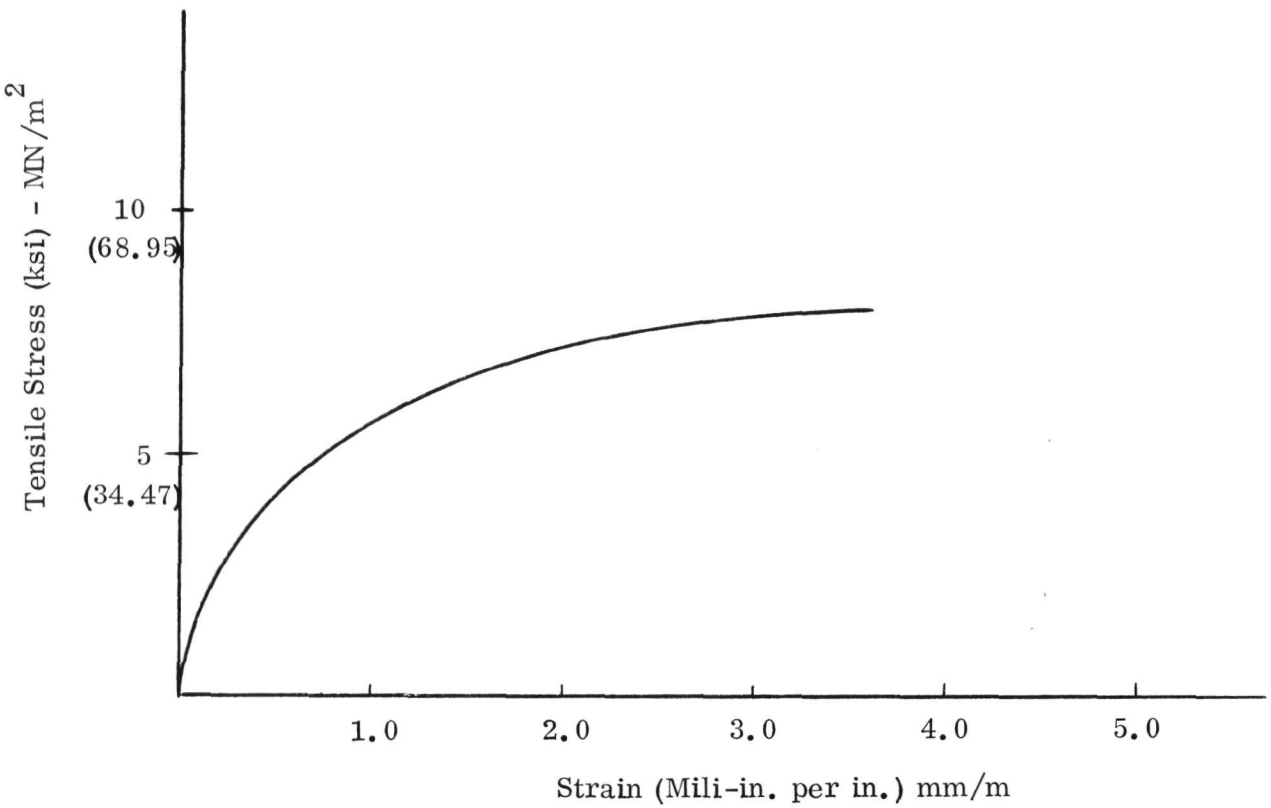

Figure 7.29. Transverse Tension Stress Strain Curves for U.D. B/Al - 588.9K (600°F).

Table 7-7. Basic Material Properties

Material	Temp.	$F_{tu_{11}}$ kN/cm^2 (ksi)	$F_{tu_{22}}$ kN/cm^2 (ksi)	$E_{tu_{11}}$ kN/cm^2 (ksi)	$E_{t_{22}}$ kN/cm^2 (ksi)	ν_{12}	ν_{21}	$\alpha \Delta T$ m/m (in./in.)	$\sqrt{F_{tu_{11}}/(E_{t_{11}} E_{t_{22}})^{1/2}}$
UD Boron/Aluminum	R.T.	122.7 (178.0)	10.3 (15.0)	22,407 (32,500)	13,789 (20,000)	0.23	0.14		0.0835
	600F	106.1 (154.0)	5.5 (8.0)	17,098 (24,800)	6,343 (9,200)			0.001620	See Figure 3
6Al-4V Annealed Titanium Alloy	F.T.	92.4 (134.0)	92.4 (134.0)	11,307 (16,400)	11,307 (16,400)	0.3	0.3		
	600F	68.3 (99.1)	68.3 (99.1)	9,239 (13,400)	9,239 (13,400)			0.000742	

varies with the calculated element crippling stress as shown in Figure 7.30. This is caused by the variation of transverse secant moduli. Accordingly, the determination of the crippling stress for each element of a UD boron/aluminum cross section must be performed on an iterative basis. The crippling stress for the titanium is obtained by the method of Reference 6.

7.3.4.2 Crippling. The crippling strength of a cross section is the maximum possible strength of a column that is short enough to avoid length effect while at the same time long enough to avoid end effects. This can usually be achieved for metal structures when the slenderness ratio (effective length divided by minimum radius of gyration of the cross section) is around 12. Open sections with flat-sided elements may be considered as made up of long rectangular plates that are simply supported along the loaded edges and may be either simply supported or free along the unloaded edges. Empirical crippling curves have been generated for isotropic metal structures by Gerard (Reference 5). It is convenient to present crippling curves in a nondimensional form for isotropic metals since one graph applies for the metal at any temperature.

7.3.4.3 Hat Section Test Results. The crippling parameter

$$(b/t)\sqrt{(F_{tu_{11}}/E_{t_{11}}E_{t_{22}})}^{1/2}$$

was used to evaluate the crippling tests. By using the material data and crippling curves presented earlier (Figure 2.3) and Reference 6 for the crippling of the titanium, the crippling analyses are performed. Comparisons with test results are shown in Table 7-8 where good correlation is obtained at room temperature and fair correlation at 589K (600F).

The thermal stresses were obtained by the use of Reference 7.

7.4 PANEL SPLICE TEST SPECIMENS

7.4.1 DESIGN. The design of the composite reinforced panel (Figure 5.6) showed a typical panel splice. In that design it was assumed that fastener locks would be transferred to the composite by means of washers of titanium brazed or adhesively bonded in place. As a result of the work accomplished in fastening methods, it was concluded that spot joining would be a more appropriate method for attachment and this method was then considered for the panel joint also.

The design philosophy required that all joining methods be compatible with scaleup for actual fabrication of orbiter hardware. This required that mechanical fasteners be used for the panel splices as spot joining would not be practical when installing large preassembled panels onto the orbiter framework.

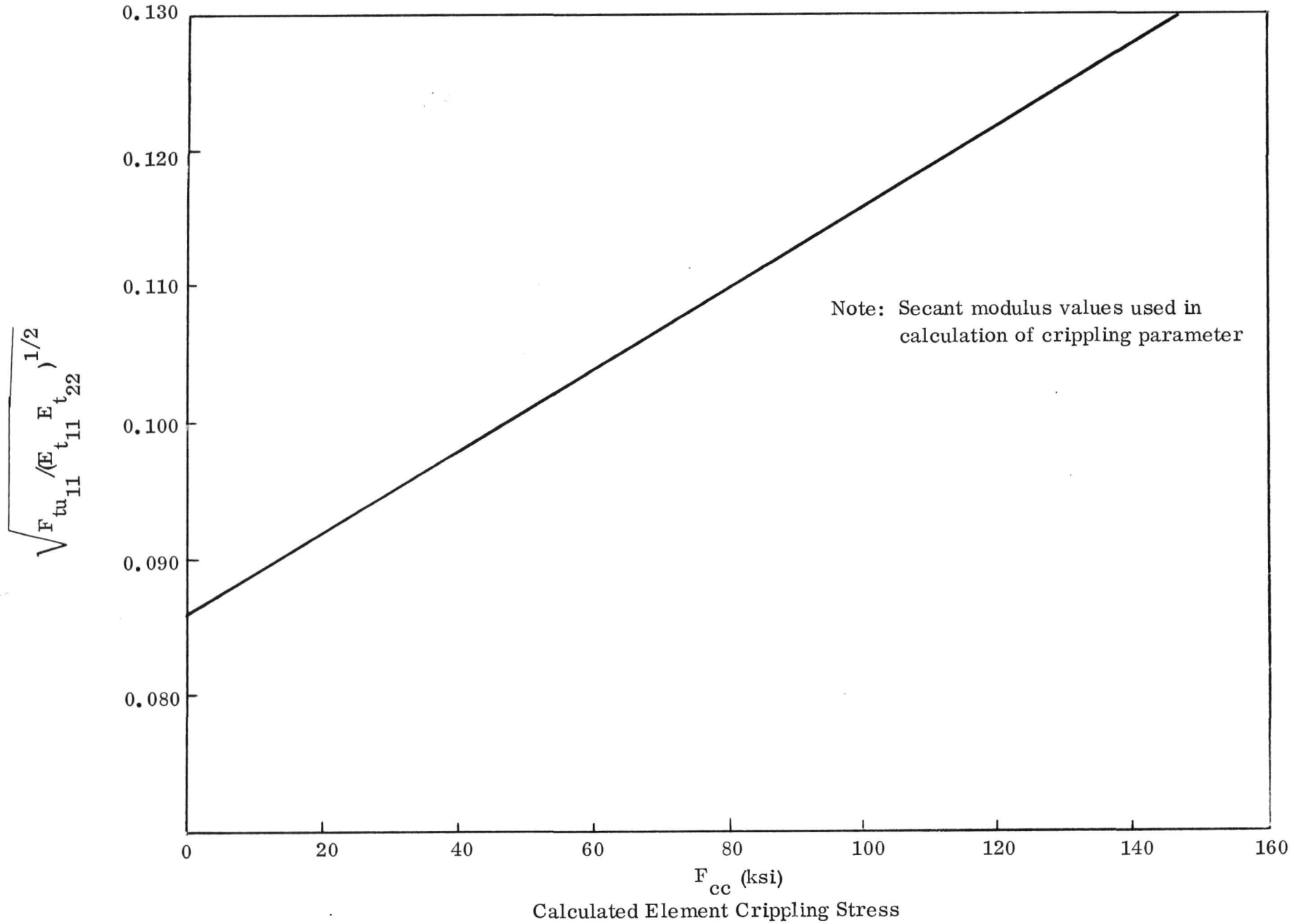

Figure 7.30. Element Crippling Parameter versus Element Stress for UD B/Al at 600F.

Table 7-8. Crippling Tests (B/Al Hat/6-4 Ti Plate)

Test Number	Temperature		t_{hat}		t_{plate}		$P_{predicted}$		P_{test}		P_{test}
	K	(F)	mm	(in.)	mm	(in.)	KN	(lbs.)	KN	(lbs.)	$P_{predicted}$
72C0068-1-01	R.T.		0.68	(0.027)	0.91	(0.036)	42.7	9608	37.8	8510	0.885
72C0068-1-02	R.T.		0.68	(0.027)	↑	↑	42.7	9608	37.7	8490	0.883
72C0068-1-03	R.T.		0.68	(0.027)			42.7	9608	42.1	9470	0.985
72C0068-3-01	R.T.		0.86	(0.034)			61.9	13921	62.0	13950	1.002
72C0068-3-02	R.T.		0.86	(0.034)			61.9	13921	5 .8	12955	0.930
72C0068-3-03	R.T.		0.86	(0.034)			61.9	13921	61.9	13920	0.999
72C0067-1-01	589	(600)	0.68	(0.027)			30.1	6773	19.5	3820	0.564
72C0067-1-02	589	(600)	0.68	(0.027)			30.1	6773	23.4	5480	0.809
72C0067-1-03	589	(600)	0.68	(0.027)			30.1	6773	29.5	5730	0.846
72C0067-3-01	589	(600)	0.86	(0.034)			41.6	10477	31.9	7170	0.684
72C0067-3-02	589	(600)	0.86	(0.034)			41.6	10477	36.6	8240	0.786
72C0067-3-03	589	(600)	0.86	(0.034)	0.91	(0.036)	46.6	10477	36.9	8300	0.762

The design which evolved utilized titanium strips and angles spot joined to the ends of the boron/aluminum hats for fastener load introduction. The shear strength values determined previously were utilized in the design.

The compression splice specimen is shown in Figure 7.31. A titanium hat is the splicing member and is attached by means of locked spindle blind rivets (NAS 1398).

The maximum compression load occurs at 589K (600F), so this specimen was designed similar to the high temperature crippling specimens.

The tension splice specimen is shown in Figure 7.32. The joint here is identical to the compression specimen, the difference being the tension fittings at the ends which introduced the load at the centroid of the combined section.

7.4.2 FABRICATION. The fabrication techniques described in 7.3.2 were utilized for the fabrication of the splice specimens. Two units of each type were built.

7.4.3 TESTING. The final subelement testing to be performed on this program was the testing of the four stringer splice specimens.

Both specimen joint configurations are identical in configuration. The difference in the specimens consists of the end load introduction configuration. The maximum tension load condition occurs when the maximum temperature is 338K (150F). The tension specimen was planned for testing at room temperature. Previous experience has shown that boron/aluminum suffers no strength degradation up to 384K (250F).

Testing of the four specimens was accomplished in a Tinium Olsen 533 KN (120,000 lb) Universal testing machine. Heating of the high temperature specimens was accomplished in a Pacific Scientific electrically heated furnace mounted in the testing machine. Temperature control was by means of an automatic temperature controller using a thermocouple attached to the specimen.

The compression specimens were mounted between adapter plates in the furnace and the temperature raised to 589K (600F). The specimens were held at this temperature for approximately 30 minutes in order for the temperature to stabilize.

The ultimate test load for the two specimens was 18.8 KN (4245 lb) and 34.8 KN (7835 lb). Design ultimate load was 27.9 KN (6288 lb). The low load capacity of the first specimen was subject for concern and the testing set reviewed.

It was determined that the size of the specimen exceeded the useable area of the furnace and that the temperatures of the extremities of the part were not being held to the desired level.

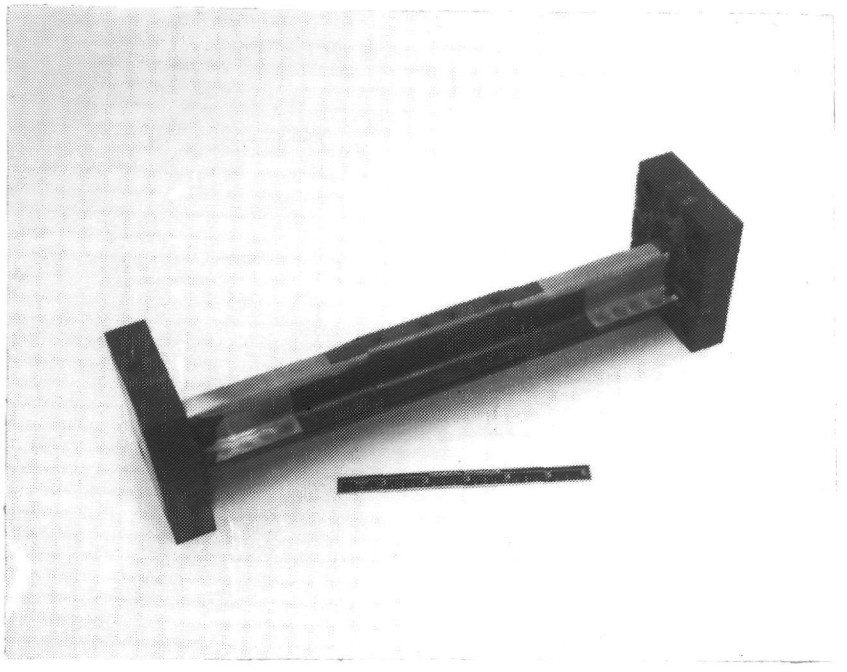

Figure 7.31. Compression Splice Specimen.

Figure 7.32. Tension Splice Specimen.

For the second part, the thermocouple was placed at the top of the part to ensure that the portion was not overheated.

The failure in both cases was due to crippling of the stringer and skin adjacent to the splice area. In both cases the crippling occurred at the top and hence hotter portion of the part.

Figure 7.33 shows the buckled area at the first specimen tested. The buckle in both cases was very similar. There was no evidence of any failure in the joint area of either specimen.

The load of 34.8 KN (7835 lb) achieved on the second test indicates that the joint design is adequate for the purpose intended.

The tension splice specimens were tested in a 533 KN (210,000 lb) capacity Tinius Olsen Universal testing machine. The end fittings of the specimens were attached to clevises on pull rods attached to the table and head of the machine.

The ultimate loads achieved for the two specimens were 81.1 KN (18,230 lb) and 95.5 KN (21,490 lb). This compares favorably with a design ultimate load of 49.1 (11,100 lb) corresponding to a tension load intensity of 640 KN/m (3660 lb/in).

The first specimen failed in the load introduction area with no apparent failure in the splice area. Figure 7.34 shows this first specimen after testing.

The second specimen was tested in a similar manner and failed in a similar manner. Figure 7.35 shows the second specimen after test. Failure in this specimen initiated at the end fitting at a load of 92.5 KN (20,800 lb). The failure of the hat section at the edge of the splice doubler through the spot welds occurred at a load of 95.5 KN (21,490 lb). The average stress in the boron/aluminum at this load was approximately 758 MN/m (110,000 psi) without considering peaking due to stress concentrations at the welds or due to bending induced by the end failure.

As a result of this testing it has been concluded that the joint as designed is more than adequate to sustain the loads to which it would be subjected in service.

The design and test load for the splice specimens are summarized in Table 7-9.

7.5 CORROSION PREVENTION

Two specimens of B/Al composite spot joined to titanium were used to evaluate four corrosion protection systems. Both specimens were vapor honed as an initial cleaning. One specimen was then alkaline cleaned, acid cleaned and given a chemical conversion

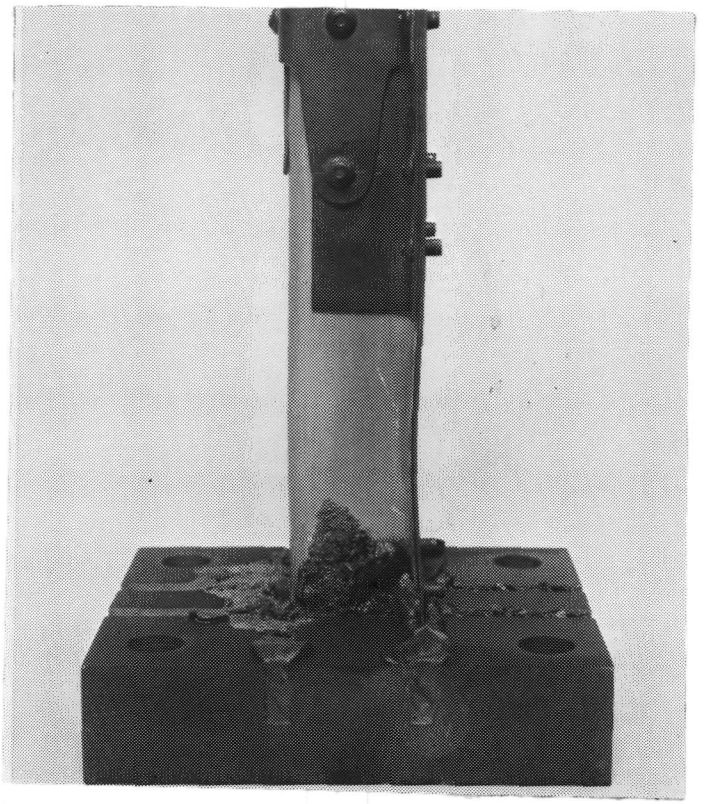

Figure 7.33. Top End of Crippled Compression Joint Specimen.

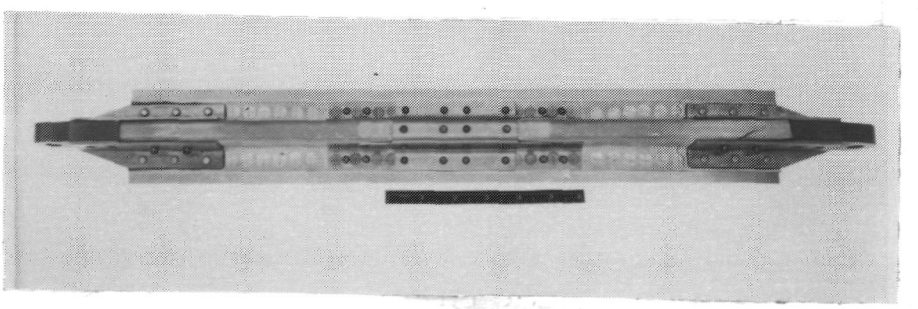

Figure 7.34. Tension Splice Specimen #1 after Testing.

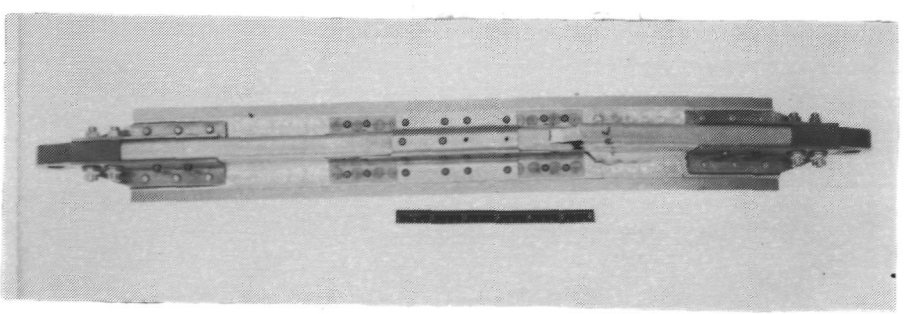

Figure 7.35. Second Tension Splice Specimen after Testing.

Table 7-9. Summary of Stringer Splice Specimen Test Loads

Specimen	Test Temp.		Design Ult. Load		Test Load		$\frac{P_{test}}{P_{design}}$
	K	(F)	K	(lbs.)	K	(lbs.)	
72C0078 (1)	295	(72)	49.4	11,100	81.1	18,230	1.64
72C0078 (2)	295	(72)	49.4	11,100	95.6	21,490	1.93
72C0079 (1)	589	(600)	27.9	6,288	18.9	4,245	0.67
72C0079 (2)	589	(600)	27.9	6,288	34.9	7.835	1.25

coating, Iridite 14-2. The other specimen was alkaline cleaned, acid cleaned, given a chromic acid anodic coating, and the coating sealed in hot water. The anodic process turned the titanium dark blue and dissolved the stainless steel rivets.

One-half of each specimen was then painted with an epoxy polyimide primer containing a corrosion inhibiting chromate pigment. A non-glossy white acrylic lacquer was applied as a top coat over the primer. The other half of each specimen was masked during the spraying of primer and topcoat. Interior surfaces between hat section and titanium were also coated by spraying coating materials into the opening at the end. Figure 7.36 shows the appearance of the 2 specimens after treatment and coating.

After the coatings had cured for one week, the effectiveness of the corrosion prevention systems was evaluated by exposing the specimens to 5% salt spray for 336 hours. This exposure caused very mild corrosion on surfaces treated with the chemical conversion coating. The anodic coating resisted corrosion better than the conversion coating, which is consistent with other corrosion tests which have been conducted on boron/aluminum composite materials. The primed and topcoated surfaces appeared unaffected by the salt spray exposure. See Figures 7.37 and 7.38.

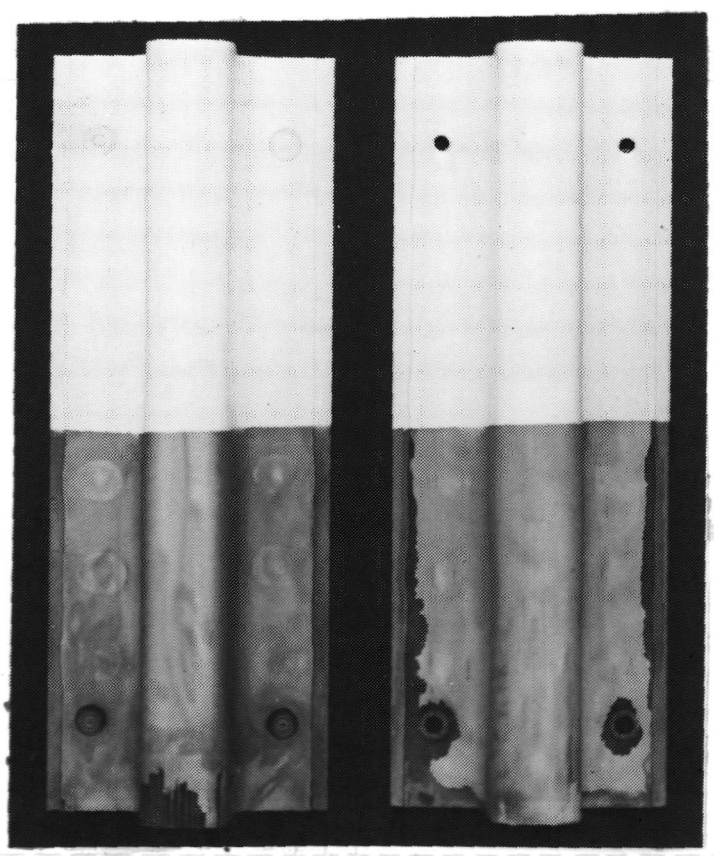

Figure 7.36. Treated Crippling Specimens Prior to Salt Spray Testing, Boron Aluminun Side.

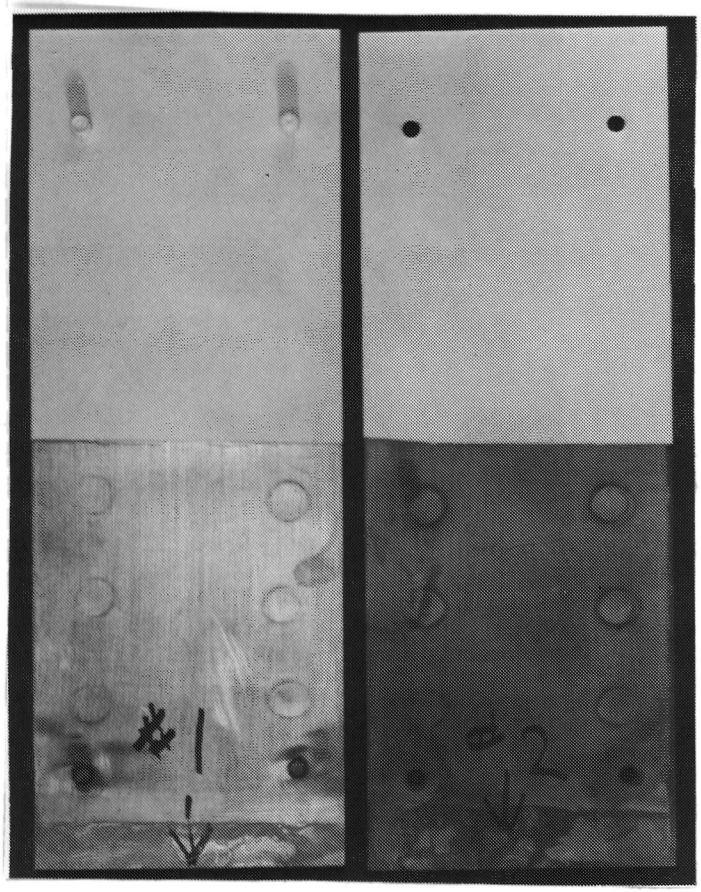

Figure 7.37. Treated Crippling Specimen after Salt Spray Testing Titanium Side.

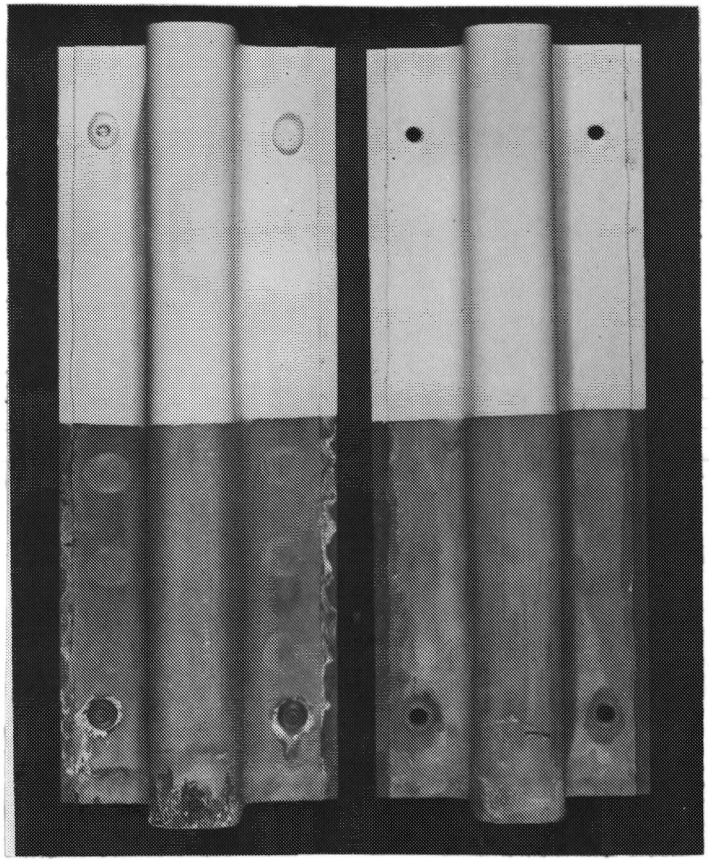

Figure 7.38. Treated Crippling Specimen after Salt Spray Testing, Boron Aluminum Side.

8

TEST PANEL DESIGN

8.1 INTRODUCTION

The orbiter composite reinforced metallic panel (Section 4) was the basis for the design of the test panels which were intended to duplicate a portion of the orbiter lower fuselage surface.

The size of the test panels was based upon the need to provide a meaningful test section at a reasonable cost. The width of the panel was set at approximately 60.9 cm (24 in), the size of a standard sheet of titanium. The stringer size and spacing then resulted in a panel with eight stringers.

It was planned to duplicate a single frame bay with simple support at the frames. The panel length was designed as a flat ended column with an effective length of 63.5 cm (25 in). Experience with flat-ended column has shown that the finite coefficient is approximately 3.6 which yields a total specimen length of 120.24 cm (47.34 in). The general arrangement of the panel is shown in Figure 8.1.

8.2 DETAIL DESIGN

The configuration of the panel stiffeners was modified somewhat from that determined in the parametric study (Section 2).

In order to improve the overall efficiency of the titanium skin in the compression panels, provide a more practical manufacturing gage, and to account for the larger bend radii necessary for forming boron aluminum, the following changes were made to the compression panel cross section. First, the spacing between the hat sections was increased from 6.22 cm (2.45 in) to 7.69 cm (3.03 in); this provides equal and slightly wider skin panels which improve the efficiency of the 0.91 mm (0.036 in) titanium skin. Second, the thickness of the hat section was increased by one ply from 0.68 mm (0.027 in) to 0.86 mm (0.034 in) to provide a more practical manufacturing gage and to improve the crippling strength. The third change was to include the effects of the larger bend radii in the final cross section and analysis. These changes resulted in a slightly improved configuration since the increased spacing and resulting increased loading was offset by the increased gage of the boron aluminum hat sections resulting from the larger corner bend radii. The results of these changes are shown in Figure 8.2, and the resulting weights and margins of safety are shown in Table 8-1.

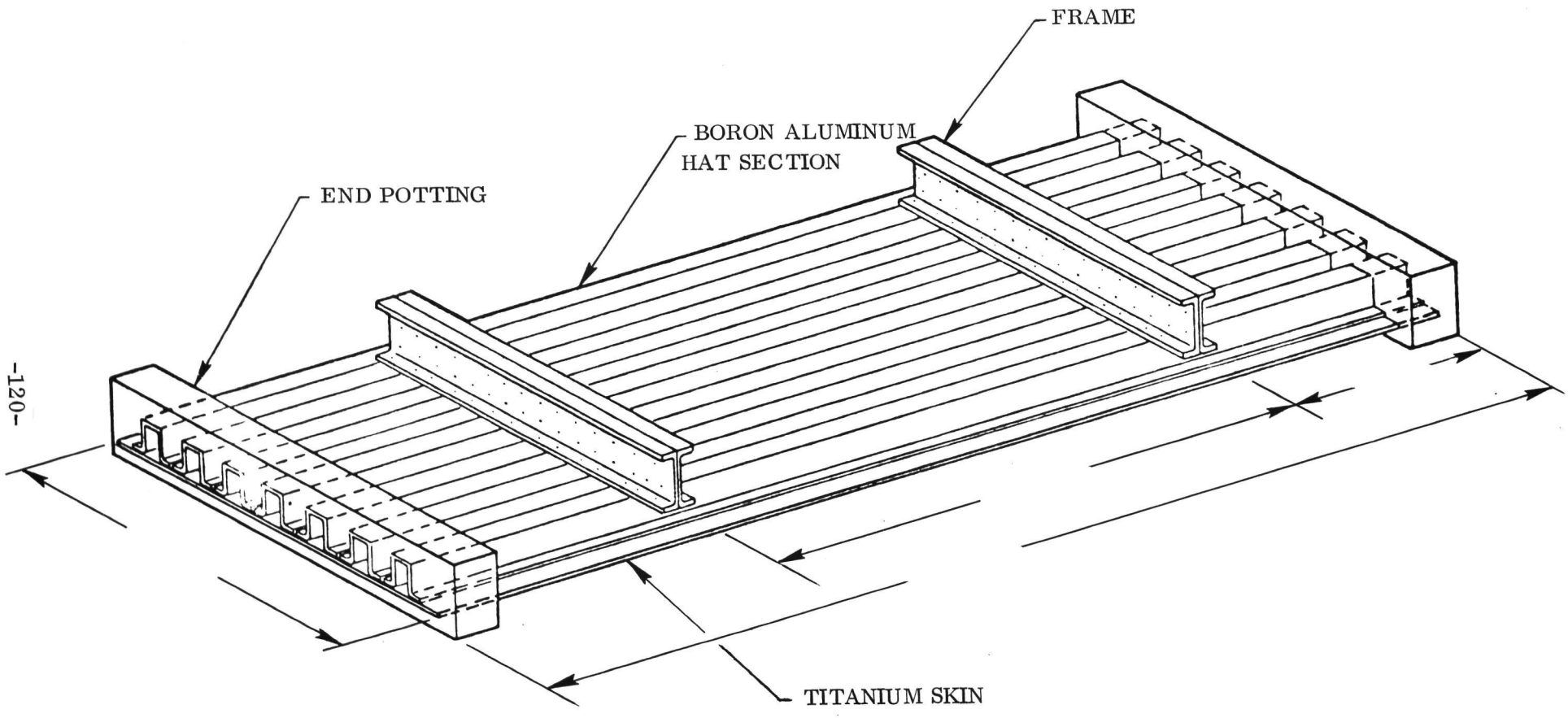

Figure 8.1. Composite-Reinforced Fuselage Panel Test Specimen.

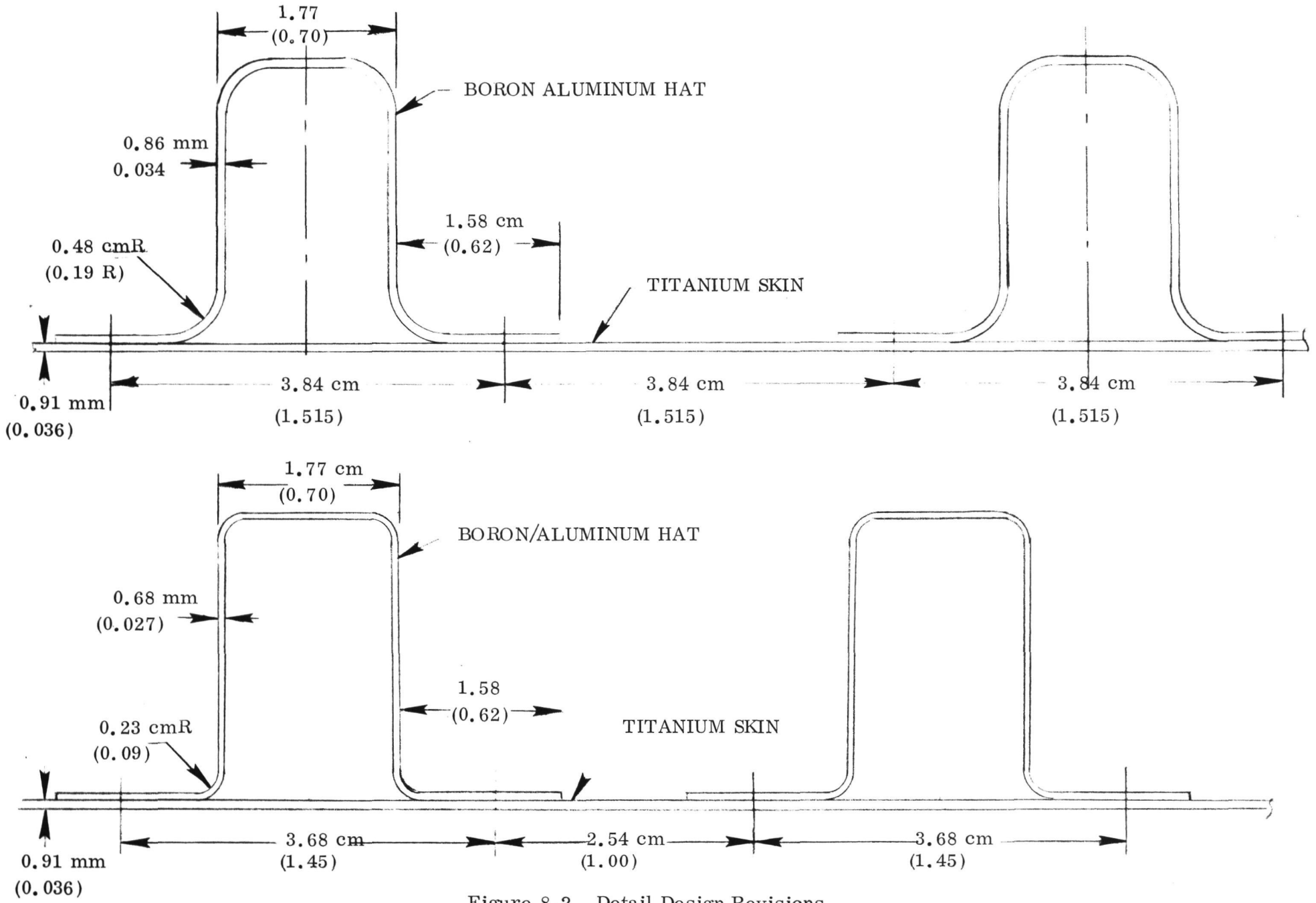

Figure 8.2. Detail Design Revisions.

Table 8-1. Weights & Margins of Safety

	Parametric Study Configuration	Final Configuration
Weight Kg/m^2 (lb/ft^2)	7.177 (1.470)	6.986 (1.431)
Skin Compression Buckling M.S.	0.14	0.02
Column M.S.	0.17	0.15
Total Section Crippling M.S.	0.44	0.46
Skin Shear Buckling M.S.	0.69	0.55
Tension M. S.	Not Critical	Not Critical

Two titanium frames were provided primarily to evaluate the structural effects of the cooler frame on the skin when at temperature. They were also planned for use to prevent torsion motion of the panel.

The frames were to be attached by means of blind fasteners into the crown of the hat section stiffeners which would be typical of alternate frames on the orbiter vehicle.

The panel ends were treated in a manner similar to the end fittings of the high temperature crippling specimens utilizing steel blocks slotted for insertion of the panel ends. The slot was filled with polyimide adhesive.

The final configuration of the test panel is shown in Figure 8.3.

This configuration represents a 33% weight saving over an all titanium panel.


SECTION C-C
TYP STRINGER
SECTION A-A
SECTION B-B
SKIN
STRINGER
ANGLE
WEB
DOUBLER
NOTES:
3. ALL DIMENSIONS ARE IN CENTIMETERS.
CONVAIR DIVISION OF GENERAL DYNAMICS
SAN DIEGO CALIFORNIA
BORON ALUMINUM
REINFORCED
COMPRESSION PANEL
14170
72C0080

Figure 3.3.

Page Intentionally Left Blank

9

TEST PANEL FABRICATION

9.1 INTRODUCTION

The fabrication of the two compression test panels was divided between the Convair factory and the R&D Laboratory of the Materials and Processes Group. The Fabrication of all detail parts utilizing composite and the final assembly of the panel were accomplished in the M&P laboratory while the detail fabrication of all steel and titanium parts was accomplished in the factory.

9.2 FABRICATION OF CONVENTIONAL METAL PARTS

The portions of the test panel fabricated by the factory were the titanium frame sections and the steel end blocks. No special handling or processing was required. The finished parts are shown in Figures 9.1 and 9.2.

9.3 FABRICATION OF COMPRESSION PANEL

9.3.1 FORMING OF HAT SECTION STIFFENERS.

9.3.1.1 Equipment and Tooling. The equipment used to form the 1.2 m (4 ft) hat section stiffeners was a specially designed machine fabricated by Convair Aerospace to hot form boron/aluminum composites.

The machine is a 4 post design with 1.82 m (72 in) x 25.4 cm (10 in) press platens and has 43 cm (17 in) of daylight and a 10 cm (4 in) stroke. Figure 9.3 is an overall view of the press in a partial stage of construction. It is designed with the lower platen movable in order to minimize heat losses (chimney effect) during separation of the tools for loading and unloading. In addition, an important feature of this design is the fine degree of control it offers in the low range of forming loads by eliminating the dead weight effect of the upper platen and tools. The machine is hydraulically powered with a 311 KN (35 ton) capacity. The forming rate is infinitely variable from 0 to 2.54 cm (1 in)/second.

The heating chamber of the press is 30.4 cm (12 in) square x 1.82 m (60 in) long. It consists of two banks of T-3 radiant lamps mounted on each side of the press to form an oven-like atmosphere for the tools and blank. This effectively provides an isothermal forming operation. Each lamp bank consists of ten Research Inc. Model AU8-612B reflector assembly modules positioned so that the lamps are mounted vertically. Temperature uniformity along the length of the heating chamber is

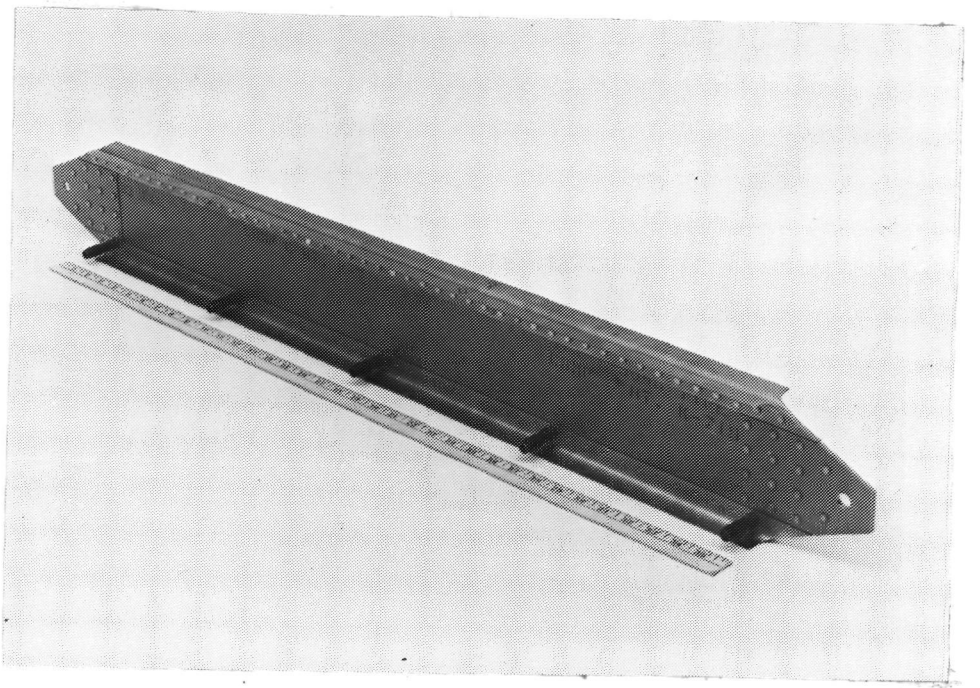

Figure 9.1. Titanium Frame Section for the Boron Aluminum Reinforced Test Panel.

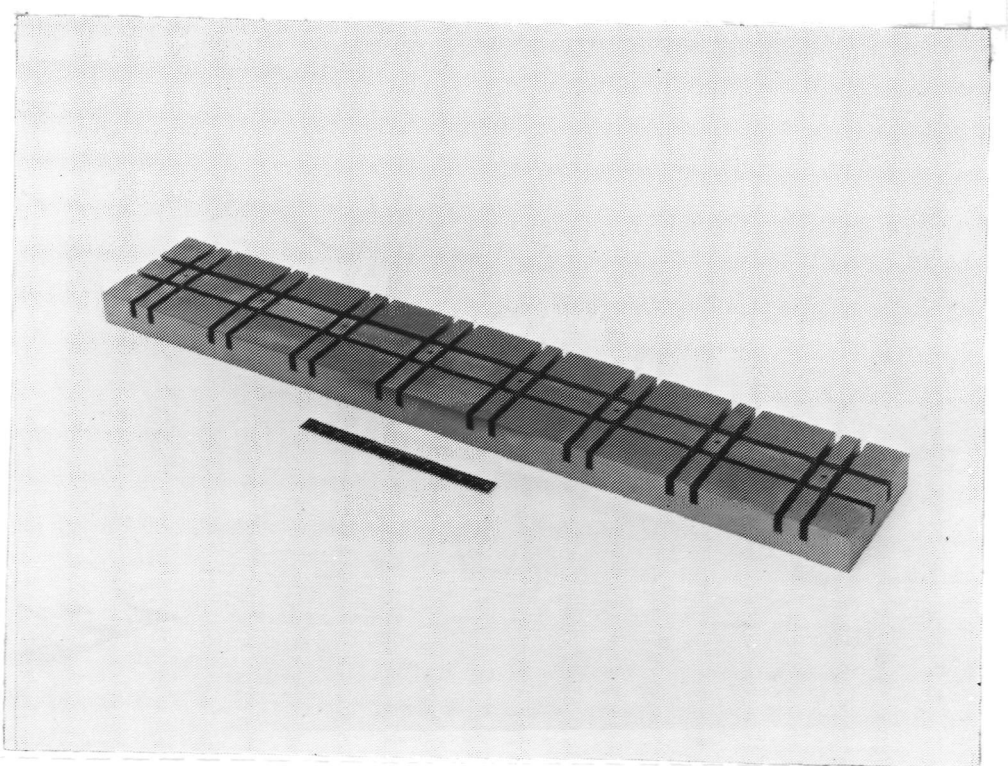

Figure 9.2. Steel End Fitting for Test Panel.

Figure 9.3. Partially Completed Heated Die Forming Press.

obtained by varying the lamp density along the length (higher lamp density of the ends of the chamber to offset "end effects"). The reflector surfaces of the modules are gold plated for maximum reflectivity. The modules utilize 1000 Watt, 240 Volt T3 quartz lamps, and are designed to provide local air cooling of the lamp end seals for longer lamp life. A 2.54 cm (1 in) diameter manifold feeds each bank of lamps and both manifolds are connected to a pressure regulator to reduce shop air to about 103-137 N/m^2 (15-20 psi). A cooling coil system is provided for water cooling the plates which are mounted to the press platens.

Power is supplied to the lamp banks by a Research, Inc. Power Supply Model No. SPG-5009W rated at 600 Volts and 600 Amps. Figure 9.4 shows an overall view of the press with the power supply and a temperature recorder. Thermocouples embedded in the tools were used to monitor temperature.

The tooling for forming the hats was 90° matched dies and was fabricated from CRES 316. Figure 9.5 shows the tooling mounted in the press. The tooling consists of a punch holder double ended punch, gooseneck punch, Vee die, die holder and die riser. The tooling arrangement provides for forming the composite material at the center of the heating zone. The system is designed so that the punch is self-centering and both

Figure 9.4. Overall View of Forming Press with Power Supply and Temperature Recorder.

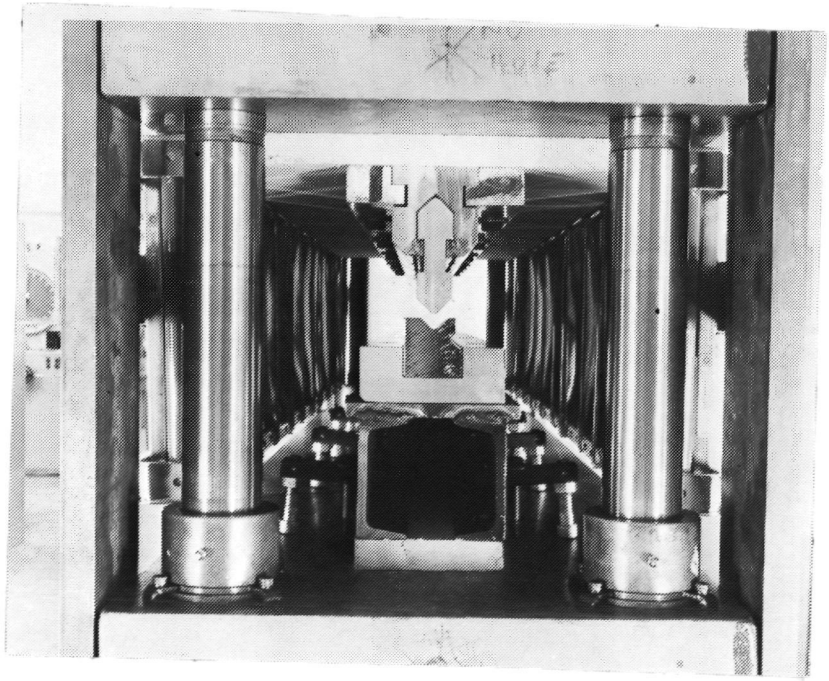

Figure 9.5. Closeup View of Dieset in Hot Forming Press.

the punch and the Vee die can be changed while hot. Blank indexing is accomplished by locating slots in the blank (which are on the bend centerline) with dowel pins on the centerline of the tools. The blanks are loaded and unloaded from one end of the press. Figure 9.6 shows a finish formed hat being removed from the press.

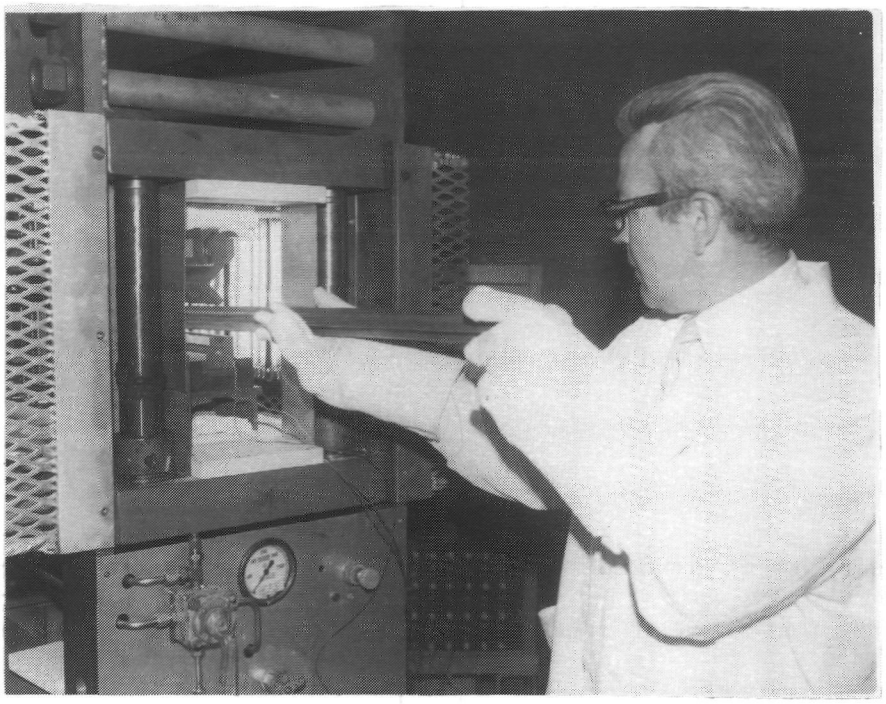

Figure 9.6. Formed Boron Aluminum Hat being Removed from Forming Press.

9.3.1.2 Fabrication Procedure.

Blank preparation. The 0.88 mm (0.035 in) boron/aluminum unidirectional material for the hat sections was produced by Amercom, Inc. and supplied in a 23 cm (9 in) x 132 cm (52 in) raw material size. Upon receipt of the sheets, visual examination and thickness measurements were made.

The sheets were sheared to a length of 123 cm (48.4 in) and sheared to a developed width of 10 cm (4.0 in). Excess trim areas were identified and retained for additional testing, if it was found necessary. After shearing, the blanks were notched along the bend centerlines to accommodate 4.7 mm (3/16 in) diameter dowel pins in the Vee die.

Initial tests. Previous work on forming hats for stringer splice test specimens indicated that crack free bends could be made at 700K (800F) without a caul sheet backup support.

During forming of the two outer bends of the first blank at 700K (800F), a binding condition was noted in the press. This was traced to thermal expansion of the platens caused by overheating. The press was modified by the installation of cooling plates. In addition microquartz insulation was placed between the hot tools and the Marinite insulation board. The final two bends of the first blank were made on the modified press. All four of the bends were made at 700K (800F) without any caul sheet backup support.

An attempt to form a second blank 1828 P-1 without a backup support resulted in intermittent cracking in the tension side of the radii. The part was loaded into the forming chamber at 700K (800F), preheated for four minutes and then formed complete without removing it from the forming chamber. The cracks generally were about 2.54 cm (1 in) in length and were randomly spaced along the entire length in all four radii.

Tests were run on excess material from the trim area of sheets 1828P and 1830P to determine the conditions necessary to improve the reliability of forming the hat sections. These tests showed that forming at 755K (900F) still resulted in slight cracking with this material but that forming at 755K (900F) with an 0.63 cm (0.025 in) annealed stainless steel backup strip resulted in crack free bends.

The transverse strength was determined for samples cut from stringer panel material. Each specimen represents a panel from which two stringers are made. See Table 9-1.

Table 9-1. Summary of Transverse Strength and Modulus Data for Boron/Aluminum Stringer Material

Specimen No.	Temp.	σ		E_y		$\epsilon_{failure}$
		MN/m^2	(psi)	GN/m^2	(psi)	
2710	RT	132	(19,177)	148	(21.5)	7,200
2711	RT	129	(18,739)	138	(20.1)	5,400
2712	RT	124	(17,976)	138	(30.1)	4,300
2713	RT	124	(17,970)	151	(21.9)	4,000
2714	RT	108	(15,729)	148	(21.4)	2,200
	Avg.	123	(17,900)	148	(21.0)	4,840

The transverse strength and modulus for the five specimens appeared to be typical of other unidirectional boron/aluminum purchased in the same period. The strain to failure however was somewhat low. The average for good material being around 7,000 microstrain and as high as 10,000, the reason for the low strain to failure was unknown. It is believed that the low strain to failure of some pieces accounted for the forming difficulty experienced. It was not expected to affect the strength of the parts during testing.

Hat fabrication. Based on these tests, the following forming conditions were used to fabricate the balance of the hats:

Temperature	755K (900F)
Preheat time	5 min.
Forming time	1 min.
Dwell time	0.7 min.
Backup support	0.63 mm (0.025 in) annealed stainless steel

The temperature variation from one end of the punch to the other was within 17K (30F); the variation from one end of the Vee die to the other was within 28K (50F). Throughout the heating and forming cycles, the average temperature of the punch was approximately 33K (60F) higher than the average temperature of the die. In order to avoid bowing and distortion of the tools, heatup was accomplished in steps at a slow rate. Typically the tools were brought up to 755K (900F) in 3 hours.

Three bends were made in the hats with the double ended punch and the fourth bend was made with the gooseneck punch (which was required for the fourth bend to accommodate the narrow width of the hat). The double ended punch was used for the first three bends because of the better forming action it provides over the gooseneck punch in matched die forming. The double ended punch is designed so that approximately 1.3 cm (0.5 in) of contact is made between the punch and die. This design results in a flat surface beyond the radius and minimizes transverse crowning.

Checking the angularity after the first three bends were made indicated that springback of approximately 2° was occurring. (The angles had an included angle of 92°.) This was primarily due to the use of the stainless steel backup strip. Prior to forming the fourth bend with the gooseneck punch, the three bends were sized without a backup strip. This brought the angles to 90°. Everlube T-50 was used as a lubricant on both the boron/aluminum blank and the stainless steel backup strip. Figure 9.7 shows seven of the sixteen 1.2 m (4 ft) hats as formed. Visual examination indicated no cracking occurred in any of the bend lines. Straightness of the parts was excellent and the hats could be held absolutely flat with very light finger pressure.

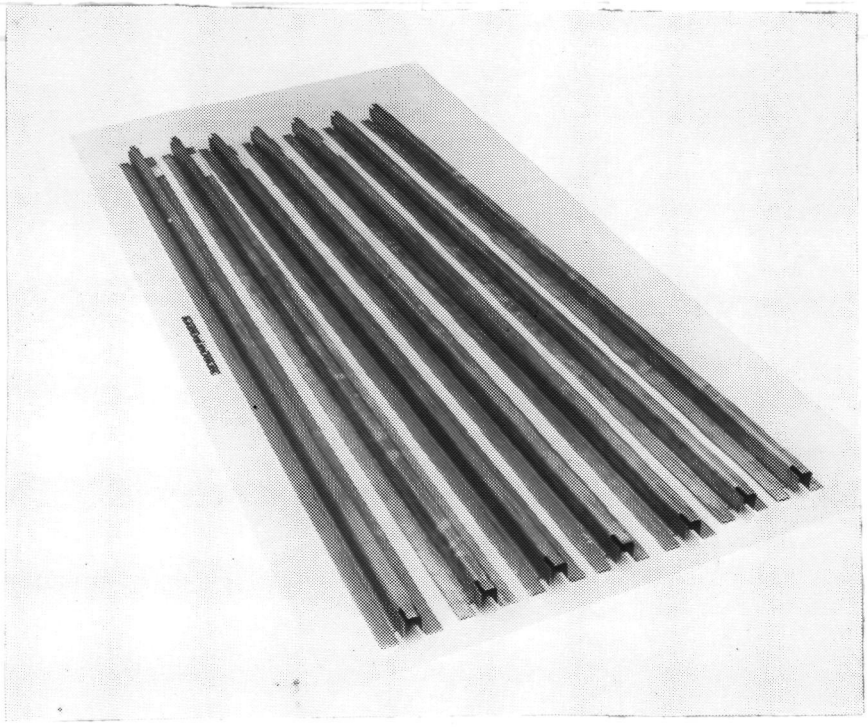

Figure 9.7. Seven Hat Sections after Forming, before Cleaning and Trimming Ends.

All of the hats were subjected to fluorescent dye penetrant inspection and no evidence of cracks was found.

9.3.1.3 Mounting Stiffeners to Skin. After forming, the hats were trimmed to a length of 120.4 cm (47-7/16 in). Cutoff of the notched ends was accomplished on a silicon carbide cutoff wheel with the hat filled with plaster in the cutoff area for support. The hats were then hand cleaned with a Scotchbrite pad and acetone to remove most of the graphite lubricant.

Holes for 2.3 mm (3/32 in) diameter bolts were punched in the flanges of the hats at both ends for mounting the hats to the titanium skin. The hats were then positioned on the titanium skin (Figure 9.8) and the machined end blocks positioned over the ends. The hats were loosely clamped to the skin and each hat adjusted so that it was centrally located in the end block recess. The hats were then clamped to the skin. After clamping, the end blocks were removed and the holes in the stringer stiffeners were transfer punched into the titanium skin. The details were disassembled, cleaned in a HF, HNO_3 solution and reassembled for the welding operation.

9.3.2 SPOT JOINING OF BORON/ALUMINUM HAT SECTIONS TO THE TITANIUM SKIN.

9.3.2.1 Tooling and Preparation. The compression panels were welded using the wooden box fixture illustrated in Figure 9.9. The welding was performed in the following sequence:

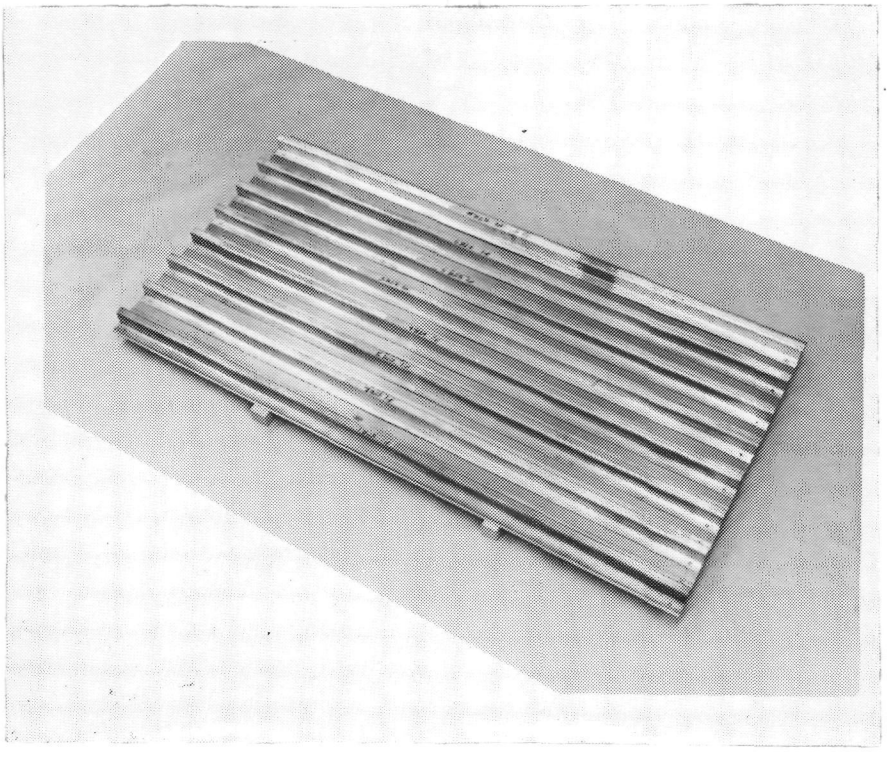

Figure 9.8. Boron/Aluminum Hat Sections Positioned on Titanium Skin.

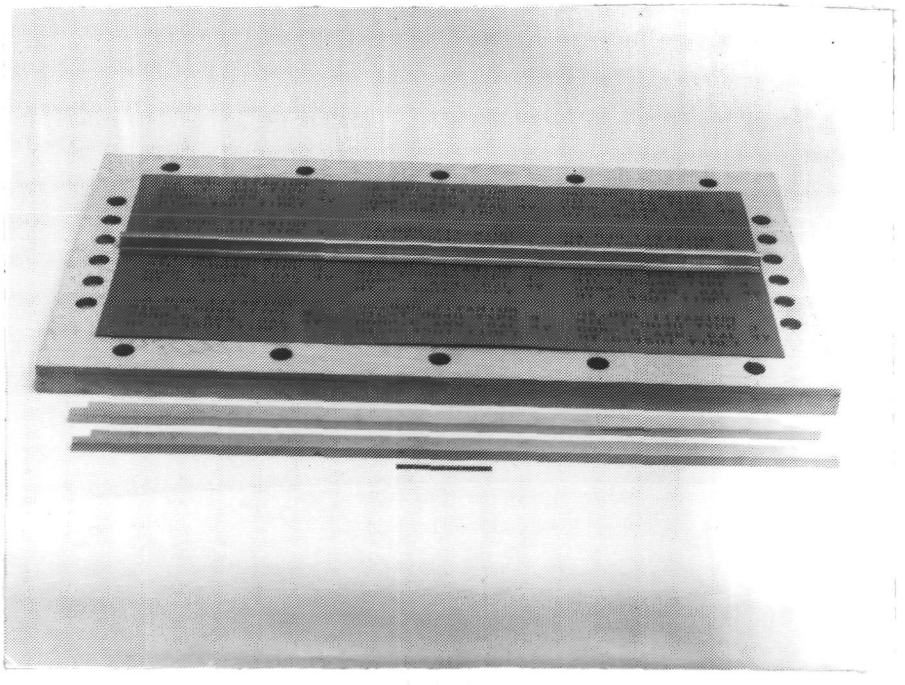

Figure 9.9. Wooden Box Fixture used during the Spot Joining of the Compression Panel, 72C0080.

a) Working from the center stringers outboard join the center 7 spots in each row.

b) Working from the center stringers outboard join 20 spots from the middle outward, alternating welding direction.

c) Working from the center stringers outboard join the remaining spots in each row. This is illustrated in Figure 9.10.

Figure 9.10. Closeup of Welding Operation.

The welding sequence was selected to minimize distortion. The sequence was only varied, within the rows described above, in order to minimize distortion. Table 9-2 contains all of the weld schedules developed for this program.

The top electrode (against the B/Al hat) was modified for use on the compression panel in order to clear the hat radii.

The weld schedule development criteria was a failure of the composite in tension at the edge of a single spot joint. The average failure load was approximately 4.48 KN (1,000 lbs) for over 40 specimens tested during development, setup and in process checks. The lowest value recorded was 3.64 KN (820 lbs).

Table 9-2. B/Al-Ti Resistance Spot Joining Schedules

	Compression Panel, Mach 133	
	Center of First Panel	Rest of First & Second Panel
Electrode on Titanium Side	Class I 1.58 cm (5/8 in) Dia. 25 cm (10 in) Tip Radius	Class I 1.58 cm (5/8 in) Dia. 25 cm (10 in) Tip Radius
Electrode on Boron/Aluminum Side	Class I 1.58 cm (5.8 in) Dia. Flat Tip	Class I 1.58 cm (5/8 in) Dia. Angle Cut Side Flat Tip
Preheat	—	4 Cycles @ 17 Phase Shift
Weld Cycles	8	8
Heat Impulses	20	18
Phase Shift	21	21
Forge Delay		
Weld Pressure N (lbs)	5.1 KN (1150)	5.1 KN (1150)
Forge Pressure N (lbs)	9.5 KN (2150)	9.5 KN (2150)

9.3.2.2 Welding of the Compression Panels. The first panel welded had expulsion of over 80 percent of the spots. This is attributed to the failure to properly clean the titanium sheet. The titanium sheet was properly cleaned for the second panel and both the frequency and seriousness of the expulsion were significantly reduced. The first panel was joined using the wooden box fixture to support the panel, but without any clamps. The fixture was pushed against the panel for each weld to keep the panel weight off of the bottom electrode. This aids in reducing distortion. Figure 9.11 illustrates the panel weld setup. The panel curvature which results from resting its weight on the lower electrode is illustrated.

The first panel welded without incident. The resultant panel had a slight bow in both directions with the center of the panel, when laying hat side up, raised approximately .64 cm (1/4 in). Figure 9.12 shows the first panel, as welded. The 1176 spot impressions were bright and shiny on the boron/aluminum side, and showed typical discoloration on the titanium side. The spot uniformity was excellent.

During the welding of the second panel the first set of spots, seven per stringer, were completed without incident. During the joining of the next set of spots distortion and twisting began to occur. Welding was stopped and the panel clamped to the tool at 16 locations. The welding then proceeded in a "work-out-the bulges" sequence, placing spots at locations which minimize or reduce the apparent distortion. The resultant panel had a slight twist and bow but little or no ripples or waves in the titanium skin.

9.3.2.3 Panel Trimming. The skin-stringer assemblies were then prepared for bonding of the end plate by trimming the hats and skin square, using a diamond coated tool.

9.3.3 NONDESTRUCTIVE EVALUATION. Nondestructive evaluation of the two test panels was accomplished using ultrasonic C-scan. The methods used were established earlier in the program during inspection of the crippling specimens. The entire panel was scanned and each joint was found to be complete. Several welds developed irregular shapes, but previous work has shown that the shape of the weld has little effect on joint strength.

Based upon previous data the tested panel had sound welds, and no difficulties should be experienced due to this fastening method.

9.3.4 ATTACHMENT OF PANEL END FITTINGS. The attachment of the steel end fittings to the panels was accomplished by Hexcel 901 foaming polyimide adhesive.

The experience gained during fabrication of the 600F crippling specimens showed that rigid fixturing was necessary in order to hold the components in proper relationship during curing of the PI material. A combination bond fixture and assembly fixture was

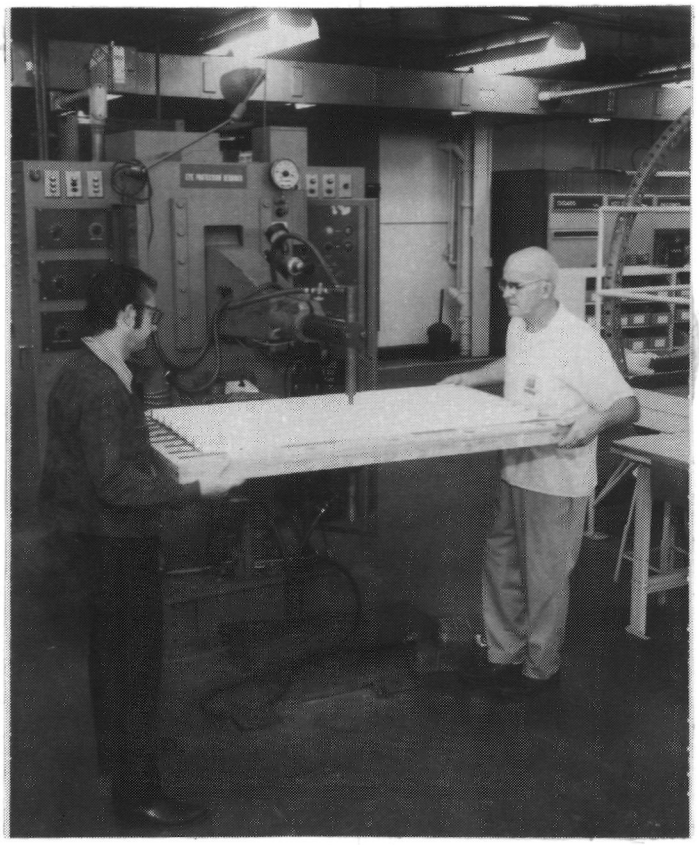

Figure 9.11. B/Al Compression Panel Weld Setup.

Figure 9.12. Front Side of B/Al-Ti Compression Panel.

fabricated in order to expedite the assembly of the test panels. The fixture consisted basically of 2 aluminum plates which served to support the panel and end blocks. Five bridge clamps were used to hold the panel flat against the tool while the end fittings were attached.

Figure 9.13 shows a completed panel in the end fitting bonding tool.

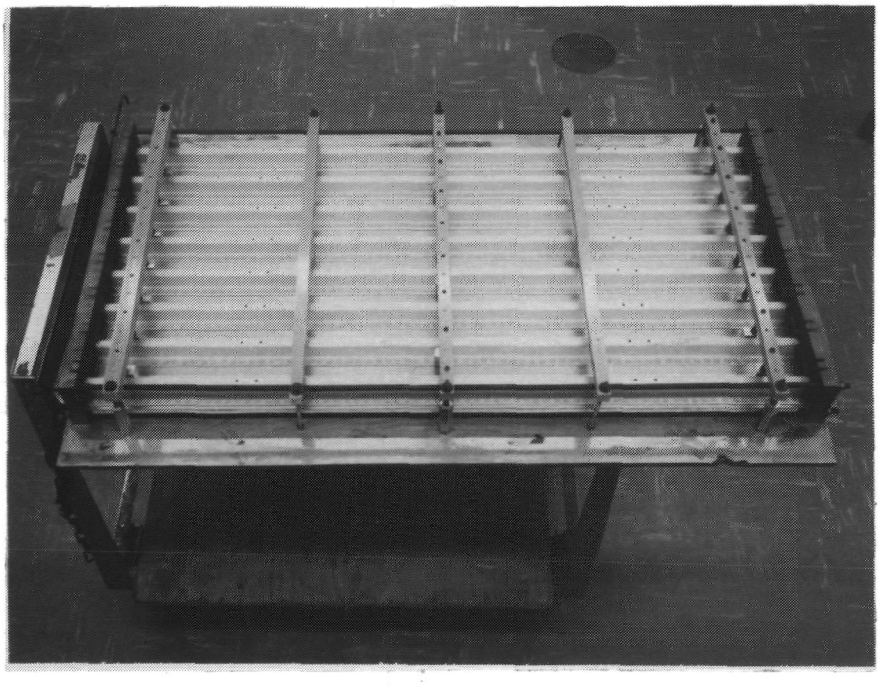

Figure 9.13 Compression Panel in Bonding Fixture Immediately after Removal from Autoclave after Postcuring.

Warpage of the titanium sheet was apparent on both panels after welding. This was attributed to the shrinking effect of the multitude of welds used to join the stringers to the sheet. The warpage was primarily a curvature in the transverse direction; however, a small longitudinal bowing was also evident. The second panel also displayed a torsional warpage.

Previous experience has shown that creep straightening of boron/aluminum could be accomplished at temperatures greater than 449K (350F). It was therefore planned to keep the panels flat against the aluminum tool, primarily to maintain alignment with the end fittings and also to attempt to straighten the panels.

The straightening effort was successful. There was no apparent transverse bow or twist in either panel after the bonding operation, and only a slight longitudinal bow. The residual longitudinal bowing of the panels was about 1 mm (0.04 in) measured at the center when supported on a flat plate.

9.3.5 ALIGNMENT OF END FITTINGS. After the end fittings had been attached, the panels were placed on a surface plate and checked for flatness and squareness at the end plates. There was a small amount of distortion of the steel end blocks due to heating so panels were placed on a milling machine for surfacing of the end blocks. After machining, the end blocks were again checked and found to be parallel within 0.05 mm (0.002 in).

9.3.6 ATTACHMENT OF FRAMES. The two titanium frames were attached to the completed panels by means of NAS1398 Monel blind rivets. The frame attachment holes had been punched prior to loading of the end plates. After the strain gages were installed, the frames were put in place and the rivets installed by a pneumatically driven rivet setter.

Figure 9.14 shows a completed panel with strain gages installed.

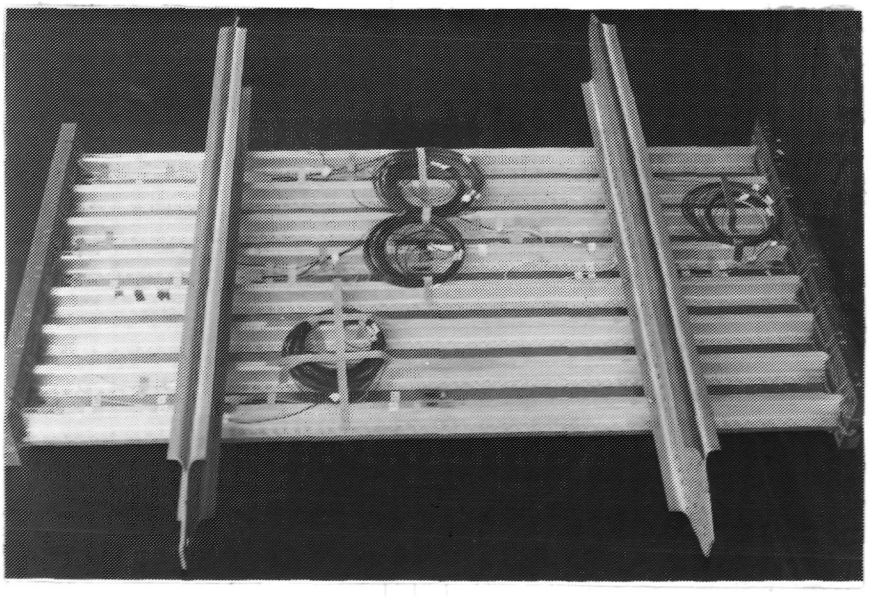

Figure 9.14. Complete Compression Panel with Instrumentation.

Page intentionally left blank

10

TESTING

10.1 INTRODUCTION

The two compression panels were to be instrumented with 33 axial strain gages, one rosette gage and 12 thermocouples. The specimen, together with the fixity fixture, was to be installed in a 2.66 MN (600,000 lb) hydraulic test machine. Pinned struts were to be installed at each of the two simulated bulkheads. These struts prevent specimen rotation but allow lateral movement. A heat reflector bank, installed on the skin sides together with Type T3 infrared lamps, was used to heat the specimens; temperatures will be continuously monitored. The heating was to be manually controlled.

10.1.1 TEST PLAN — PANEL NO. 1.

1. Install specimen in test machine, carefully centering the specimen's neutral axis and the machine centerline. Apply load and check strain gages for uniform load distribution. Shim compression head if necessary.

2. Apply tare load (20% limit) of 34.5 KN (7,760 lb). Keep this load constant while exercising the gages by applying heat to 589K ±14K (600 ±25F). Exercise the gages three times minimum.

3. When gages have stabilized at tare load and 589K (600F), begin test by loading panel to design limit (D.L.) in 10% D.L. increments, recording instrumentation at each increment.

4. Reduce load to 20% D.L. in 10% D. L. increments.

5. Repeat steps 3 and 4.

6. Increase load in 10% D.L. increments to 259 KN (58,250 Lb) (Design Ultimate). Hold this load 5 minutes; if no failure has occurred, continue loading in 10% D. L. increments to failure, keeping the 589 K ±14K (600 ±25F) constant.

10.1.2 TEST PLAN — PANEL NO. 2.

1. Install specimen in test machine, carefully centering the specimen's neutral axis and the machine centerline. Apply load and check strain gages for uniform load distribution. Shim compression head if necessary.

2. Apply tare load (20% limit) of 34.5 KN (7,760 lb). Keep this load constant while exercising the gages by applying heat to 589 K ±14 K (600 ±25F). Exercise the gages three times minimum.

3. When gages have stabilized at tare load and 589 K (600F), begin test by loading panel to 80% D. L. of 138 KN (31,070 lb) in 10% D.L. increments.

4. Reduce load to 20% D.L. in increments of 10% D.L., recording the instrumentation.

5. Repeat steps 3 and 4 for 100 cycles except instrumentation is to be recorded only on cycles 1, 2, 5, 10, and each subsequent 10 cycles for a total of 13 recording cycles.

6. Increase load in 10% D. L. increments to Design Ultimate - 259 KN (58,250 Lb). Hold this load 5 minutes. If failure has not occurred, continue loading in 10% D. L. increments to failure.

10.1.3 DOCUMENTATION.

1. Photograph failed panels, giving particular attention to details of local failure areas.

2. Reduce test data.

3. Prepare one reproducible and two copies of test report.

10.1.4 DATA ACQUISITION. Strain gage data will be recorded on a Redor 785 magnetic tape recorder with associated signal conditioning equipment. Digital printout of the strain data will be accomplished on a coupled Kleinschmidt typewriter.

10.2 TEST OF FIRST PANEL

10.2.1 TEST PANEL INSTRUMENTATION AND TESTING. The instrumentation of the first test panel consisted of 33 axial strain gages and a 3-axis rosette making a total of 36 strain gage channels. In addition, 10 thermocouples were installed on the panel. Figure 10.1 illustrates the location of all the instrumentation on this panel.

Initially it was planned to use Rockide gages on the panel, but much difficulty was experienced in obtaining satisfactory adhesion between the gages and the boron/aluminum. Several attempts were made to obtain satisfactory gage installations. The problems occurred as gages were installed and the overspray from the plasma spraying operation hit previously installed gages and dislodged them. Finally, polyimide

"Page missing from available version"

gages were used to replace those damaged. Gages 10, 14, 20, and 30 were replaced with WK06 modified foil gages with polyimide backing. Gages 11, 15, 28, and 34A, B, and C were replaced with WK125 gages.

Figure 10.2 shows the placement of the test panel in the Tinius Olsen 2.66 MN (600,000 lb) Universal testing machine. Figure 10.3 is a schematic diagram showing the location of the test panel and heat lamps in the testing machine.

The test was run in accordance with the test plan. Initially a force load of 20% of limit was applied and the strain gages recorded.

Table 10-1 summarizes the strain gage readings at 20% limit load. It should be noted that the 8 gages had been lost by this time and several others gave questionable readings. These initial readings gave evidence of non-uniform load application which data unfortunately were not examined in detail prior to proceeding with the test.

Table 10-2 lists the thermocouple readings during the entire test. Strain readings were taken at the same time increments. The temperature gages show that non-uniform heating was occurring.

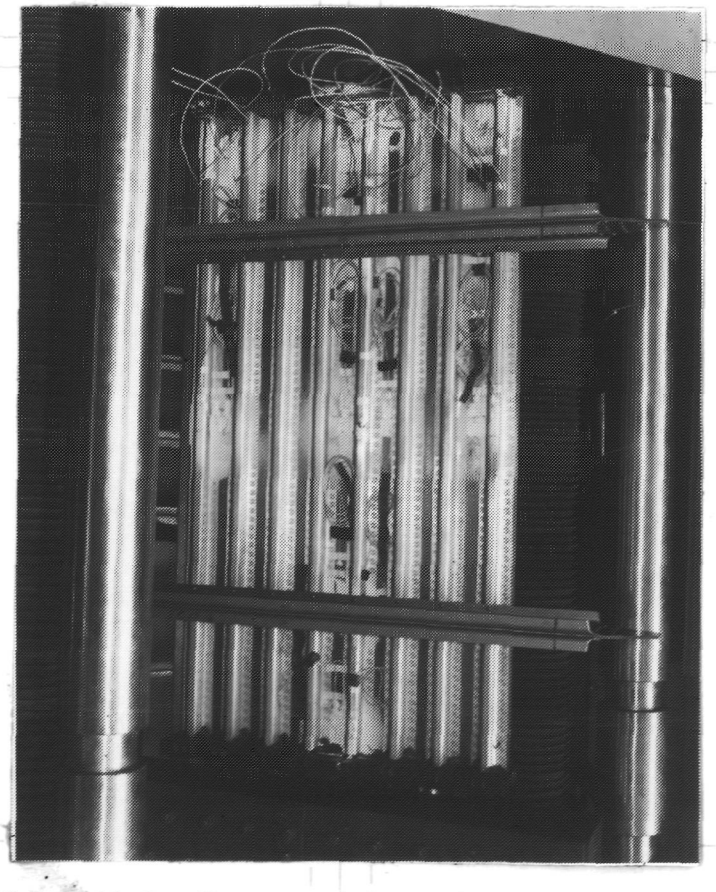

Figure 10.2. Compression panel in Test Machine.

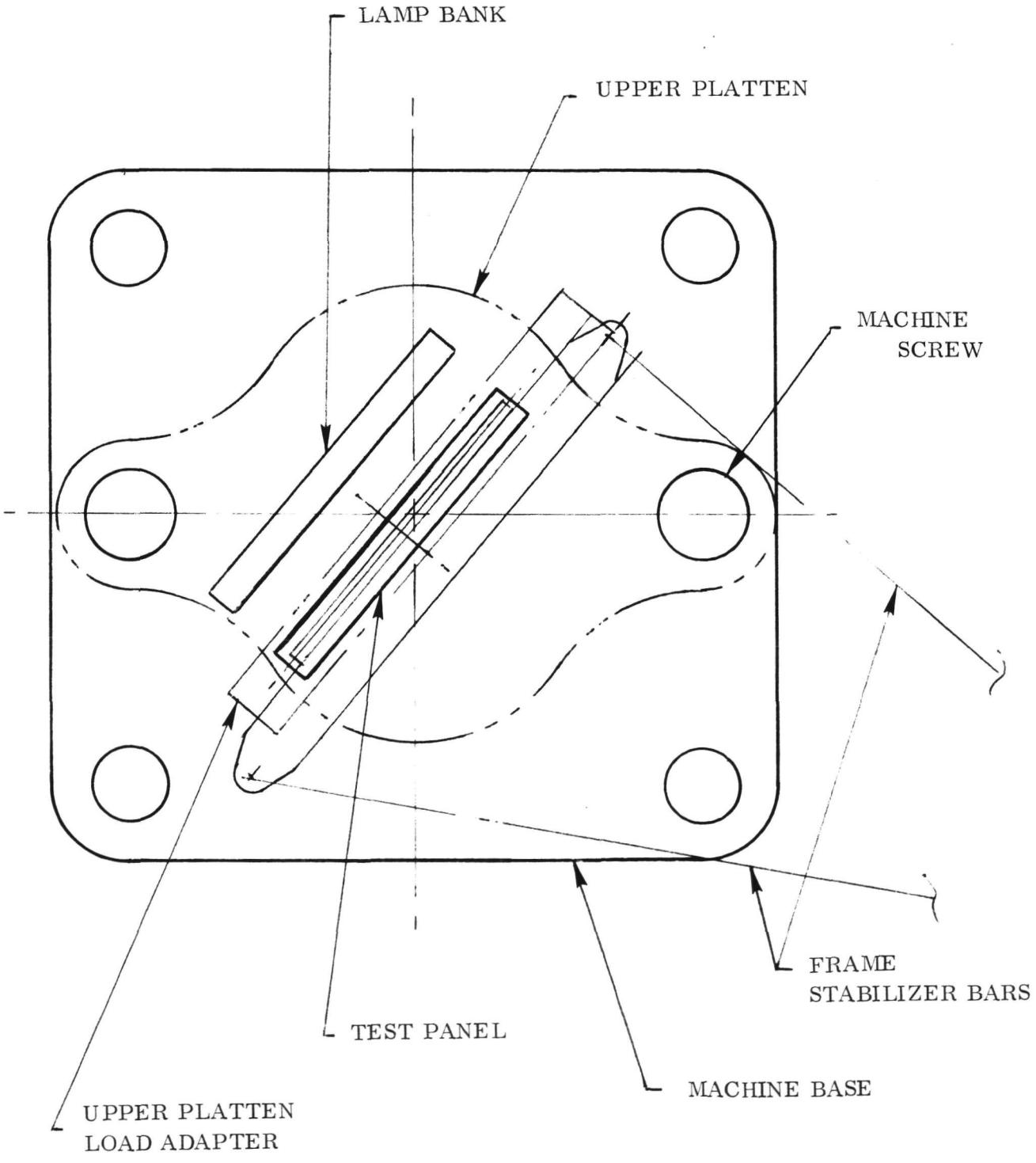

Figure 10.3. Schematic of Test Setup.

Table 10-1. Strain Gage Readings at 20% Tare Load

Gage	Microstrain	Gage	Microstrain
1	+ 94.9	18	- 391.9
2	- 149	19	+ 9
3	Out	20	- 16
4	- 112.9	21	- 400
5	+ 87.2	22	Out
6	- 129.5	23	- 167
7	- 141.6	24	-2549
8	- 171.9	25	Out
9	- 236.4	26	Out
10	- 183.8	27	- 180
11	- 23.6	28	Out
12	Out	29	- 78.6
13	- 78.4	30	- 65
14	-1554	31	-3320
15	Out	32	- 18.6
16	- 253.6	33	+ 2
17	+ 9	34A	Out
		34B	
		34C	

Table 10-2. Panel Temperatures K (F)

Load % Limit	Time	Thermocouple No. 1	2	3	4	5	6	7	8	9	10
		298	298	298	298	298	298	298	298	298	298
20	1330	(78)	(78)	(78)	(78)	(78)	(78)	(78)	(78)	(78)	(78)
		361		344	332	339	353	333	355	372	361
20	1340	(190)	INOP	(160)	(140)	(150)	(175)	(140)	(180)	(210)	(190)
		389		355	350	361	383	355	291	422	394
20	1345	(240)		(180)	(170)	(190)	(230)	(180)	(245)	(300)	(250)
		441		400	378	394	422	372	433	474	435
20	1350	(335)		(260)	(220)	(250)	(300)	(210)	(320)	(395)	(320)
		494		439	394	422	450	389	455	505	
20	1355	(430)		(330)	(250)	(300)	(350)	(240)	(360)	(450)	(400)
		513		449	433	444	478	400	478	530	491
20	1400	(465)		(350)	(320)	(340)	(400)	(260)	(400)	(495)	(425)
		549		466	444	478	505	422	510	560	533
20	1405	(530)		(380)	(340)	(400)	(450)	(300)	(460)	(550)	(500)
		589		511	466	510	533	450	561	594	544
20	1410	(600)		(460)	(380)	(460)	(500)	(350)	(550)	(610)	(520)
		605		510	472	505	561	466	578	622	583
20	1415	(630)		(460)	(390)	(450)	(550)	(380)	(580)	(660)	(590)
		578		505	505	505	566	472	572	622	583
20	1420	(580)		(450)	(450)	(450)	(560)	(390)	(570)	(660)	(590)
		605		605	478	522	572	478	583	583	594
20		(630)		(480)	(400)	(480)	(570)	(400)	(590)	(680)	(610)
		614		528	483	524	583	478	594	644	597
30		(645)		(490)	(410)	(485)	(590)	(400)	(610)	(700)	(615)
		605		528	483	524	583	472	589	583	597
40		(630)		(490)	(410)	(485)	(590)	(390)	(600)	(690)	(615)
		616		528	486	524	585	475	589	644	597
50		(650)	INOP	(490)	(415)	(485)	(590)	(395)	(600)	(700)	(615)

An error in recording the location of the thermocouples transposed thermocouples 6 and 9. Number 6 was being used to monitor the temperature at the panel since it was thought to be in the center of the panel and hence would show the highest reading. As the results show, gage 9 was in reality in the center of the pane and showed a panel temperature of 644K (700F). Subsequent examination of the panel showed discoloration in a roughly 48 cm (19 in) circular area in the center of the panel indicating temperatures of 589 K (600F) or greater.

After the panel had reached test temperature, the load was increased in 10% of limit load steps with the gages read at each step. The loading continued through 60% of limit and the panel failed in local buckling as the load was being raised to 70%. The failure load was 67.5 % of limit or 120 KN (27,000 lb). The buckle was located slightly below the mid-point of the panel and extending nearly all the way across the panel. The buckle did not completely cross the #1 stringer. Figures 10.4 and 10.5 show the appearance of the panel after removal from the test machine.

10.2.2 FAILURE ANALYSIS. The test data was examined in detail to determine the reason for the disappointingly low failure load. The test panel was also examined in detail for any clue to the failure. This investigation disclosed several major discrepancies in the testing procedure and instrumentation.

10.2.2.1 Instrumentation. The Rockide gages chosen exhibit extremely high apparent strain reaction to temperature. This amounts to 16,000 microstrain at the test temperature. This apparent strain is an order of magnitude higher than the true strain expected during the test. The temperature correction factors for the gages where applied to the test readings failed to give meaningful data on most of the gages.

Every attempt to determine the true strain readings at the test temperature led to misleading and ambiguous results. The most meaningful data obtainable was all based upon strain relative to the strain reading (at temperature) at 20% of limit load.

These data did, however, indicate major load non-uniformities in the panel throughout the load application to failure.

The Rockide gages were very vulnerable to damage and are not reliable enough for this type of test. Each of these gages is equipped with an integral thermocouple. This feature enables thermal strain corrections to be made. The thermocouples, however, were not all utilized.

The raw strain gage data are not presented here because they were meaningless in that form.

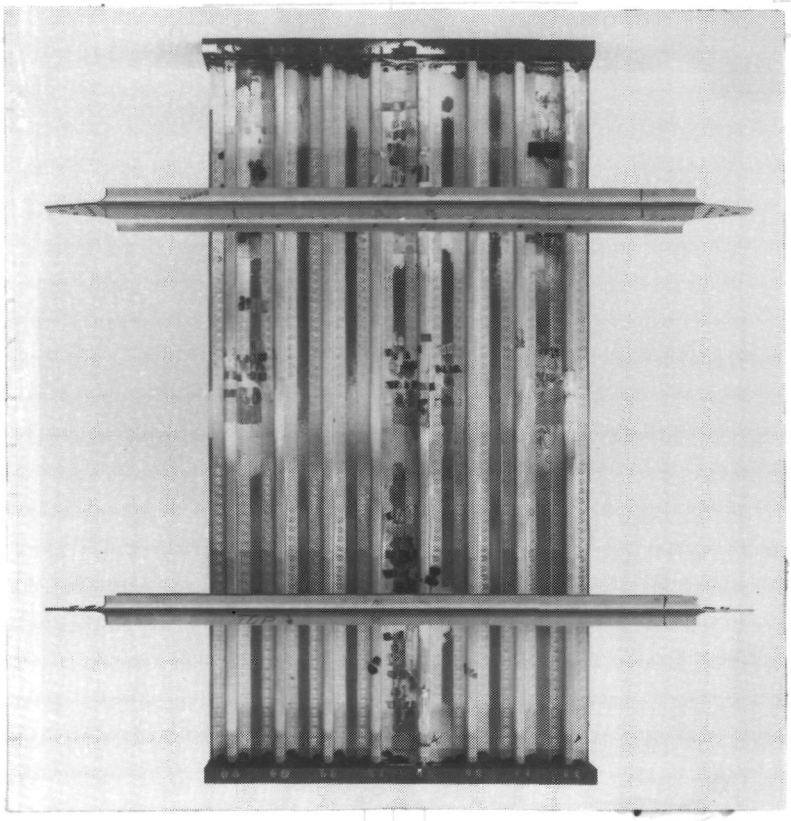

Figure 10.4. Stringer Side of Compression Panel after Testing.

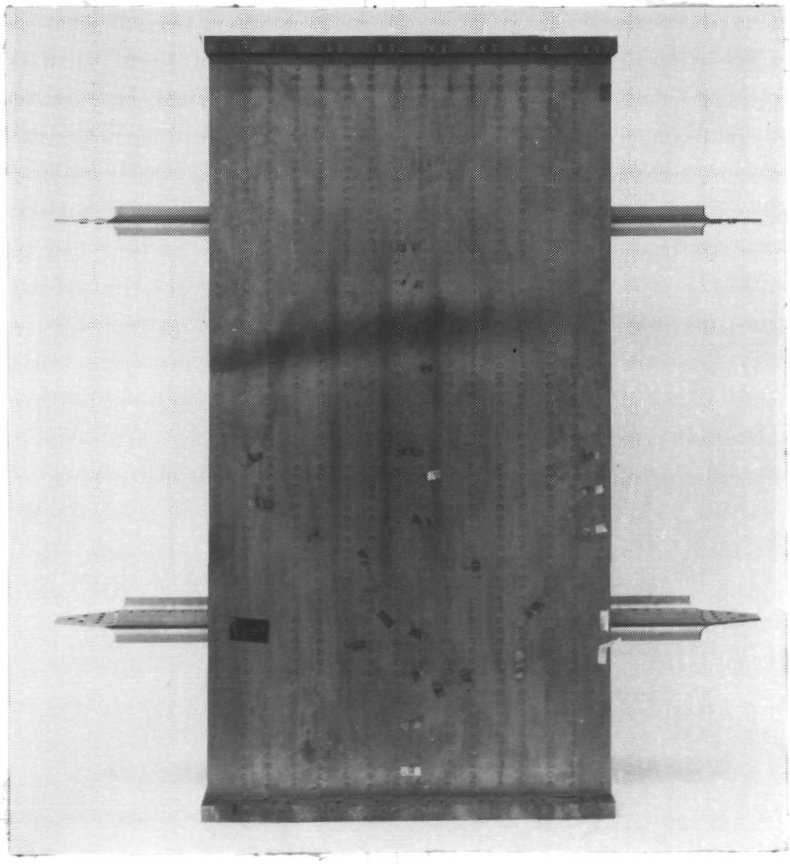

Figure 10.5. Skin Side of Compression Panel after Testing.

Figure 10.6 is a plot of 5 strain gages made by taking the 20% tare load strain at room temperature and adding to it the corrected strain readings at temperature as the load was increased. The absolute value of the strains is in question but the trends appear to be valid. The diagonal straight line extending beyond the plotted data represents the average strain which could be expended for a perfectly uniform stress distribution. It is apparent that some buckling or load redistribution occurred between 40 and 50% limit load; however, this was not apparent to observers watching the panel.

10.2.2.2 Thermocouples. As indicated above, insufficient temperature measurements were available to satisfactorily evaluate the test. Future tests should include more numerous temperature measurements.

After the test, there was some question as to the accuracy of the skin temperature measurements in that they were all on the stringer side of the panel. Prior to removing the failed panel from the test machine, the thermocouples were revised in order to evaluate any temperature gradients through the skin.

The thermocouples were arranged as shown in Figure 10.7. The panel was heated using the lamp banks until the stringer side gages indicated readings as close as possible to the test condition. The face or heated side gages were then read. Table 10-3 summarizes the temperature readings. It is apparent that there was no sizable gradient through the skin and that the stringer side thermocouples truly indicated skin temperatures.

10.2.2.3 Temperature Control. Heating of the panel was accomplished by a group of quartz lamps connected to a single controller. It was apparent that multiple temperature controls using a wider lamp bank was necessary. In addition, some method of insulating the specimen from the machine platens was desirable. The large mass of the machine platens makes it impossible to keep the ends at the desired temperature.

10.2.2.4 Test Setup and Procedure. The non-uniform load distribution in the panel as indicated by the nature of the failure and the strain gage data were reason to question the setup of the panel in the test machine. As indicated by Figure 10.8, the centroid of the panel did not exactly coincide with the centroid of the load axis of the machine. In order to evaluate the effects of this eccentricity, a pair of steel columns were placed between the load heads with their centroid placed at the centroid of the panel. Loads up to 222 KN (50,000 lb) were applied while dial indicators were used to measure the deflection of the upper load introduction plate with respect to the base of the machine.

The columns used for this test were steel pipe 137 cm (54 in) long with a cross section of 45 cm^2 (7 in^2). The large variation in deflection between the ends of the platen was noted. This amount of moment caused the machine to be unstable.

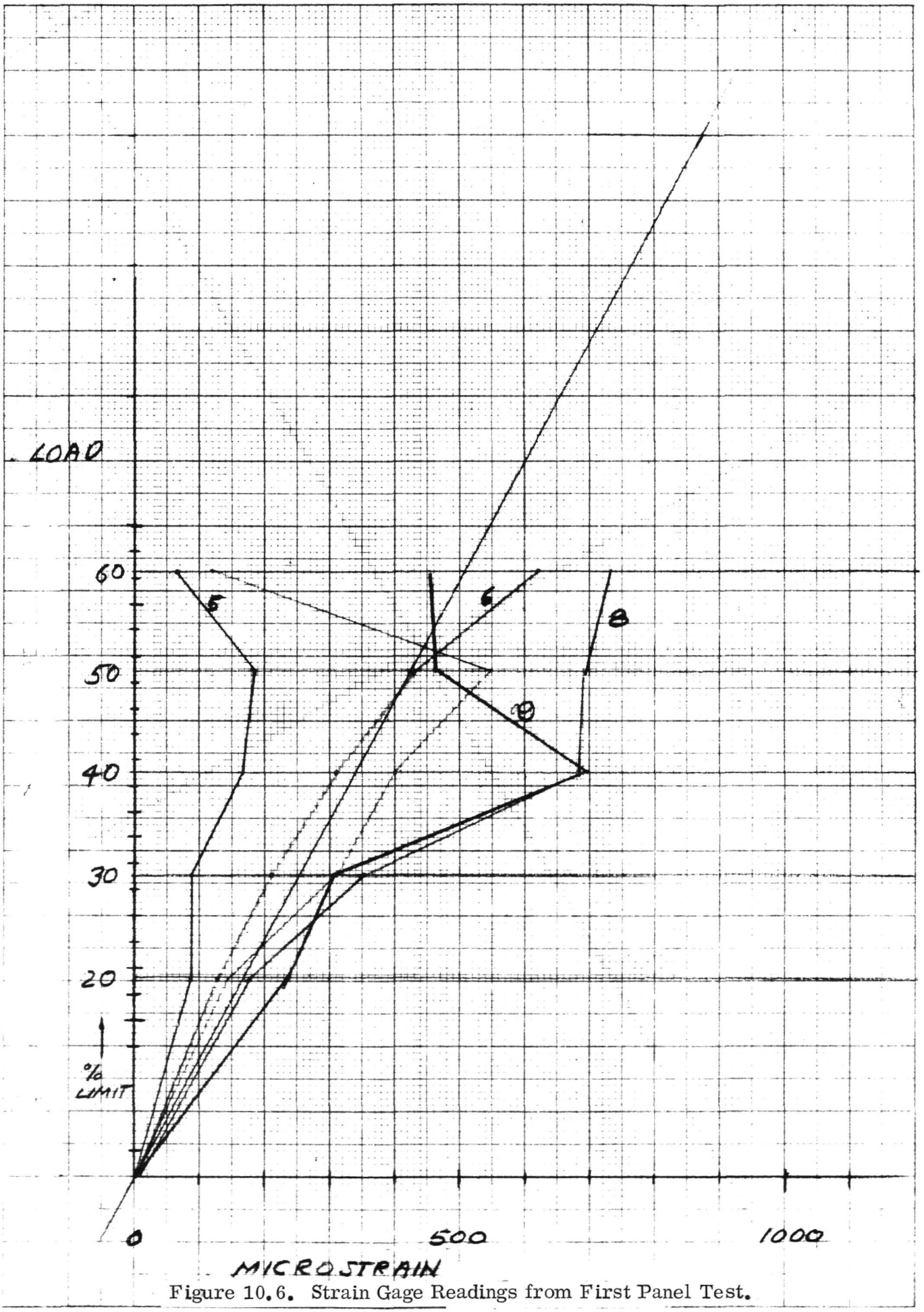

Figure 10.6. Strain Gage Readings from First Panel Test.

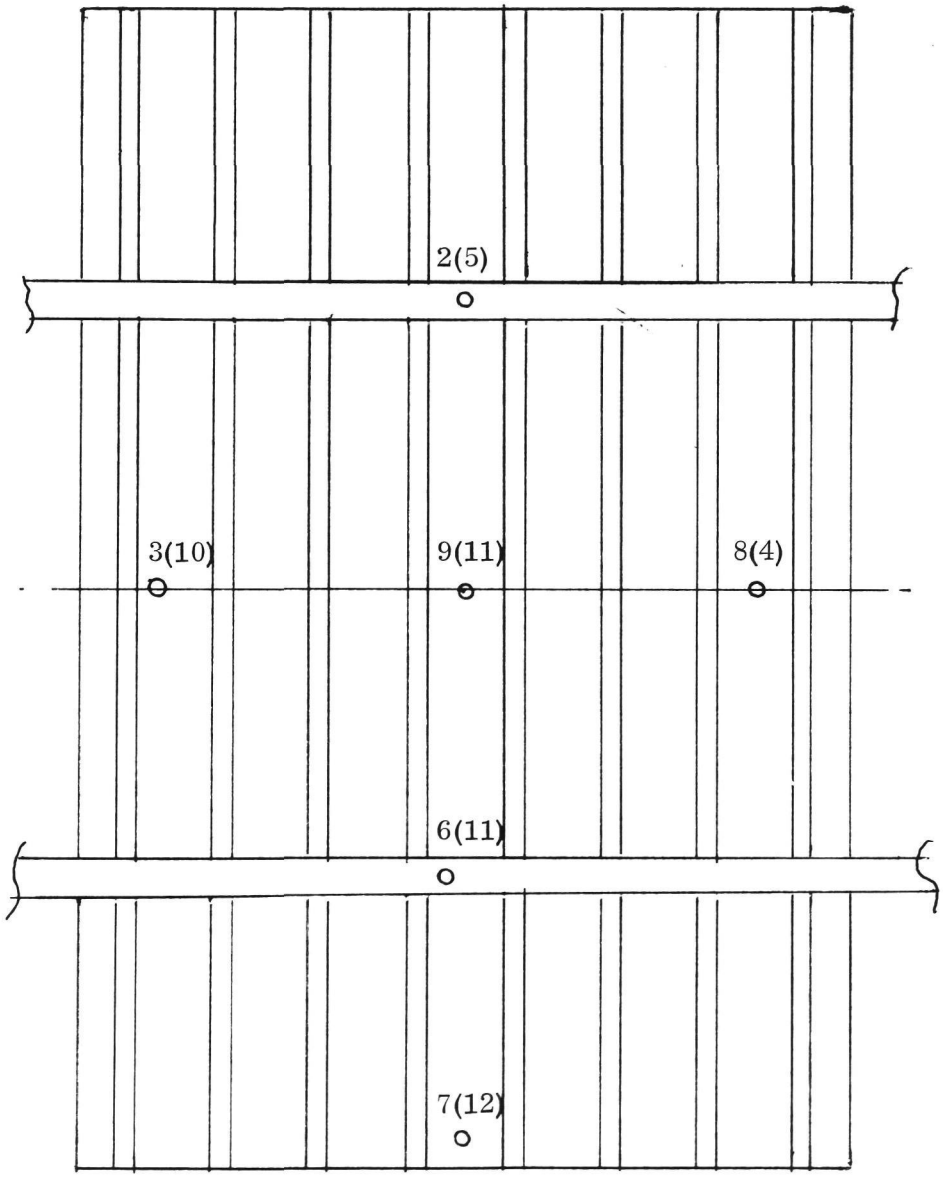

Figure 10.7. Thermocouple Location for Thermal Gradient Survey. Gage numbers in parentheses are on skin side.

Table 10-3. Summary of Thermocouple Readings for Thermal Gradient Survey

2	5	3	10	9	1	8	4	6	11	7	12
303	303	303	303	303	303	303	303	303	303	303	303
(85)	(85)	(85)	(85)	(85)	(85)	(85)	(85)	(85)	((85)	(85)	(85)
469	466	405	439	486	478	433	433	422	447	378	366
(385)	(380)	(270)	(330)	(415)	(400)	(340)	(320)	(300)	(345)	(220)	(200)
522	522	441	493	536	539	489	480	478	489	411	394
(480)	(480)	(335)	(410)	(505)	(510)	(420)	(405)	(400)	(420)	(280)	(250)
578	572	489	522	586	589	533	522	533	536	439	422
(580)	(570)	(420)	(480)	(595)	(600)	(500)	(480)	(500)	(505)	(330)	(300)
633	630	528	572	647	658	583	578	589	594	478	461
(680)	(675)	(490)	(570)	(705)	(725)	(590)	(580)	(600)	(610)	(400)	(370)
			5 Minute Soak								
628	622	519	558	628	641	569	564	583	586	478	458
(670)	(660)	(475)	(545)	(670)	(695)	(565)	(555)	(590)	(595)	(400)	(365)

Note: 1. Thermocouple numbers are given in matching pairs. The first number in each pair denotes the gage on the stringer side of the panel.

2. Temperatures in Degrees

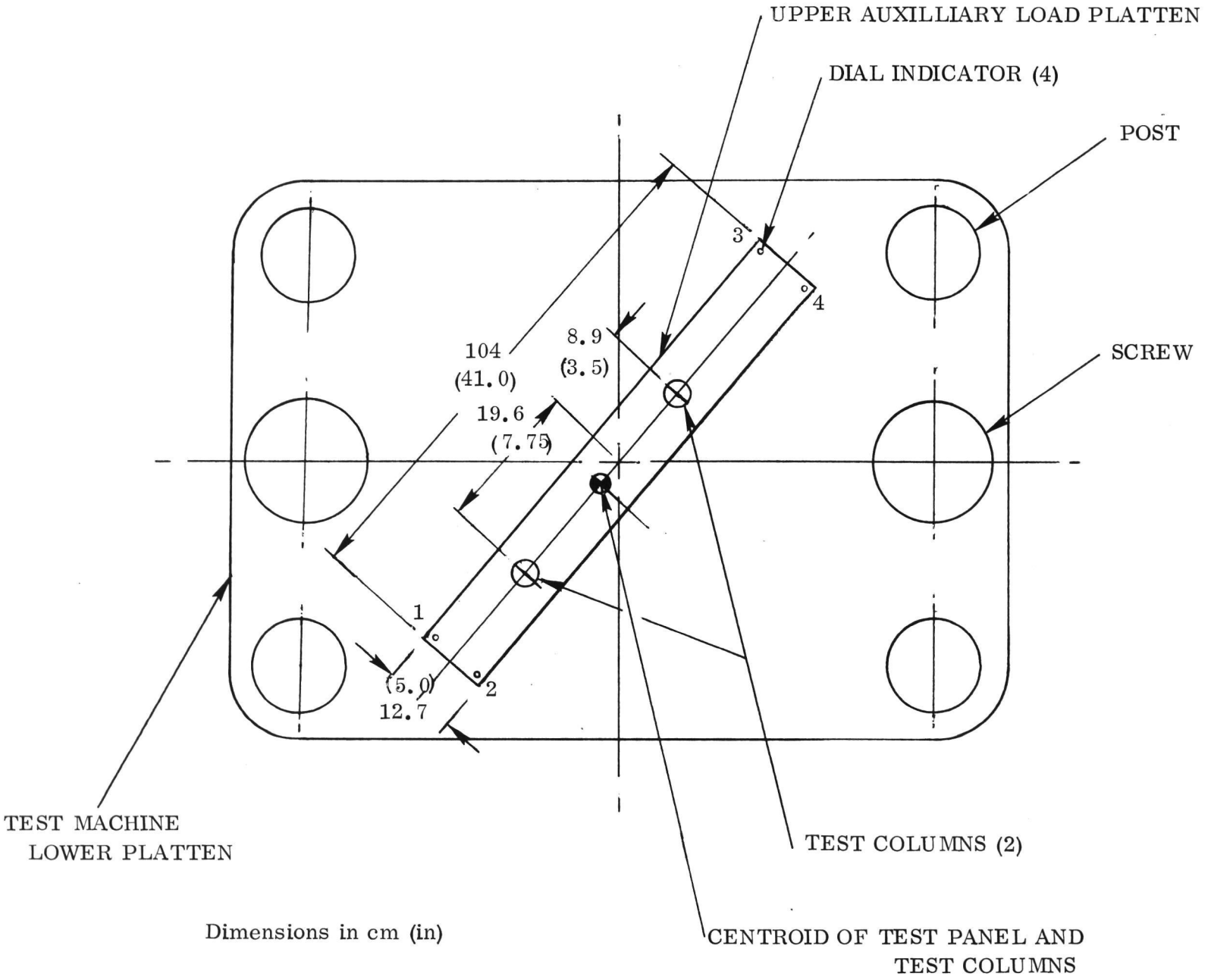

Figure 10.8. Schematic Diagram of Test Machine.

The machine was modified to enable the compression specimen to be placed on the centroid of the machine to preclude this type of problem.

10.2.2.5 Recommendations. The following recommendations were a result of the failure analysis and should be followed for the test of the second panel.

1. The lamp bank should be zoned such that there are at least 5 independently controlled channels for the heat lamps.

2. The heat lamps should extend a few inches past the panel edges; more heat is required near the edges and much more on the ends.

3. The end fixity fixture should be thermally insulated from the test machine head.

4. Every strain gage should have a thermocouple at the same location.

5. Several heat runs should be made prior to test to exercise the strain gages and adjust heat lamp spacing.

6. Static loads up to approximately 40%-50% of limit should be applied to the cold panel to verify evenly distributed load introduction.

10.3 TESTING OF SECOND PANEL

10.3.1 INTRODUCTION. As a result of the premature failure of the first compression panel, it was decided to subject the second panel to the static test plan rather than the fatigue plan as originally proposed. Special precautions were taken to prevent a recurrence of the test problems encountered during the first test.

10.3.2 TEST PREPARATION. The testing machine was recalibrated and the special load introduction heads were removed, checked for flatness and reinstalled such that the centroid of the test panel coincided with the centroid of the testing machine.

The heat lamp system was extensively modified to provide 5 zones of control, one for each of the lamp assemblies. After an initial heating test, one thermocouple in each zone was chosen to be monitored continually during the test. These same thermocouples were wired to the thermal control system and to an overheat warning alarm.

Several loading cycles up to 40% of limit were run at room temperature in order to verify the uniformity of load introduction. Initial tests were run using thin asbestos sheets between the specimen ends and the machine platens to block the flow of heat into the heavy steel structure.

The asbestos proved to be too resilient and was removed. Thereafter, reasonably uniform strain distribution was obtained.

Several heating cycles were attempted in order to tune the lamp bank controllers. During what was planned to be the last test before the actual panel structural tests, a thermocouple became dislodged from the specimen as the specimen was approaching 589K (600F). The thermocouple which became loose was connected, for that zone, to the controller, temperature monitor and alarm. The controller sensed a drop in temperature and turned full on in an effort to maintain the temperature.

The test conductor was unaware of this discrepancy and continued the test for several minutes. No mechanical load was applied during this time. When the heat was turned off, the specimen was checked and found to be severely overheated and locally buckled. All of the strain gages in the overheated area were dislodged. Several buckles were apparent on the edge of the panel and extended across 3 stringers.

Figures 10.9 and 10.10 show the size and extent of the buckles.

The panel was removed from the test machine for further evaluation.

10.3.3 POST TEST EVALUATION. The panel was inspected and the extent of the damage determined. The overheated area and buckles are limited to the 3 stringers on one side of the panel and between the two frames.

Temperature data from the test during which the panel was damaged has been reviewed. Only one burst of data was recorded during the time that the overheat condition existed, and this did not record the maximum temperature. The maximum temperature recorded in the damaged area was 719K (835F) with other temperatures showing 644-700K (700-800F).

Figure 10.11 shows the skin side of the panel with the darkened area caused by overheating. The original photo in color shows this to be dark blue in color. An attempt was made to determine the local temperature reached during the test. Samples of similar gage titanium were exposed to radiant heat and raised to various temperatures. The resulting discoloration was compared to the color of the test panel. It has been decided that the maximum temperature reached locally was from 755K to 811K (950F to 1000F).

10.3.4 PANEL REPAIR. The instrumentation was removed from the panel and the two frames removed. The panel was then placed on a surface plate and the buckles evaluated.

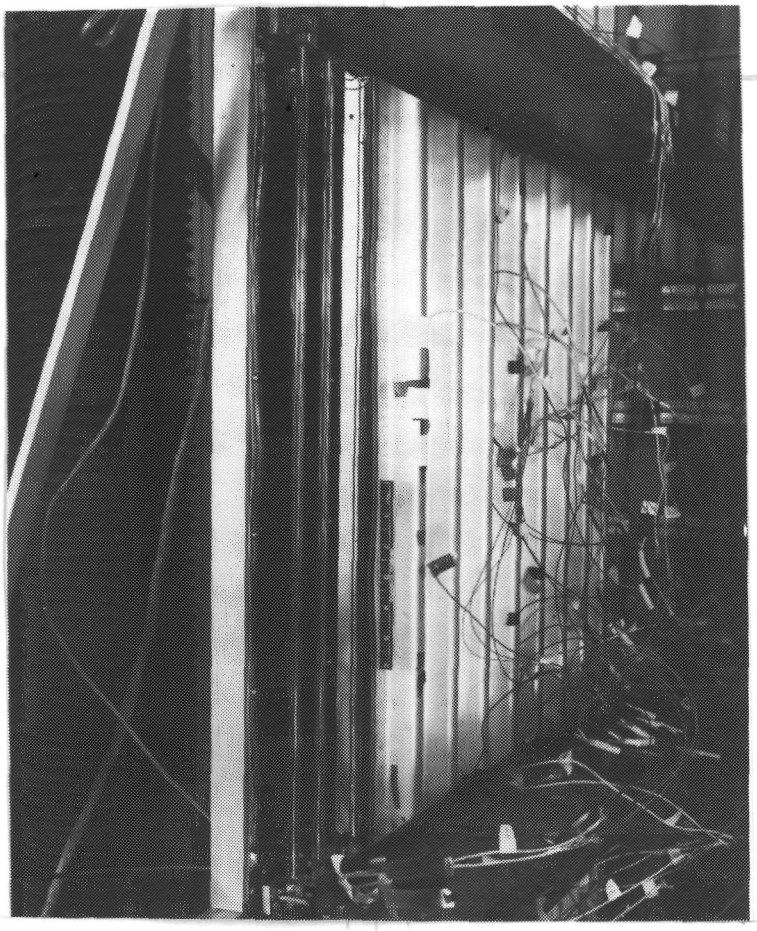

Figure 10.9. Edge of Compression Panel Buckled due to Overheating.

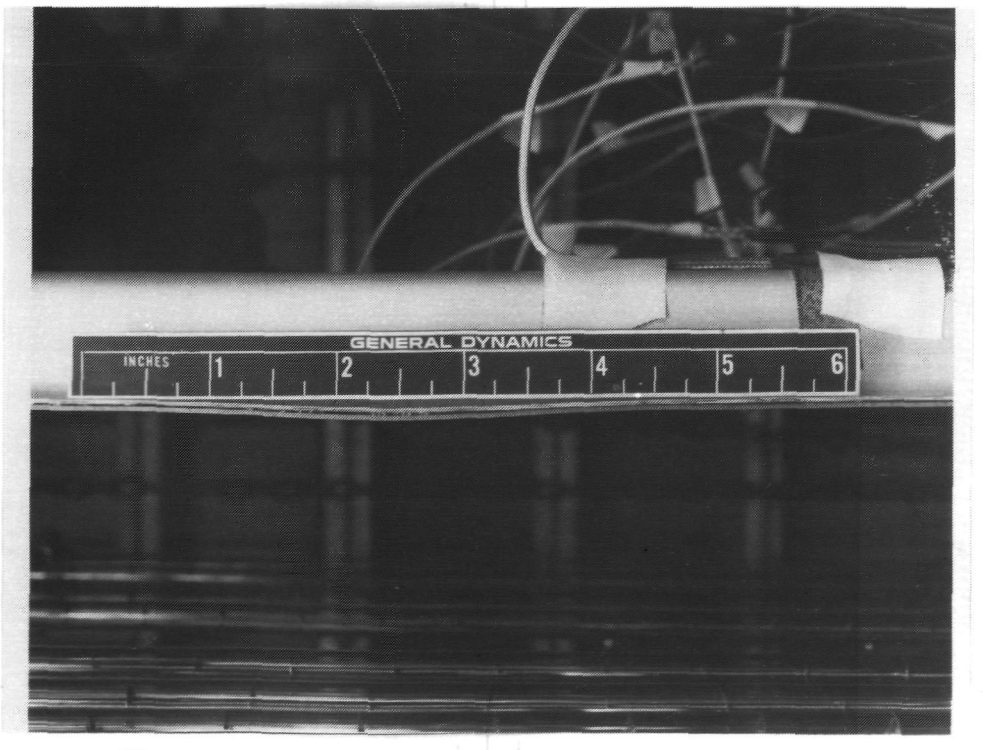

Figure 10.10. Closeup of Buckled Edge of Panel.

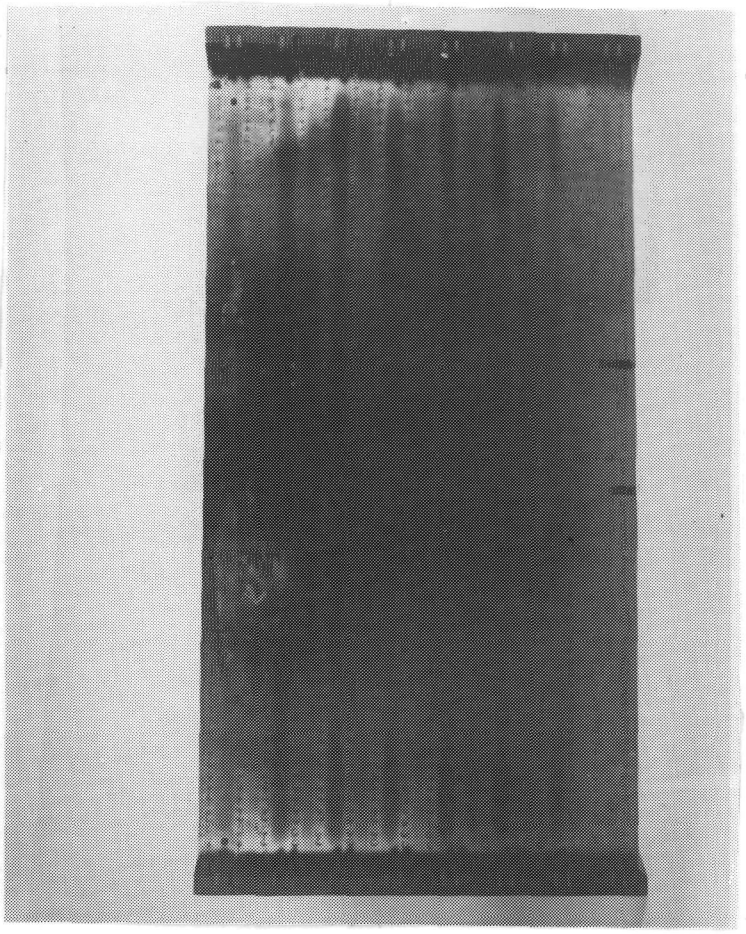

Figure 10.11. Discoloration of Skin due to Overheating.

A decision was made to repair the panel and attempt to test it again. The buckled stiffeners were successfully straightened using the local application of heat and pressure. Because it was not possible to obtain perfectly straight stringer flanges and the possibility that the boron was degraded due to overheating locally, it was decided to reinforce the skin flanges of the three damaged stringers.

Five boron/aluminum angles $[0_6]$ 1.09 mm thick were hot formed. The angles were attached to the stringers by means of rivets and adhesive bonding. Hexcel 951 material was used for the bonding operation. An 0.81 mm (0.032) titanium doubler was added to the skin side of the panel. Figures 10.12 and 10.13 illustrate the repared panel.

One of the end blocks was found to be loosened and this was removed, cleaned and rebonded to the panel. The panel was then checked for flatness and the end blocks machined flat and parallel.

10.3.5 FAILURE MODE AND EFFECTS ANALYSIS. Prior to testing the repaired compression panel, a detailed study was made of all potential failure modes. A systems analysis approach was utilized to determine potential means by which the panel could be damaged by human error or equipment failure during testing.

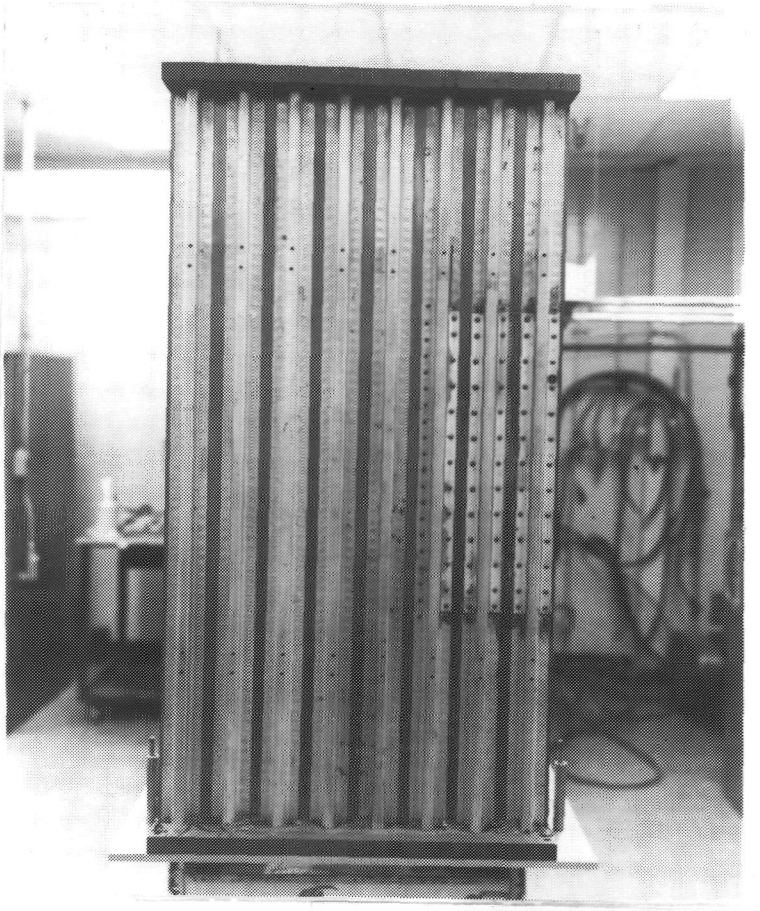

Figure 10.12. Stringer Side of Repaired Compression Panel.

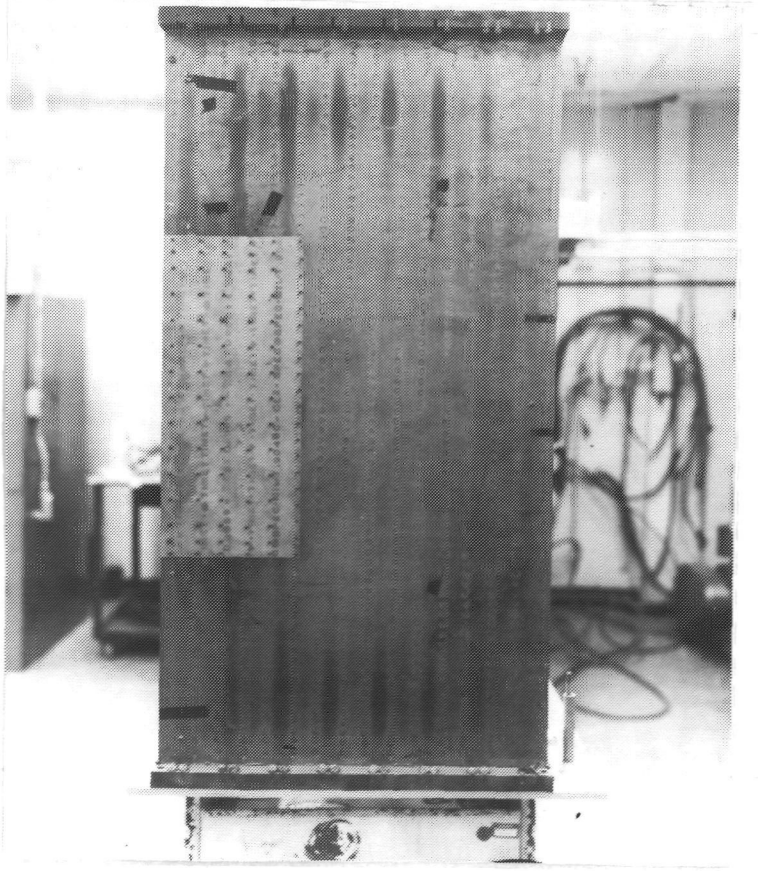

Figure 10.13. Stringer Side of Repaired Panel.

The purpose of this analysis was to:

(a) Analyze those elements necessary to test a composite compression plate stringer at elevated temperature.

(b) Determine the probable mode of failure of each element.

(c) Determine the probable effect of these failures on the test specimen.

(d) Plan preventive action.

Assumptions

1. It is assumed in this analysis that all personnel conducting the tests and obtaining test data are sufficiently qualified to operate the necessary equipment.

2. It is assumed in this analysis that the test is conducted in an area and time such that outside influences have negligible effect; i.e., all equipment and personnel are dedicated solely to this test during the test period.

Figures 10.14 and 10.15 delineate the test systems and operations.

Table 10-4 identifies the failure modes, failure effects and preventive action.

The definition of the failure classes is as follows:

Class

I Catastrophic - Data lost and specimen damaged beyond repair or severe capital equipment damage.

II Severe specimen damage but repairable — major data invalidation but some is available.

III Minor data invalidation or test delay rectified by system repair and reruns.

IV Data acquisition or setup error but recoverable by rerun without repair.

V Minor test delay.

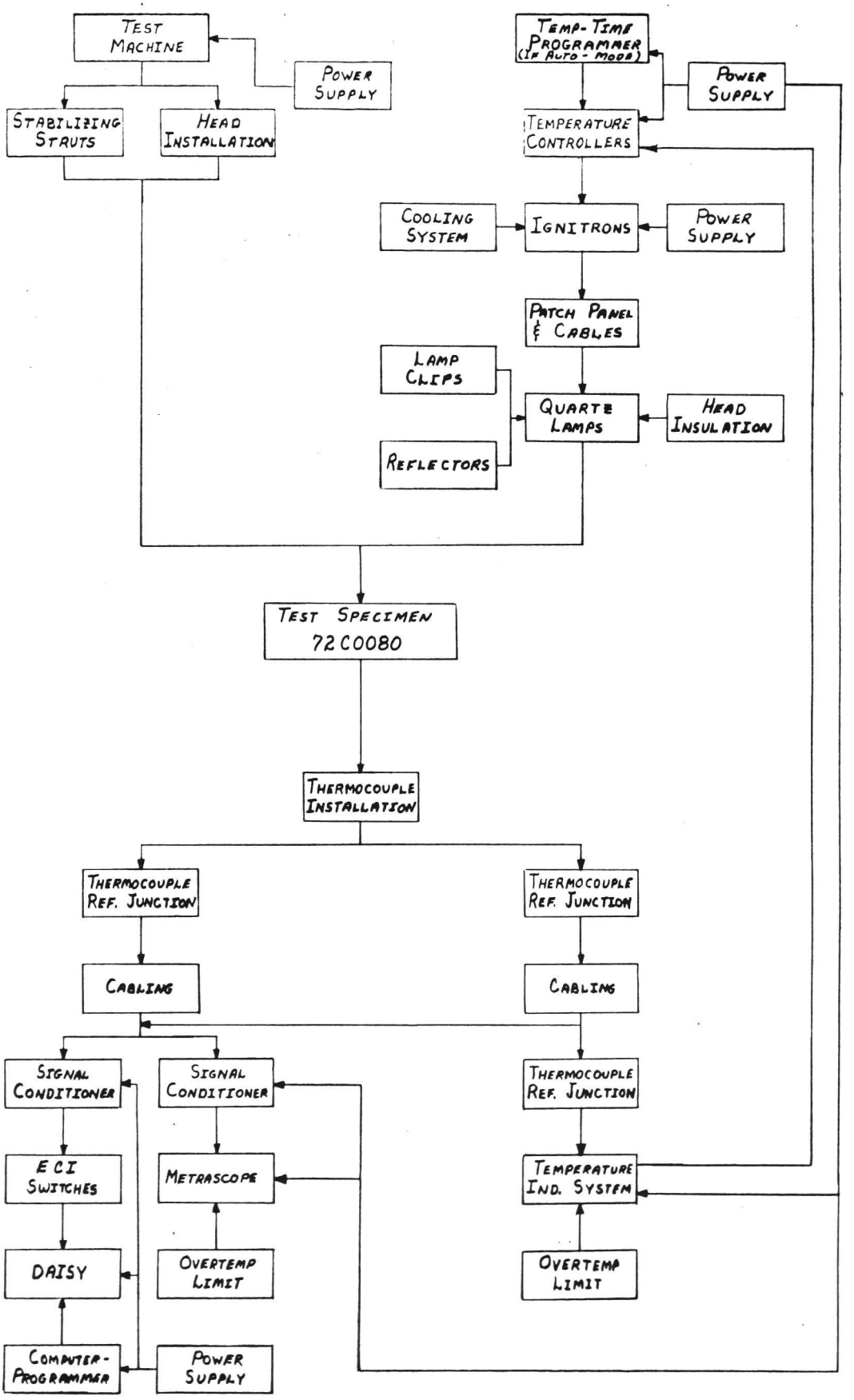

Figure 10.14. Equipment Logic Diagram.

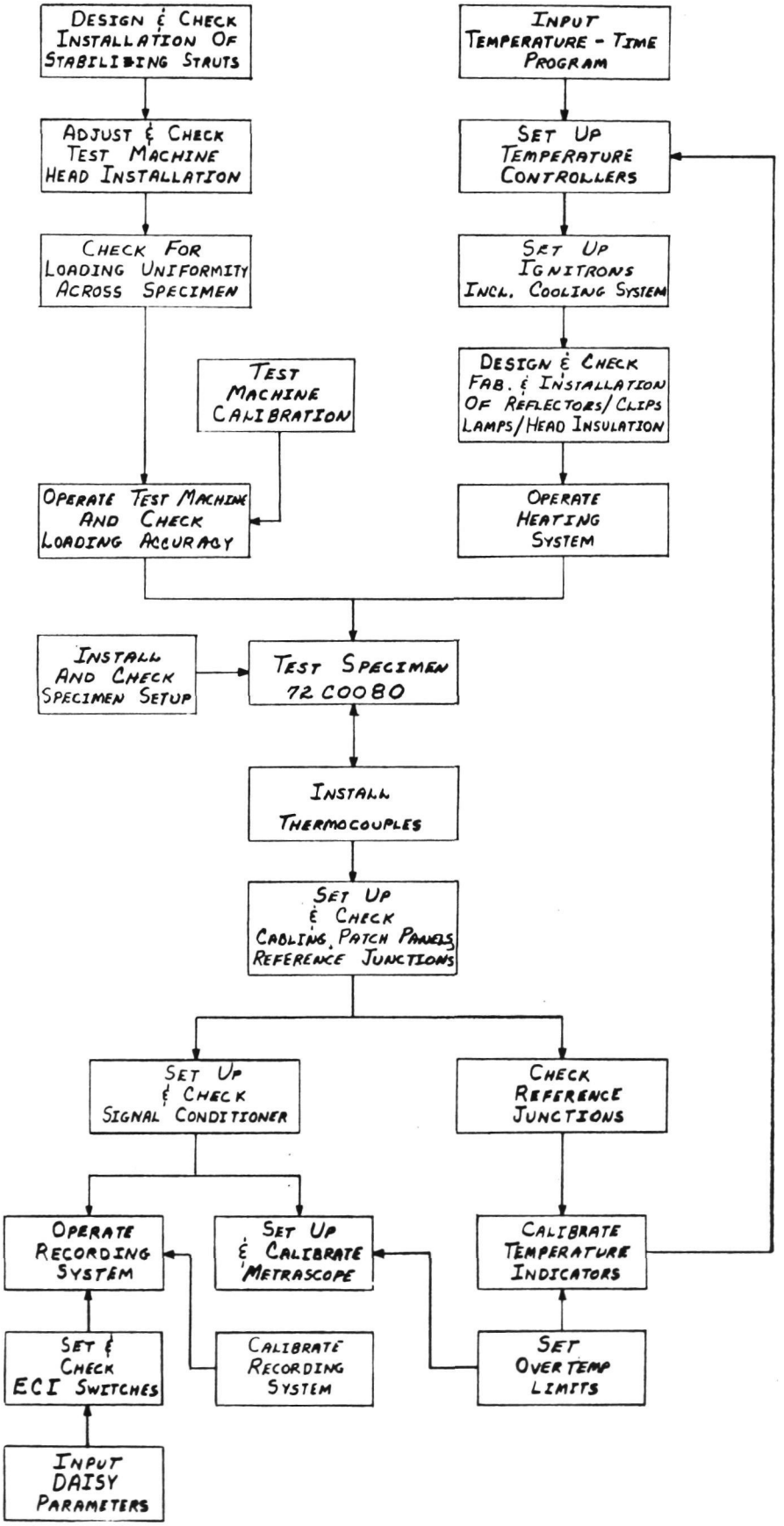

Figure 10.15. Operations Logic Diagram.

Table 10-4. Failure Modes and Effects Analysis

SYSTEM / SUBSYSTEM	FUNCTION	FAILURE MODE	FAILURE EFFECT	FAILURE CLASS	PREVENTIVE ACTION
Heat System					
Programmer - temperature indicator.	Provides indication of temperature and servo error voltage control	Component failure which drives indication up.	Reduces heat power in servo control mode. Provides erroneous monitor data.	IV	Set programmer alarm and overtemp so entire system is shut down. Failure not predictable.
		Component failure which drives indication down.	Causes full power in servo control mode. Strong specimen failure potential. Erroneous monitor data.	I	Set monitor alarm to alert observer. System shut down by automatic alarm switch to be considered. Set error voltage limiter to control maximum control voltage available.
Programmer - drum drive.	Rotates drum containing control curve.	Component failure drives one drum out of phase with remainder of the system.	Slow drum will cause low power on one channel and uneven heat distribution.	III	Set up redundant monitor system. Test conductor to determine action.
			Fast drum will cause high power on one channel and uneven heat distribution but will not exceed test requirements.	III	Redundant monitor system. Set error voltage limiter. Test conductor or automatic alarm to shut down system.
Programmer - probe follower.	Follows control curve.	Component failure-probe wanders or drives up or down.	Probe drives down. Reduces power on one heat channel.	III	Set up redundant monitor system. Test conductor to determine action.
			Probe drives up. Can cause full power and strong specimen failure potential.	I	Set up monitor alarm and consider automatic alarm switch. Set error voltage limiter.
Ignitron-tube or pulser.	Controls power proportionate to programmer output.	Component failure causing power reduction or increase.	Reduction will reduce heat and uneven distribution.	III	Set up redundant monitor system. Test conductor to determine action.
			Increase will cause up to full power on one or more heat channels.	I	Redundant monitor and controller alarms systems set for automatic shut down.
Reflector Installation	Lamp holder and infra-red reflection.	Uneven specimen heat.	Specimen local buckles, Damaged Material, Unuseable data.	II	Run dummy specimen. Increase number of control channels and adjust number of lamps and locations as required. Make check runs on test specimen. Provide insulation at specimen ends.
		Shorted lamp bank or incorrect cable attachment.	Arcing on test machine and damage to data acquisition system	I	Perform two independent secondary checks of the reflector design and engineering inspections of the reflector manufacture and installation. Provide adequate insulation and grounding.
		Lamp breakage.	Shorted lamp bank arced and damaged specimen.	I	Incorporate adequate lamp and reflector support in design.
		Reflector support failure	Shorted lamp bank, arced and damaged specimen.	I	Incorporate adequate lamp and reflector support in design.
		Incorrect cable hookup.	Shorted lamp bank.	I	Perform two checks of design and hookup installation.

Table 10-4. Failure Modes and Effects Analysis

SYSTEM / SUBSYSTEM	FUNCTION	FAILURE MODE	FAILURE EFFECT	FAILURE CLASS	PREVENTIVE ACTION
Load System					
Head installation	Apply contact loads	Uneven load application.	Undesireable strain distribution.	V	Verify head installation is centered, square, parallel, and that the base is smooth, flat, and clean.
Machine setup procedure	Proper load application and indication.	Insufficient hyd. bed. Insufficient oil. Machine out of calibration.	Incorrect (low) load.	IV	Pretest verification of proper operating procedures per manufacturer's manual. Inspection of machine condition by qualified personnel. Verification of setup by second independent check.
			Incorrect (high) load - Potential specimen failure without valid data.	I	
Machine load system	Apply and indicate test loads.	Load surge.	Specimen damage.	II	Apply loads at low rate and in increments.
		Overload.	Specimen damage or destruction -	II	Provide test operator observer to verify applied loads.
		Rotation of load system.	Induced bending of specimen and binding of the test machine.	III	Pretest verification of head and specimen center lines. In-test deflection verification of proper machine alignment.
Specimen installation.	Provides test data.	Uneven specimen heat.	See reflector installation	III	Provide heat barrier between specimen and test machine and use heat absorption paint as required.
		Uneven strain and induced bending.	Unreliable data to support design verification.	V	Grind specimen ends flat and square. Shim specimen as required. Make low load test runs to verify equitable distribution.

Table 10-4. Failure Modes and Effects Analysis

SYSTEM / SUBSYSTEM	FUNCTION	FAILURE MODE	FAILURE EFFECT	FAILURE CLASS	PREVENTIVE ACTION
Data Acquisition					
Instrumentation installation.	Provides strain and temperature sensors.	Wrong location.	Incorrect data and design criteria evaluation and analysis.	III	Perform quality assurance inspection of instrumentation layout and installation location. Provide specific sign off.
		Deviated installation procedure.	Sensor bond failure. Low resistance to ground or high circuit resistance.	III	Perform quality assurance and/or engineering inspection and verification of conformance to authorized written procedures.
		Sensor bond failure.	Erroneous control or evaluation data. - See heat controllers.	III	Pretest verification of applicable installation procedure. See bond failure effect. Provide redundant thermocouples on analog monitor system. Use split junction and parallel circuit thermocouples where applicable.
		Incorrect thermocouple material used or sensor connection misidentified.	Erroneous data on two or more channels.	III	Second independent check of installation and materials. Pretest verification and calibration of sensor output.
Thermocouple suitcase.	Provides constant reference junction temperature.	Equivalent to power off - i.e., reference temperature low.	All temperatures read higher than actual. Improper data for evaluation and analysis.	IV	Monitor constant reference junction temperature on continuous read out equipment. Record junction temperature with test data for permanent record. Redundant thermocouples to use redundant suitcase. Temperature change alarm to be used on monitor.
		Control switch stays closed. - i.e., reference temperature high.	All temperatures read lower than actual. Improper data and potential specimen destruction.	I	
Visual monitor equipment.	Dual observation of real time temperatures.	Solid state components.	Erroneous readings on one or more channels.	III	Not predictable - comparison to programmer direct readout to provide data for test conductor to initiate hold or stop.
		Poor pin contact.	Same as above.	III	Perform pretest cleaning and checkout maintenances.
		Improper calibration and scaling.	Same as above.	III	Provide complete second independent check of all settings.
		Improper scaling of alarms.	Potential specimen failure.	I	Same as above.
Signal conditioner balance pot.	Signal adjustment for zero balance.	Zero drift.	Erroneous data on affected channel.	IV	Pretest clean up of pot by verifying signal condition with oscilloscope.
DAISY ECI switches. DAISY parameters. DAISY switch settings. DAISY computer Reference tables.	Condition and record temperature and strain data.	Improper setup of input computer.	Same as above.	IV	Perform second independent check of each step written setup procedure, with Real verification prior to test start. Clean and check ECI switches.

10.4 PANEL NO. 2 SECOND TEST

10.4.1 PREPARATION. Based upon the failure analysis, a test procedure was prepared which incorporated fail safe procedures and necessitated the use of redundant sensing and alarm systems.

A special network of 12 thermocouples distributed around the panel was connected to a real time monitor which also included an over temperature cutoff and alarm on each of the 12 channels. These thermocouples were used in addition to the 32 thermocouples used for each strain gage location.

Special operating procedures were written for the testing machine operator with a second person in attendance to verify proper operation of the loading controls.

In an effort to reduce the heat loss into the machine platens, blocks of Marinite insulation were placed between the steel end blocks of the specimen and the machine platens. This material was approximately 2.5 cm (1 in) thick and was machined flat and parallel before use. Several samples of the material were tested in compression to verify that the material had sufficient strength and stiffness.

In order to eliminate minor inaccuracies in the flatness of the steel end blocks and the insulation, the faying surfaces of these members were coated with Epoxylite high temperature epoxy which was then cured with a slight compression load applied.

Considerable time was spent in assuring that uniform load application was obtained. The specimen centroid was placed on the load center of the machine and stainless steel foil shims were used locally between the insulation blocks and machine platens. Numerous loading cycles of room temperatures to 40% of limit load were made prior to testing of temperature.

Several heat runs were made and the lamp bank zones adjusted to achieve uniform heat distribution. The insulation blocks improved the temperature drop off at the end from that previously experienced.

Flat black graphite paint was applied to local areas of the panel to help raise the panel temperature in these areas.

10.4.2 MODIFIED TEST PLAN.

10.4.2.1 Room Temperature Run to 40% Design Limit.

a) Verify that strain gages and thermocouples have been checked end-to-end.

b) Verify that the temperature indicating dials are functioning.

c) Center specimen in test machine.

d) Raise machine bed 5 cm (2.0 in) assuring that upper head has adequate clearance.

e) Install side braces (4) and adjust so that they are supported in a level position and are not applying load to specimen.

f) Real and Zero-cal instrumentation.

g) Apply approximately 448 N (100 lb) to specimen and check that it is centered and level and that side braces are adequately supported.

h) Apply 10%, 20%, 30%, and 40% design limit load, recording instrumentation after each load application increment.

j) Review strain data for uniformity of strain distribution. Shim specimen as necessary.

10.4.2.2 No Load Run with 589K (600F) Skin Temperature.

a) Verify that strain gages and thermocouples are in proper working order.

b) Install a protective metal shield between infrared heaters and specimen.

c) Check wiring from panel distribution box to specimen and from specimen to instrumentation monitor and controls.

d) Go through Structures Test Manual to prepare heat equipment for test.

e) Verify that Metrascope limits are set at 380K (225F) and that the dump circuit is operative.

f) Verify that the manual dump circuit is operative.

g) Set the programmer overtemperature switches to 385K (230F).

h) Place the reflector at least six inches from the shielded specimen.

i) Station an observer at the specimen, one at the Metrascope and one test conductor at the heat controller.

j) Take ambient temperature data.

k) Start heating, gradually increasing the voltage to a maximum of 480 volts.

l) Verify that all heaters are operative.

m) Remove all voltage from lamps.

n) Remove protective shield specimen.

o) Apply voltage to heat lamps and adjust settings as necessary to stabilize temperatures at 366K (200F) and record instrumentation.

p) If it is obvious that the voltages will exceed 480 volts at 589K (600F), remove all voltage and move reflector to 4 inches from specimen and repeat paragraph "o".

q) Set Metrascope to 491K (425F) and overtemperature switches to 494K (430F).

r) Increase voltage as necessary to stabilize panel at 489K (400F) and record instrumentation.

s) Set Metrascope to 603K (625F) and overtemperature switches to 616K (650F).

t) Increase voltage as necessary to stabilize panel at 589K (600F) and record instrumentation.

u) Obtain program manager's approval of data before proceeding.

10.4.2.3 40% Limit Run at 489K (400F).

a) Set Metrascope limit at 380K (225F) and overtemperature switches at 383K (230F).

b) Apply 40% design limit load; read instrumentation.

c) Gradually heat specimen to 366K (200F) and record instrumentation.

d) Set Metrascope limit to 491K (425F) and overtemperature switches to 494K (430F) while continuing to maintain 40% design limit load. Record instrumentation.

e) Obtain program manager's approval before beginning test.

10.4.2.4 Test.

a) Make checks - Paragraphs 10.4.2.1 a, c, d, and e.

b) Perform checks - Paragraphs 10.3.2.2 c, d, e, f, and i.

c) The skin temperature limits are 589K ±14K (600F ±25F) except for ends which are 589K $^{+28K}_{-83K}$ (600F $^{+50F}_{-150F}$).

d) Record 10% limit load and 589K (600F) temperature data as tare.

e) Set Metrascope to 616K (650F) and overtemperature switches to 619K (655F).

f) Apply 20% design limit load and record data.

g) While maintaining the 589K (600F) temperature, increase the load to 40% and record data. Continue to load in 20% design limit increments to 100% design limit, recording data at each increment.

h) Record data at 110, 120, 130, 140, 150% of design limit loading.

i) Continue loading in 10% design limit increments to specimen failure.

10.4.3 PANEL NO. 2 SECOND TEST. Testing was accomplished in accordance with the previously defined plan. The specimen was heated to 589K (600F) and loads applied incrementally up to 80% limit in steps of 20% limit. Data recording was expedited to minimize the creep effects of holding a load at temperature. The total time from 20% limit to 80% limit was approximately 13 minutes.

Strains and temperatures measured during this test are shown in Table 10-5. It should be noted that 20% D.L.L. was "tare" and strains were set at 0. The specimen failed at 172 KN (38,750 lb) (99.8% D.L.L.) by crippling between the bulkhead and specimen end. The crippling initiated on the edge of the panel which had been repaired and spread most of the way across the panel.

Figure 10.16 shows the appearance of the panel after cooling and removal from the test machine. The buckle was more prominent while under load and at temperature. The shape of the buckle and the nature of the failure in the stringers are shown in Figures 10.17 and 10.18.

Table 10-5. Panel #2 Test Data Microstrain and Temperatures.

SS-CPNL 600 20 % DATE: 5 / 11 / 73 TIME: 13 : 59 : 2

FILE: 1 RECORD: 76 CHANNELS 3 THROUGH 77

CHAN							
3	-32.	S1	-54.	S2	-77.	S3	-69. S4
7	-101.	S5	-54.	S6	-56.	S7	-124. S8
11	-134.	S9	-57.	S10	-129.	S11	-96. S12
15	-106.	S13	-139.	S14	+.		-29. S16
19	-111.	S17	-165.	S18	-106.	S19	-101. S20
23	-39.	S21	-47.	S22	+.	S23	-33. S24
27	-48.	S25	-63.	S26	-104.	S27	-114. S28
31	+.		-122.	S30	-252.	S31	-198. S32
35	-186.	S33	-2.	S34A	-74.	S34B	-29. S34C
39	+495.	T1	+540.	T2	+493.	T3	+557. T4
43	+504.	T5	+544.	T6	+561.	T7	+567. T8
47	+509.	T9	+500.	T10	+585.	T11	+523. T12
51	+602.	T13	+595.	T14	+521.	T15	+415. T16
55	+480.	T17	+471.	T18	+539.	T19	+522. T20
59	+446.	T21	+574.	T22	+573.	T23	+595. T24
63	+603.	T25	+582.	T26	+584.	T27	+602. T28
67	+627.	T29	+612.	T30	+513.	T31	+569. T32
71	+573.	T33	+508.	T34	+587.	T22C	+586. T24C
75	+582.	T26C	+582.	T27C	+570.	T32C	

SS-CPNL 600 40 % DATE: 5 / 11 / 73 TIME: 14 : 10 : 3

FILE: 1 RECORD: 80 CHANNELS 3 THROUGH 77

CHAN							
3	-79.	S1	-250.	S2	-141.	S3	-274. S4
7	-198.	S5	-146.	S6	-204.	S7	-332. S8
11	-330.	S9	-74.	S10	-370.	S11	-297. S12
15	-282.	S13	-330.	S14	+.		-81. S16
19	-384.	S17	-564.	S18	-283.	S19	-292. S20
23	-168.	S21	-310.	S22	+.	S23	-165. S24
27	-206.	S25	-203.	S26	-365.	S27	-252. S28
31	+.		-260.	S30	-573.	S31	-507. S32
35	-548.	S33	-9.	S34A	-179.	S34B	-69. S34C
39	+505.	T1	+543.	T2	+488.	T3	+552. T4
43	+505.	T5	+542.	T6	+562.	T7	+573. T8
47	+512.	T9	+493.	T10	+571.	T11	+516. T12
51	+590.	T13	+580.	T14	+510.	T15	+419. T16
55	+476.	T17	+486.	T18	+548.	T19	+521. T20
59	+453.	T21	+579.	T22	+563.	T23	+597. T24
63	+605.	T25	+582.	T26	+587.	T27	+587. T29
67	+600.	T29	+592.	T30	+501.	T31	+574. T32
71	+566.	T33	+510.	T34	+587.	T22C	+584. T24C
75	+583.	T26C	+590.	T27C	+574.	T32C	

Table 10-5. Panel #2 Test Data Microstrain and Temperatures (continued)

SS-CPNL 600 60 % DATE: 5 / 11 / 73 TIME: 14 : 11 : 15

FILE: 1 RECORD: 81 CHANNELS 3 THROUGH 77

CHAN							
3	-104.	S1	-442.	S2	-151.	S3	-549. S4
7	-282.	S5	-260.	S6	-377.	S7	-526. S8
11	-466.	S9	-253.	S10	-586.	S11	-526. S12
15	-461.	S13	-548.	S14	+.		-411. S16
19	-511.	S17	-912.	S18	-397.	S19	-408. S20
23	-563.	S21	-532.	S22	+.	S23	-334. S24
27	-385.	S25	-376.	S26	-577.	S27	-449. S28
31	+.		-493.	S30	-777.	S31	-695. S32
35	-807.	S33	-19.	S34A	-296.	S34B	-114. S34C
39	+505.	T1	+548.	T2	+488.	T3	+552. T4
43	+504.	T5	+544.	T6	+562.	T7	+571. T8
47	+513.	T9	+493.	T10	+571.	T11	+516. T12
51	+590.	T13	+581.	T14	+510.	T15	+418. T16
55	+478.	T17	+487.	T18	+549.	T19	+521. T20
59	+452.	T21	+578.	T22	+567.	T23	+598. T24
63	+605.	T25	+581.	T26	+586.	T27	+588. T28
67	+613.	T29	+596.	T30	+504.	T31	+573. T32
71	+566.	T33	+509.	T34	+586.	T22C	+586. T24C
75	+582.	T26C	+584.	T27C	+572.	T32C	

SS-CPNL 600 80 % DATE: 5 / 11 / 73 TIME: 14 : 12 : 55

FILE: 1 RECORD: 82 CHANNELS 3 THROUGH 77

CHAN							
3	-134.	S1	-658.	S2	-158.	S3	-834. S4
7	-352.	S5	-396.	S6	-570.	S7	-720. S8
11	-575.	S9	-413.	S10	-827.	S11	-759. S12
15	-672.	S13	-774.	S14	+.		-712. S16
19	-657.	S17	-1256.	S18	-519.	S19	-527. S20
23	-814.	S21	-726.	S22	+.	S23	-482. S24
27	-609.	S25	-557.	S26	-782.	S27	-641. S28
31	+.		-735.	S30	-994.	S31	-896. S32
35	-1053.	S33	-29.	S34A	-410.	S34B	-149. S34C
39	+507.	T1	+551.	T2	+488.	T3	+550. T4
43	+502.	T5	+540.	T6	+562.	T7	+565. T8
47	+508.	T9	+489.	T10	+567.	T11	+514. T12
51	+583.	T13	+584.	T14	+508.	T15	+417. T16
55	+473.	T17	+492.	T18	+550.	T19	+521. T20
59	+452.	T21	+579.	T22	+565.	T23	+591. T24
63	+607.	T25	+581.	T26	+583.	T27	+586. T28
67	+615.	T29	+600.	T30	+505.	T31	+573. T32
71	+563.	T33	+509.	T34	+592.	T22C	+580. T24C
75	+582.	T26C	+574.	T27C	+570.	T32C	

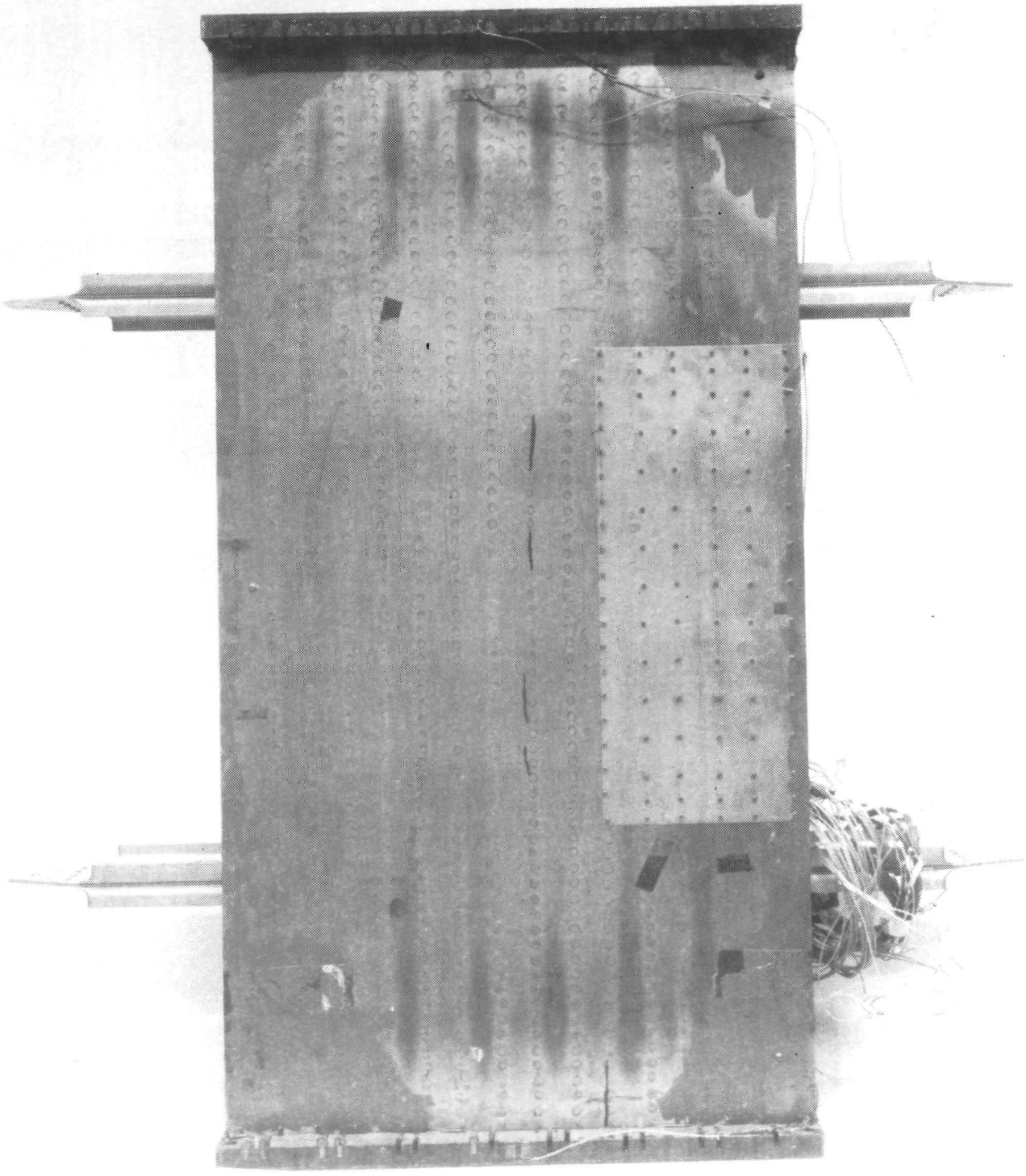

Figure 10.16. Skin Side of Panel after Testing. Buckle is at the Top of the Panel.

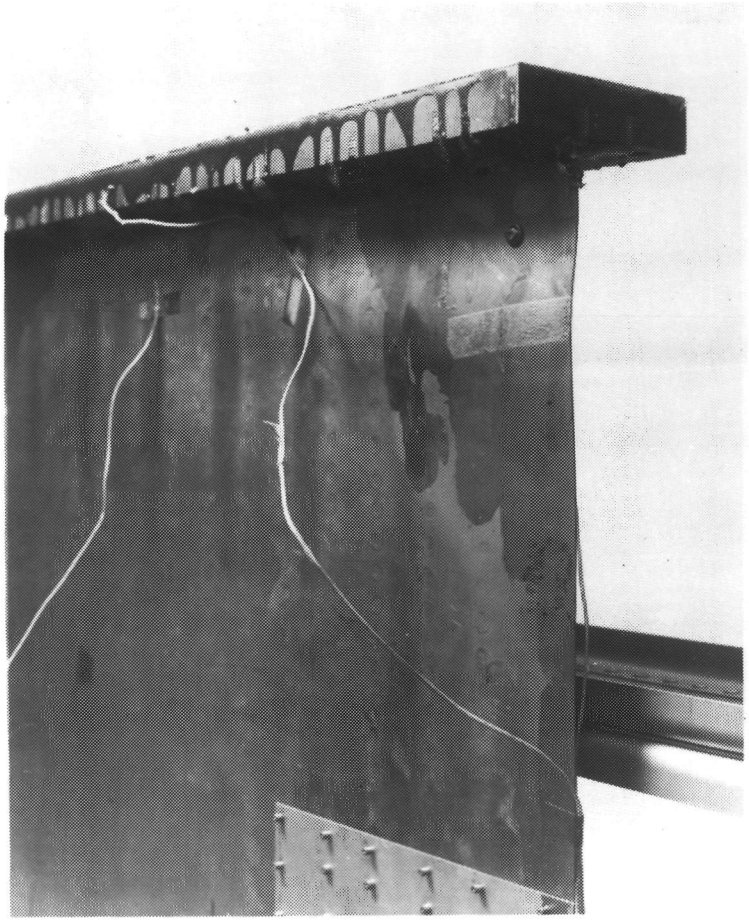

Figure 10.17. Closeup of Buckle in Skin of Compression Panel.

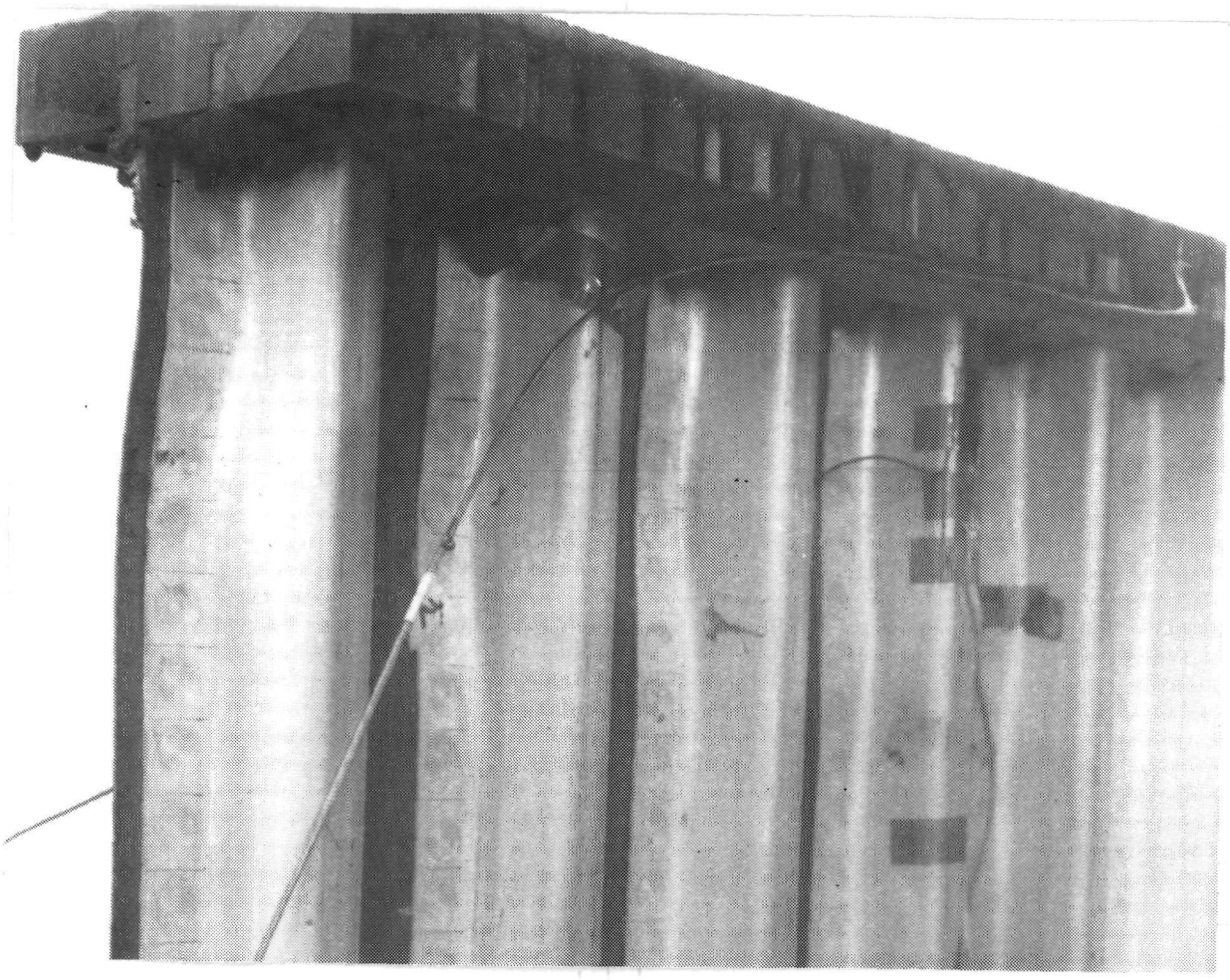

Figure 10.18 Buckles in Stringers at End of Compression Panel.

10.4.4 ANALYSIS. The strain readings for several groups of strain gages are plotted in Figures 10.19 through 10.24. In each of these figures, the group of gages is located together on the skin, hat section skin flange and hat section crown. The phantom line in each graph is the theoretical average strain for the panel.

The group of gages in Figure 10.19 was located at the top center of the panel and shows that despite the efforts to get uniform load introduction, the skin side of the panel was being loaded more heavily than the stiffener.

Figure 10.20 shows the strain readings of gages located at the center of the panel on the side with the patch. The strain here was fairly uniform and considerably lower than the unpatched areas of the panel.

Figures 10.21 and 10.22 are from groups of gages located at the center of the panel of the vertical centerline and at the edge opposite the patch. The strain distribution here is quite uniform — the gages at the center are somewhat lower in value due to the influence of the patch.

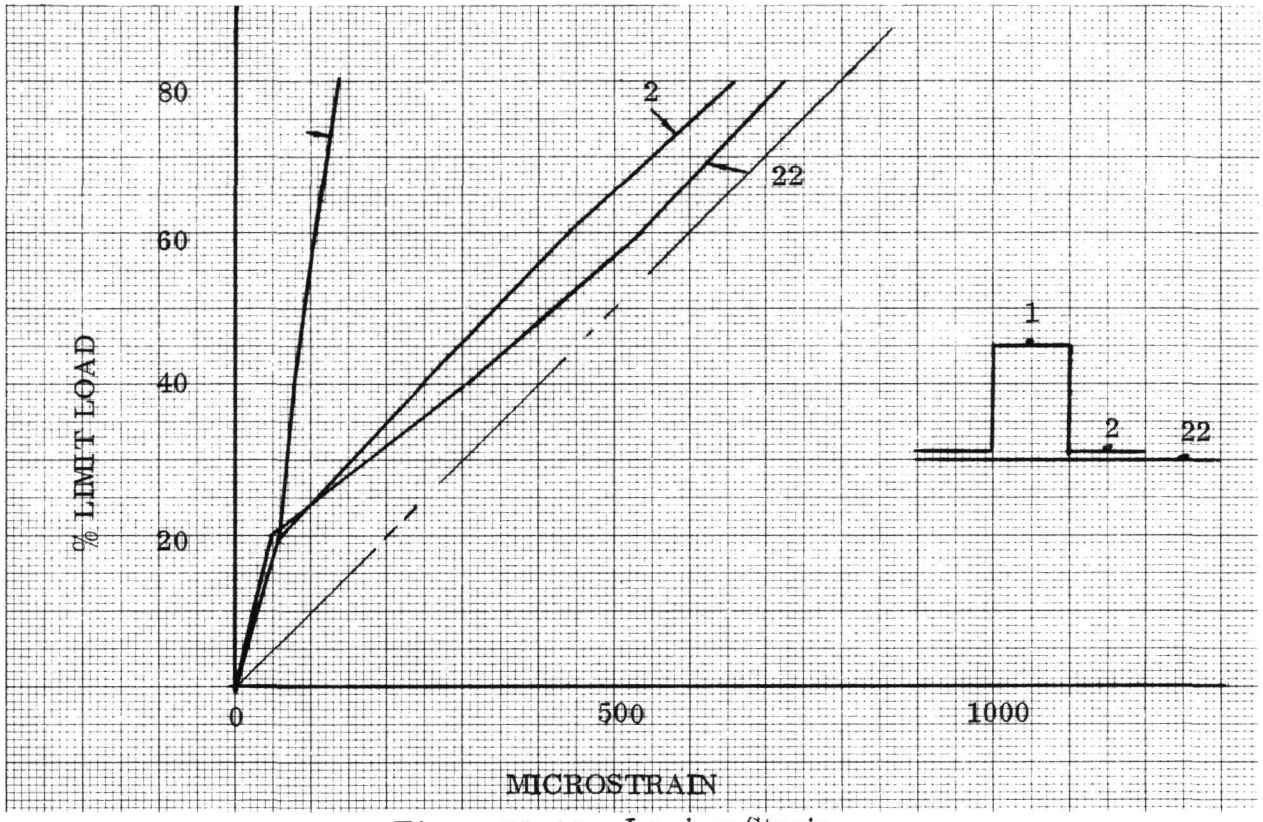

Figure 10.19. Load vs Strain.

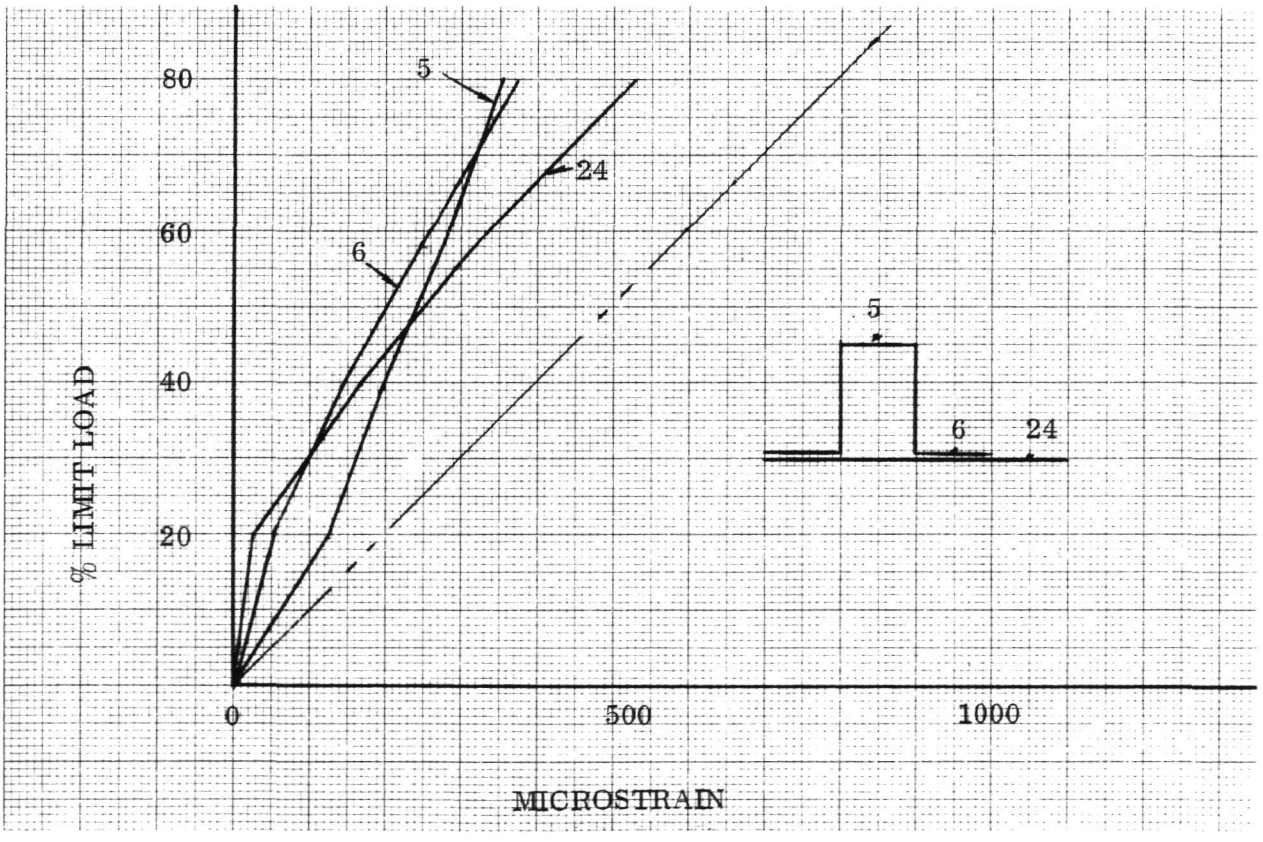

Figure 10.20. Load vs Strain.

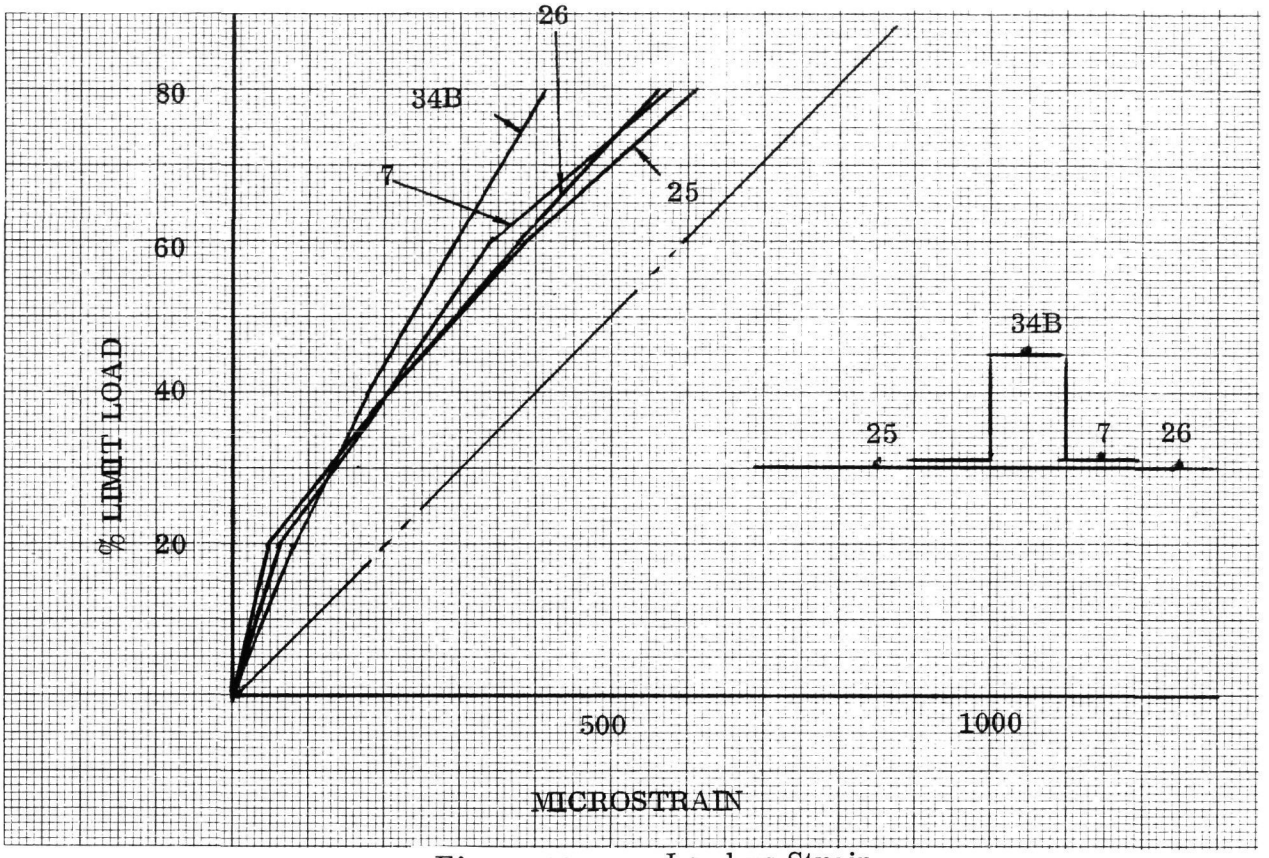

Figure 10.21. Load vs Strain.

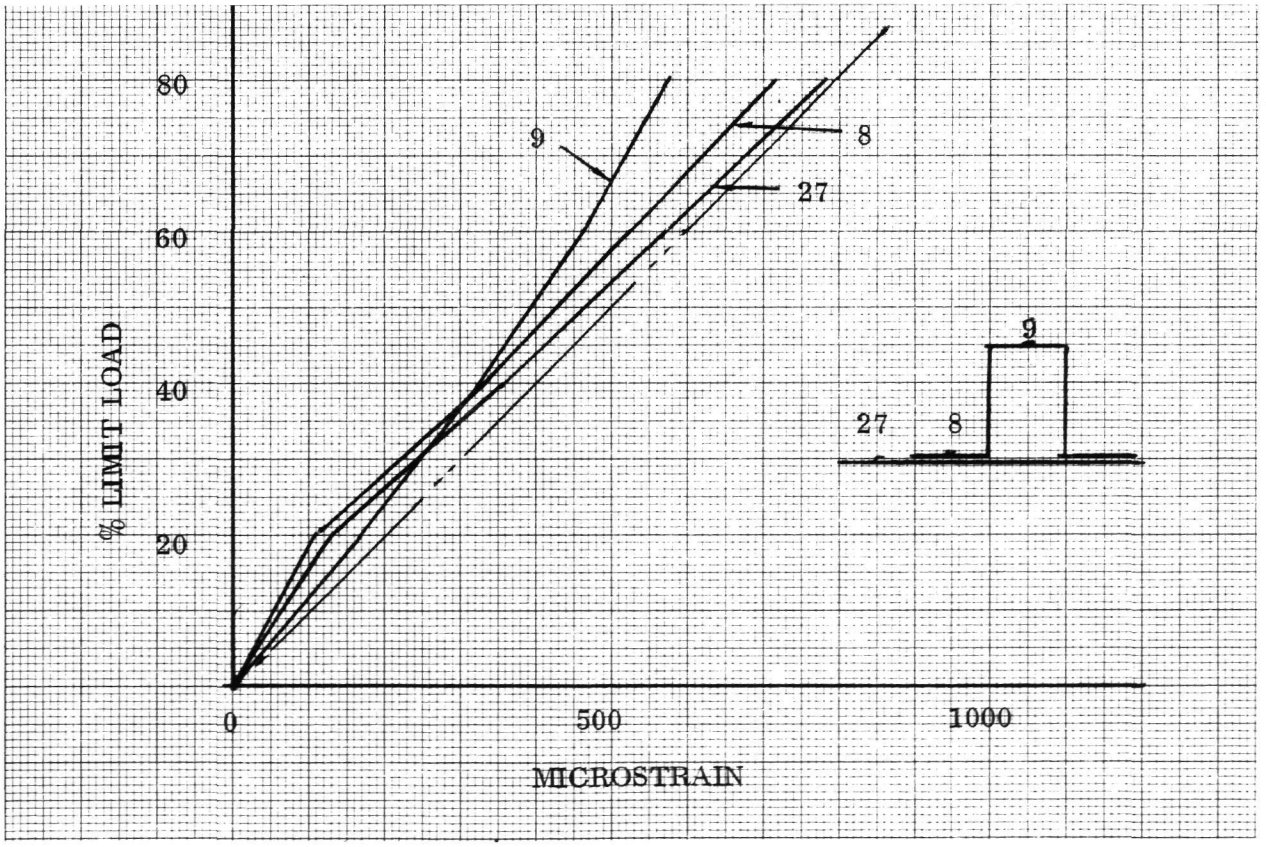

Figure 10.22. Load vs Strain.

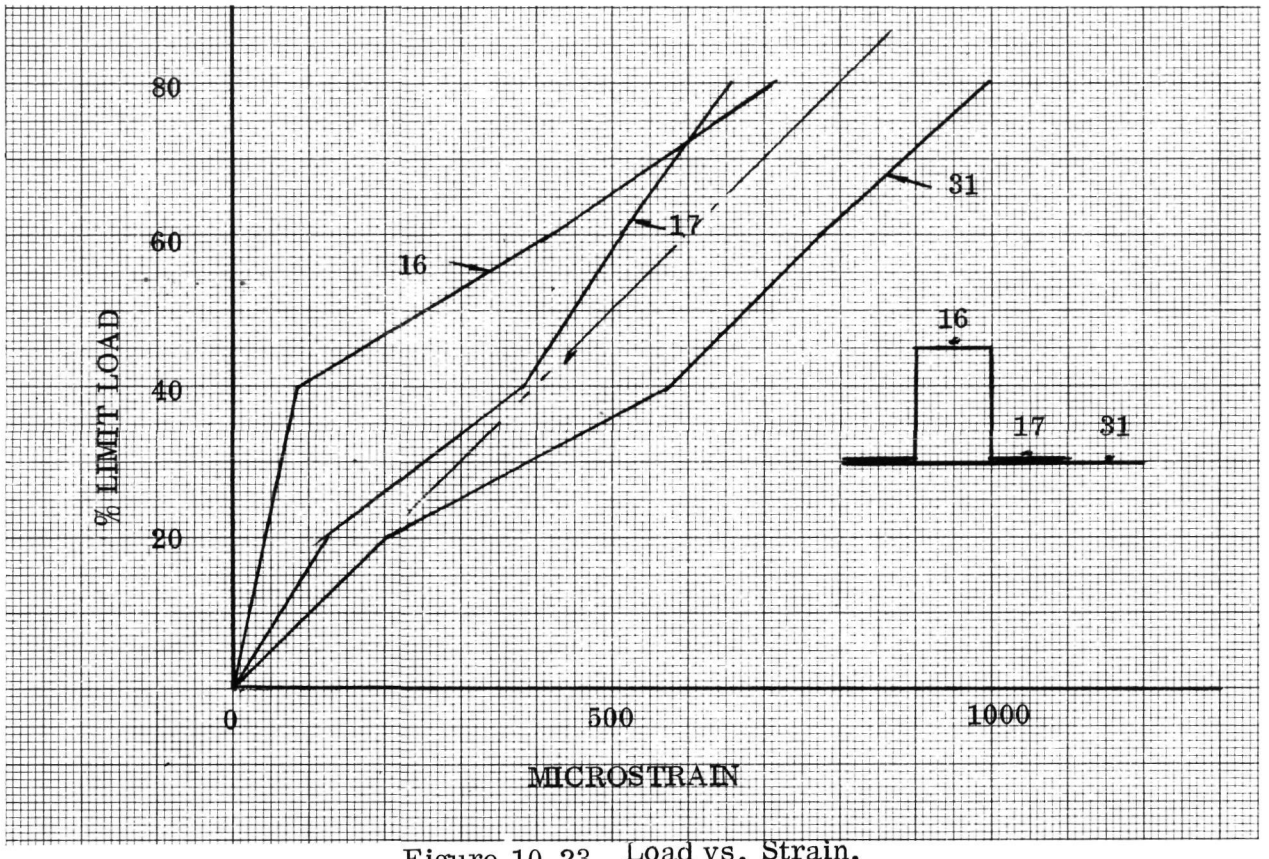

Figure 10.23. Load vs. Strain.

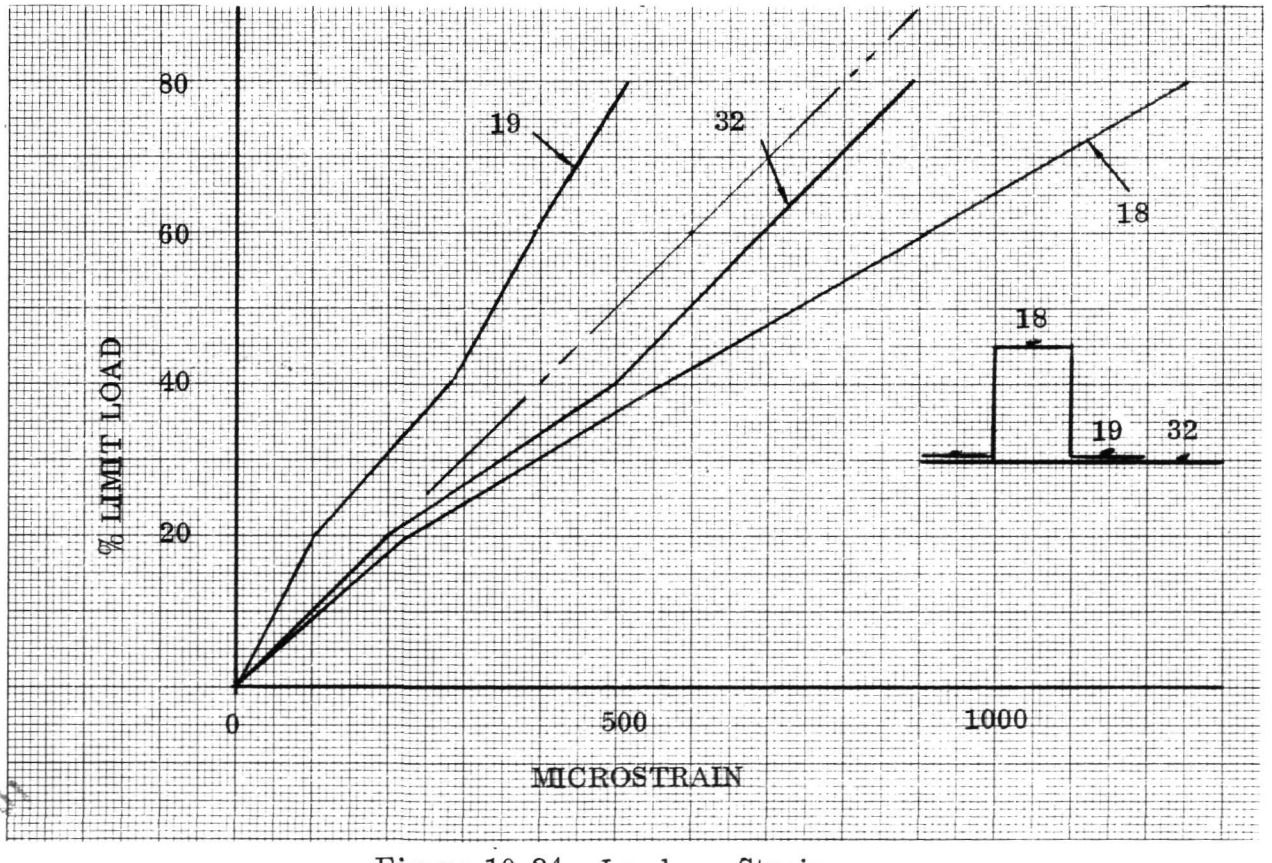

Figure 10.24. Load vs. Strain.

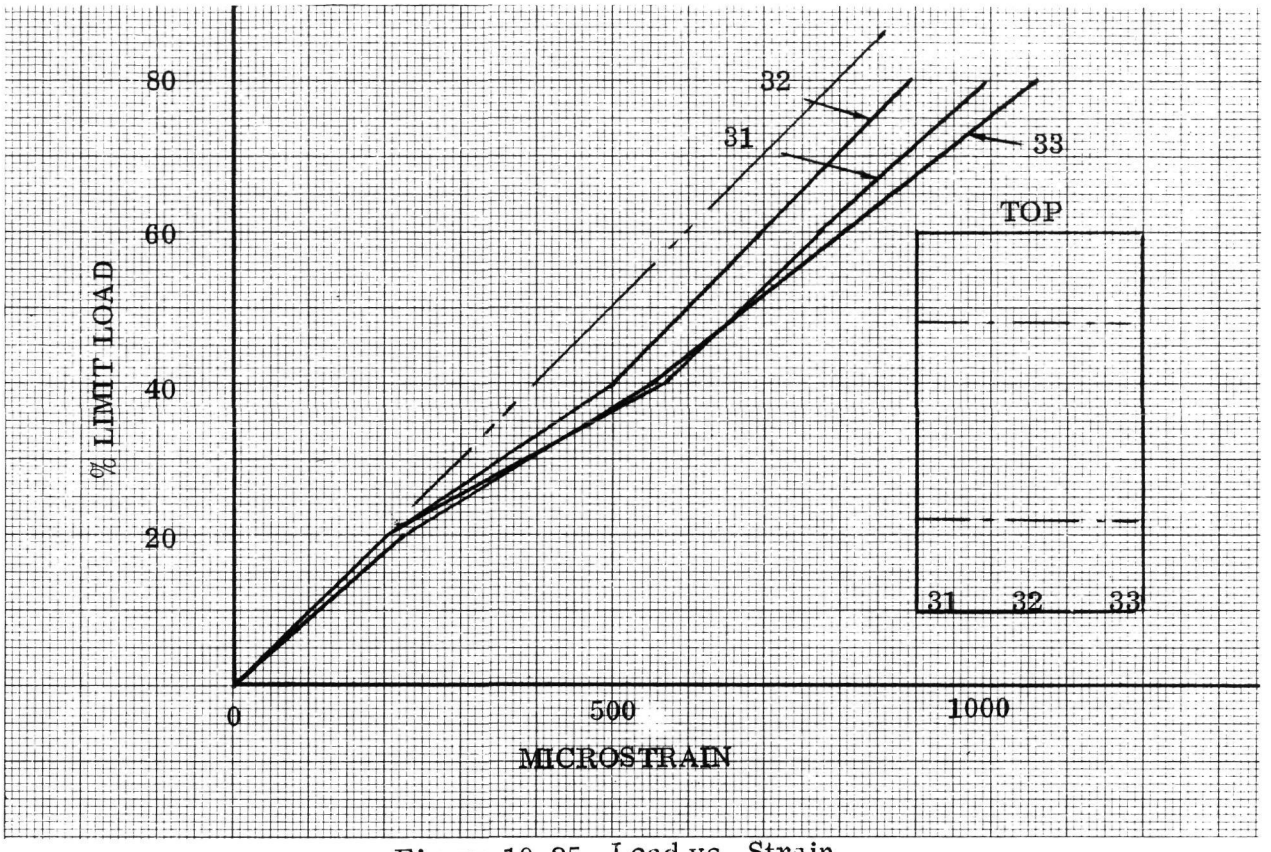

Figure 10.25. Load vs. Strain.

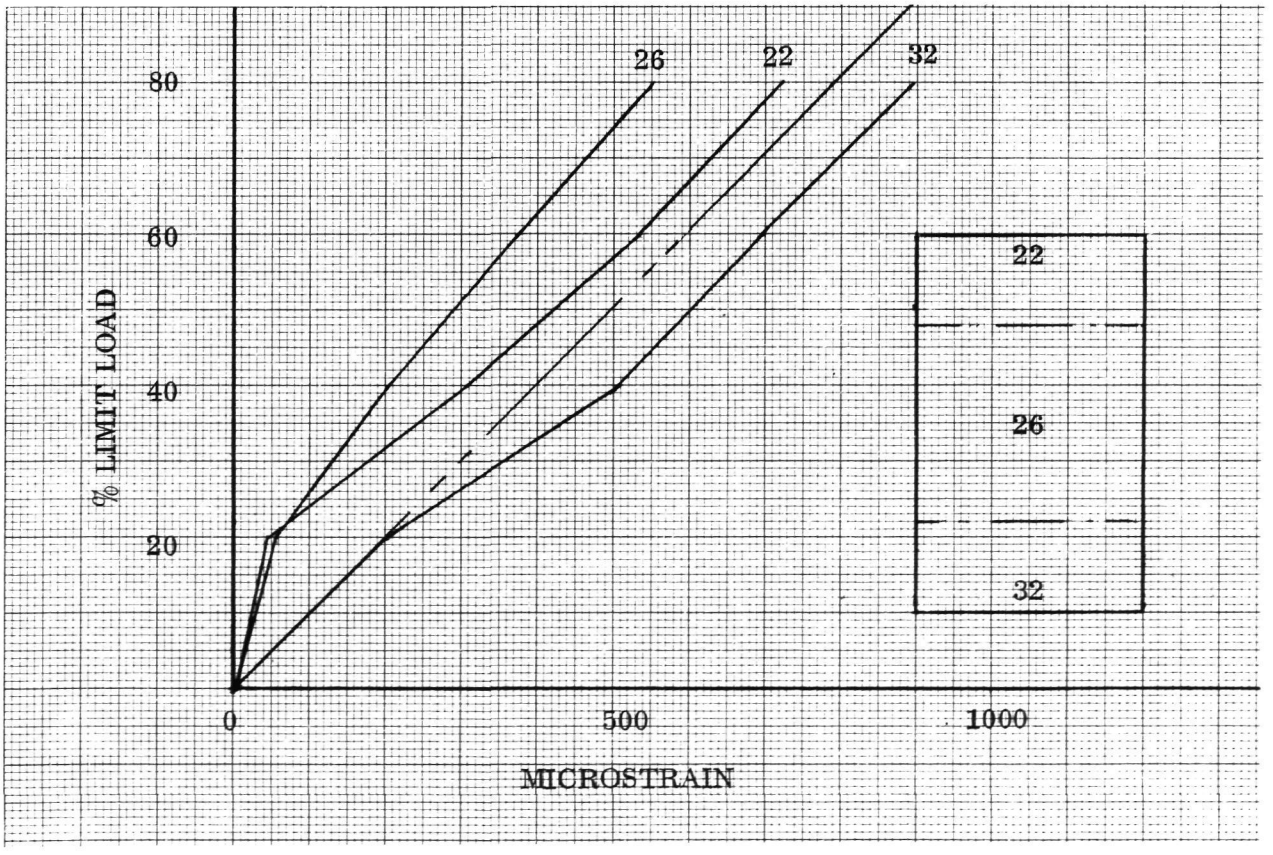

Figure 10.26. Load vs. Strain.

Figures 20.23 and 10.24 show the strain readings from gages at the bottom of the panel. Here again, evidence of nonuniformity is apparent but the differences are in the opposite direction.

Since skin buckling is the critical parameter for the panel failure, it is important to note the variation in skin strain around the panel.

Figure 10.25 shows the variation in skin strain across the bottom of the panel.

It is apparent that the strains are relatively uniform across the panel width and that the skin strains were higher than the theoretical uniform panel strain. Figure 10.26 shows the variation in skin strains about the vertical centerline of the panel. The skin strain at the center (Gage 26) is below the average due to the influence of the patch.

A close inspection of both panels revealed that there was no evidence of spot weld failure at any of the buckles in any of the tests. The use of this fastening method did not contribute to the failure.

Page intentionally left blank

11

CONCLUSIONS

11.1 The preliminary design and parametric study work showed that a boron/aluminum reinforced titanium panel had a definite weight advantage over an all titanium panel or any of the composite reinforced panels.

11.2 A method of predicting the crippling of unidirectional boron/aluminum compression members was developed and was demonstrated to be accurate.

11.3 Splicing of composite stringers solely by means of mechanical fasteners was demonstrated both at room temperature and at 589K (600F) in tension and compression.

11.4 The testing of the first panel was accomplished without sufficient preparation and the failure load of 61.5% of design limit cannot be construed to be a true measure of the panel's strength. The nature of the failure was cause for concern, however. This panel displayed a tendency for the titanium skin to buckle with the boron/aluminum stringer following the skin buckle and unable to prevent the buckle from continuing across the panel.

11.5 The failure of panel no. 2 displayed a similar mode to that noted for panel 1, although at a higher load. It may be argued that the initiation of the failure could have been caused by the stiffeners introduced by the patch and reinforcement of the repaired area. The repair of the panel may have influenced the failure; however, the primary cause for failure appears to be that the boron/aluminum stringers failed to provide sufficient support for the titanium skin so that skin buckling was initiated at a lower stress than predicted. Secondly, the stringers also failed to prevent the buckle, once initiated, from spreading across the panel.

A review of the margin of safety for the panel summarized in the stress analysis (Phase I Summary) shows that minimum margin of safety for the panel was 2% for skin buckling.

Aerospace design practice dictates that the thickness of stringers shall be at least one gage heavier than the skin being stiffened. This practice was not adhered to for these panels, the skin and stringer gages being approximately equal. The low transverse strength of the boron/aluminum at 589K (600F) aggravated this condition.

Although the test panels did not achieve the desired loads, the program did establish several important goals. It showed that boron/aluminum can be fabricated using modified sheet metal techniques; it can be joined successfully and reliably to titanium by means of spot diffusion bonding; and boron/aluminum displays usable strength up to 589K (600F) provided that sufficient attention is given to the low transverse strength and modulus at elevated temperatures.

REFERENCES

1. Emero, D. H., "Optimization of Multirib and Multiweb Wing Box Structures Under Shear and Moment Loads," published in the Proceedings of the AIAA 6th Structures and Materials Conference, April 1965.

2. Bruhn, E. F., "Analysis and Design of Flight Vehicles Structures," Tri-State Offset Co.

3. Unpublished Communication by James Anderson, Langley Research Center.

4. Perry, D. N., "Aircraft Structures," 1950 McGraw-Hill Book Co.

5. Gerard, G., "Structural Stability Theory," Figure 3.11, McGraw-Hill, 1962.

6. Lockheed Stress Memo Number 126, "Prediction of Crippling Strength," January 25, 1966.

7. Convair Aerospace Fort Worth Structures Manual, Page 11.2.1a, 1960.